

THERMOSENSITIVE BIODEGRADABLE mPEG-PLLA BLOCK
COPOLYMERS: SYNTHESSES, CHARACTERIZATIONS AND
APPLICATIONS IN DRUG DELIVERY SYSTEMS; SYNTHESIS AND
PROPERTIES OF NOVEL ELECTROCHROMIC POLYTHIENYLPYRROLE

A THESIS SUBMITTED TO
THE GRADUATE SCHOOL OF NATURAL AND APPLIED SCIENCES
OF
MIDDLE EAST TECHNICAL UNIVERSITY

BY

OLCAY MERT

IN PARTIAL FULFILLMENT OF THE REQUIREMENTS
FOR
THE DEGREE OF DOCTOR OF PHILOSOPHY
IN
POLYMER SCIENCE AND TECHNOLOGY

MAY 2011

Approval of the thesis:

**THERMOSENSITIVE BIODEGRADABLE mPEG-PLLA BLOCK
COPOLYMERS: SYNTHESSES, CHARACTERIZATIONS AND
APPLICATIONS IN DRUG DELIVERY SYSTEMS; SYNTHESIS AND
PROPERTIES OF NOVEL ELECTROCHROMIC
POLYTHIENYLPYRROLE**

submitted by **OLCAY MERT** in partial fulfillment of the requirements for the degree of **Doctor of Philosophy in Polymer Science and Technology Department, Middle East Technical University** by,

Prof. Dr. Canan Özgen _____
Dean, Graduate School of **Natural and Applied Sciences**

Prof. Dr. Necati Özkan _____
Head of Department, **Polymer Science and Technology**

Prof. Dr. Ayhan S. Demir _____
Supervisor, **Chemistry Dept., METU**

Examining Committee Members:

Prof. Dr. Leyla Aras _____
Chemistry Dept., METU

Prof. Dr. Ayhan S. Demir _____
Chemistry Dept., METU

Prof. Dr. Levent Toppare _____
Chemistry Dept., METU

Prof. Dr. Duygu Kısakürek _____
Chemistry Dept., METU

Prof. Dr. M. Yakup Arıca _____
Biology Dept., GAZİ University

Date: 24.05.2011

I hereby declare that all information in this document has been obtained and presented in accordance with academic rules and ethical conduct. I also declare that, as required by these rules and conduct, I have fully cited and referenced all material and results that are not original to this work.

Name, Last name: Olcay Mert

Signature:

ABSTRACT

THERMOSENSITIVE BIODEGRADABLE mPEG-PLLA BLOCK COPOLYMERS: SYNTHESSES, CHARACTERIZATIONS AND APPLICATIONS IN DRUG DELIVERY SYSTEMS; SYNTHESIS AND PROPERTIES OF NOVEL ELECTROCHROMIC POLYTHIENYLPYRROLE

Mert, Olcay

Ph.D., Department of Polymer Science and Technology

Supervisor: Prof. Dr. Ayhan S. Demir

May 2011, 222 pages

Syntheses of biodegradable PLLA homopolymers and PLLA-mPEG diblock copolymers for the formation of thermo-sensitive gels were performed. The sol-gel transition temperature of the matrix was adjusted by altering the length of each PEG and LA component. PLLA-mPEG biocompatible copolymers, having appropriate length of each block component, showed sols at around 42-45 °C, suitable for the injection, then a gel with subsequent rapid cooling to body temperature. Topotecan and camptothecin were selected as anti-cancer drugs. Both drugs can easily hydrolyze at physiological conditions (pH=7.4). This causes the loss of its activity, and it turns into inactive toxic carboxylate form from active lactone state. To keep those anti cancer drugs in the lactone form, they were efficiently loaded into PLLA-mPEG gels in different loading ratios. Their stability in gel was fully examined with HPLC and fluorescence spectroscopy. It was found that both drugs were highly stable and in active form in the prepared gels (>95 %). Then, both release profile of drugs at different loading ratios showed prolonged release over weeks. Mechanistic studies on the stabilization of CPT anti cancer drug with PLLA-mPEG gels were carried out

using ATR-FTIR, confocal and optic microscopes. The cytotoxic efficacy of TPT in the PLLA-mPEG platform (PLLA-mPEG-TPT) was evaluated on LLC-1 and 4T1 cancer cell lines by MTT assay. *In vivo*, the administration of PLLA-mPEG-TPT to the mice bearing breast tumours established with 4T1 cells resulted in a significant reduction in tumour size and better survival percentages. Additionally, stabilization of CPT and TPT with gels may find another application on solid tumors in brain via local injection.

A novel conducting polymer was successfully synthesized via electropolymerization of 1-(1H-pyrrol-1-yl)-2,5-di(thiophen-2-yl)-1H-pyrrole. The electrochemical and electro-optical properties of the corresponding polymer, which was the first example of polymer containing 1,1'-bipyrrole units, were elaborated using electroanalytical and spectroscopic techniques. Cyclic voltammograms and electrooptical studies showed that the polymer has a stable and well-defined reversible redox process as well as electrochromic behavior. The processable polymer film also possessed a yellowish orange light emitter property.

Keywords: Camptothecin, Topotecan, PLLA-mPEG, Stability, Release, Pyrrole

ÖZ

ISIYA HASSAS BİYOBOZUNAN mPEG-PLLA BLOK KOPOLİMERLERİ: SENTEZ, KARAKTERİZASYON VE İLAÇ SALIM SİSTEMLERİNDE UYGULAMALARI; YENİ ELEKTROKROMİK POLİ (TİYONİL PİROL) SENTEZİ VE ÖZELLİKLERİ

Mert, Olcay

Doktora, Polimer Bilimi ve Teknolojisi Bölümü

Tez Yöneticisi: Prof. Dr. Ayhan S. Demir

Mayıs 2011, 222 sayfa

Biyobozunur ve biyouyumlu PLLA homopolimerleri ve PLLA-PEG kopolimerleri sıcaklığa bağımlı özellikleri incelenmek üzere sentezlenmiştir. Her bir PLLA-mPEG bileşeninin uzunluğu ayarlanarak, polimerin 42-45 °C de enjeksiyona hazır olması (sol), soğutmayla da vücut sıcaklığında jel oluşturması sağlanmıştır. Topotekan ve Kamptotesin anti-kanser ilaç olarak seçilmiştir. Topotekan ve Kamptotesin pH= 7.4 de kolaylıkla hidroliz olabilmektedir. Bahsedilen ilaçların lakton formu belirtilen pH'da aktif olmayan ve toksik olan karboksilat formuna dönüşmektedir. İlaçları lakton formunda tutabilmek için, ilaçlar PLLA-mPEG jellerinin içerisine etkin bir şekilde çeşitli oranlarda yüklenmiştir. İlaçların jel içindeki kararlılığı detaylı bir şekilde HPLC ve floresans spektroskopisi ile incelenmiştir. Her iki ilacın jel içerisinde oldukça kararlı ve aktif olduğu bulunmuştur (>95 %). Daha sonra çeşitli yükleme oranlarında bu ilaçların jelden salım çalışmaları yapılmış ve ilaçların uzun bir süre boyunca salım gösterdiği bulunmuştur. CPT antikanser ilacının PLLA-mPEG jelleriyle kararlılığının mekanizması ATR-FTIR, konfokal ve optik mikroskopla aydınlatılmıştır. PLLA-mPEG jeli içindeki topotekanın sitotoksik etkinliği MTT yöntemiyle LLC-1 ve 4T1 kanser hücre hatlarında

değerlendirilmiştir. In vivo olarak, 4T1 hücreleriyle hazırlanan meme kanseri tümörlerine PLLA-mPEG-TPT verilmesi sonucunda tümör büyümesinde azalma ve sağkalım oranlarında artış gözlemlenmiştir. Ayrıca bu ilaçların jel içerisindeki kararlılığı lokal enjeksiyon yolu ile beyindeki katı tümörlerin tedavisinde uygulama bulacağı düşünülmektedir.

Yeni iletken polimer film başarılı bir şekilde 1-(1H-pirol-1-yl)-2,5-di(tiyofen-2-yl)-1H-pirol' ün elektropolimerizasyonu sonucunda sentez edilmiştir. Bu 1,1'-bipirol ünitesi içeren ilk polimerdir. Sentez edilen polimer elektroanalitik ve spektroskopik teknikler kullanılarak incelenmiştir. Siklik voltamogramlar ve elektro-optiksel çalışmalar polimerin kararlı ve tersinir redoks prosesine ve ayrıca elektrokromik özelliğe sahip olduğunu göstermiştir. Filmin sarımsı turuncu ışık emme özelliğine sahip olduğu gözlenmiştir.

Anahtar Kelimeler: Kamptotesin, Topotekan, PLLA-mPEG, Kararlılık, Salım, Pirol

*To the memory of people who sacrificed themselves for the sake of peace of
their country*

ACKNOWLEDGEMENTS

I am deeply indebted to my supervisor Prof. Dr. Ayhan S. Demir whose valuable guidance, criticism, suggestions and encouragement lead to the creation of thesis. It is a great honor for me to be his student, and his intellectual approach will continue to inspire me. In addition, just like everyone else who has an opportunity to work with him, I always feel great admiration about his wide scientific knowledge and infinite energy. Scientific experiences earned at Demir Research Group will be cornerstones of my future academic life.

I would like to thank my former and current lab-mates helping me in our research group. For their kind helps, I greatly thank and strongly express my regards to all people in chemistry department, as well.

I would like to thank Dr. Atilla Cihaner, Dr. Güneş Esendağlı, and Dr. A. Lale Doğan for their kind helps and contributions in the electrochemical polymerizations, in vivo studies and in vitro studies, respectively.

I express my endless thanks to Dr. Yıldırım Erbil at GYTE, Dr. Turan Öztürk at İTÜ, Dr. Levent Demirel at Koç University, Dr. Levent Toppare at METU, Dr. Cavit Uyanık at Kocaeli University, Dr. Mehmet S. Eroğlu at Marmara University, Dr. Meral Arca at Marmara University, Dr. Tayfur Öztürk at METU, Dr. Yunus Kışalı at Kocaeli University, Dr. Justin Hanes, Dr. Samuel K. Lai, Dr. Ming Yang at Johns Hopkins University at USA for their contributions to my academic career during or prior to the thesis.

I would like to thank to my all PST-502 lab. colleagues Dr. Gralp zko, Dr. Elif Vargn, Glden Eroęlu, Ali Sinan Dike for their friendship and making student lab an enjoyable place. Also, special thanks go to Ali Sinan Dike for his kind help about supplying electronic books, papers and other documents.

I also wish to thank my dear friends: Fatih Bay at Bern Univ., İdris Candan at METU, Uęur Cengiz at GYTE and Erdin Doęancı at Kocaeli University. I have spent great time with them almost a decade. I would like to thank Dr. Adnan Bulut at Kırıkkale University and Dr. Sleyman Aydın at Malatya University for their kind friendship and insight.

I would also like to thank Kocaeli University for the financial support during my thesis via Faculty Development Program (YP) and TUBITAK 2214 Scholarship Program.

For the part of building block system for the development of electrochemical reactors, we gratefully thank the European Union within the Seventh Framework Programme for the financial support of the Small Scale Collaborative Project ERUDESP.

My special thanks go to my parents, Rahime and Muammer Mert, and my sister, Oya Mert, for their endless love and always being with me whenever I need them. I always feel how lucky I am.

TABLE OF CONTENTS

ABSTRACT	iv
ÖZ.....	vi
ACKNOWLEDGEMENTS	ix
TABLE OF CONTENTS	xi
LIST OF TABLES	xix
LIST OF FIGURES	xxi
ABBREVIATIONS	xxxiii
CHAPTERS	1
1. INTRODUCTION.....	1
1.1. Thermosensitive Biodegradable mPEG-PLLA Block Copolymers: Syntheses, Characterizations and Applications in Drug Delivery Systems	1
1.1.1. Thermosensitive Biodegradable Polymers	2
1.1.1.1. PLLA Homopolymer and PLLA-mPEG Copolymers	3
1.1.1.2. PLGA Homopolymer and PLGA-PEG Copolymers.....	9
1.1.1.3. Polyphosphazenes.....	11
1.1.1.4. Poly(sebacic acid) (PSA) Homopolymer and PSA-PEG Copolymers	14
1.1.1.5. Poly(peptides).....	17
1.1.2. Application of Thermosensitive Polymers	18
1.1.2.1. General Applications	18
1.1.2.2. Applications in Drug Delivery Systems	19
1.1.3. Other Drug Delivery Techniques	22
1.1.3.1. Drug Loaded Implant Polymers	22
1.1.3.2. pH Sensitive Polymers.....	24

1.1.3.3. Light Sensitive Polymers.....	25
1.1.3.4. Ultrasound-Responsive Polymers	26
1.2. Synthesis, Properties and Applications of Novel Electrochromic Polythienylpyrroles.....	27
1.2.1. General Concepts.....	27
1.2.2. Building Block System for Development of Electrochemical Reactors	33
1.3. Pyrrole Coupling Chemistry: Investigation of Electroanalytic Spectroscopic and Thermal Properties of N-Substituted Poly(Bis-Pyrrole) Films	35
1.4. The Aim of This Study	37
1.4.1. Thermosensitive Biodegradable mPEG-PLLA Block Copolymers: Synthesis, Characterizations and Applications in Drug Delivery Systems	37
1.4.2. Preparation of Polymeric PEG:PSA Particles for the Camptothecin Anticancer Drug Delivery System.....	39
1.4.3. Synthesis and Properties of Novel Electrochromic Polythienylpyrrole .	39
1.4.4. Pyrrole Coupling Chemistry: Investigation of Electroanalytic Spectroscopic and Thermal Properties of N-Substituted Poly(Bis-Pyrrole) Films	41
2. EXPERIMENTAL	42
2.1. Materials	42
2.2. Equipments	43
2.2.1. Nuclear Magnetic Resonance Spectroscopy (NMR).....	43
2.2.2. FTIR and ATR-FTIR Spectroscopy	43
2.2.3. High Performance Liquid Chromatography (HPLC)	43
2.2.4. Fluorescence Spectroscopy.....	44
2.2.5. Confocal Spectroscopy	44
2.2.6. Optical Microscope.....	44
2.2.7. Cyclic Voltammetry (CV) System and Spectroelectrochemistry	44

2.3. Procedure	45
2.3.1. Thermosensitive Biodegradable mPEG-PLLA Block Copolymers: Syntheses, Characterizations and Applications in Drug Delivery Systems	45
2.3.1.1. Homopolymerization of L-Lactide	45
2.3.1.2. Copolymerization of L-Lactide with mPEG-2000 (PLLA-mPEG2k)	45
2.3.1.3. Copolymerization of L-Lactide with mPEG-5000 (PLLA-mPEG5k)	46
2.3.1.4. Copolymer Film Preparation	47
2.3.1.5. General Procedure for Determining Gel to Sol Transition Temperature.....	47
2.3.1.6. CPT and TPT Loading into Copolymer Gel.....	48
2.3.1.7. Preparation of Tris Buffer	49
2.3.1.8. Preparation of Free CPT and TPT Stock Solution	49
2.3.1.9. Preparation of Triethylamine Acetate (TEAA) Buffer.....	49
2.3.1.10. HPLC Analysis	50
2.3.1.11. Fluorescence Analysis	50
2.3.1.12. Release Experiments	51
2.3.1.12.1. Preparation of Standard Curve	52
2.3.1.13. Examination of CPT Loaded Gel with ATR-FTIR	52
2.3.1.14. In vitro and In Vivo Studies	53
2.3.1.14.1. Cell Culture	53
2.3.1.14.2. MTT Assay.....	53
2.3.1.14.3. Animals and Tumor Formation	54
2.3.1.14.4. Statistical Analysis	55
2.3.2. Preparation of Polymeric Particles for the Camptothecin Anticancer Drug Delivery System	55
2.3.2.1. Synthesis of Sebacic Acid Prepolymer.....	55
2.3.2.2. Synthesis of PEG Prepolymer	56

2.3.2.3. Synthesis of PEG:PSA Copolymer.....	56
2.3.2.4. Nanoparticle and Microparticle formulations of PEG:PSA Copolymer	56
2.3.3. Synthesis and Properties of Novel Electrochromic Polythienylpyrrole .	57
2.3.3.1. Synthesis of N-Aminophthalimide 10.....	57
2.3.3.2. Synthesis of N-Phthalimidopyrrole 12	58
2.3.3.3. Synthesis of N-Aminopyrrole 13.....	59
2.3.3.4. Synthesis of 1,1'-Bipyrrole 14	60
2.3.3.5. Synthesis of 1,4-Bis(2-thienyl)butane-1,4-dione 17.....	60
2.3.3.6. Synthesis of 1-(1H-pyrrol-1-yl)-2,5-di(thiophen-2-yl)-1H-pyrrole (SNSN) 18	61
2.3.3.7. Electropolymerization and Characterization of SNSN 33.....	62
2.3.4. Building Block System for Development of Electrochemical Reactors	63
2.3.4.1. Synthesis of 2-(2,5-di(thiophen-2-yl)-1H-pyrrol-1-yl)ethanamine 35	63
2.3.4.2. Synthesis of 2-(4-(bromomethyl)pyridin-2-yl)-4-methylpyridine 37	64
2.3.4.3. Synthesis of N-((2-(4-methylpyridin-2-yl)pyridin-4-yl)methyl)-2-(2,5-di(thiophen-2-yl)-1H-pyrrol-1-yl)ethanamine 38	64
2.3.4.4. Synthesis of N-((2-(4-methylpyridin-2-yl)pyridin-4-yl)methyl)-2-(2,5-di(thiophen-2-yl)-1H-pyrrol-1-yl)ethanamine-Rh Complex 39	65
2.3.4.5. Synthesis of 4-((2-(2,5-di(thiophen-2-yl)-1H-pyrrol-1-yl)ethylamino) methyl) phenylboronic acid 41.....	66
2.3.4.6. Synthesis of 5-((2-(2,5-di(thiophen-2-yl)-1H-pyrrol-1-yl)ethylamino) methyl)thiophen-2-yl-2-boronic acid 43.....	67
2.3.4.7. Synthesis of SNS-EA-Ph-BA-NAD 45	68
2.3.4.8. Synthesis of 1-(3-(triethoxysilyl)propyl)-2,5-di(thiophen-2-yl)-1H-pyrrole 47.....	68

2.3.4.9. Synthesis of Silane-Boronic–NAD Compound 51	69
2.3.5. Pyrrole Coupling Chemistry: Investigation of Electroanalytic Spectroscopic and Thermal Properties of N-Substituted Poly(Bis-Pyrrole) Films	70
2.3.5.1. Materials and Methods	70
3. RESULTS AND DISCUSSION.....	73
3.1. Thermosensitive Biodegradable mPEG-PLLA Block Copolymers: Syntheses, Characterizations and Applications in Drug Delivery Systems	73
3.1.1. Synthesis of Poly(L-Lactide) Homopolymer	74
3.1.2. Syntheses of mPEG-PLLA Diblock Copolymers	75
3.1.3. Properties of mPEG-PLLA Diblock Copolymers	78
3.1.3.1. Copolymer Film Preparation	78
3.1.3.2. Comparison of Surface ATR of Copolymer Films.....	79
3.1.3.3. Comparison of Bulk FTIR and Surface ATR.....	80
3.1.3.4. Surface Free Energy Properties and Contact Angle Measurements	81
3.1.4. Determination and Regulation of Thermosensitivity of the Polymers	83
3.1.5. Camptothecin Class Topoisomerase I Anticancer Drugs: Structures, Clinic Limitations and Properties	84
3.1.5.1. Camptothecin.....	84
3.1.5.2. Clinic Limitation for CPT Derivatives	85
3.1.5.3. Topotecan (TPT).....	86
3.1.5.4. Mechanism of Action of Camptothecin with Topoisomerase 1	88
3.1.6. Thermosensitive mPEG-PLLA Drug Delivery Systems	89
3.1.6.1. Formulation of the Polymer-Drug Conjugate.....	89
3.1.6.2. Stability of the Drugs.....	89
3.1.6.2.1. Fluorescence Spectroscopy Analysis.....	89
3.1.6.2.2. Analysis of R_L and R_C Values of Free CPT and TPT via Fluorescence Spectroscopy.....	90

3.1.6.2.3. Analysis of R_L and R_C Values for CPT and TPT in Gel via Fluorescence Spectroscopy.....	91
3.1.6.2.4. Analysis of Lactone Conversion of Free CPT and TPT via Fluorescence Spectroscopy.....	91
3.1.6.2.5. Analysis of Lactone Conversion of CPT and TPT in Gel via Fluorescence Spectroscopy.....	93
3.1.6.2.6. HPLC Analysis.....	95
3.1.6.2.7. Analysis of Lactone Conversion of Free CPT and TPT via HPLC	95
3.1.6.2.8. Analysis of Lactone Conversion of CPT and TPT in Gel via HPLC	97
3.1.6.2.9. Concentration Effect on Drug Stability	99
3.1.6.2.10. Mechanistic Outlook to the Stabilization of CPT via PLLA-mPEG Gels	99
3.1.6.3. Controlled Release of the Drugs.....	104
3.1.6.3.1. Standard Curves of Free CPT and TPT	104
3.1.6.3.2. Release Studies of CPT and TPT Anticancer Drugs from Gels .	105
3.1.6.4. In Vivo and In Vitro Experiments with Polymer-Drug Conjugate	110
3.1.6.4.1. In Vitro Studies.....	110
3.1.6.4.2. In Vivo Studies	112
3.1.7. Performance of the Current Platform vs. Literature	115
3.2. Preparation of Polymeric PEG:PSA Particles for the Camptothecin Anticancer Drug Delivery System.....	119
3.2.1. Synthesis of Sebacic Acid Prepolymer.....	119
3.2.2. Synthesis of PEG Prepolymer	119
3.2.3. Synthesis of PEG:PSA Copolymer.....	120
3.2.4. Nanoparticle and Microparticle formulations of PEG:PSA Copolymer	121
3.2.5. Analysis of CPT loaded particles by HPLC	122

3.3. Synthesis and Properties of Novel Electrochromic Polythienylpyrrole ..	123
3.3.1. Synthesis of 1,1'-Bipyrrole.....	123
3.3.2. Synthesis of 1-(1H-pyrrol-1-yl)-2,5-di(thiophen-2-yl)-1H-Pyrrole (SNSN)	124
3.3.3. Electropolymerization of SNSN.....	125
3.3.4. Characterization of PSNSN with FTIR	128
3.3.5. Electro-Optical Properties of SNSN and of Its Derived Polymer PSNSN.....	130
3.3.6. Studies of Switching and Stability of PSNSN.....	132
3.3.7. Spectroscopic Studies	135
3.3.8. Building Block System for Development of Electrochemical Reactors	135
3.3.8.1. Synthesis of a SNS-Mediator	137
3.3.8.2. Synthesis of SNS-NAD ⁺	138
3.3.8.3. Electropolymerization of SNS-Ethylene Amine (SNS-EA) 35.....	139
3.3.8.4. Electropolymerization of SNS-EA-Bipyridine 38.....	140
3.3.8.5. Electropolymerization of SNS-EA-Bipy-Rh Complex 39	140
3.3.8.6. Electro-copolymerization of SNS-EA-Bipyridine Rh Complex 39 with Pyrrole	141
3.3.8.7. SNS-EA-Bipy Rh Complex-Pyrrole 39 After NAD Addition	142
3.3.8.8. Electropolymerization of SNS-EA-pBA and Copolymerization with 3,4-Ethylene Dioxythiophene (EDOT).....	143
3.3.8.9. Film Stability of SNS-EA-PBA-EDOT in Various Mediums.....	144
3.3.8.10. Electropolymerization of SNS-EA-PBA with Thiophene.....	145
3.3.8.11. Electropolymerization of Pyrrole and Its Copolymer with SNS-EA-PBA 41	146
3.3.8.12. Film Stability of SNS-EA-PBA-Pyrrole Before and After NAD Immobilizations	146

3.4. Pyrrole Coupling Chemistry: Investigation of Electroanalytic Spectroscopic and Thermal Properties of N-Substituted Poly (Bis-Pyrrole) Films	148
3.4.1. Electrochemical Behavior of Monomer I and Synthesis of Corresponding Polymer	148
3.4.2. Spectroelectrochemical Behavior of PI	151
3.4.3. Thermal Behavior of PI	154
3.4.4 Electrical Properties.....	155
3.4.5. Voltammetric Recognition of Na ⁺ Ions	155
3.4.6. Preconcentration and Voltammetric Recognition of Ag ⁺ Ions	157
4. CONCLUSIONS	160
4.1. Thermosensitive Biodegradable mPEG-PLLA Block Copolymers: Syntheses, Characterizations and Applications in Drug Delivery Systems ...	160
4.2. Preparation of Polymeric PEG:PSA Particles for the Camptothecin Anticancer Drug Delivery System.....	163
4.3. Synthesis and Properties of Novel Electrochromic Polythienylpyrrole ..	163
4.4. Pyrrole Coupling Chemistry: Investigation of Electroanalytic Spectroscopic and Thermal Properties of N-Substituted Poly(Bis-Pyrrole) Films	165
REFERENCES	167
APPENDICES	180
A. HPLC	180
B. NMR	208
CURRICULUM VITAE	218

LIST OF TABLES

TABLES

Table 1.1 Properties of synthetic biodegradable polymers.....	10
Table 2.1 Conditions for poly(L-lactide) synthesis	45
Table 2.2 Conditions for PLLA-mPEG2k synthesis	46
Table 2.3 Conditions for PLLA-mPEG5k synthesis	47
Table 2.4 Concentrations of PLLA, PLLA-mPEG2k and PLLA-mPEG5k tested determining gel to sol transition temperature.	48
Table 2.5 CPT and TPT loading into copolymer gel.....	49
Table 2.6 Excitation and emission wavelength values of CPT and TPT used in HPLC analysis	50
Table 2.7 Excitation and emission wavelength values of CPT and TPT used in fluorescence analysis	51
Table 2.8 Gel preparation with CPT and TPT drugs at different loading ratios ..	52
Table 3.1 The molecular weight of PLLA homopolymers.....	74
Table 3.2 The molecular weight of PLLA-mPEG diblock copolymers.....	76
Table 3.3 Determination of sol-gel temperature.....	83
Table 3.4 R_L and R_C values for free CPT and TPT	91
Table 3.5 Lactone conversion of free CPT.....	92
Table 3.6 Lactone conversion of free TPT	93
Table 3.7 CPT in gel, 0.015 % loading	94
Table 3.8 TPT in gel, 0.015 % loading.....	94
Table 3.9 L % of CPT and TPT in gel, HPLC analysis.....	98
Table 3.10 Formulations of CPT and TPT loaded gels	105
Table 3.11 Release data of formulation 28	107

Table 3.12 Release data of formulation 29	108
Table 3.13 Release data of formulation 30	109
Table 3.14 Release data of formulation 31	110
Table 3.15 Electrochemical and/or optical data for SNS, SNSN, SNSF and SNSNP as well as their polymers.	126
Table 3.16 Voltammetric and spectroelectrochemical data with the conductivities of PPy and P-I at 300 K.....	155
Table 3.17 Syntheses and sol-gel characteristics of PLLA and PLLA-mPEG polymers	163

LIST OF FIGURES

FIGURES

Figure 1.1 Comparison of conventional and controlled-release profiles.....	2
Figure 1.2 Structures of L- and D- Lactides.....	3
Figure 1.3 Syntheses of PLLA (A and B) and PDLA (C and D).	4
Figure 1.5 DOX or β -lap loaded PEG(5k)-b-PLA(5k) diblock copolymer micelle.	6
Figure 1.6 Synthesis of PLGA from lactide and glycolide monomers.....	9
Figure 1.7 Hydrolysis of PLGA	10
Figure 1.8 The synthetic route of the PLGA–PEG diblock (a) and PLGA–PEG– PLGA triblock copolymers (b).	11
Figure 1.10 Degradation routes of aminoacid ester–substituted polyphosphazenes.	12
Figure 1.11 Synthesis of poly(organo phosphazene)s	13
Figure 1.12 Synthesis of poly(organo phosphazenes) bearing mPEG and amino acid esters	14
Figure 1.13 Synthesis of poly(sebacic acid).....	15
Figure 1.14 Synthesis of PEG:PSA copolymer	16
Figure 1.15 Transformation from the aqueous solution into gel for PEG–SA gel (a) PEG–SA solution at rt, (b) the gel at 37 °C.....	16
Figure 1.16 Amino acid sequences of the the proteins (A) and physical gel-sol change of monodisperse triblock copolymer (B).	17
Figure 1.17 Structure of PEG-g-PLGA and PLGA-g-PEG copolymers (A) and in vivo efficacy in diabetic rats of PLGA-g-PEG depot systems (B).....	18

Figure 1.18 % of transplanted MDSCs at the wound site (A), wound closure analysis after mixing or covering the MDSCs with the PEG–PLGA–PEG hydrogel (B).....	19
Figure 1.19 Efficacies of intratumoral OncoGel™ vs. systemic i.v. (A) and i.p. (B) and in vitro release of paclitaxel from OncoGel (C).....	20
Figure 1.20 Photographs of the representative rat bladders	21
Figure 1.21 Antitumor effects against S-180 solid tumor.	22
Figure 1.22 First figure represents polymer wafer with BCNU being placed into a tumor resection cavity while second shows multiple polymer wafers covered with surgical for being safe.....	23
Figure 1.23 pH-sensitive hydrogels in consideration of delivery of oral colon-specific drugs.....	24
Figure 1.24 Schematic illustration of drug release process in AEA system.....	25
Figure 1.25 Light-activated mesostructured silica nanoparticles having azobenzene derivatives	26
Figure 1.26 Effect of ultrasound on drug loaded pluronic triblock copolymer micelles.....	26
Figure 1.27 Structure of 2,5-Di(2-thienyl)pyrroles (SNS)	27
Figure 1.28 Synthesis of SNS starting from thiophene	27
Figure 1.29 Resonance structures of SNS	28
Figure 1.30 α - α and β "- β " couplings of SNS	29
Figure 1.31 Substituted SNS derivatives	29
Figure 1.32 Capacitance of poly(SNS) films at different potentials vs. electrogeneration time at 25 °C.	30
Figure 1.33 1-aryl-2,5-di(2-thienyl)pyrrole derivatives bearing an electron-withdrawing group.....	31
Figure 1.34 Schematic representation of enzyme immobilization.	31
Figure 1.35 Electrochemical polymerization of SNS-Crown and ion recognition by the PSNS-Crown film to give PSNS-Crown-M.	32

Figure 1.36 Chemical structure of PTPTB.	32
Figure 1.37 Reaction scheme of functionalized CdSe/ZnS quantum dots	33
Figure 1.38 Enzymatic electrochemical chiral synthesis of L-Lactate via NADH cofactor	34
Figure 1.39 Immobilization of the modified GatDH and cofactor regeneration for the oxidation of alcohols	34
Figure 1.40 N-, alfa- and beta-linked bisPy with different types of spacers	35
Figure 1.41 1-(3-(2-(2-(3-(1H-pyrrol-1-yl)propoxy)ethoxy)ethoxy)propyl)-1H-pyrrole.....	36
Figure 1.42 An injectable biodegradable polymeric system is developed for the efficient preserving of the active form and delayed-release of camptothecin anticancer drugs.....	38
Figure 1.43 Synthesis of SNSN and 1,1'-bipyrrole.....	40
Figure 2.1 Synthesis of N-aminophthalimide 10 from phthalimide 9	57
Figure 2.2 Synthesis of N-phthalimidopyrrole 12 from N-aminophthalimide 10	58
Figure 2.3 Synthesis of N-aminopyrrole 13 from N-phthalimidopyrrole 12	59
Figure 2.4 Synthesis of 1,1'-bipyrrole 14 from N-aminopyrrole 13	60
Figure 2.5 Synthesis of 1,4-Bis(2-thienyl)butane-1,4-dione 17	60
Figure 2.6 Synthesis of SNSN 18	61
Figure 2.7 Electrochemical polymerization of SNSN 33	62
Figure 2.8 Synthesis of compound 35	63
Figure 2.9 Synthesis of compound 37	64
Figure 2.10 Synthesis of compound 38	65
Figure 2.11 Synthesis of compound 39	66
Figure 2.12 Synthesis of compound 41	67
Figure 2.13 Synthesis of compound 43	67
Figure 2.14 Synthesis of compound 45	68
Figure 2.15 Synthesis of compound 47	69
Figure 2.16 Synthesis of compound 51	70

Figure 3.1 PLLA-mPEG polymerization starting from L-lactide and mPEG	75
Figure 3.2 Representative ¹ H-NMR of copolymer 21	77
Figure 3.3 FTIR spectrum of copolymer 25	78
Figure 3.4 Comparison of surface ATR of copolymer Films 21 and 25	80
Figure 3.5 Comparisons of bulk FTIR and surface ATR of copolymer 25	81
Figure 3.6 Structure of camptothecin	84
Figure 3.7 CPT producing plants	85
Figure 3.8 Camptothecin hydrolysis to water soluble sodium salt	86
Figure 3.9 Structure of topotecan	87
Figure 3.10 Synthesis of topotecan	87
Figure 3.11 Mechanism of action of camptothecin	88
Figure 3.12 L % and C % of free CPT and TPT with FL analysis (a. circle: L % of free TPT in buffer; b. diamond: L % of free CPT in buffer)	92
Figure 3.13 Lactone conversion for CPT and TPT in gel, 0.015 % loading via FL (a. up-triangle: L % of CPT in gel; b. plus: L % of TPT in gel).	94
Figure 3.14 HPLC Chromatograms of the conversion of lactone to carboxylate of free CPT and TPT with time elapsed, respectively.	96
Figure 3.15 Conversions of lactone to carboxylate of free CPT and TPT with HPLC (a. down-triangle: L % of free CPT in buffer; b. star: L % of free TPT in buffer). Polynomial fitting of data was performed.	97
Figure 3.16 CPT and TPT in Gel with HPLC Analysis, 0.015 % loading (a. cross: L % of TPT in gel; b. square: L % of CPT in gel)	98
Figure 3.17 Proposed mechanism of conversion of lactone ring to carboxylate form of CPT	100
Figure 3.18 ATR-FTIR spectra of powder CPT (A) and CPT loaded copolymer gel (B) in the range of 2000-4000 cm ⁻¹	101
Figure 3.19 ATR-FTIR spectra of powder CPT (A) and CPT loaded copolymer gel (B) in the range of 600-1800 cm ⁻¹	102

Figure 3.20 Confocal microscope image of drug loaded gel (A); optical microscope image of drug loaded gel (B)	103
Figure 3.21 TPT standard curve	104
Figure 3.22 CPT standard curve	104
Figure 3.23 CPT and TPT release curves	106
Figure 3.24 Effect of TPT released from PLLA-mPEG gels on the viability of LLC-1 and 4T1 cancer cells.	111
Figure 3.25 Effect of high doses of TPT on the viability of 4T1 cancer cells ...	112
Figure 3.26 Size of 4T1 breast tumours during 14-day follow-up (A and B) and survival percentages of the mice during the treatment period (C).	114
Figure 3.27 Representative photographs of two mice bearing 4T1 tumors.....	115
Figure 3.28 Structure of the poly(ethylene oxide)- <i>b</i> -poly(propylene oxide)- <i>b</i> -poly(ethylene oxide)- <i>g</i> -poly(acrylic acid), Pluronic-PAA, copolymers	118
Figure 3.29 The preparation of monomeric SA prepolymer	119
Figure 3.30 The preparation of acetylated PEG prepolymer.....	120
Figure 3.31 The preparation of PEG: PSA copolymer.....	120
Figure 3.32 Size distribution report by volume for CPT loaded nanoparticles..	121
Figure 3.33 Particle images of Confocal, SEM and Light Microscopes.....	122
Figure 3.34 Representative HPLC Chromatogram of CPT loaded polymeric microparticles	123
Figure 3.35 Synthesis of dipyrrole and SNSN	124
Figure 3.36 Cyclic voltammetry of 1,1'-bipyrrrole and SNSN.....	126
Figure 3.37 (a) Redox behavior of PSNSN film at different scan rates and (b) relationship of anodic and cathodic current peaks as a function of scan rate in 0.1 M TBAP/DCM.	127
Figure 3.38 FT-IR spectra of SNSN and PSNSN (a) between 4000 cm ⁻¹ and 600 cm ⁻¹ and (b) between 900 cm ⁻¹ and 600 cm ⁻¹	129
Figure 3.39 Polymerization of SNSN.....	130

Figure 3.40 The changes in the electronic absorption spectra of 3.0×10^{-2} M of SNSN in 0.1 M TBAP/DCM during in situ electrolysis at 1.1 V.	131
Figure 3.41 Electronic absorption spectra of PSNSN in 0.1 M TBAP/DCM at various applied potentials between 0.0 V and 1.1 V.	132
Figure 3.42 Optical transmittance changes for PSNSN at 444 nm, 661 nm and 1000 nm.	134
Figure 3.43 Emission spectra of SNSN (excited at 350 nm) and PSNSN (excited at 440 nm) in DMF.	135
Figure 3.44 Design of electrochemical reactor.	136
Figure 3.45 Synthesis of Mediator.	137
Figure 3.46 Synthesis of NAD- SNS Complex.	138
Figure 3.47 Synthesis of the compound 43	139
Figure 3.48 Electropolymerization of SNS-ethylene diamine 35 (red) and monomer free medium (blue).	139
Figure 3.49 Electropolymerization of SNS-EA-Bipy.	140
Figure 3.50 Electropolymerization of SNS-EA-Bipy-Rh Complex.	141
Figure 3.51 Electropolymerization of pyrrole (A) and copolymer of SNS-EA-Bipy Rh Complex.	142
Figure 3.52 Copolymer film of SNS-EA-Bipy Rh complex 39 before (A) and after (B) the addition of NAD.	143
Figure 3.53 Electropolymerization of SNS-EA-PBA (A-red) and its copolymer with EDOT (B-blue).	144
Figure 3.54 Film stability of SNS-EA-PBA-EDOT in 0.1 M TBAP in DCM (A) and 0.1 M LiClO ₄ in water (B).	145
Figure 3.55 Electropolymerization of SNS-EA-PBA-Thiophene.	145
Figure 3.56 Electropolymerization of pyrrole (A) and copolymer of SNS-EA-PBA-Pyrrole (B).	146

Figure 3.57 Film stability of SNS-EA-PBA- pyrrole in 0.1 M LiClO ₄ in water before (A) and after (B) NAD immobilization; (C) structure of immobilization of NAD to SNS-EA-PBA-Pyrrole	147
Figure 3.58 1-(3-(2-(2-(3-(1H-pyrrol-1-yl)propoxy)ethoxy)ethoxy)propyl)-1H-pyrrole.....	148
Figure 3.59 Cyclic voltammograms of 3.0x10 ⁻² M sample I in 0.1 M TBAClO ₄ /acetonitrile solution (a) between 0.0 V and 2.0 V and (b) repetitive cycling between 0.0 V and 1.1 V at a 100 mV/s scan rate.	149
Figure 3.60 (a) Scan rate dependence of PI film (100 mC/cm ²) on a platin disk electrode in 0.1 M TBAClO ₄ in ACN solution at various scan rates between 20 mV/s and 140 mV/s. (b) Dependence of anodic (<i>i_{ac}</i>) and cathodic (<i>i_{cc}</i>) current peaks on the scan rate for neutral and oxidized PI	150
Figure 3.61 Electrochemical polymerization of monomer I	151
Figure 3.62 (a) <i>In-situ</i> absorption spectra for PI (50 mC/cm ² on ITO) was enrolled at 0.1 M TBAClO ₄ in ACN at several applied potentials (vs. Ag-wire) and (b) Optical responses of PI (50 mC/cm ² on ITO) at 315 nm, 484 nm, and 1000 nm as a function of applied potentials in 0.1 M TBAClO ₄ /acetonitrile (vs. Ag-wire).	153
Figure 3.63 TGA thermogram of PI (polymerization charge of 5 C/cm ²).....	154
Figure 3.64 Voltammetric responses of the PI (100 mC/cm ²) with respect to an increasing Na ⁺ ion concentration in a 0.1 M TBAClO ₄ /acetonitrile solution at a scan rate of 50 mV/s.	157
Figure 3.65 (a) Cyclic voltammograms recorded for PI (100 mC/cm ²) after 30 s conditioning at -0.5 V in various concentrations of AgBF ₄ in a 0.1 M TBAClO ₄ /acetonitrile solution at a scan rate of 50 mV/s and (b) the amount of the charge of accumulated silver calculated by the integration of the anodic peak.	158
Figure 3.66 SEM pictures obtained (a) PI without Ag ⁺ ions, (b) PI after the applied -0.5 V for 5 minutes in a 0.1 M TBAClO ₄ /acetonitrile solution containing	

1.0x10 ⁻³ M AgBF ₄ . (c) PI after the applied -1.0 V for 5 min in a 0.1 M TBAClO ₄ /acetonitrile solution containing 1.0x 10 ⁻³ M AgBF ₄	159
Figure 4.1 Stability of CPT and TPT in gels (0.015 %) versus rapid hydrolysis in physiological environment	161
Figure 4.2 1,1'-bipyrrole	164
Figure 4.3 1-(1H-pyrrol-1-yl)-2,5 di(thiophen-2-yl)-1H-pyrrole (SNSN)	164
Figure A.1. First measurement of three independent data for free CPT in tris buffer at pH=7.4 at t=0 min	180
Figure A.2. First measurement of three independent data for free CPT in tris buffer at pH=7.4 at t=20 min	181
Figure A.3. First measurement of three independent data for free CPT in tris buffer at pH=7.4 at t=39 min	181
Figure A.4. First measurement of three independent data for free CPT in tris buffer at pH=7.4 at t=58 min	182
Figure A.5. First measurement of three independent data for free CPT in tris buffer at pH=7.4 at t=78 min	182
Figure A.6. First measurement of three independent data for free CPT in tris buffer at pH=7.4 at t=97 min	183
Figure A.7. First measurement of three independent data for free CPT in tris buffer at pH=7.4 at t=117 min	183
Figure A.8. First measurement of three independent data for free CPT in tris buffer at pH=7.4 at t=136 min	184
Figure A.9. First measurement of three independent data for free CPT in tris buffer at pH=7.4 at t=155 min	184
Figure A.10. First measurement of three independent data for free CPT in tris buffer at pH=7.4 at t=175 min	185
Figure A.11. First measurement of three independent data for free CPT in tris buffer at pH=7.4 at t= 194 min	185

Figure A.12. First measurement of three independent data for free CPT in tris buffer at pH=7.4 at t=213 min.....	186
Figure A.13. First measurement of three independent data for free CPT in tris buffer at pH=7.4 at t=232 min.....	186
Figure A.14. First measurement of three independent data for free CPT in tris buffer at pH=7.4 at t=252 min.....	187
Figure A.15. First measurement of three independent data for free CPT in tris buffer at pH=7.4 at t=271 min.....	187
Figure A.16. First measurement of three independent data for free CPT in tris buffer at pH=7.4 at t=290 min.....	188
Figure A.17. First measurement of three independent data for free CPT in tris buffer at pH=7.4 at t=310 min.....	188
Figure A.18. First measurement of three independent data for free TPT in tris buffer at pH=7.4 at t=0 min.....	189
Figure A.19. First measurement of three independent data for free TPT in tris buffer at pH=7.4 at t=20 min.....	189
Figure A.20. First measurement of three independent data for free TPT in tris buffer at pH=7.4 at t=39 min.....	190
Figure A.21. First measurement of three independent data for free TPT in tris buffer at pH=7.4 at t=58 min.....	190
Figure A.22. First measurement of three independent data for free TPT in tris buffer at pH=7.4 at t=78 min.....	191
Figure A.23. First measurement of three independent data for free TPT in tris buffer at pH=7.4 at t=97 min.....	191
Figure A.24. First measurement of three independent data for free TPT in tris buffer at pH=7.4 at t=117 min.....	192
Figure A.25. First measurement of three independent data for free TPT in tris buffer at pH=7.4 at t=136 min.....	192

Figure A.26. First measurement of three independent data for free TPT in tris buffer at pH=7.4 at t=155 min.....	193
Figure A.27. First measurement of three independent data for free TPT in tris buffer at pH=7.4 at t=175 min.....	193
Figure A.28. First measurement of three independent data for free TPT in tris buffer at pH=7.4 at t=194 min.....	194
Figure A.29. First measurement of three independent data for free TPT in tris buffer at pH=7.4 at t=213 min.....	194
Figure A.30. First measurement of three independent data for free TPT in tris buffer at pH=7.4 at t=232 min.....	195
Figure A.31. First measurement of three independent data for free TPT in tris buffer at pH=7.4 at t=252 min.....	195
Figure A.32. First measurement of three independent data for free TPT in tris buffer at pH=7.4 at t=271 min.....	196
Figure A.33. First measurement of three independent data for free TPT in tris buffer at pH=7.4 at t=290 min.....	196
Figure A.34. First measurement of three independent data for free TPT in tris buffer at pH=7.4 at t=310 min.....	197
Figure A.35. First measurement of three independent data for CPT in gel at 0.015% loading at t= 0 min	197
Figure A.36. First measurement of three independent data for CPT in gel at 0.015% loading at t= 45 min	198
Figure A.37. First measurement of three independent data for CPT in gel at 0.015% loading at t= 90 min	198
Figure A.38. First measurement of three independent data for CPT in gel at 0.015% loading at t= 135 min	199
Figure A.39. First measurement of three independent data for CPT in gel at 0.015% loading at t= 180 min	199

Figure A.40. First measurement of three independent data for CPT in gel at 0.015% loading at t= 225 min	200
Figure A.41. First measurement of three independent data for CPT in gel at 0.015% loading at t= 270 min	200
Figure A.42. First measurement of three independent data for CPT in gel at 0.015% loading at t= 315 min	201
Figure A.43. First measurement of three independent data for TPT in gel at 0.015% loading at t= 0 min	201
Figure A.44. First measurement of three independent data for TPT in gel at 0.015% loading at t= 45 min	202
Figure A.45. First measurement of three independent data for TPT in gel at 0.015% loading at t= 90 min	202
Figure A.46. First measurement of three independent data for TPT in gel at 0.015% loading at t= 135 min	203
Figure A.47. First measurement of three independent data for TPT in gel at 0.015% loading at t= 180 min	203
Figure A.48. First measurement of three independent data for TPT in gel at 0.015% loading at t= 225 min	204
Figure A.49. First measurement of three independent data for TPT in gel at 0.015% loading at t= 270 min	204
Figure A.50. First measurement of three independent data for TPT in gel at 0.015% loading at t= 315 min	205
Figure A.51. First measurement of three independent data for CPT in gel at 1.0% loading (representative example), t= 120 min.....	205
Figure A.52. First measurement of three independent data for CPT in gel at 10.0% loading (representative example), t= 120 min.....	206
Figure A.53. First measurement of three independent data for TPT in gel at 1.0% loading (representative example), t= 120 min.....	206

Figure A.54. First measurement of three independent data for TPT in gel at 10.0% loading (representative example), t= 120 min.....	207
Figure B.1. ¹ H spectrum of polymer 19.....	208
Figure B.2. ¹³ C spectrum of polymer 19.....	209
Figure B.3. ¹ H spectrum of polymer 20.....	209
Figure B.4. ¹ H spectrum of polymer 21.....	210
Figure B.5. ¹ H spectrum of polymer 22.....	210
Figure B.6. ¹ H spectrum of polymer 23.....	211
Figure B.7. ¹ H spectrum of polymer 24.....	211
Figure B.8. ¹ H spectrum of polymer 25.....	212
Figure B.9. ¹ H spectrum of polymer 26.....	212
Figure B.10. ¹ H spectrum of polymer 27.....	213
Figure B.11. ¹ H spectrum of SNSN 18.....	213
Figure B.12. ¹³ C spectrum of SNSN 18.....	214
Figure B.13. ¹ H spectrum of the compound 38.....	214
Figure B.14. ¹³ C spectrum of the compound 38.....	215
Figure B.15. ¹ H spectrum of the compound 39.....	215
Figure B.16. ¹³ C spectrum of the compound 39.....	216
Figure B.17. ¹ H spectrum of the compound 41.....	216
Figure B.18. ¹ H spectrum of the compound 43.....	217
Figure B.19. ¹ H spectrum of the compound 47.....	217

ABBREVIATIONS

CPT	Camptothecin
TPT	Topotecan
FDA	Food and Drug Administration
TOPO-I	Topoisomerase I enzyme
FITC	Fluorescein Isothiocyanate
d-DMSO	Deuterated-dimethylsulfoxide
NAD ⁺	Nicotinamide Adenine Dinucleotide
MTT	3-(4,5-Dimethylthiazol-2-yl)-2,5-diphenyltetrazolium bromide
BCNU	Bis-chloroethylnitrosourea
TEAA	Triethylamine-acetic acid
BBB	Blood-Brain Barrier
MWD	Molecular Weight Distribution
SEM	Scanning Electron Microscope
FL	Fluorescence Spectroscopy
PLLA	Poly-L-Lactic Acid
PLLA-mPEG	Poly-L-Lactic Acid Methoxy Polyethyleneglycol
ATR-FTIR	Attenuated Total Reflection FTIR Spectroscopy

CHAPTER 1

INTRODUCTION

1.1. Thermosensitive Biodegradable mPEG-PLLA Block Copolymers: Syntheses, Characterizations and Applications in Drug Delivery Systems

Drug delivery can be simply expressed as the delivery of a pharmaceutical substance to humans or animals. Drug delivery systems have now reached at the most advance stage of a multi-billion dollar pharmaceutical industry with versatile applications of many research area of medicine. Also, it will undoubtedly continue to be one of important research areas in future life. One of the aims of controlled drug delivery is to keep the drugs at proper therapeutic level for a specific duration of time for maximum therapeutic benefits, as indicated controlled release profile in Figure 1.1. On the other hand, for conventional methods lower doses than therapeutic level show no effective response while higher doses cause toxicity. Immediate high release of a single dose of medications with using conventional methods (i.e. tablets) may exceed maximum level in the beginning, and then decrease in drug level reaches to minimum ineffective level. Also, multiple doses of drug are much required for the continuation of therapy via conventional ways [1].

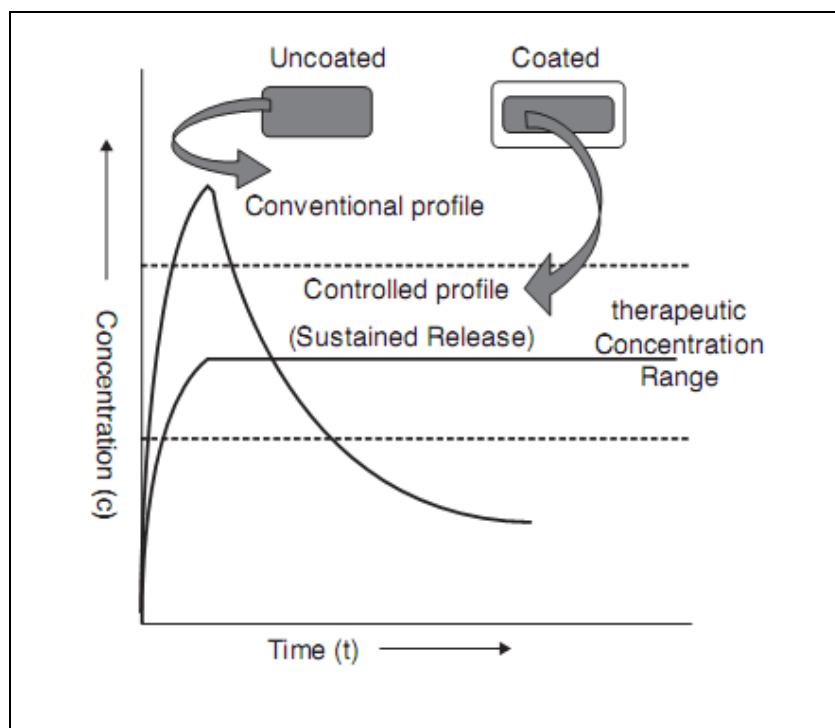


Figure 1.1 Comparison of conventional and controlled-release profiles

Local targeted drug delivery has become very attractive over last decades since medicine is delivered to a patient in a manner that the concentration of the medicine raises at the target location without causing systemic toxicity. The medicine generally can be taken via oral ingestion or intravascular injection in traditional drug delivery systems so that it enters the systemic blood circulation. On the other hand, local targeted delivery aims to concentrate medicine in infected tissues while keeping healthy tissues safe in body. This leads to more efficient therapy and less side effects.

1.1.1. Thermosensitive Biodegradable Polymers

Thermosensitive biodegradable polymers are one of most preferred polymers in the biomedical field in last 10-15 years because they can easily be subjected to a

physical change with an external heat due to their property of thermosensitivity, and no effort is needed to remove them from the body due to their property of degradability. PEG based copolymers of poly(lactide), poly(lactic-co-glycolic acid) (PLGA), poly(sebacic acid), polypeptides and polyphosphazenes are some of many examples of the thermosensitive biodegradable polymers. Syntheses, characterizations and interesting properties of those polymers together with their copolymers with PEG are described in detail below.

1.1.1.1. PLLA Homopolymer and PLLA-mPEG Copolymers

Poly lactide homopolymer is the polymer of the cyclic dimer of lactic acid, which exists as two optical isomers, D and L. L-lactide is the naturally occurring isomer, and DL-lactide is the synthetic blend of D-lactide and L-lactide. Structures of L- and D- monomers are shown in Figure 1.2.

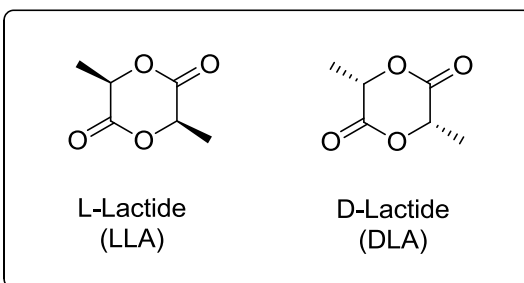


Figure 1.2 Structures of L- and D- Lactides

PLLA homopolymer is a semicrystalline thermoplastic showing high-tensile strength and low elongation and can be used for load-bearing purposes like sutures, dental and drug delivery systems and orthopedic fixation. PLLA roughly has a 37 % crystalline state having a melting around 175-178 °C and a T_g around 60-65 °C [2]. PLLA exhibits good biocompatibility, very good processability and biodegradability mainly by hydrolysis at the ester links and has a degradation

time of the order of 6 months to 2 years, which compares to 500-1000 years for conventional commercial polymers [2,3]. PLLA hydrolyzes to lactic acid which is a normal product of muscular contraction in humans and animals. The lactic acid is then further metabolized through the tricarboxylic acid cycle and then degraded carbon dioxide and water [2].

PLLA and PDLA syntheses take place with two methods: polycondensation of lactic acids and ring opening polymerization of lactide monomer (Figure 1.3).

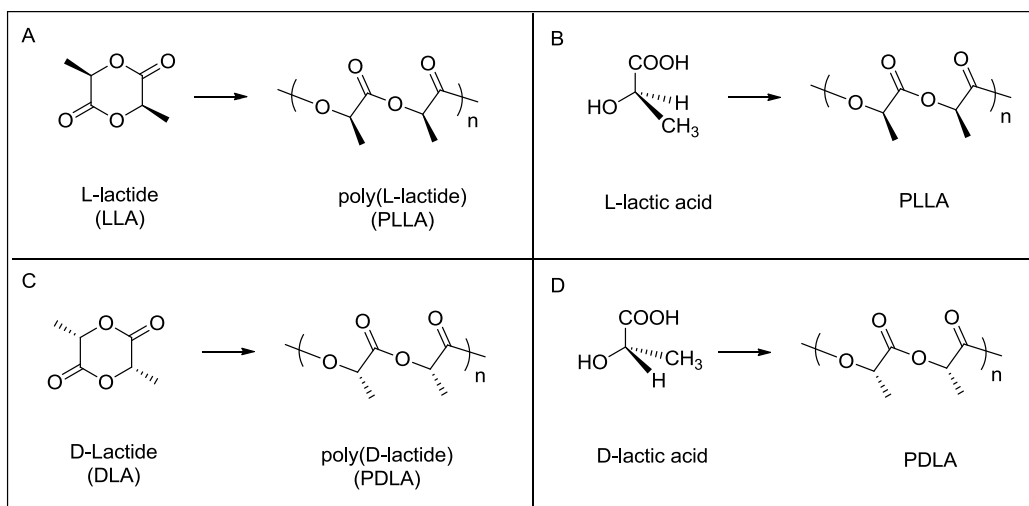


Figure 1.3 Syntheses of PLLA (A and B) and PDLA (C and D).

Many polymerization mechanisms were reported so that a proposed mechanism was called a cationic [4], the other was termed as a complexation mechanism or second order insertion mechanism [5].

The most preferred catalyst for polymerization of L-lactide is stannous 2-ethyl-hexanoate ($\text{Sn}(\text{Oct})_2$) due to almost complete conversions and low toxicity compared to other heavy metal salts. Mechanism of polylactide in the presence of

$\text{Sn}(\text{Oct})_2$ is shown in Figure 1.4. The polymerization mechanism of several tin compounds was also studied [6, 7].

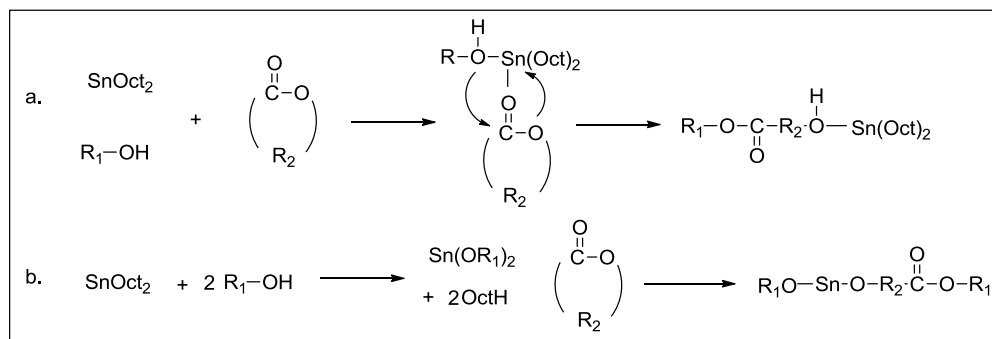


Figure 1.4 Coordination-insertion mechanism of L-lactide polymerization

The surface modification is important to increase the biocompatibility of any polymeric implant because biological interactions between the host tissue and the implant mainly take place at the surface of the implant. Several PLLA block copolymers were synthesized by using biocompatible polymers in order to increase the hydrophilicity of the relatively hydrophobic PLLA and simultaneously decrease its crystallinity to achieve rapid biodegradation. Among these biocompatible polymers, methoxy polyethylene glycol (mPEG) is definitely the most commonly used for this purpose due to its inherent properties of water and organic solvent solubility, high flexibility, strong hydration, non-toxicity, absence of antigenicity and weak immunogenicity, which are essential properties to formulate the drugs [8]. mPEG is effective to prevent the adsorption of proteins and adhesion cells possibly by their extreme hydrophilic character, i.e. their high molecular mobility in aqueous media. It also has approval from the Food and Drug Administration (FDA). These two polymers have complementary functions: PLLA is a rather hydrophobic polymer having good mechanical properties and biodegradable, whereas mPEG is hydrophilic and not biodegradable due to the non-degradability of etheric linkages. The

copolymerization of mPEG with LLA monomer results in obtaining new materials with original physical, chemical, and biological properties adaptable to many uses [9-15].

Aqueous solutions of diblock PLA-PEG copolymers form micelles at low concentrations where hydrophobic interactions due to the packing of the hydrophobic PLA blocks control the micelle shape and size. Usually, spherical micelles form in aqueous media. The hydrophobic PLA blocks form the core of the micelle while the hydrophilic PEG blocks build the outer shell (Figure 1.5). The micelles associate at high copolymer concentration levels forming a gel at a lower temperature and become a sol at a higher temperature. The increase in the PLA block length increases the aggregation tendency of the block copolymer in aqueous phase resulting in a steep sol-gel transition curve. These block copolymers can be used as matrices for sustained release drug delivery systems [16-27].

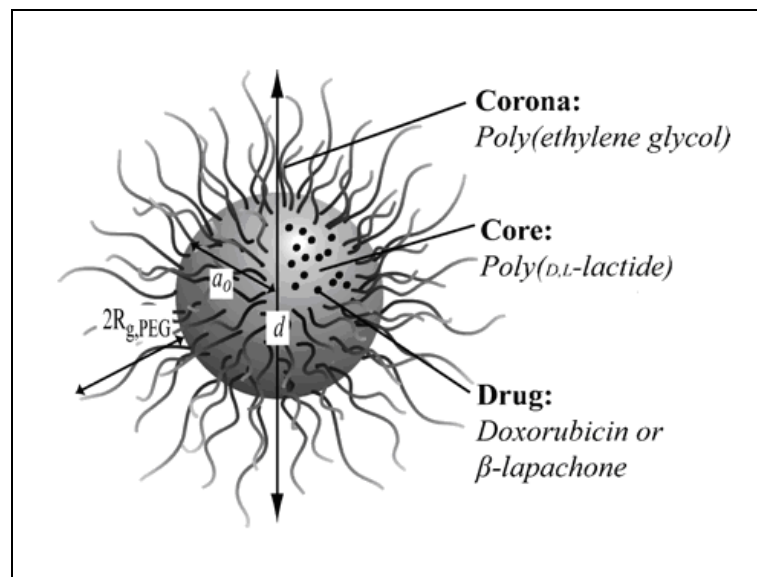


Figure 1.5 DOX or β -lap loaded PEG(5k)-b-PLA(5k) diblock copolymer micelle. d , hydrodynamic diameter of the micelle; $2R_{g,PEG}$, thickness of corona [20].

The hydrophobic micelle core serves as a microenvironment for incorporating hydrophobic drugs such as anti-cancer drugs, while the hydrophilic outer shell serves as a stabilizing interface between the hydrophobic drug and the external medium [19-22]. These particles were less than 40 nm in size and were biodegradable to nontoxic, biocompatible degradation products within the body. The sol-gel transition temperature is adjustable by changing the length of each component. Aqueous solutions of these copolymers are sols at around 42-45° C, and they are loaded with bioactive molecules, and after the injection of this sol and consecutive fast cooling to body temperature, the loaded copolymer makes a gel that could serve as a sustained-release matrix for medicines [23].

The size, drug loading capacity, stability, release kinetics and biodistribution of micelles are affected by the molecular weight of the blocks, and the chemical structure of the diblock copolymer [24-27]. The effect of the length of the PLLA and PEG blocks on the critical micelle concentration (CMC) values of diblock PLLA-PEG copolymers in aqueous and salt solutions were examined in detail and it was found that the role of the PLLA block is more significant than that of the PEG block in micelle formation [16]. The addition of NaCl can decrease the CMC values of diblock copolymers containing short PLLA blocks [28].

PLLA-PEG diblock copolymers together with PDLA (polymeric enantiomer of PLLA)-PEG diblock copolymers were used to prepare the bioresorbable hydrogels in which stereo-complexation takes place between PLLA and PDLA blocks, which is important for sustained delivery of bioactive molecules [29]. Triblock (PLLA/PEO/PLLA) copolymers were also synthesized and their hydrolytic degradation was investigated [30-32].

Crystallization behavior and biodegradability of PLLA-PEG diblock copolymers were also examined in detail. Diblock copolymers degrade much faster than

PLLA homopolymer of the same molecular weight [33]. It was found that the crystallization tendency of one block influences the crystalline structure of the other block in a PLLA-PEG copolymer chain. In addition, these copolymers can form spherulites with banded textures. Single crystals with abundance of screw dislocations were also observed [34].

Morphological investigation of PLLA-PEG nanoparticles showed that core-shell nanoparticles self-organize on the surface with a novel process. The crystallization-induced morphological changes of diblock copolymer were examined from sphere to band via disk. This process is useful to understand the mechanism of phase separation and segment crystallization of the block copolymers [35]. A review has been published on the macromolecular organization of PLLA-PEG diblock copolymers, which covers dynamic macromolecular organization of block copolymer nanoparticles into bioinspired nano-architectures [36].

Heterobifunctional PLLA-PEG diblock copolymers containing an acetal terminal group at the PEG chain end were reported [37-39]. Transformation of acetal into aldehyde group on the micelle surface was succeeded. No change in the micelle size and shape was observed before and after the conversion of the acetal end groups to aldehyde groups on the micelle. This functionalized micelle, in particular the one carrying terminal groups, is expected to have a wide utility not only in biomedical applications (e.g. surface modification through the coupling of bioactive substances) but also for the construction of the supramolecular architecture [37-39].

The surface modification of PLLA is applied with Langmuir Blodgett (LB) technique to prepare well organized stable brush structures of amphiphilic PLLA-PEG diblock copolymers [40]. In that study, the dynamic contact angles were

measured to examine the stability of the LB-films transferred on the PLLA support and changes in the surface properties on incubation of surfaces in water. Diblock copolymer of PLLA-PEG on the macro-porous PLLA scaffolds was also examined by thermal induced phase separation [41]. It seems to be a promising method for controlling the pore size of open, regular and well-interconnected macroporous scaffolds for the growth and culture of cells.

1.1.1.2. PLGA Homopolymer and PLGA-PEG Copolymers

A copolymerization of lactide and glycolide monomers leads to the synthesis of poly(D,L-lactic acid-co-glycolic acid) (PLGA) in the presence of catalysts like tin(II) 2-ethylhexanoate, tin(II) alkoxides, or aluminum isopropoxide (Figure 1.6). During copolymerization, ester linkages are obtained in the production of linear aliphatic polyester.

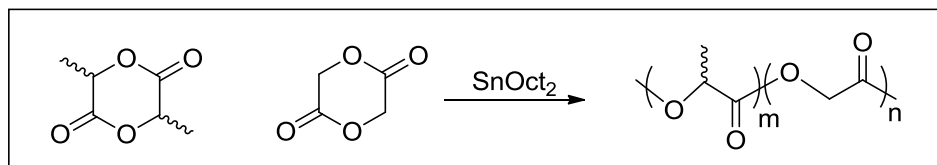


Figure 1.6 Synthesis of PLGA from lactide and glycolide monomers

Poly(L-lactide-*co*-glycolide) gradually degrades into lactic and glycolic acid in acidic medium due to its great biocompatible and biodegradable properties (Figure 1.7). These hydrolysis products can be metabolized via the tricarboxylic acid (TCA) with the formation of carbon dioxide and water [42].

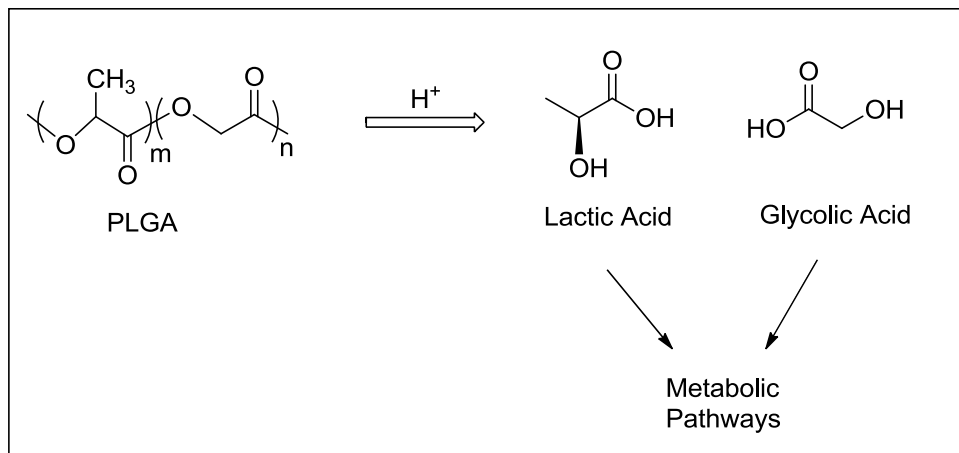


Figure 1.7 Hydrolysis of PLGA

Poly(glycolide) is a highly crystalline homopolymer and the most hydrophilic among all of them. The melting point of poly(glycolide) is much higher than poly(L-lactide) (224°C to 226°C vs. 175-178 °C), and the degradation rate of poly(glycolide) is much higher than that of poly(L-lactide) (Table 1.1). Also, different ratios of lactide (LA) and glycolide (GA) in random PLGA copolymers cause different degradation rates from weeks to months for the different application areas. PLGA copolymer consisting of 50% glycolide and 50% dl-lactide degrades faster than their homopolymers [43-45].

Table 1.1 Properties of synthetic biodegradable polymers

Polymers	Structure	Mw/kD	Degradation Rate
Poly(glycolide)	Crystalline 224-230 °C	–	100 % in 2–3 months
Poly(glycolic acid-co-L-lactic acid)	Amorphous State	40–100	100 % in 50–100 days
Poly(L-lactide)	Semicrystalline 175-178 °C	100–300	50 % in 1–2 years

Thermosensitive biodegradable PLGA-PEG block copolymers can be produced by using hydrophilic, biocompatible poly(ethylene glycol) (PEG) with biodegradable and biocompatible PLGA. Appropriate adjustment of each block leads to different thermosensitive properties. Syntheses of PLGA-PEG block copolymers are performed by ring-opening polymerization of cyclic lactide and glycolide with PEG in the presence and absence of the catalyst. Stannous octoate is widely used as catalyst. The terminal hydroxyl groups of dihydroxy PEG or monomethoxy PEG initiate the block copolymerization, leading to A-B-A or A-B type block copolymers, respectively (Figure 1.8) [46].

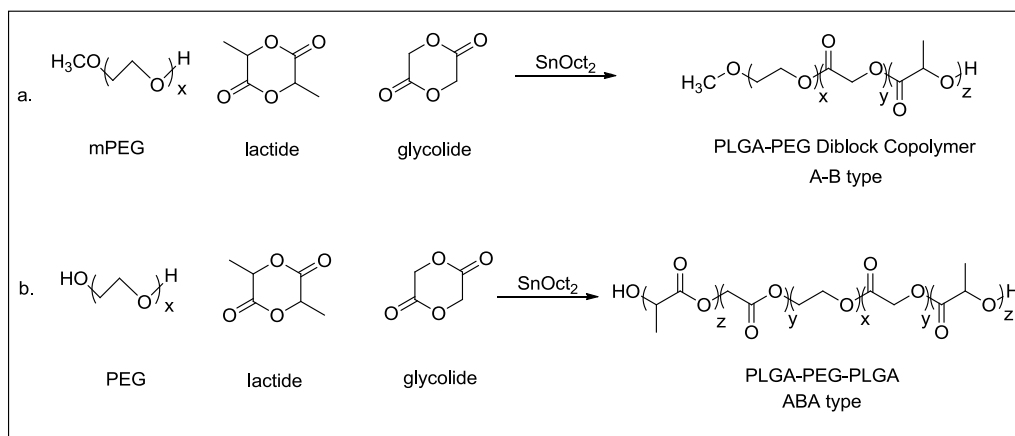


Figure 1.8 The synthetic route of the PLGA–PEG diblock (a) and PLGA–PEG–PLGA triblock copolymers (b).

1.1.1.3. Polyphosphazenes

Polyphosphazenes, also regarded as ‘hybrid inorganic–organic polymers’, contain inorganic elements in the backbone and organic substitutes in side-groups [47] (Figure 1.9). Two organic side groups attached to the phosphorus atom play important role to change the characteristics of the polymer. For example, biodegradable polyphosphazenes can be produced by the substitution of

hydrolytically sensitive side groups such as glucosyl, glycerol, imadazolyl and lactide, glycolide, and amino acid esters [48-52].

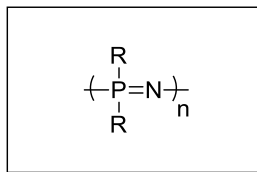


Figure 1.9 Polyphosphazenes

The phosphorus–nitrogen backbone can be sensitized by hydrolytically sensitive side groups, and degradation occurs with the formation of various by-products in a few hours to years based on the side groups (Figure 1.10) [47, 53, 54].

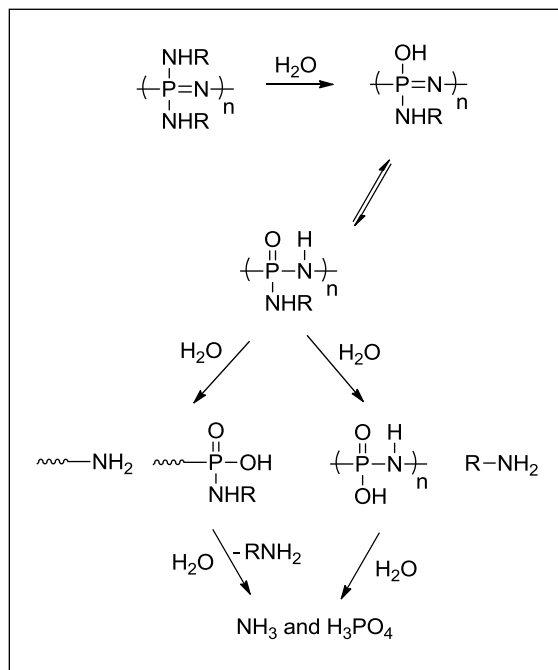


Figure 1.10 Degradation routes of amino acid ester–substituted polyphosphazenes. The formation of body-friendly degradation products (amino acids and ammonium phosphate buffer) was obtained.

Figure 1.11 basically describes ring-opening polymerization followed by macromolecular substitution for the synthesis of poly(organo phosphazene)s. This is the earliest and most widely preferred pathway to obtain poly(organo phosphazene)s [55–65]. The macromolecular intermediate poly(dichloro phosphazene) **2** are easily synthesized from commercially available cyclic trimer hexachlorocyclo triphosphazene **1** and heat at 220 to 250 °C with or without an appropriate initiator. Then, nucleophilic attack to chlorine atoms of the intermediate results in the substitution of organic side groups with the use of alkoxide, amino or aryloxy reagents, as indicated types **3**, **4** and **5**.

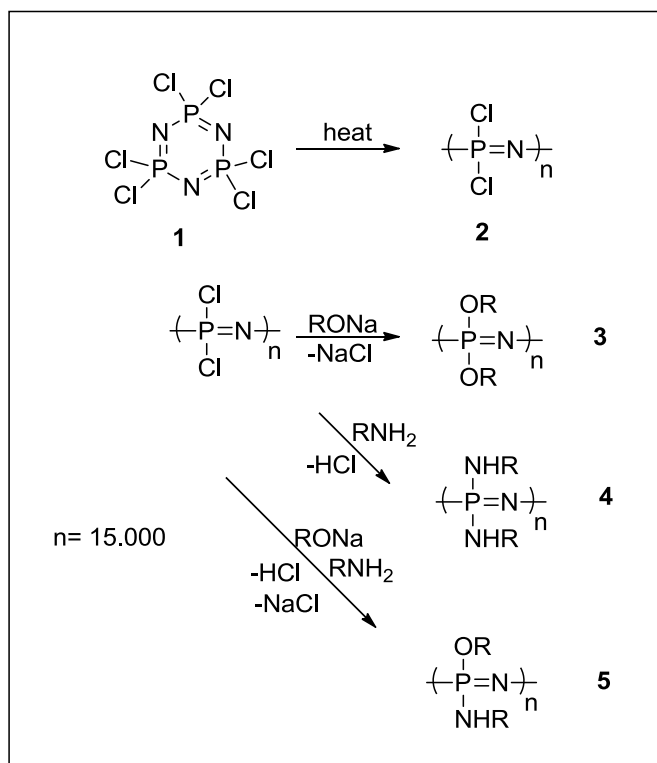


Figure 1.11 Synthesis of poly(organo phosphazene)s

Thermosensitive biodegradable amphiphilic polyphosphazenes can be synthesized with substitution of thermosensitive polymer chains to

polyphosphazene backbones. Methoxy-poly(ethylene glycol) (mPEG) and amino acid esters substituted poly (organophosphazenes) have been synthesized and characterized (Figure 1.12), and their lower critical solution temperature (LCST) was found [66]. Polymer **7** was first synthesized from poly(dichlorophosphazene) **6** and the sodium salt of mPEG in room temperature in THF at 5 hrs. Then, polymer **8** was obtained from the addition of excess amount of amino acid esters to polymer **7** at 50 °C in the presence of triethyl amine in 2-3 days. The mole ratio and variation of the amino acid esters and the mPEG lead to the synthesis of many different copolymers. Then, they were all characterized by (¹H, ¹³C, ³¹P) NMR spectroscopies, UV, DSC, GPC, and elemental analysis.

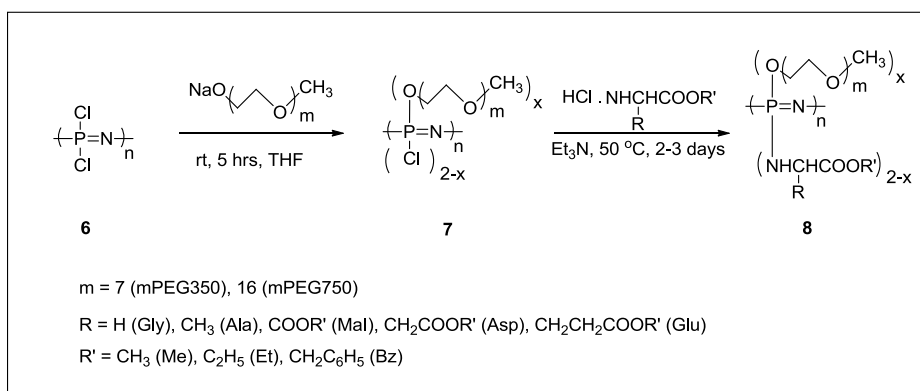


Figure 1.12 Synthesis of poly(organophosphazenes) bearing mPEG and amino acid esters

1.1.1.4. Poly(sebacic acid) (PSA) Homopolymer and PSA-PEG Copolymers

Polyanhydrides such as poly(sebacic acid) (PSA), poly(adipic acid) (PAA) and poly(dodecanoic anhydride) have properties of biocompatibility due basically to the hydrolytic instable anhydride linkages and biodegradability through surface erosion, and they have growing remarkable interest in the applications of sustained drug delivery systems [67-69]. Poly(sebacic acid)s can be synthesized by melt-polycondensation method in vacuum just after obtaining their

prepolymers via refluxing sebacic acid and acetic anhydride (Figure 1.13) [69,70].

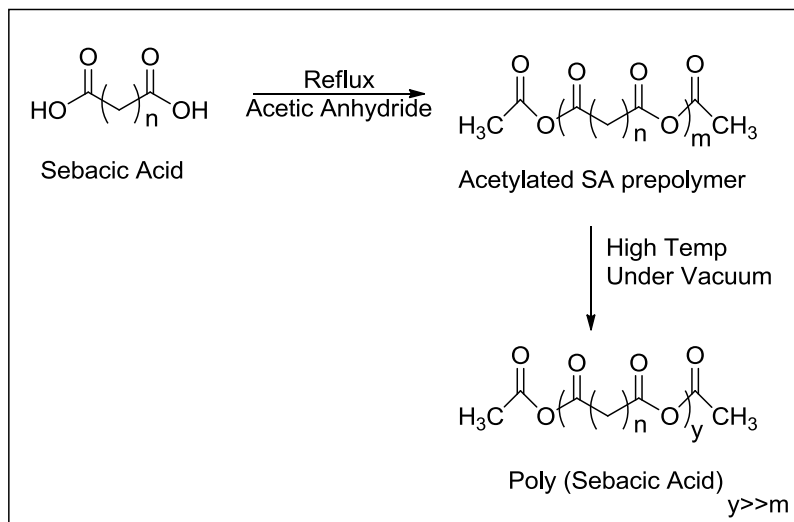


Figure 1.13 Synthesis of poly(sebacic acid)

Biodegradable poly(sebacic acid)s-PEG copolymers can be synthesized with melt polymerization after acetylations of sebacic acid prepolymer and PEG prepolymer are performed, as indicated in Figure 1.14 [71-72]. Also, the reaction of sebacyl chloride with PEG yields a thermosensitive PEG-SA copolymer. Variation in molecular weight and composition leads to change in sol-gel transition temperature [73] (Figure 1.15). Additionally, the release of model drug, FITC-dextran, is tested from the gel over 24 h [73]. For the drug delivery applications, nanoparticles of PEG-PSA copolymers are tested in human cervicovaginal mucus, and they show rapid penetration through mucosal barrier [74], and PEG-PSA particles show improved efficacy of local etoposide delivery against small cell lung cancer in vivo [75].

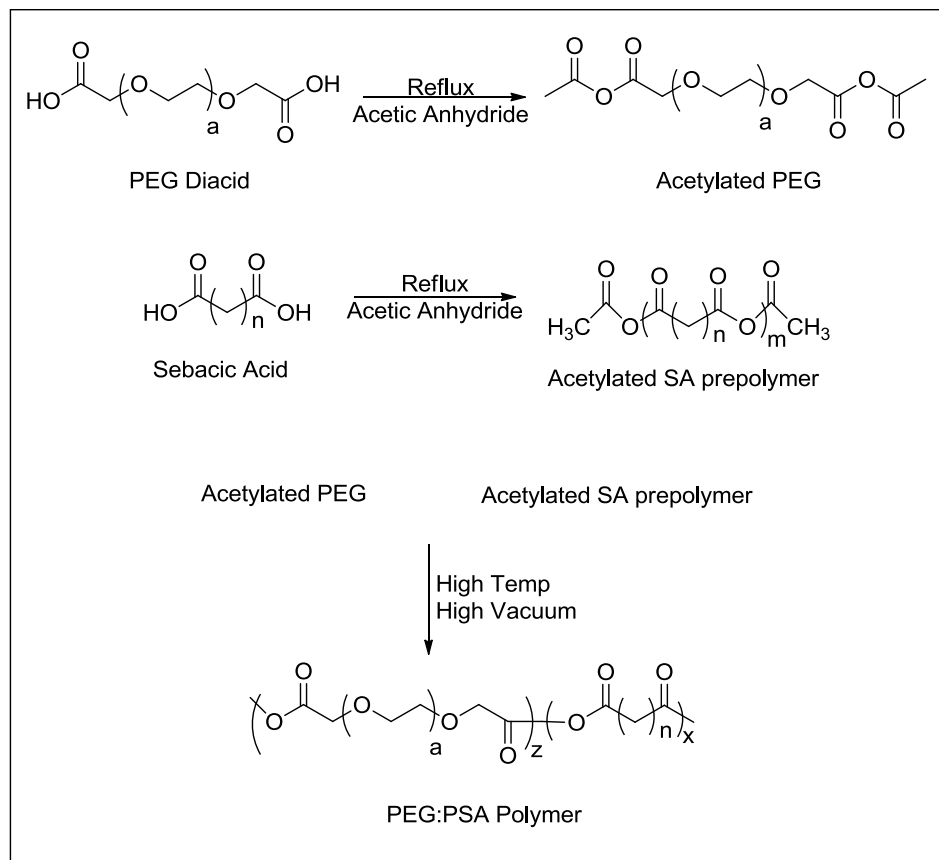


Figure 1.14 Synthesis of PEG:PSA copolymer

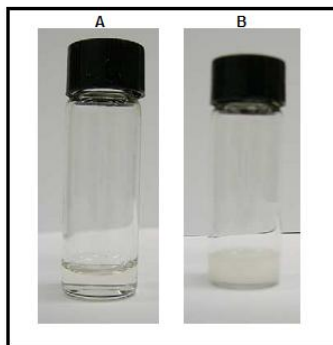


Figure 1.15 Transformation from the aqueous solution into gel for PEG–SA gel
 (a) PEG–SA solution at rt, (b) the gel at 37 °C.

1.1.1.5. Poly(peptides)

Biocompatibility and biodegradability properties of polypeptides and poly(amino acids) enhance their usage as biomedical materials. Artificial multidomain proteins produced by recombinant DNA methods in Fig 1.16-A can display reversible gelation in response to alterations in temperature or pH (Fig. 1.16-B). The triblock architecture, indicated in Fig. 1.16-A, contains relatively short “leucine zipper” end blocks and a water-soluble polyelectrolyte domain. The formation of coiled-coil aggregates of the terminal domains leads to gelation of the protein while the middle polyelectrolyte part keeps solvent in the network structure and hinders the formation of precipitates [76].

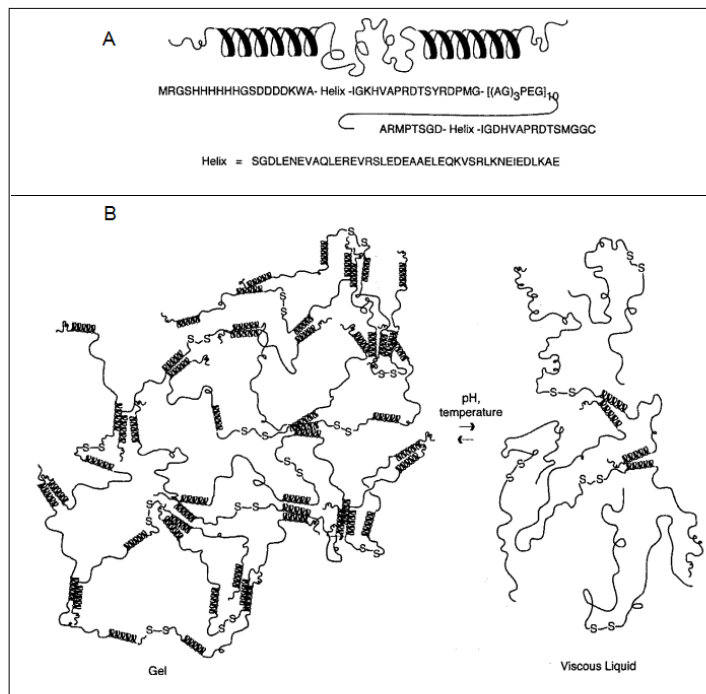


Figure 1.16 Amino acid sequences of the the proteins (A) and physical gel-sol change of monodisperse triblock copolymer (B). It has 230 amino acids (aa) with the Helix repeats (84 aa of all) and alanyl-glycine- rich repeats (90 aa of all). Single-letter abbreviations for the amino acid residues are as follows: A, Ala; C, Cys; D, Asp; E, Glu; F, Phe; G, Gly; H, His; I, Ile; K, Lys; L, Leu; M, Met; N, Asn; P, Pro; Q, Gln; R, Arg; S, Ser; T, Thr; V, Val; and W, Trp.

1.1.2. Application of Thermosensitive Polymers

Drug delivery, three dimensional cell culture, and cell therapy/tissue engineering can be regarded as biomedical applications of thermosensitive systems. Some representative examples are given for the applications of general and drug delivery systems, respectively.

1.1.2.1. General Applications

PEG-g-PLGA and PLGA-g-PEG copolymers (Figure 1.17-A) were tested for the studies of diabetic control and cartilage repair via insulin and chondrocyte cell deliveries, respectively. The control of blood glucose level was succeeded up to 16 days in diabetic rats with an injection of PLGA-g-PEG copolymer (Figure 1.17-B). Thermogelling PLGA-g-PEG was also applied for cartilage repair, and cartilage defect was remarkably repaired [77].

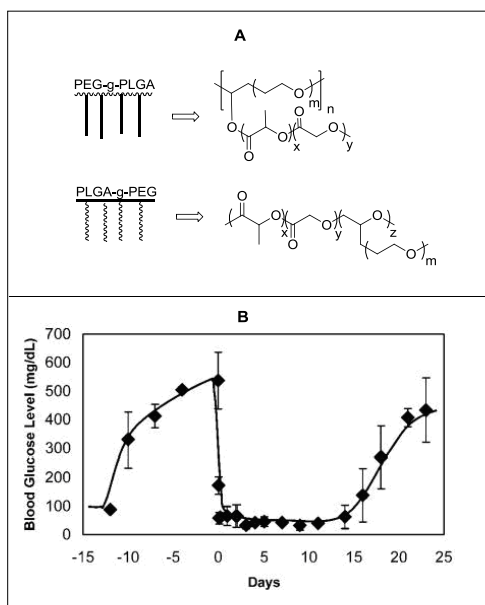


Figure 1.17 Structure of PEG-g-PLGA and PLGA-g-PEG copolymers (A) and in vivo efficacy in diabetic rats of PLGA-g-PEG depot systems (B)

PEG–PLGA–PEG triblock thermosensitive hydrogel was used as a wound dressing and scaffold for the regeneration new tissues via cell transplantation. Stem cells and then hydrogel onto upper part (MDSC + hydrogel) were applied to wound site. After transplantation, 30 % and 15% of the transplanted MDSCs (muscle-derived stem cells) were found to remain in the diabetic wound bed at days of 9th and 20th, respectively (Figure 1.18-A). The higher engraftment led to better wound healing as shown at Figure 1.18-B likely by keeping the cells at the wound site for more time [78].

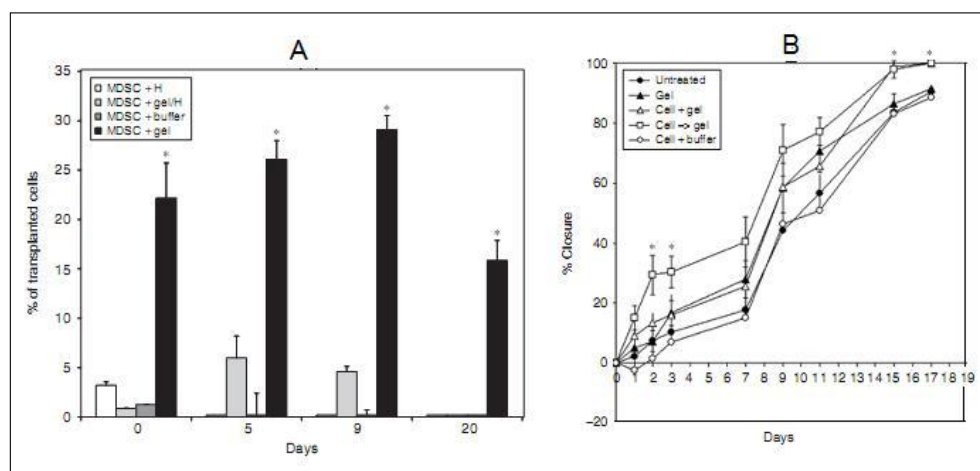


Figure 1.18 % of transplanted MDSCs at the wound site (A), wound closure analysis after mixing or covering the MDSCs with the PEG–PLGA–PEG hydrogel (B)

1.1.2.2. Applications in Drug Delivery Systems

In vivo applications of thermosensitive polymers in drug delivery have been extensively increased in last decade [79-83]. One of those polymers (OncoGel) has become commercially available, and it has been just started to be tested clinically.

OncoGel (ReGel/paclitaxel), clinically one of the most intensively studied systems, is a unique formulation composed of thermosensitive PLGA-PEG-PLGA gel and chemotherapeutic paclitaxel drug. It can be intratumorally injected into local solid tumors. Lower paclitaxel dosing in OncoGel (a single dose at 60 mg/kg level) rather than the maximum tolerated systemic dose of the commercial paclitaxel (multiple 5 doses with 20 mg/kg per day; total dose: 100 mg/kg) exhibited better anti-tumor efficacy (Figure 1.19-A and B) and lower drug-related adverse effects. Higher in vivo survival probability may probably be related with the continuation of slow release of paclitaxel from OncoGel. It continues about 6 weeks in vitro experiments (Figure 1.19-C) [81].

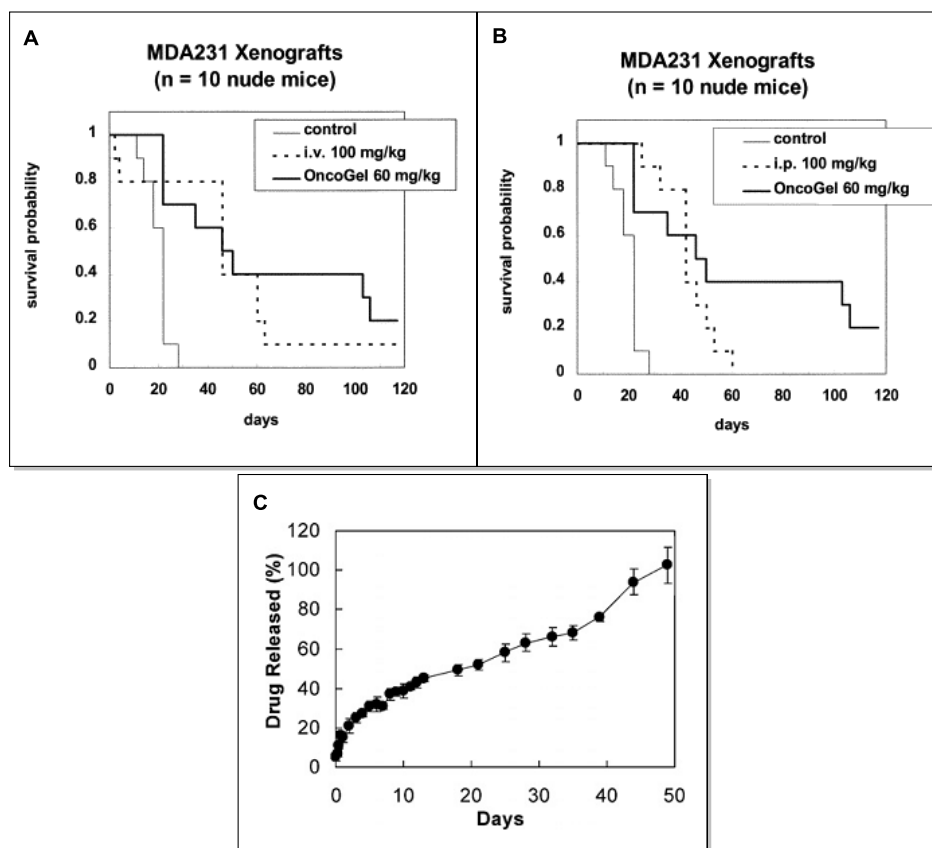


Figure 1.19 Efficacies of intratumoral OncoGel™ vs. systemic i.v. (A) and i.p. (B) and in vitro release of paclitaxel from OncoGel (C).

With the administration of Oncogel directly into solid tumors, preliminary antitumor activity, pharmacokinetics and the toxicity were characterized in phase 1 study [82]. The study confirmed that the administration of Oncogel intralesionally was well tolerated, and it was found to remain at the injection region beside not significantly available at the systemic circulation. Stable and progressive diseases were observed among six and eight patients, respectively. In a phase 2 study a combined therapy of OncoGel with external-beam radiation was applied to patients having inoperable esophageal cancer [83]. Dose-limiting toxicities were not obtained, and a decrease in tumor size in most patients was observed. Thus, OncoGel formulation deserves continued clinical research.

Biodegradable thermosensitive PEG-PLGA-PEG copolymers with FITC and misoprostol are firstly tested for prolonged drug delivery by intravesical path. The aqueous solutions of PEG-PLGA-PEG copolymers (30% w/v) are in liquid form at room temperature while they display a gel state at body temperature. Direct introduction of polymer-drug solution to bladder via a urethral catheter is performed to prevent adverse effects of medicines employed for bladder diseases. Bright green fluorescence of FITC is observed in rats after instillation of FITC loaded PEG-PLGA-PEG hydrogels into bladders is carried out. On the other hand, only background fluorescence is visible after instillation of free FITC to same region (Figure 1.20). Thus, it has been proved that thermosensitive PEG-PLGA-PEG copolymers are very powerful candidates for intravesical drug delivery [84].

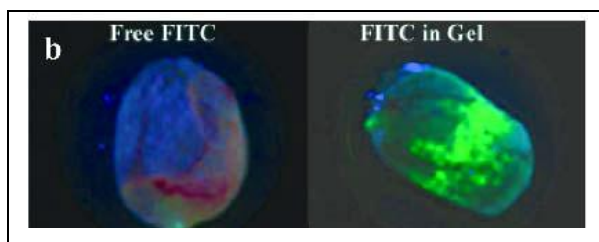


Figure 1.20 Photographs of the representative rat bladders

A study centered on the use of PEG-CPT drug reports that the released drug from hydrogels formed by a thermally gelling and hydrolytically degradable polymer PLGA-PEG-PLGA shows good anti-tumor efficacy in vivo (group 6 in Figure 1.21) [85].

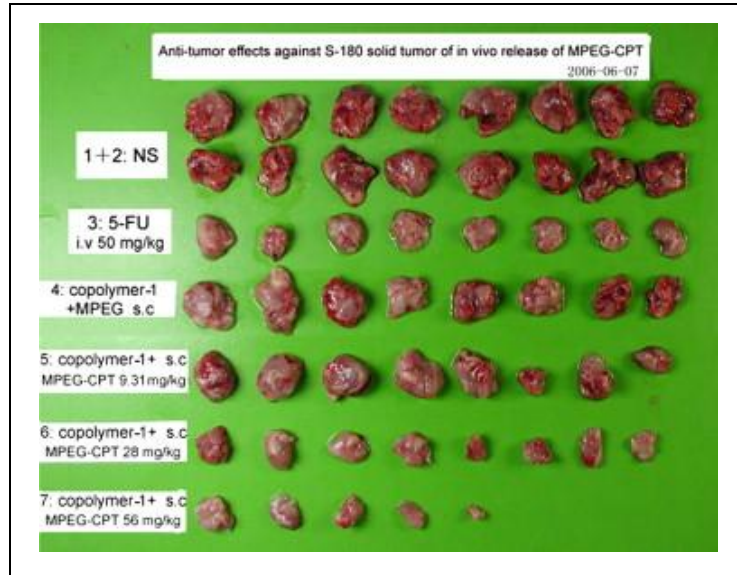


Figure 1.21 Antitumor effects against S-180 solid tumor. (i.v.: intravenous injection; s.c.: subcutaneous injection; NS: the negative control with just the physiological saline solution; 5-FU: the positive control with a sufficient amount of 5-FU.

1.1.3. Other Drug Delivery Techniques

In addition to temperature sensitive polymers used in delivery applications, implant polymers, pH sensitive polymers, light sensitive polymers and ultrasound responsive polymers can be applied for efficient therapy.

1.1.3.1. Drug Loaded Implant Polymers

First clinical application of drug loaded polymer system approved by FDA in 1996 is Gliadel wafers. It delivers carmustine drug (BCNU) directly to the site of

a brain tumor via controlled release from the polymer-drug matrix after implantation. The composition of gliadel matrix is 3.85 % BCNU and poly-[bis-p-(carboxyphenoxy)propane-sebacic acid] copolymer (PCPP-SA) in a 20:80 formulation with 1.4 cm diameter and 1.0 mm thickness [86].

First human study using those wafers for Phase I-II trial is seen in Figure 1.22. In this clinical test, 1.93 %, 3.85 % and 6.35 % doses of drug were tested on 21 patients. Mean survival was found 65, 64, and 32 weeks, respectively. 3.85 % dose seemed effective and safe so Phase III studies were initiated. Phase III was carried out 27 centers with 222 patients [87]. Randomization of patients was performed in course of surgery to take the polymer with BCNU or empty polymer. Results indicated that 23 weeks survival for polymer without drug versus 31 weeks survival for BCNU-polymer matrix. In the subgroup of patients having glioblastoma, 60 % increase in 6-month survival was observed for drug loaded polymer group (64 % vs. 44 %).

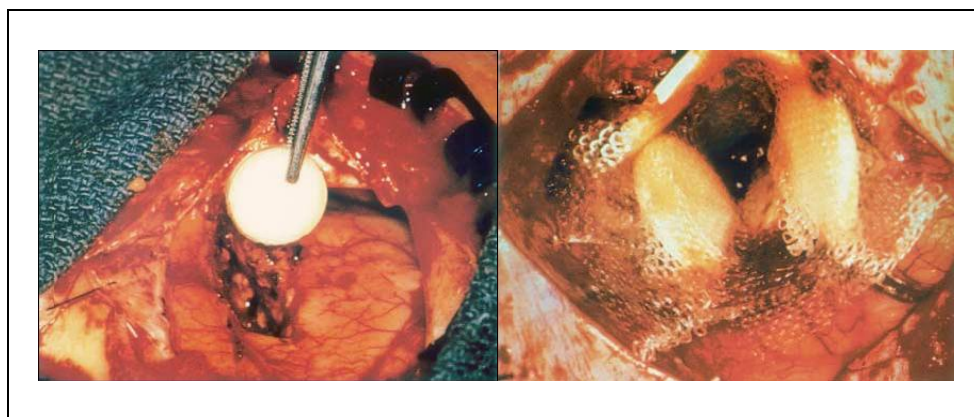


Figure 1.22 First figure represents polymer wafer with BCNU being placed into a tumor resection cavity while second shows multiple polymer wafers covered with surgical for being safe.

1.1.3.2. pH Sensitive Polymers

pH-sensitive acrylic acid and acrylic amide based hydrogels consisting of ionizable acidic groups at high pH and azoaromatic moieties can be used in delivery of drugs to colon because an azoaromatic crosslink can easily be degraded in the presence of enzymes produced by the microbial flora of the colon, as indicated in Figure 1.23. Polymeric system displays low swelling degree due to the low pH environment in stomach. Therefore, the drug is safe and stable in the pH of stomach. However, increase in pH in the gastrointestinal tract leads to increase in extends of swelling. Finally, higher swelling in colon causes easy access of azoreductase enzymes for the degradation of azo bands. Thus, drug is released into colon environment [88].

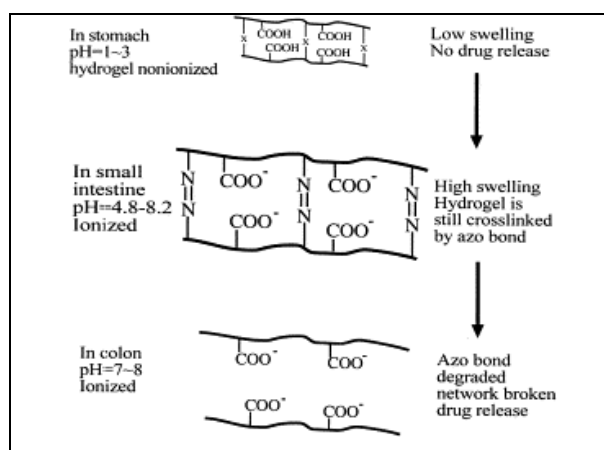


Figure 1.23 pH-sensitive hydrogels in consideration of delivery of oral colon-specific drugs.

Poly(vinylacetaldiethylaminoacetate) (AEA) shows hydrogel property upon increase in pH from 4 to 7.4 (Figure 1.24) [89,90]. Fast release of chlorpheniramine maleate drug in AEA solution in neutral pH slowed down after hydrogel is obtained. pH dependable sol-gel AEA polymer is tested for nasal

delivery in rats, and AEA Hydrogel formation is observed in the rat nasal cavity after administration [89,90].

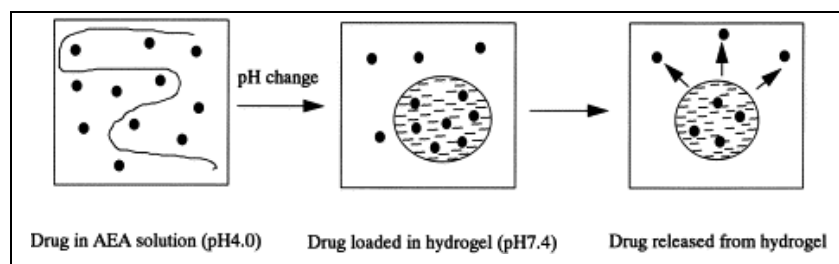


Figure 1.24 Schematic illustration of drug release process in AEA system, •. Drug molecule; wavy line: polymer in solution; lined circle, hydrogel.

1.1.3.3. Light Sensitive Polymers

Release of a drug into living cells is possible via phototherapy in the presence of a photo-activated material under remote control at proper time and location. Light-activated mesostructured silica (LAMS) nanoparticles can be used for the release of drugs (i.e. camptothecin) in cancer cell medium (Figure 1.25) [91]. Irradiation time and light intensity play important role in terms of quantity of released drugs. Nanoparticles are constantly illuminated at 413 nm leading to cis-trans photoisomers via N=N bond. Those wagging motion of N=N bonds results in the release of drugs (Figure 1.25).

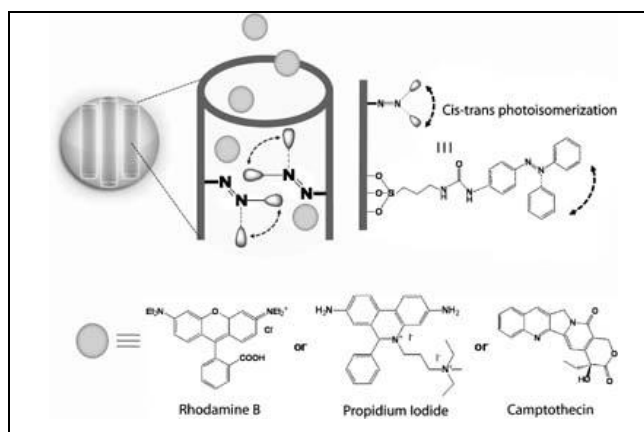


Figure 1.25 Light-activated mesostructured silica nanoparticles having azobenzene derivatives

1.1.3.4. Ultrasound-Responsive Polymers

Ultrasound can be used as effective stimulus for the release of drugs at the tumor environment, and it makes better the intracellular drug uptake by tumor cells within the body. It is noninvasive method and can be controlled from outside. Dissociation of polymeric materials is observed upon exposition of ultrasound (Figure 1.26) [92]. Release of doxorubicin anticancer drug from pluronic micelles and intracellular uptake are examined. Intratumoral distribution survival rates and drug biodistribution of mice having ovarian carcinoma tumors are evaluated after 1 MHz ultrasound is applied [92].

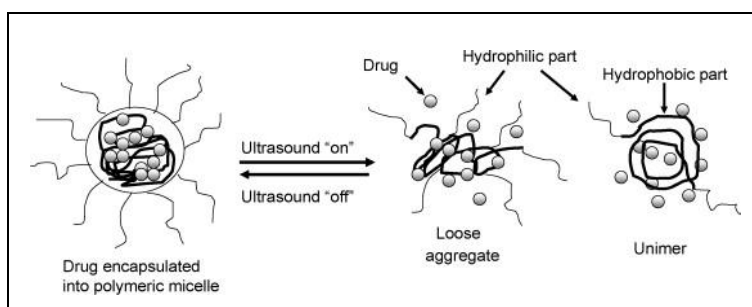


Figure 1.26 Effect of ultrasound on drug loaded pluronic triblock copolymer micelles

1.2. Synthesis, Properties and Applications of Novel Electrochromic Polythienylpyrroles

1.2.1. General Concepts

2,5-Di(2-thienyl)pyrroles (SNS) (Figure 1.27) contain thiophene and pyrrole rings interconnected by their α -positions.

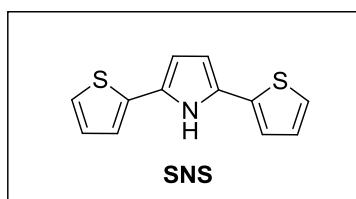


Figure 1.27 Structure of 2,5-Di(2-thienyl)pyrroles (SNS)

Synthesis of SNS was performed with 1,4-di(2-thienyl)-butane-1,4-dione [93], prepared by Friedel-Crafts acylation of thiophene with succinyl chloride, and ammonium acetate in glacial acetic acid and acetic anhydride at refluxing temperature under nitrogen atmosphere (Figure 1.28) [94].

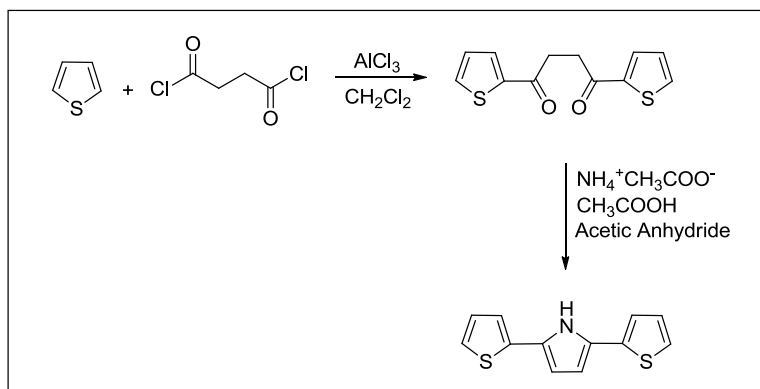


Figure 1.28 Synthesis of SNS starting from thiophene

Electrochemical synthesis of poly(SNS) was examined in several reports [94-97]. Acetonitrile (AN), ethanol, propylene carbonate (PC), tetrahydrofuran (THF) were used as the solvents. Para-toluene sulphonate and lithium perchlorate (LiClO_4) were employed as the supporting electrolytes. Films of poly(SNS) were analyzed using electroanalytical and spectroscopic techniques. FT-IR experiments proved that the polymerization process goes through α - α' positions preferentially. The electrogenerated poly(SNS) film is soluble in MeOH, acetone, THF and partially soluble in AN and insoluble in LiClO_4 -AN couple. The electrochemically reduced p(SNS) is soluble in LiClO_4 -AN couple [96].

SNS has three resonance structures, resulting in the cation radical (Figure 1.29). Unpaired radical electron is situated on different carbon atoms on rings, whereas the positive charge is localized on the nitrogen in pyrrole unit. Radical coupling of these structures leads to a linear shape (α - α') and several branched shapes of polymer (α - β' , α - β'' , β' - β' , β'' - β'' , β - β''). Substitutions on nitrogen and on β'' position of pyrrole as well as α , β and β' positions on thiophene determine the degree of linear vs. branched shape, resulting in the properties of final polymer. For example, α - α' and β'' - β'' couplings are shown in Figure 1.30 [98].

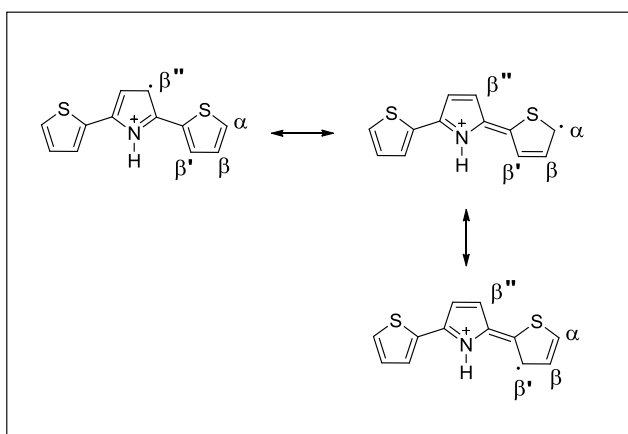


Figure 1.29 Resonance structures of SNS

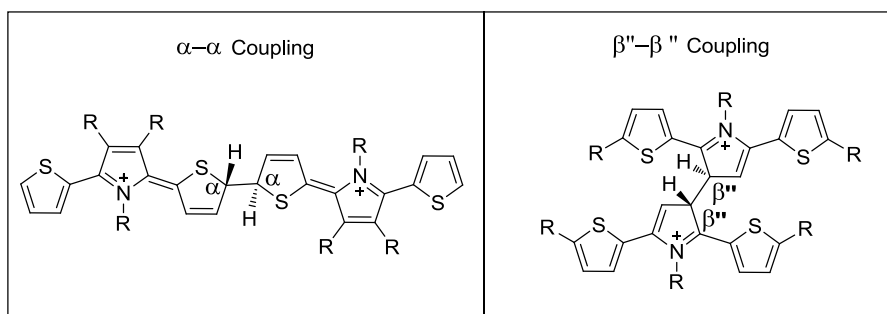


Figure 1.30 α - α and β'' - β'' couplings of SNS

Methyl or bromo substituted SNS and unsubstituted SNS was chosen to investigate kinetically linearity and branching degrees (Figure 1.31). Electro-oxidation of the compounds having bromo and methyl substitutions at alpha position led to low rate constant when compared to no substitution at alpha position. ($14,000 \text{ M}^{-1}\text{s}^{-1}$ and $17,000 \text{ M}^{-1}\text{s}^{-1}$ for substituted ones vs. $36,000 \text{ M}^{-1}\text{s}^{-1}$ for no substitution) [98].

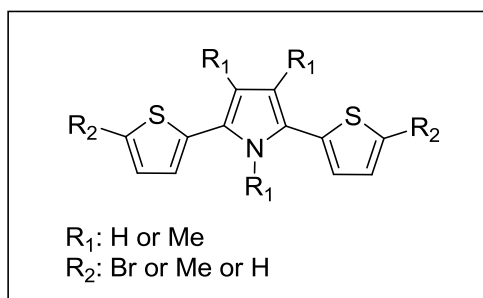


Figure 1.31 Substituted SNS derivatives

Electrochemical impedance spectroscopy (EIS) was used to measure the capacitance and charge storage capacity of oxidized and reduced poly (2,5-di-(2-thienyl)-pyrrole) films. Firstly, films of P(SNS) were anodically produced on platin electrode using $\text{LiClO}_4 + \text{CH}_3\text{CN}$ as the electrolyte solvent couple. Then, they were reduced in mixture of water and CH_3CN with 0.1 M LiClO_4 at -200

mV vs. SSCE. It was observed that film capacitances increase while going from reduced state at -200 mV to the first oxidation one at 300 mV. The formation of positive charges (polarons) along the poly(SNS) chain resulted in high charge storage capacity of films. Increase in C_f was observed with elapsed time of electrogeneration (Figure 1.32). But, gradual oxidation from 300 mV to 1020 mV led to a decrease in the slope of graph. This might be due to raising degradation and/or crosslinking in the polymer [99].

SNS and its polymerized form play a key role in many areas like photovoltaic cells, electroluminescent (EL) devices, light emitting diodes, electrochromic devices, biological and voltammetric sensors [100-111].

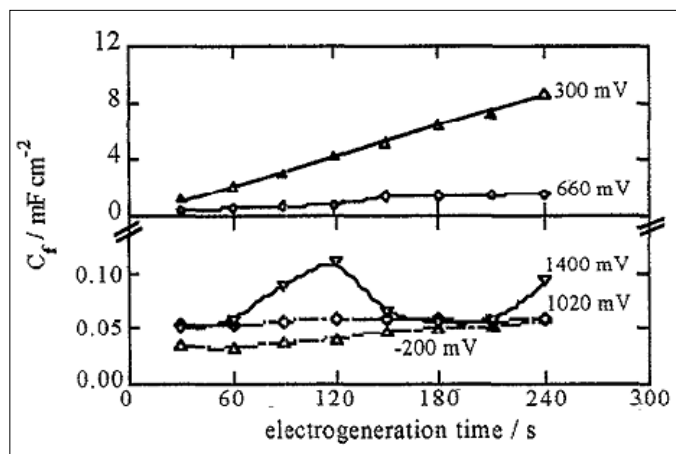


Figure 1.32 Capacitance of poly(SNS) films at different potentials vs. electrogeneration time at 25 °C.

It was found that 1-aryl-2,5-di(2-thienyl)pyrrole derivatives bearing an electron-withdrawing group emitted strong fluorescence, making them promising material for the field of electroluminescent (EL) devices. Especially, 1-(4-methoxyphenyl)-2-(5-((E)-2-(methylthio)-2-tosylvinyl) thiophen-2-yl)-5-

(thiophen-2-yl)-1H-pyrrole (Figure 1.33) exhibited extremely high performance (the highest luminous efficiency: 5.9 cd/A) [100].

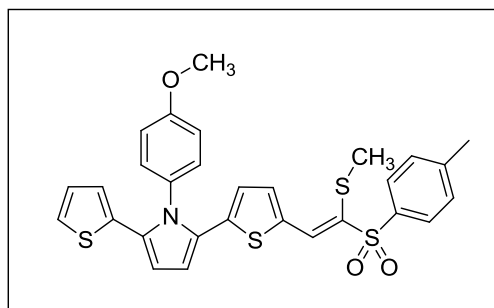


Figure 1.33 1-aryl-2,5-di(2-thienyl)pyrrole derivatives bearing an electron-withdrawing group

Immobilization studies were performed with poly(SNS) derivatives with the objective of biosensors. Immobilization of gluconobacter oxydans cells into polymer of 4-(2,5-di(thiophen-2-yl)-1H-pyrrol-1-yl)benzenamine (poly(SNS-NH₂)) led to glucose detection in real samples [101]. Also, polyphenol oxidase was immobilized into a copolymer of 1-(4-nitrophenyl)-2,5-di(2-thienyl)-1H-pyrrole [SNS(NO₂)] with pyrrole ([SNS(NO₂)]/PPy) via electrochemical polymerization for the substrates of catechol and l-tyrosine biosensor [102]. Representative scheme for the immobilization was depicted in Figure 1.34.

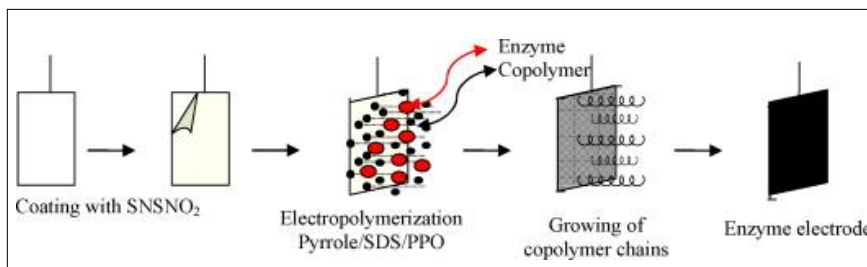


Figure 1.34 Schematic representation of enzyme immobilization.

Poly(SNS) derivatives were also used for ion sensing purposes of alkali metals with voltammetry. For example, benzo-SNS-15-crown-5 (SNS-Crown) was electropolymerized in TBAClO₄/ethanol solution to yield its corresponding polymer (Figure 1.35). It was seen that Na⁺ ions gave best interaction with crown cavity of PSNS-Crown in both neat water and organic media (ethanol) among alkali metal cations (Li⁺, Na⁺ and K⁺) [103].

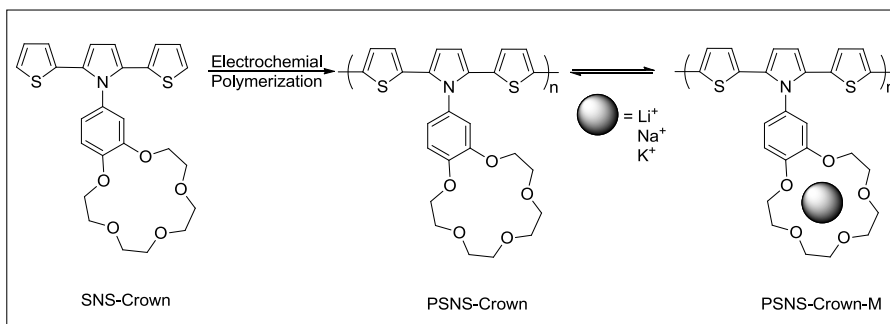


Figure 1.35 Electrochemical polymerization of SNS-Crown and ion recognition by the PSNS-Crown film to give PSNS-Crown-M.

Poly(N-dodecyl-2,5,-bis(2'-thienyl)pyrrole-2,1,3- benzothiadiazole) (PTPTB) (Figure 1.36) was used as the energy-acceptor material for the improvement exciton harvesting in organic-inorganic hybrid photovoltaic cells via resonance energy transfer [104].

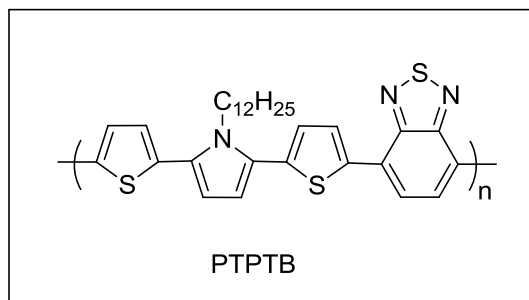


Figure 1.36 Chemical structure of PTPTB.

The recent studies about SNS bearing p-substituted (H, F, CH₃, NH₂, NO₂) benzene [105-109] as well as fluorescent and anchoring groups like naphthyl and fluoren [110-111] mainly focused on the investigation of both electrochemical and optical properties of those polymers for possible use in light emitting diodes, electrochromic devices and analytical sensors.

1.2.2. Building Block System for Development of Electrochemical Reactors

Synthesis of CdSe/ZnS quantum dots (QDs) bearing phenyl boronic acid groups which bind NAD⁺ or NADH is performed. The quenching of luminescence of quantum dots by the reduced cofactor, NADH, is less efficient way than quenching them by the NAD⁺. This dissimilarity allows us the use of NAD⁺/NADH-sensitive quantum dots as luminescent probes which help sensing of ethanol and the conversion of ethanol to acetaldehyde in the presence of alcohol dehydrogenase (AlcDH) (Figure 1.37) [112].

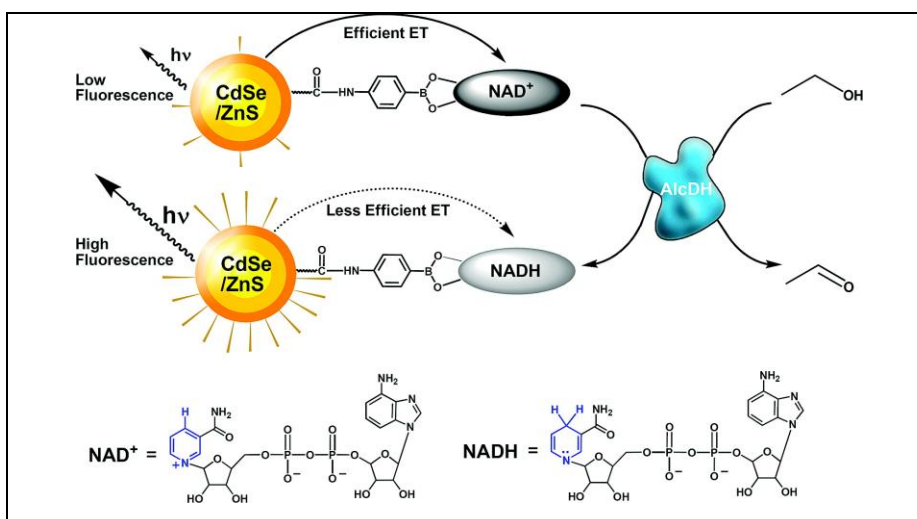


Figure 1.37 Reaction scheme of functionalized CdSe/ZnS quantum dots

Electrochemical microreactor is designed for the continuous regeneration of NADH from NAD⁺ by exploiting of flavin as mediator in the presence of formate

dehydrogenase (FDH enzyme. NADH regeneration is confirmed with the enzymatically conversion of pyruvate (Figure 1.38b and c) to L-lactate. [113].

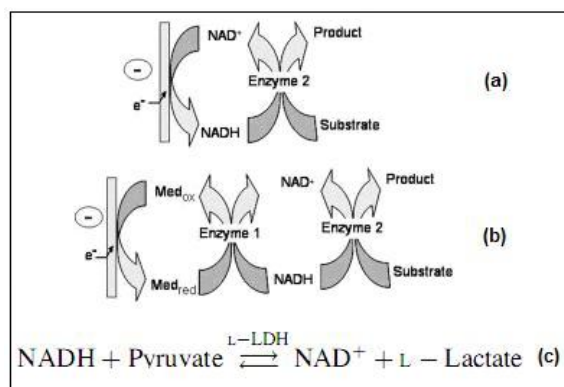


Figure 1.38 Enzymatic electrochemical chiral synthesis of L-Lactate via NADH cofactor, (a) directly, (b) indirectly, (c) enzymatic model reaction.

Multifunctional galactitol dehydrogenase enzyme (GatDH) catalyzes the reactions of aliphatic alcohols to ketones in the presence of NAD^+ . It is shown that immobilization of enzyme on gold electrode surfaces via thiol bonds oxidizes 1,2-hexanediol substrate to corresponding ketone in the presence of the redox mediator CTFM (4-carboxy-2,5,7-trinitrofluorenylidene-malonnitrile) and the cofactor NAD^+ (Figure 1.39) [114].

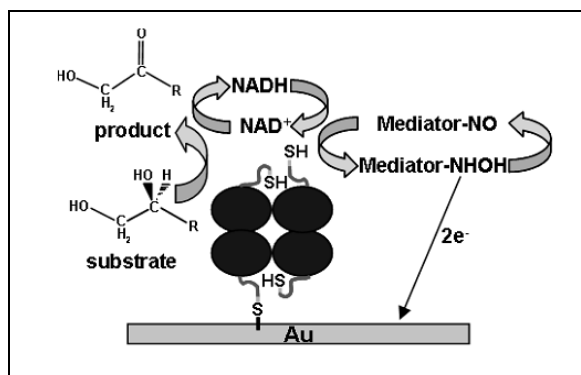


Figure 1.39 Immobilization of the modified GatDH and cofactor regeneration for the oxidation of alcohols

1.3. Pyrrole Coupling Chemistry: Investigation of Electroanalytic Spectroscopic and Thermal Properties of N-Substituted Poly(Bis-Pyrrole) Films

N-, alfa- and beta-linked bispyrroles (bisPy) and their corresponding polymers, which bear no further substitutions, have recently received increased attention due to their unique, interesting electrochemical and optical properties, as well as a wide variety of usages for different purposes, such as organic phase biosensors, intermediates in porphrin syntheses, and any kind of ion and gas sensing platform (Figure 1.40) [115-131].

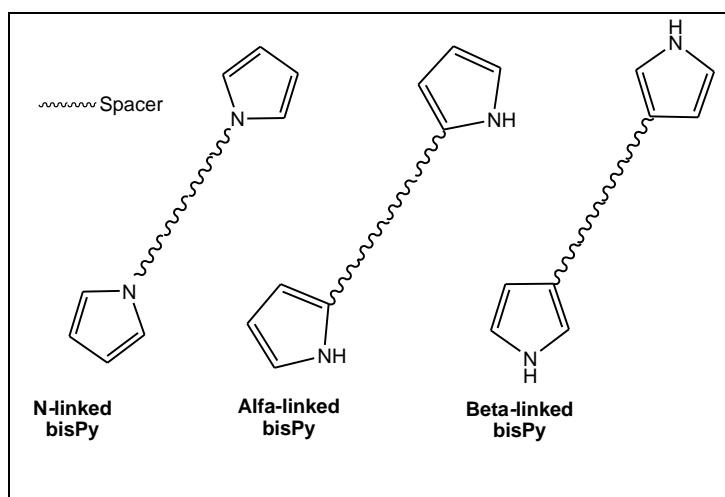


Figure 1.40 N-, alfa- and beta-linked bisPy with different types of spacers

The electrochemical behaviors of N-substituted bisPy and their corresponding polymers with more or less flexible and bulky spacers (linear alkylic, etheric, and aromatic) were examined, in which it was found that the structures of the spacer groups change the electrochemical properties of these materials [115]. N-substituted bisPy with Ni(II) macrocyclic complex spacers were prepared with different lengths of amino alkyl pyrroles. The usefulness of N-pendant pyrrole groups that bear nickel, cobalt, or iron ions was evaluated for their use as oxygen

carriers, in turn suggesting the possible application of these films as oxygen sensors or O₂/N₂ separators [116]. In addition, One of N-substituted polybisPy analogues, having shorter flexible intrachains than poly(1-(3-(2-(2-(3-(1H-pyrrol-1-yl)propoxy)ethoxy)ethoxy)propyl)-1H-pyrrole) **PI**, was used as ionophoric resins in order to extract radioactive ions via a macro scale deposition process [117,118], while it and its copolymers were investigated with impedance spectroscopy, cyclic voltammetry, ESR, UV-Vis spectroscopy and thermal techniques [119-122]. N-substituted bisPy derivative with ethering spacer **I** was electro-oxidized in water to form a polymer film on the electrode surface, and glucose oxidase immobilization was performed for the detection of glucose [123]. The same group also detected catechol by using organic phase enzyme electrodes with polyphenol oxidase [124] (Figure 1.41). Also, **PI**'s shorter analogues were tested for the extractions of radioactive and non-radioactive ionic molecules in appropriate conditions [117-122].

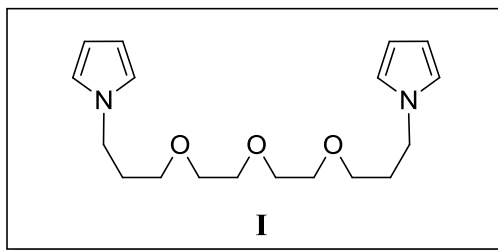


Figure 1.41 1-(3-(2-(2-(3-(1H-pyrrol-1-yl)propoxy)ethoxy)ethoxy)propyl)-1H-pyrrole

Electrochemical studies of common alpha-linked bisPy such as pyrromethanes, pyrromethene, and pyrroketones have attracted increasingly more attention due to their importance in porphrin syntheses [125]. Alpha-linked bisPy monomers with aza spacers have been evaluated as precursors of narrow band gap conducting polymers, which make them a suitable candidate for optoelectronic applications [126]. Alpha-linked bisPy bearing electron withdrawing quinone or dicyano

subunits are specific binders of F^- in organic solvents, in which they display remarkable, binding-induced changes in their color and optical and electrochemical signatures [127]. Alfa-linked bisPy with a carboxamide moiety for anion recognition were also studied wherein these materials showed great selectivity towards the cyanide anion over other common inorganic anions [128]. Langmuir-Blodgett films of bis(pyrrolyl)fluorene derivatives were investigated and were shown to be good candidates for the elements of the gas sensing devices of different types of artificial noses or a neuronal network [129]. A short review about the syntheses, oxidative polymerizations, and electronic structures of alfa-linked bisPy with arylenes, carbazoles, fluorenes, and naphthalenes was published [130].

Beta-linked bisPys were synthesized with an efficient synthetic route by using Suzuki coupling methodology. Conjugated polymer films containing polycyclic aromatic residues were electroactive and robust electrochromic materials [131].

1.4. The Aim of This Study

1.4.1. Thermosensitive Biodegradable mPEG-PLLA Block Copolymers: Synthesis, Characterizations and Applications in Drug Delivery Systems

The aim of the work is the development of injectable sol-gel system which can preserve the camptothecin family drugs in active form and make sustainable release of the drug in local position (Figure 1.42).

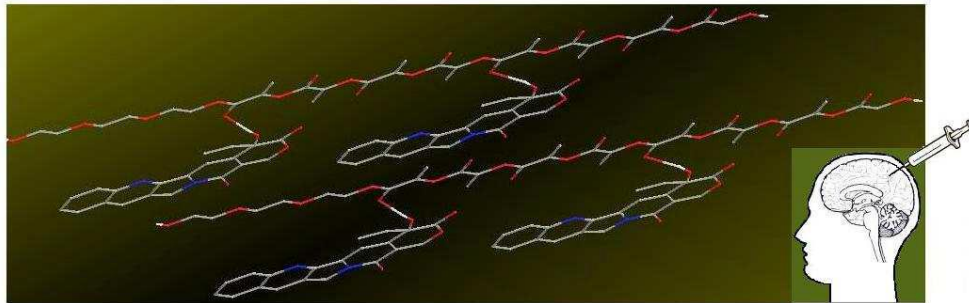


Figure 1.42 An injectable biodegradable polymeric system is developed for the efficient preserving of the active form and delayed-release of camptothecin anticancer drugs.

Most challenging problem for the family of camptothecin anti-cancer drugs is the conversion of active lactone ring into inactive toxic carboxylate form at physiological conditions ($\text{pH} = 7.4$) at body. Our primary goal is to improve an efficient and simple method which keeps topotecan and camptothecin in lactone form, especially for brain tumor therapies such as local injection since the treatments of surgery, radiotherapy, and chemotherapy have produced only modest increases in median survival time from a few months to over a year for primary malignant brain tumors. Thus, the major part of the thesis aims:

- (a) To design suitable platforms which stabilize highly the lactone species of CPT and TPT,
- (b) To prepare efficient homogenous drug loadings,
- (c) To perform sustained-release matrix of CPT and TPT anticancer drugs over weeks,
- (d) To investigate mechanistic aspects of gel-drug interactions,
- (e) To develop a model application of a local injection in malignant breast tumours in vivo after making cell line tests by MTT in vitro. This model application may follow local injection therapy of primary malignant brain tumors, as well.

1.4.2. Preparation of Polymeric PEG:PSA Particles for the Camptothecin Anticancer Drug Delivery System

Apart from above drug loaded mPEG-PLLA polymeric system for local injection, the aim of this part is to formulate nano and microcarriers synthesized with different type of biodegradable polymers for the stabilization of camptothecin anti cancer drug for possible systemic delivery applications (*i.e.* i.v.).

1.4.3. Synthesis and Properties of Novel Electrochromic Polythienylpyrrole

Aim of this part of the thesis is

- (a) To synthesize a novel 1-(1H-pyrrol-1-yl)-2,5 di(thiophen-2-yl)-1H-pyrrole (SNSN) **18** from 1-aminopyrrole **13** and 1,4-dithien-2-yl-butane-1,4-dione **17** in the presence of PTSA as indicated at Figure 1.43.
- (b) To synthesize 1,1'-bipyrrole **14** at several steps, starting from phthalimide **9**, for testing its electropolymerization characteristics for better understanding of electropolymerization mechanism of SNSN (Figure 1.43).
- (c) To synthesize poly(SNSN) homopolymer electrochemically under suitable conditions.
- (d) To elaborate the electrochemical and electro-optical properties of poly(SNSN) using electroanalytical and spectroscopic techniques, and to discuss them in comparison with previously reported polySNS derivatives.
- (e) To examine fluorescence characteristics of p(SNSN) with fluorescence spectroscopy.

Lastly, to perform immobilizations of all necessary SNS based components (NAD⁺ cofactor, mediator and enzymes) into surface layer of electrode for the construction of building block system for the development of electrochemical reactors.

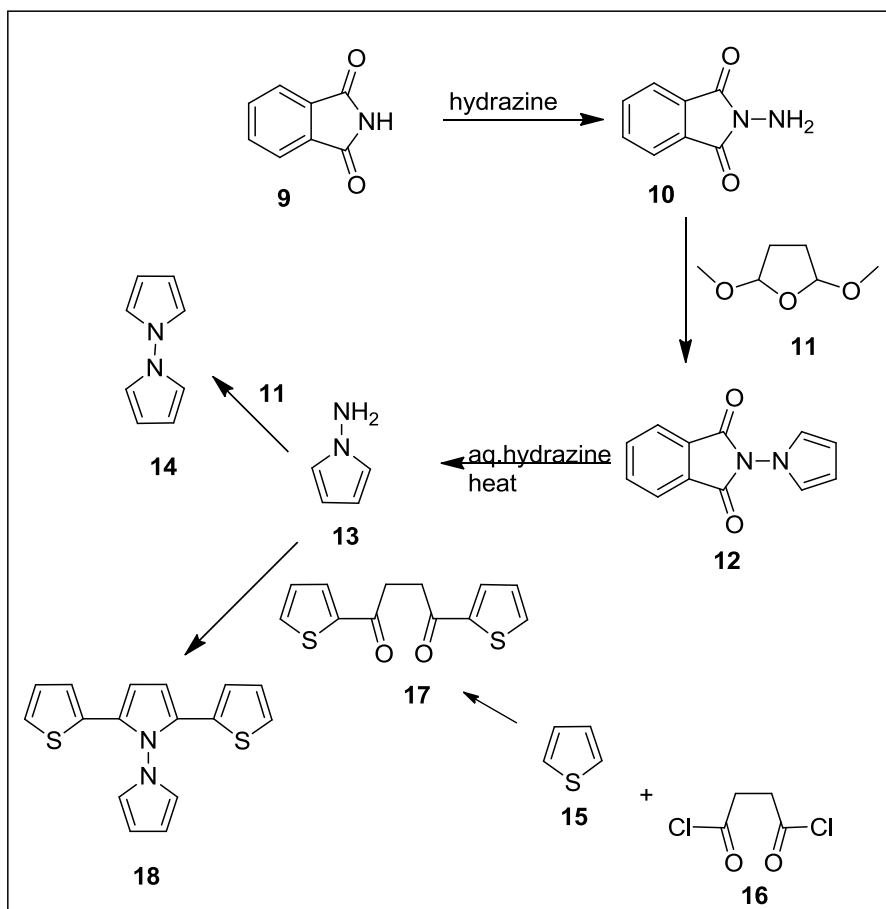


Figure 1.43 Synthesis of SNSN and 1,1'-bipyrrrole

1.4.4. Pyrrole Coupling Chemistry: Investigation of Electroanalytic Spectroscopic and Thermal Properties of N-Substituted Poly(Bis-Pyrrole) Films

Aim of this part of the thesis is

- To fully characterize **PI** films by electroanalytic, spectroscopic, thermal, and four probe techniques.
- To investigate stability, multi-electrochromic behavior and a reversible redox process of **PI** films.
- To examine **PI** films for selective voltammetric response towards Na^+ among the alkali series in an organic medium
- To detect Ag^+ ions in the solution via **PI** films by using cyclic voltammetry without precipitants or complexing ligands.

CHAPTER 2

EXPERIMENTAL

2.1. Materials

L-lactide monomer (Aldrich), mPEG-2000 homopolymer (Aldrich), mPEG-5000 homopolymer (Fluka), stannous 2-ethyl-hexanoate (Sigma), benzyl alcohol (Sigma) were used in the syntheses of poly(L-lactide) and PLLA-mPEG diblock copolymer. Diethyl ether (J.T. Baker) and dichloromethane (J.T. Baker) were employed in purification steps. Trisma-base (Aldrich), NaOH (Aldrich) and HCl (Aldrich) were employed in the buffer preparations. Camptothecin and topotecan were purchased from Chengdu Haojie Pharmchem in China and used as received. Triethylamine (Aldrich), acetonitrile (J.T. Baker) and acetic acid (J.T. Baker) were employed in preparation of mobile phase and filtered out with filtration system prior to use.

Aluminum chloride (AlCl_3) (Aldrich), succinyl chloride (Aldrich), toluene (Sigma), phthalimide, absolute ethanol (Sigma), dimethoxytetrahydrofuran (Aldrich), dioxane (Aldrich), hydrazine (Aldrich), Na_2SO_4 (Aldrich), methanol (Aldrich), hexane (Aldrich), p-toluenesulfonic acid were used as received in the synthesis of 1-(1H-pyrrol-1-yl)-2,5-di(thiophen-2-yl)-1H-pyrrole (SNSN) and 1,1'-bipyrrole. Thiophene (Sigma) and dichloromethane (Merck) were purified by conventional distillation procedures prior to use. Tetrabutylammonium

perchlorate (TBAP) (Aldrich) as the supporting salt was used without purification for the electrochemical polymerization of SNSN.

2.2. Equipments

2.2.1. Nuclear Magnetic Resonance Spectroscopy (NMR)

^1H and ^{13}C NMR experiments were carried out for the structural analysis of all monomers, homopolymers and copolymers. For ^1H - and ^{13}C -NMR measurements, 400 and 100 MHz frequencies were used, respectively. Also, determination of number average molecular weight of homopolymers and copolymers were performed with ^1H -NMR. Bruker Avance DPX 400 and Avance III Ultrashield instruments were employed. Samples were prepared with deuteriochloroform (CDCl_3) in NMR tubes.

2.2.2. FTIR and ATR-FTIR Spectroscopy

FT-IR spectra of polymers were recorded on a Bruker Vertex 70 by making KBr pellets. The attenuated total reflection FTIR spectroscopy (ATR-FTIR) was a Bruker Vertex 70, equipped with the PIKE MIRacle universal ATR sampling accessory (Diamond/ZnSe crystal plate with fixed angle of incidence of 45 with 2.0 μ depth penetration).

2.2.3. High Performance Liquid Chromatography (HPLC)

HPLC spectra were recorded on Thermo Finnigan HPLC with Fluorescence dedector. Data was analyzed with Chromquest software program. Nova-Pak C-18 4 μm 3.9x150 mm HPLC Column was used for the analysis of carboxylate and lactone forms of anti cancer drugs.

2.2.4. Fluorescence Spectroscopy

Fluorescence measurements were recorded on Perkin Elmer LS-50 fluorescence spectroscopy. Double Wavelength and single read programs with Win-Lab software were used for the analysis of lactone and carboxylate conversions and release experiments of anti-cancer drugs. Measurements were performed in quartz cell. A Varian Cary Eclipse Fluorescence spectrophotometer was also used for fluorescence measurements of SNSN and p(SNSN).

2.2.5. Confocal Spectroscopy

Zeiss LSM 510 Confocal Microscope equipped with Argon laser (488 nm) and LP505 emission filter was employed. 40X magnification were performed.

2.2.6. Optical Microscope

Zeiss Axioskop 2 plus optic microscope with 100X magnification with Hitachi CCD camera was used for the measurements of CPT loaded and unloaded gel.

2.2.7. Cyclic Voltammetry (CV) System and Spectroelectrochemistry

A Volta-Lab 40 and/or Gamry PCI4/300 potentiostat–galvanostat were used for getting electroanalytical measurements. A spectrometer of Hewlett–Packard 8453A was employed for performing electro-optic analyses. Moreover, the method of square wave helped to find out switching ability of the final polymeric film between its neutral and doped cases.

2.3. Procedure

2.3.1. Thermosensitive Biodegradable mPEG-PLLA Block Copolymers: Syntheses, Characterizations and Applications in Drug Delivery Systems

2.3.1.1. Homopolymerization of L-Lactide

3 g of L-lactide (21 mmol), 107 mg of benzyl alcohol (1 mmol), and 84 mg of Sn(Oct)₂ (0.21 mmol) were added into 45 mL of dry toluene, followed by refluxing using Dean-Stark apparatus for 2 h under a nitrogen atmosphere. Toluene was evaporated under reduced pressure. Homopolymer was dissolved in 100 mL methylene chloride and precipitated with an excess amount of cold diethyl ether (1 L). Then, it was dried under vacuum. Yield of poly(L-Lactide) **19** was about 80 %. ¹H NMR (CDCl₃) δ (ppm): 1.5 (d, 3H), 5.1 (q, H); ¹³C NMR (CDCl₃) δ 16.6, 68.9, 169.3

Poly(L-lactide) **20** was synthesized with same methodology as above. Experimental conditions were indicated in Table 2.1.

Table 2.1 Conditions for poly(L-lactide) synthesis

ID	Lactide	Sn(Oct) ₂	Time	Benzyl Alcohol	Toluene
19	3.0 g	84 mg	3 hrs	107 mg	45 mL
20	6.8 g	84 mg	3 hrs	104 mg	45 mL

2.3.1.2. Copolymerization of L-Lactide with mPEG-2000 (PLLA-mPEG2k)

1.2 g of mPEG-2000 (0.6 mmol), 5 g of L-lactide (35 mmol), and 100 mg of Sn(Oct)₂ (0.25 mmol) were added to 120 mL of dry toluene and refluxed for 10.5 hrs under nitrogen atmosphere. During the experiment, the reaction was monitored by thin layer chromatography (TLC, silica gel, 1:1 DCM/MeOH

solvent mixture), and the plate was developed with Dragondorf Reagent. mPEG and diblock copolymer exhibited different R_f values (mPEG: 0.24, diblock copolymer: 0.28) Later, toluene was evaporated under reduced pressure. The copolymer product **21** was dissolved in 100 mL dichloromethane and precipitated with an excess amount of cold diethyl ether (1L). ¹H NMR (CDCl₃) δ (ppm): 1.5 (d, 3H), 3.63 (s, 2H), 5.1 (q, H); ¹³C NMR (CDCl₃) δ 16.6, 68.9, 71, 169.3

PLLA-mPEG2k **22**, **23** and **24** were synthesized with the same methodology as above. Experimental conditions were indicated in table 2.2.

Table 2.2 Conditions for PLLA-mPEG2k synthesis

ID	mPEG 2k mass (g)	Lactide mass (g)	Sn (Oct)₂ (mg)	Time (h)	Toluene (mL)
21	1.2	5.0	100	10.5	120
22	1.2	3.0	100	10.5	120
23	1.2	1.5	100	10.5	120
24	1.2	1.5	100	24	120

2.3.1.3. Copolymerization of L-Lactide with mPEG-5000 (PLLA-mPEG5k)

3 g of mPEG-5000 (0.6 mmol), 5 g of L-lactide (35 mmol), and 100 mg of Sn(Oct)₂ (0.25 mmol) were added to 120 mL of dry toluene and refluxed for 10.5 hrs under nitrogen atmosphere. Then, toluene was evaporated under reduced pressure. The copolymer product **25** was dissolved in 100 mL dichloromethane and precipitated with an excess amount of cold diethyl ether (1L). ¹H NMR (CDCl₃) δ (ppm): 1.5 (d, 3H), 3.63 (s, 2H), 5.1 (q, H); ¹³C NMR (CDCl₃) δ 16.6, 68.9, 71, 169.3

PLLA-mPEG5k **26** and **27** were synthesized with the same methodology as above. Experimental conditions were indicated in Table 2.3.

Table 2.3 Conditions for PLLA-mPEG5k synthesis

ID	mPEG 5k mass (g)	Lactide mass (g)	Sn (Oct)₂ mg	Time (h)	Toluene (mL)
25	3	5	100	10.5	120
26	3	3	100	10.5	120
27	6	4	200	10.5	120

2.3.1.4. Copolymer Film Preparation

Standard glass slides initially cut into halves of dimensions 26 mm x38 mm were cleaned in chromic acid, rinsed with a few times with distilled water, and dried. Chloroform and toluene were used as the solvents to prepare homo- and copolymers. Polymer concentration was kept at 20 mg/mL. For full dissolution of polymer it was heated up to 50 °C followed by cooling to room temperature. A mechanical dipper with a removal rate of 67 mm/min was used for coating of glass slides with polymer solution. At each experiment, the slides were kept for 2 min in polymer solution. A vacuum oven was employed to dry the coated slides [132].

2.3.1.5. General Procedure for Determining Gel to Sol Transition Temperature

PLLA homopolymer **19-20** and diblock PLLA-mPEG copolymers **21-27** were mixed with distilled water to make various concentrations as seen in Table 2.4. They were vortexed to get homogenous mixture if available, and they were immersed in a temperature controlled water bath. The gel-to sol transitions of copolymers were examined between 20 and 80 °C with 2.0 °C increments. The tubes were maintained in water baths for 5 min at each temperature point before tilting. The critical gel to sol temperature was determined as the temperature at which the gel turned into sol form immediately after tilting the tube.

Table 2.4 Concentrations of PLLA, PLLA-mPEG2k and PLLA-mPEG5k tested determining gel to sol transition temperature.

ID	Concentration % (mg/ μl)
19	3
20	3
21	3
22	3
23	3, 5 ,10, 30, 45
24	3
25	3
26	30
27	30

2.3.1.6. CPT and TPT Loading into Copolymer Gel

0.015, 1.0, and 10 % loadings of topotecan or camptothecin into copolymer gel **23** were performed (Table 2.5). For example, the 0.015 % loading of CPT into copolymer was prepared with following way: 100 mg PLGA-PEG, 0.015 mg CPT and 200 μ l of tris buffer at pH: 7.4 were mixed to form gel at RT.

Measurements of <1 mg CPT and TPT: 1-2 mg of drugs were dissolved in a mixture of MeOH: DCM. Then, appropriate volume of drug solution, corresponding to 0.015 mg in weight, was placed into 1 ml eppendorph tube followed by evaporation with lyophilizator overnight for full removal of solvents.

For higher loadings, we directly mixed camptothecin or topotecan powders with copolymer. Then appropriate volume of distillated water was added to form gels having drugs.

Table 2.5 CPT and TPT loading into copolymer gel

Amount of Polymer 23 (mg)	Drug	Amount of drug (mg)	Buffer at pH:7.4 (μL)
100	CPT	0.015	200
115	CPT	1.15	140
120	CPT	12	150
100	TPT	0.015	200
120	TPT	1.2	150
120	TPT	12	150

2.3.1.7. Preparation of Tris Buffer

606 mg trisma-base was added to 250 ml of distilled water. Then, it was stirred for complete dissolution. Medium of pH was adjusted to 5.0, 7.4 or 9.9 with diluted hydrochloric acid or sodium hydroxide solutions.

2.3.1.8. Preparation of Free CPT and TPT Stock Solution

8.7 mg of CPT powder was dissolved in 25 ml of DMSO in a volumetric flask. Final concentration is 10^{-3} M. It was covered with aluminum foil and stored at 4 °C in fridge. It was brought to room temperature and kept about 1 hr for dissolution of solvent prior to use in analysis.

10.5 mg of TPT powder was dissolved in 25 ml of DMSO in volumetric flask. Final concentration is 10^{-3} M. It was covered with aluminum foil and stored at 4 °C in fridge. It was brought to room temperature and kept about 1 hr for dissolution of solvent prior to use in analysis.

2.3.1.9. Preparation of Triethylamine Acetate (TEAA) Buffer

10 ml of triethyl amine was added to 990 mL of distilled water in volumetric flask. pH of system was adjusted to 5.5 with glacial acetic acid. Suction filtration

was performed for the removal of potential dusts, and it was degassed prior to use.

2.3.1.10. HPLC Analysis

5 μL of drug loaded gel was diluted with about 1 mL of pH=7.4 tris buffer in vial. Then, it was immediately analyzed with HPLC having C18 reverse phase column and fluorescence detector. Excitation and emission wavelengths used in HPLC analysis were shown in Table 2.6. Also, mobile phase used was 23:77 (v/v) ACN-TEAA buffer (1 %, v/v, pH: 5.5) for CPT analysis in gel and 12:88 (v/v) ACN-TEAA buffer (2 %, v/v, pH: 5.5) for TPT analysis in gel.

Table 2.6 Excitation and emission wavelength values of CPT and TPT used in HPLC analysis

Drug	Excitation λ (nm)	Emission λ (nm)
CPT	370	432
TPT	381	516

For control experiments; 3 μL of 10^{-3} M CPT in DMSO was diluted with 1 mL pH= 7.4 tris buffer in vial. Also, 5 μL of 10^{-3} M TPT in DMSO was diluted with 1 mL pH= 7.4 tris buffer in vial. Then, it was immediately analyzed with HPLC equipped with fluorescence detector using wavelengths in Table 2.6.

2.3.1.11. Fluorescence Analysis

5 μL of drug loaded gel was diluted with about 3 mL of pH=7.4 tris buffer in quartz cell. Then, it was immediately analyzed with fluorescence spectroscopy using double wavelength program. Wavelengths employed were shown in Table 2.7.

For control experiments; 3 μL of 10^{-3} M CPT in DMSO were diluted with 3 mL pH= 7.4 tris buffer in quartz cell. Also, 5 μL of 10^{-3} M TPT in DMSO were diluted with 3 mL pH= 7.4 tris buffer in quartz cell. Then, it was immediately analyzed with fluorescence spectroscopy measured with double wavelength program using wavelengths in Table 2.7.

Table 2.7 Excitation and emission wavelength values of CPT and TPT used in fluorescence analysis

ID	λ excitation (nm)	λ_1 emission (nm)	λ_2 emission (nm)
Free CPT	370	432	480
Free TPT	381	516	580

2.3.1.12. Release Experiments

Topotecan or camptothecin were loaded into copolymer gel with 0.015 % and 1.0 % loading ratios. For example, 0.0375 mg TPT and 250 mg polymer were mixed homogeneously in eppendorph tube. 350 μL of pH=7.4 tris buffer was added to form a gel at room temperature. 350 μL of buffer was suitable to keep matrix as a gel form at 35 °C. 0.5 ml of pH=5 Tris buffer was added into upper side of gel. System contains two layers; first layer is gel with drug while second layer is supernatant. Other formulations were prepared with the same manner and indicated in Table 2.8. Then, they were put into a shaker having constant speed at 160 rpm and 35 °C. In different time points, supernatants were replaced with the fresh one. Measurements were carried out using fluorescence spectroscopy with single read measurements at appropriate wavelengths of drugs shown in Table 2.6. Dilutions were performed prior to measurements if necessary. Also, a blank formulation, with no drug, was prepared for the elimination of low fluorescence characteristic of polymer.

Table 2.8 Gel preparation with CPT and TPT drugs at different loading ratios

ID	Loading %	Drug	Polymer Mass (mg)	Drug Mass (mg)	Buffer (μL)
28	0.015	TPT	250	0.0375	350
29	1.0	TPT	160	1.6	225
30	0.015	CPT	250	0.0375	350
31	1.0	CPT	250	2.5	350
32	NA	NA	250	NA	350

2.3.1.12.1. Preparation of Standard Curve

2.1 mg of CPT were dissolved in 50 ml MeOH. Then, 0.1 ml of stock solution were diluted with 2.9 mL of pH=5.0 tris buffer. Further dilutions were performed before the intensity measurements of each sample with fluorescence spectroscopy using single read program. Final volume of sample was always kept as 3.0 mL for all standard curves and release experiments. Intensity vs. mass of drug were plotted to obtain standard curve equation.

1.7 mg of TPT was dissolved in 1.0 ml MeOH. Then, 20 μ l of stock solution was diluted with 2.98 mL of pH=5.0 tris buffer. Further dilutions were performed before the intensity measurements of each sample with fluorescence spectroscopy using single read program. Final volume of sample was always kept as 3.0 mL for all standard curve and release experiments. Intensity vs. mass of drug were plotted to obtain standard curve equation.

2.3.1.13. Examination of CPT Loaded Gel with ATR-FTIR

For the stabilization mechanism, ATR-FTIR spectra of powder CPT and CPT loaded copolymer gel were recorded, respectively. For CPT loaded gel sample, highly concentrated copolymer solution (almost like gel) was prepared with PLLA-mPEG and distilled water. It was recorded as background. Then, a 1-2

mg of powder CPT were added into the same vial before it was stirred with high speed vortex for the complete homogenization. ATR-FTIR spectrum of drug loaded gel was recorded and then background was subtracted.

2.3.1.14. In vitro and In Vivo Studies

2.3.1.14.1. Cell Culture

4T1 mouse mammary carcinoma cell line (American Type Culture Collection, ATCC; Manassas, VA, USA) and Lewis lung carcinoma (LLC-1) cells kindly gifted by Dr. Sven Brandau, University Duisburg-Essen, Germany, was cultured in 75 cm² culture flasks having RPMI 1640 culture media enriched with heat disabled fetal bovine serum (10%), 2 mM L-glutamine (Thermo Scientific, HyClone, Logan, UT, USA), 100 units/ml penicillin and 100 µg/ml streptomycin (Biochrom, Berlin, Germany) at 37°C in a humidified incubator containing 5% CO₂.

2.3.1.14.2. MTT Assay

Topotecan (TPT) was dissolved in DMSO (80 mg/ml) as a stock solution and test concentrations were prepared freshly in culture media. TPT in PLLA-mPEG platform (0.25% loading) overlaid by culture media was allowed for the release of the drug during two hours. Then, the culture media was collected and test dilutions were prepared for MTT assay. The same procedure was performed with PLLA-mPEG gel as a negative control. The amount of released TPT in the culture media was fluorometrically quantitated prior to cytotoxicity assay.

The methylothiazolyltetrazolium (MTT) assay was used to evaluate cell viability. Shortly, 50 µl of cell suspensions consisting of 3x10⁴ or 1x10⁴ 4T1 and 1x10⁴ LLC-1 cells were seeded in 96-well flat-bottom plates and varying concentrations

of freshly dissolved TPT or TPT released from the PLLA-mPEG gel were added into each well (50 μ l/well). All concentrations were studied in quadruplicates. Then, the cells were kept for a period of 24 h at 37°C in a humidified incubator containing 5% CO₂. After incubation period for 24 h, 25 μ l of 5 mg/ml MTT solution were supplied into each well, and the incubation of plates was done for 4h more. The solubilization of formazan precipitate was observed after the addition of 80 μ l lysing buffer (pH=4.7) comprising 23% SDS (Sigma) dissolved in 45% N,N-dimethylformamide solution (Sigma). After an overnight incubation at 37°C, the optical densities (OD) were read at 570 nm using a microplate reader (Spectramax Plus, Molecular Devices, Sunnyvale, CA, USA). Cells incubated in the culture medium alone served as a control for cell viability (untreated wells). Cell viability (%) was calculated as (OD of treated wells/OD of untreated wells) x 100.

2.3.1.14.3. Animals and Tumor Formation

Six- to eight-week-old inbred female BALB/c mice (Kobay As., Ankara, Turkey) were housed under environmentally controlled standard conditions. The Guiding Principles in the Care and Use of Laboratory Animals together with those described in the Declaration of Helsinki were strictly adhered in the conduct of all the experimental procedures described. In vivo study was approved by the Institutional Ethical Committee of Hacettepe University, Ankara, Turkey (Approval Number: 2010/10-10) before its commencement.

4T1 mouse mammary carcinoma cells at the fourth passage (5×10^4 cells suspended in 0.1 ml phosphate-buffered saline) were inoculated subcutaneously into the right dorsal flank of the syngeneic BALB/c mice. The mice were distributed into four experimental groups: Control group (injected with physiological saline, 0.9% NaCl, 0.13 ml/30 gr), PLLA-mPEG control group

(injected with PLLA-mPEG gel, 0.13 ml/30 gr), TPT group (injected with Topotecan dissolved in physiological saline (0.35 mg/ml), 0.045 mg TPT/kg) and PLLA-mPEG-TPT group (injected with PLLA-mPEG-TPT gel (0.35 mg/ml (0.08% TPT loading)), 0.045 mg TPT/kg). Peri-tumoral subcutaneous injections were performed at the second week post-inoculation coinciding with the appearance of palpable tumors. The size of the tumors was measured twice a week, and the mean diameter was calculated as the square root of the product of the two perpendicular diameters.

2.3.1.14.4. Statistical Analysis

Arithmetic mean \pm standard deviation (SD) is used for all values. Student's paired *t*-test is employed for statistical difference between experimental groups. Differences are counted as statistically significant when $P \leq 0.05$.

2.3.2. Preparation of Polymeric Particles for the Camptothecin Anticancer Drug Delivery System

2.3.2.1. Synthesis of Sebacic Acid Prepolymer

10.0 g sebacic acid and 100 mL of acetic anhydride were placed into 250 ml two necked round flask. N₂ was passed through the system, and the flask was immersed into oil bath. It was refluxed at 145 °C for 15 min before mixture was brought into room temperature. The solvent was evaporated under reduced pressure with rotawap. Recrystallization was performed with dry toluene, and then residual solvent was removed with reduced pressure over a few hours. ¹H-NMR (CDCl₃) δ (ppm): 2.45 (t, 4H, CH₂), 2.33 (s, 6H, CH₃), 1.66 (m, 4H, CH₂), 1.33 (m, 8H, CH₂) [71,72].

2.3.2.2. Synthesis of PEG Prepolymer

10.0 g PEG diacid and 200 mL of acetic anhydride were placed into 250 ml two necked round flask. N₂ was passed through system, and the flask was immersed into oil bath. It was refluxed at 145 °C for 30 min before mixture was brought into room temperature. The solvent was evaporated under reduced pressure with rotawap. The residue was extracted with anhydrous ether and dried in vacuum. ¹H-NMR (CDCl₃) δ (ppm): 4.27 (s, CH₂), 3.65 (s, OCH₂CH₂), 2.25 (s, CH₃) [71,72].

2.3.2.3. Synthesis of PEG:PSA Copolymer

1.0 g acyl-PEG_{0.6k} and 1.0 g acyl-SA prepolymer were placed into three necked 50 mL flask under nitrogen. Then, it was directly immersed into 185°C oil bath. It was mixed about 1 min before vacuum was opened. Pump pressure was 3.2x10⁻¹ mbar. It was stirred about 15 min. Then, the vacuum channel was closed for 30 s to provide nitrogen gas sweep. Polymerization continued for 10-12 min more. After it was cooled down, chloroform was added into mixture followed by precipitation with 40-50 mL of petroleum ether. Then, product was dried under vacuum for few hours. Amount obtained: 1.50 g. ¹H-NMR (CDCl₃): δ (ppm): 4.27 (s, CH₂), 3.65 (s, OCH₂CH₂), 2.45 (t, 4H, CH₂), 1.66 (m, 4H, CH₂), 1.33 (m, 8H, CH₂). [71,72]

2.3.2.4. Nanoparticle and Microparticle formulations of PEG:PSA Copolymer

Nanoprecipitation (Solvent Diffusion) and Single Emulsion methods were performed to formulate camptothecin loaded PEG-SA nanoparticles and microparticles. For diffusion method, copolymer and camptothecin were

dissolved in DMSO then it was added dropwisely into 1 % PVA aqueous phase followed by 3 hrs stirring. Lastly, particles were washed with water three times using centrifuge at 10 k rpm before freeze-dried. For single emulsion method, copolymer and CPT were dissolved in chloroform methanol mixture (4:1). 200 μ l water was added before probe sonication was performed. Then, emulsion was poured into 40 ml of 1 % PVA solution. Particles were washed with water three times using centrifuge at 10 k rpm.

2.3.3. Synthesis and Properties of Novel Electrochromic Polythienylpyrrole

2.3.3.1. Synthesis of N-Aminophthalimide **10**

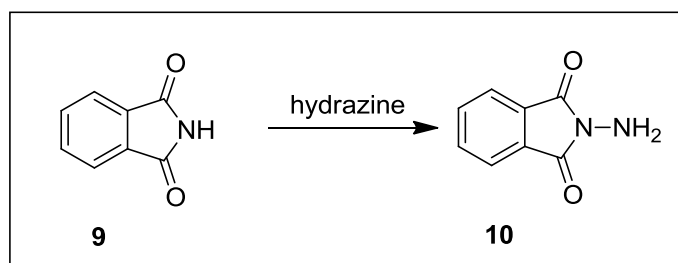


Figure 2.1 Synthesis of N-aminophthalimide **10** from phthalimide **9**

4.9 g phthalimide **9** in 80 ml of absolute ethanol was stirred under water-ice bath at 5 °C for 15 min. 1.5 ml of 99 % hydrazine was dropwisely added to flask. The mixture was stirred at 5 °C for 2 h. Viscosity of reaction medium increased with time passed. 50 mL of ice-water, after grinding, was added to reaction mixture. It was then filtered with vacuum filtration, and white precipitate was washed with 3-5 mL of water. Excess volume of water (higher than 5 mL) causes an increase in the lost of product. Then, it was dried well. The yield of the compound **10** was 75 % [133-135]. Ice-water bath prevents the formation of phthalhydrazide [136].

It had ^1H NMR (400 MHz, CDCl_3) δ (ppm) 4.0 (brs, 2H), 7.7 (dd, 2H), 7.8 (dd, 2H) ppm.

2.3.3.2. Synthesis of N-Phthalimidopyrrole **12**

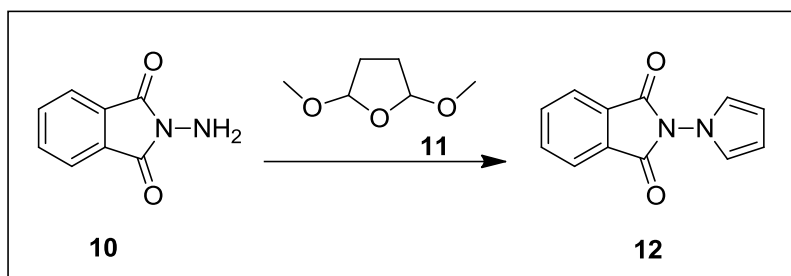


Figure 2.2 Synthesis of N-phthalimidopyrrole **12** from N-aminophthalimide **10**

2.5 mL 2,5-dimethoxytetrahydrofuran **11** were added into 2.5 g N-Aminophthalimide **10** in 25 mL dioxane. While the mixture was in the form of suspension initially, it turned into yellow solution at reflux temperature of 110 °C. After maintaining the mixture for 5-10 min at reflux temperature, 2.5 mL of 5 N HCl were added dropwise from septum cap. Solution became darker, and black solution was obtained. The mixture was cooled, and the flask was kept in ice-water bath to precipitate crystals. Vacuum filtration was performed for the separation of crystals. Crystals were washed with 5-10 mL of 1:3 dioxane-water mixtures. White crystals were dried in vacuum. The yield of the compound **12** was about 66 %. [135-137]. It had ^1H NMR (400 MHz, CDCl_3) δ (ppm) 6.3 (dd, 2H), 6.7 (dd, 2H), 7.8 (dd, 2H) and 7.9 (dd, 2H) ppm.

2.3.3.3. Synthesis of N-Aminopyrrole **13**

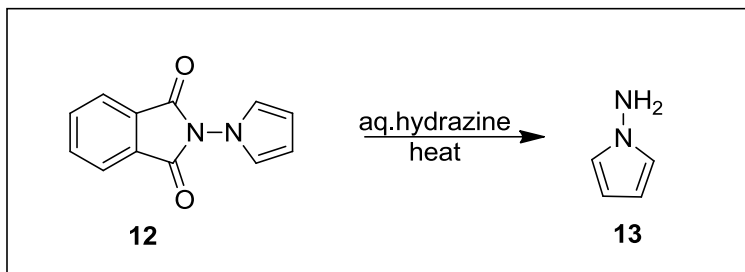


Figure 2.3 Synthesis of N-aminopyrrole **13** from N-phthalimidopyrrole **12**

8.5 g N-phthalimidopyrrole **12** were dissolved in 70 mL of CH₃OH. The suspension turned into yellow solution with the addition of 2.5 mL of 99 % hydrazine monohydrate. The reaction was refluxed for 45-60 min. It was brought into room temperature followed by addition of 1.25 ml of acetic acid. The mixture was refluxed for 20 min again, and then vacuum filtration was performed. The filtrate was evaporated in reduced pressure, and the solid residue was treated with 50 ml of 60 % aq. NaOH until complete dissolution of the solid residue. Extraction was carried out using diethyl ether. Then, it was washed with NaHCO₃ and brine. Ether phase was dried with Na₂SO₄, and removed with reduced pressure. The yield of the compound **13** was about ~65 % [137-138]. It had ¹H NMR (400 MHz, CDCl₃) δ (ppm) 4.8 (brs, 2H), 6.1 (dd, 2H) and 6.7 (dd, 2H) ppm.

2.3.3.4. Synthesis of 1,1'-Bipyrrole **14**

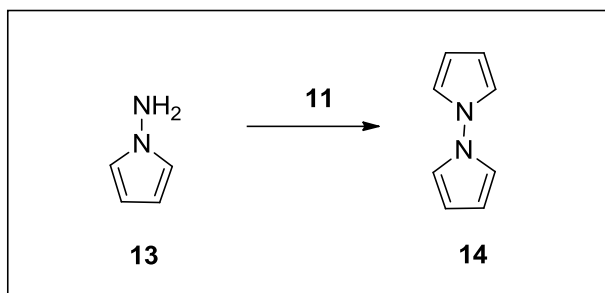


Figure 2.4 Synthesis of 1,1'-bipyrrole **14** from N-aminopyrrole **13**

1 g N-aminopyrrole **13** was dissolved in 20 mL of 1,4-dioxane. Then, 2 mL 2,5-dimethoxytetrahydrofuran **11** were added into flask. Color of solution turned from dark yellow to light green. The solution was refluxed for 3 days, and then 4 ml 5 N HCl were added while the flask was warm. Color became brown. The solution was extracted with n-hexane four times (4 x50 mL). Hexane was removed with reduced pressure after it was dried over Na₂SO₄. Yield of the compound **14** was about 35 % [135]. ¹H NMR (400 MHz, CDCl₃) δ (ppm) 6.1 (dd, 4H) and 6.8 (dd, 4H) ppm

2.3.3.5. Synthesis of 1,4-Bis(2-thienyl)butane-1,4-dione **17**

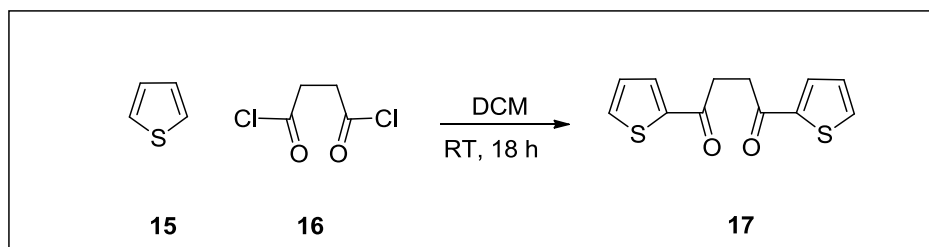


Figure 2.5 Synthesis of 1,4-Bis(2-thienyl)butane-1,4-dione **17**

1.6 g AlCl₃ were added into 10 mL of DCM in a round flask. 575 μL of succinyl chloride **16**, 1.0 mL of thiophene **15** and 2.5 mL of DCM in a funnel were added into flask dropwisely. Color of mixture turned red from yellow. It was stirred at room temperature for 18 h. Grinded ice and 0.5 mL of concentrated HCl were added into the flask for quenching, respectively. The reaction was further stirred for 2.5 hrs. Organic phase was washed two times with 1M HCl, two times with H₂O, two times with NaHCO₃. Then it was dried over Na₂SO₄. Column chromatography (SiO₂, CH₂Cl₂: hexane (1: 4)) and the treatment of charcoal were carried out for purification, respectively. Yield of the compound **17** was 72 % [139]. ¹H-NMR: (400 MHz; CDCl₃) δ (ppm) 3.38 (s, 4H); 7.13 (dd, 2H); 7.63 (dd, 2H); 7.80 (dd, 2H); ¹³C-NMR: (100 MHz; CDCl₃) 33.20; 128.18; 132.15; 133.69; 143.78; 191.4.

2.3.3.6. Synthesis of 1-(1H-pyrrol-1-yl)-2,5-di(thiophen-2-yl)-1H-pyrrole (SNSN) **18**

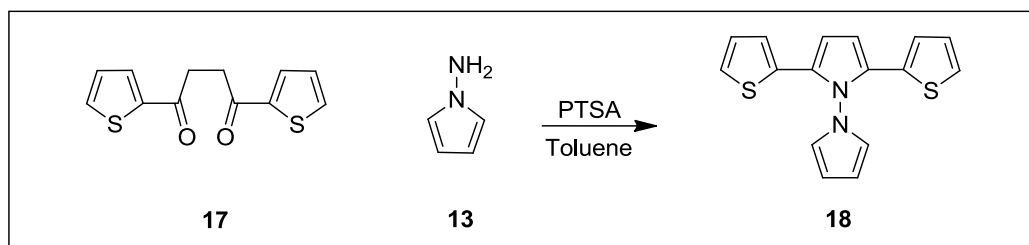


Figure 2.6 Synthesis of SNSN **18**

1,4-Dithien-2-yl-butane-1,4-dione **17** (178 mg, 0.71 mmol), 1-aminopyrrole **13** (290 mg, 3.56 mmol), and *p*-toluenesulfonic acid (PTSA, 45.0 mg, 2.6 mmol) were all added into toluene (30 mL). The reaction was refluxed for about 120 mins via a Dean–Stark apparatus. The reaction was followed by thin layer chromatography. The removal of solvent was performed under reduced pressure, and then the left over was washed with CHCl₃ and water. The removal of CHCl₃

was done under reduced pressure. The recrystallization of left over was done with about 5.0 mL of ethyl acetate and the product **18** was acquired as white crystals in a 60% yield. M.p. 186–189 °C. ^1H NMR (300 MHz, CDCl_3): δ (ppm) 7.15 (dd, $J = 1.0, 5.2$ Hz, 2H); 6.89 (dd, $J = 3.7, 5.0$ Hz, 2H); 6.85 (t, $J = 2.2$ Hz, 2H); 6.52 (s, 2H); 6.36 (m, 4H). ^{13}C NMR (75 MHz, CDCl_3): δ 131.6, 129.0, 127.2, 123.6, 121.9, 121.7, 108.4, and 106.5.

2.3.3.7. Electropolymerization and Characterization of SNSN **33**

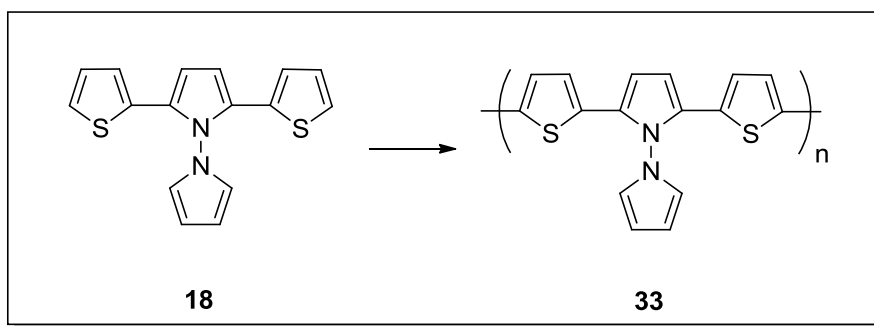


Figure 2.7 Electrochemical polymerization of SNSN **33**

Electrolyte solution employed was 0.1 M tetrabutylammonium perchlorate (TBAP), the supporting salt, in freshly prepared dichloromethane (DCM) distilled over CaH_2 under N_2 atmosphere. Working electrode was a platinum disk (0.02 cm^2), and platinum wire were employed as the counter electrode. Reference electrode was Ag/AgCl in a 3 M NaCl(aq) solution.

Repetitive cycling at 100 mV/s scan rate or steady potential electrolysis of the monomer **18** led to film of PSNSN **33**. Then, the film on working electrode was washed with DCM. Then, it was placed into a cell consisting of only 0.1 M TBAP/DCM electrolyte solutions (no monomer at all) for examining the redox behavior of the PSNSN film after the polymerization.

Spectroelectrochemical studies were carried out using an indium–tin oxide (ITO, Delta Tech. 8–12 Ω , 0.7 cm \times 5 cm) as working electrode together with platinum wire as counter electrode and silver wire as reference electrode in UV cuvette. Calibration of Ag wire as a pseudo-reference electrode was performed with 5 mM electrolyte solution of ferrocene/ferrocenium couple. Electropolymerization of 3.0×10^{-2} M of SNSN in 0.1 M TBAP/DCM electrolyte solutions during in situ electrolysis at 1.1 V led to successful coating of polymer on ITO.

The PSNSN film **33** on ITO was switched between the neutral and doped states several times for the equilibration of the film's redox behavior in a monomer-free electrolyte solution prior to optical studies.

2.3.4. Building Block System for Development of Electrochemical Reactors

2.3.4.1. Synthesis of 2-(2,5-di(thiophen-2-yl)-1H-pyrrol-1-yl)ethanamine **35**

0.8 g 1,4-di(thiophen-2-yl)butane-1,4-dione **17**, 1.3 mL ethylene diamine **34** and 0.2 g PTSA were added into dry toluene (30 mL). It was refluxed for about 10 hrs under argon atmosphere with Dean-Stark apparatus. 2-(2,5-di(thiophen-2-yl)-1H-pyrrol-1-yl) ethanamine **35** was purified with silica gel 95:5 (DCM:MeOH). The yield was 90% [140].

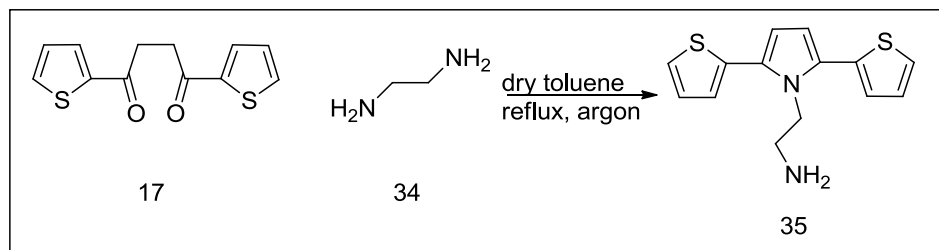


Figure 2.8 Synthesis of compound **35**

2.3.4.2. Synthesis of 2-(4-(bromomethyl)pyridin-2-yl)-4-methylpyridine **37**

3.6 g of 4-methyl-2-(4-methylpyridin-2-yl) pyridine **36**, 3.6 g NBS and 0.16 g of AIBN were added to 100 mL of CCl₄. It was refluxed at approx. 80°C under argon atmosphere for 5 hours. The reaction mixture was cooled and filtered before the solvent was evaporated. The product **37** (1.2 g) was purified with column chromatography (SiO₂, Acetone: CH₂Cl₂ (2: 98)). H-NMR: (400 MHz; CDCl₃) 8.6 (d, 1H), 8.5 (d, 1H), 8.3 (s, 1H), 8.1 (s, 1H), 7.3 (d, 1H), 7.1 (d, 1H), 4.5 (s, 2H), 2.4 (s, 3H) [141].

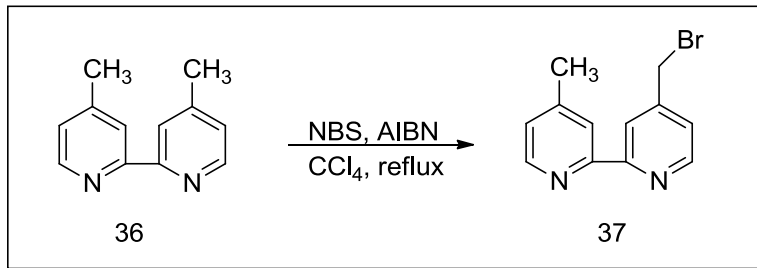


Figure 2.9 Synthesis of compound **37**

2.3.4.3. Synthesis of N-((2-(4-methylpyridin-2-yl)pyridin-4-yl)methyl)-2-(2,5-di(thiophen-2-yl)-1H-pyrrol-1-yl)ethanamine **38**

110 mg 2-(2,5-di(thiophen-2-yl)-1H-pyrrol-1-yl)ethanamine **35** and 90 mg 2-(4-(bromomethyl)pyridin-2-yl)-4-methylpyridine **37** were dissolved in 7 ml of dry ACN and 3 ml of dry DMF in the presence of 34 mg K₂CO₃ and 3 mg of KI. It was mixed for approx. 3.5 hrs at 35°C. The solvent was evaporated. The product **38** (110 mg) was purified with column chromatography (SiO₂, MeOH: CHCl₃ (2: 98)). H-NMR: (400 MHz; CDCl₃) 8.4 (t, 2H), 8.1 (d, 2H), 7.2 (dt, 2H), 7.0 (m, 6H), 6.2 (s, 2H), 4.3 (t, 2H), 3.6 (s, 2H), 2.7 (t, 2H), 2.4 (s, 3H), 1.4 (broad s, 1H). ¹³C NMR (100 MHz, CDCl₃): δ 156.2, 155.9, 150.3, 149.2, 149.0, 148.1, 134.6,

128.5, 127.4, 126.4, 125.5, 124.7, 122.7, 122.0, 120.3 111.2, 52.1, 49.2, 44.9, 21.2

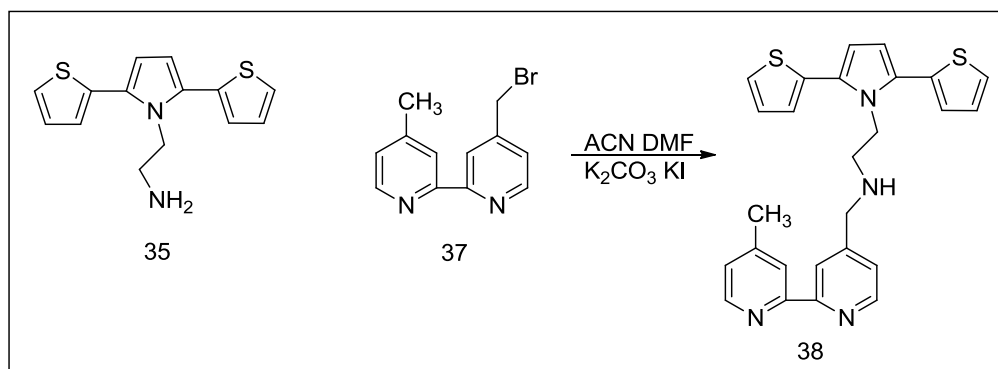


Figure 2.10 Synthesis of compound **38**

2.3.4.4. Synthesis of N-((2-(4-methylpyridin-2-yl)pyridin-4-yl)methyl)-2-(2,5-di(thiophen-2-yl)-1H-pyrrol-1-yl)ethanamine-Rh Complex **39**

15.6 mg [Cp*RhCl₂]₂ in 2 ml of methanol were dropwise added into 23 mg of N-((2-(4-methylpyridin-2-yl)pyridin-4-yl)methyl)-2-(2,5-di(thiophen-2-yl)-1H-pyrrol-1-yl) ethanamine **38** in 4 ml of methanol. It was stirred about half an hour at room temperature. Then, methanol was evaporated. The yield was 100%. H-NMR: (400 MHz; CDCl₃) 8.78 (s, 1H), 8.69 (d, 1H), 8.67 (d, 1H), 8.59 (s, 1H), 7.61 (d, 1H), 7.51 (d, 1H), 7.26 (d, 2H), 7.13 (d, 2H), 7.05 (dd, 2H), 6.25 (s, 2H), 4.38 (t, 2H), 3.85 (s, 2H), 2.8 (t, 2H), 2.6 (s, 3H), 1.70 (s, 15H). ¹³C NMR (100 MHz, CDCl₃): δ 155.3, 154.1, 153.0, 150.6, 150.5, 134.5, 129.2, 128.6, 127.6, 127.4, 126.3, 125.6, 125.4, 123.5, 111.0, 96.8, 96.7, 51.3, 48.9, 44.7, 21.4, 9.1, HRMS: Calculated : 729.1360 g/mol, Founded: 729.1368 g/mol

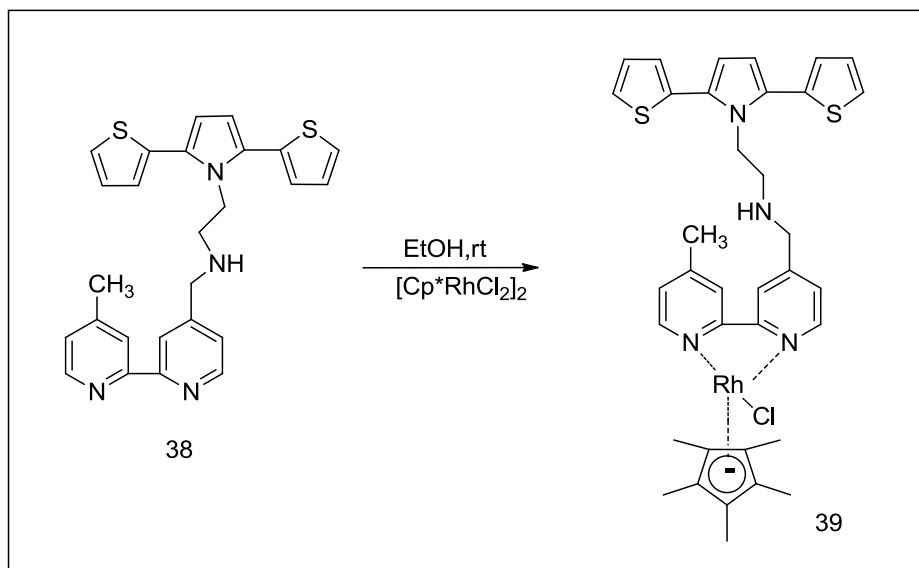


Figure 2.11 Synthesis of compound **39**

2.3.4.5. Synthesis of 4-((2-(2,5-di(thiophen-2-yl)-1H-pyrrol-1-yl) ethylamino) methyl) phenylboronic acid **41**

195 mg 2-(2,5-di(thiophen-2-yl)-1H-pyrrol-1-yl)ethanamine **35** and 105 mg 4-formylphenylboronic acid **40** were added into 10 ml of dry toluene and 10 ml of methanol. Then, 88 mg of NaCNBH₃ was added into the reaction mixture followed by stirring at room temperature under argon atmosphere overnight. The product **41** was purified with silica gel (solvent: ethyl acetate). The amount obtained was 205 mg. Yield was 72%. H-NMR: (400 MHz; d-dms_o) 7.95 (s, 2H), 7.7 (d, 2H), 7.55 (d, 2H), 7.1 (m, 6H), 6.3 (s, 2H), 4.25 (t, 2H), 3.5 (s, 2H), 2.56 (t, 2H). HMRS: Calculated MH⁺: 409.1216 g/mol, Founded MH⁺: 409.1223 g/mol.

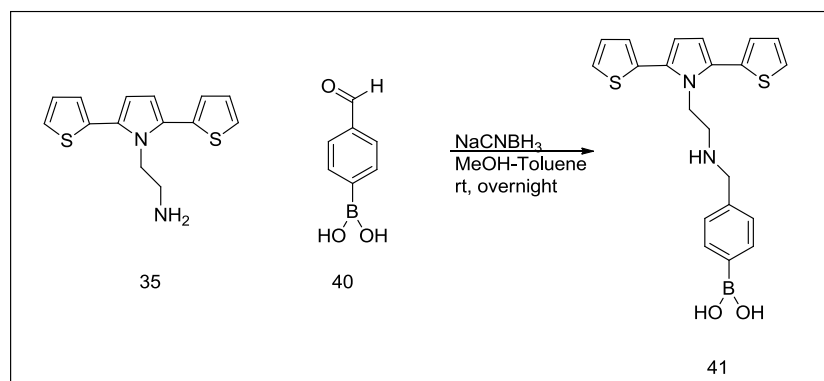


Figure 2.12 Synthesis of compound **41**

2.3.4.6. Synthesis of 5-((2-(2,5-di(thiophen-2-yl)-1H-pyrrol-1-yl)ethylamino)methyl)thiophen-2-yl-2-boronic acid **43**

130 mg 2-(2,5-di(thiophen-2-yl)-1H-pyrrol-1-yl)ethanamine **35** and 73 mg 5-formylthiophen-2-yl-2-boronic acid **42** were added into 10 ml of dry toluene and 10 ml of methanol. Then, 60 mg NaCNBH_3 were added into a reaction mixture. It was stirred at room temperature under argon atmosphere overnight. The product **43** was purified with silica gel (S: EtAc). Amount obtained was 110 mg. The yield was 56%. H-NMR: (400 MHz; d-dmsO) 7.98 (s, 2H), 7.42 (d, 2H), 7.32 (d, 1H), 7.01 (m, 4H), 6.7 (d, 1H), 6.18 (s, 2H), 4.11 (t, 2H), 3.6 (s, 2H), 2.52 (t, 2H).

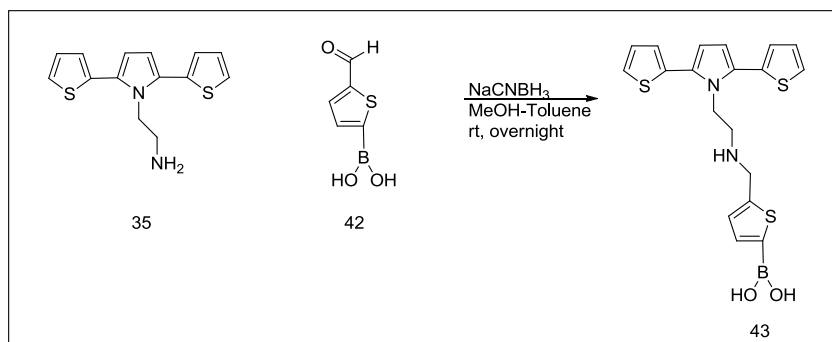


Figure 2.13 Synthesis of compound **43**

2.3.4.7. Synthesis of SNS-EA-Ph-BA-NAD 45

6.5 mg NAD⁺ **44** (1 ev) and 3.6 mg 4-((2-(2,5-di(thiophen-2-yl)-1H-pyrrol-1-yl)ethylamino)methyl) phenylboronic acid **41** (1.1 eV) were added into 0.7 mL d-dmsol. It was stirred overnight at room temperature. The white suspension became soluble with time.

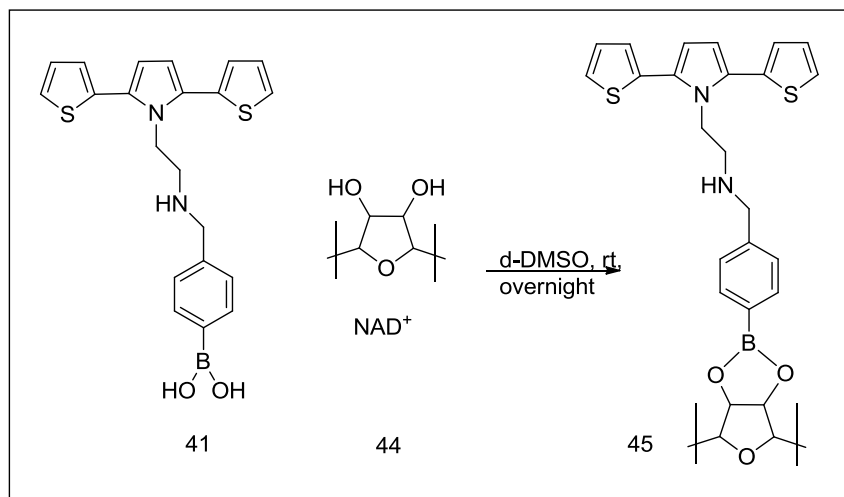


Figure 2.14 Synthesis of compound **45**

2.3.4.8. Synthesis of 1-(3-(triethoxysilyl)propyl)-2,5-di(thiophen-2-yl)-1H-pyrrole **47**

25 mg 1,4-bis(2-thienyl)butane-1,4-dione **17** and 0.2 mL 3-(triethoxysilyl)propan-1-amine **46** and 250 mg of Al₂O₃ were placed into a shlenk tube. It was stirred about 30 min under microwave conditions (800 W). It was passed through a short silica column with dichloromethane to eliminate impurities. ¹H-NMR: (400 MHz; CDCl₃) 0.4 (t, 2H), 1.1 (t, 9H), 1.60 (m, 2H), 3.62 (q, 6H), 4.05 (t, 2H), 6.26 (s, 2H); 7.00 (d, 4H); 7.25 (t, 2H).

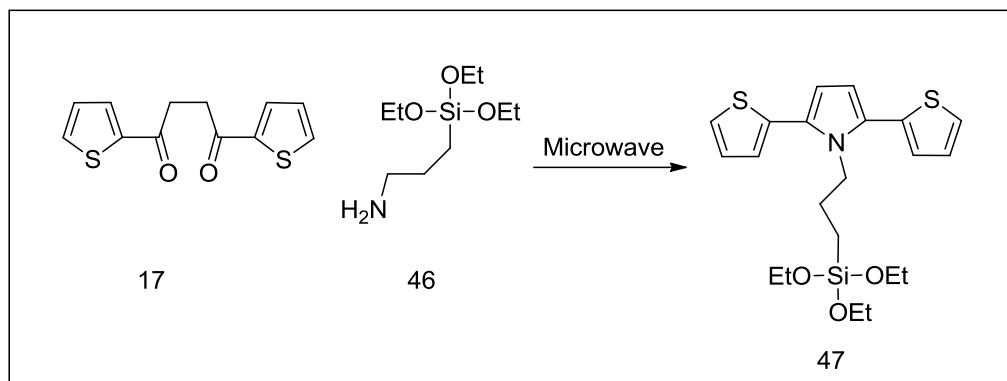


Figure 2.15 Synthesis of compound 47

2.3.4.9. Synthesis of Silane-Boronic-NAD Compound 51

0.22 mL compound 48 (1 mmol) and 155 mg compound 49 (1 mmol) in 20 mL THF were refluxed at 80 °C about 1 hour to obtain compound 50. After cooling to room temperature, 63.2 mg NAD (0.095 mmol) in 2 mL 10mM pH= 8.8 phosphate buffer was dropwise added into 2.0 mL compound 50-THF solution (0.095 mmol compound 50). Yellow suspension turned into yellow solution. The mixture was stirred about 2 hrs at room temperature before lyophilization.

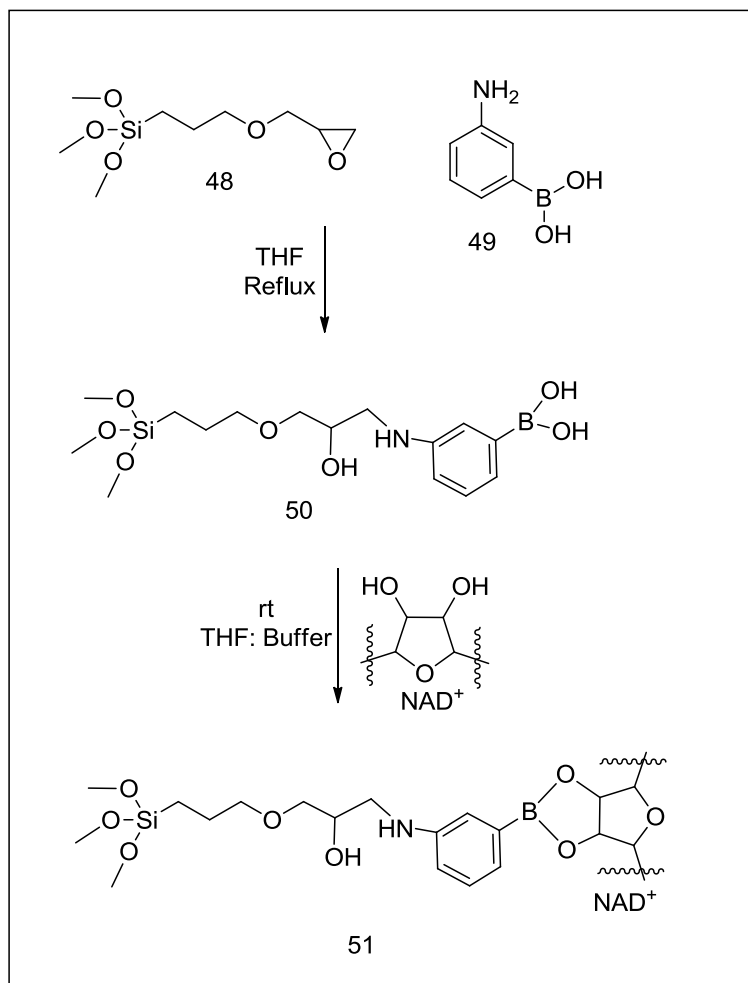


Figure 2.16 Synthesis of compound **51**

2.3.5. Pyrrole Coupling Chemistry: Investigation of Electroanalytic Spectroscopic and Thermal Properties of N-Substituted Poly(Bis-Pyrrole) Films

2.3.5.1. Materials and Methods

2,5-Dimethoxytetrahydrofuran, 4,7,10-trioxa-1,13-tridecanodiamine, acetic acid, CH₂Cl₂, NaClO₄, LiClO₄, KClO₄, AgBF₄, and tetrabutylammonium perchlorate

(TBAClO₄) were acquired from Aldrich and Merck and were used without further purification. Acetonitrile was dried over CaH₂ and distilled under an inert atmosphere before use. The monomer **I** was synthesized as previously described [123].

The polymers were synthesized from 0.1 M TBAClO₄ in an acetonitrile solution containing monomer **I** via repetitive cycling at a scan rate of 100 mV/s between 0.0 V and 1.1 V, or steady potential electrolysis at 1.1 V vs Ag/AgCl. The coating of the polymer on a platinum electrode (BAS, 0.02 cm²) or indium-tin oxide (ITO, Delta Tech. 8–12 Ω, 0.7 x 5 cm) was performed. A platinum wire was employed as the counter electrode and Ag/AgCl in a 3 M NaCl(aq) solution as the reference. After polymerization is completed, the films were washed with acetonitrile in order to remove monomer and oligomeric species and then were passed into a different cell having an electrolytic solution without monomer. Electrochemical production and measurements were done with VoltaMaster 4 potentiostat-galvanostat.

For spectroelectrochemical studies, platinum and silver wires were used as the counter and the pseudo-reference electrodes, respectively. Calibration of the latter electrode was done externally with a 5 mM electrolyte solution of ferrocene/ferrocenium couple. Coating of the polymer film was performed on ITO at 1.1 V and, the film was washed and switched several times between neutral and doped states in order to equilibrate its redox behavior in a monomer-free electrolytic solution. *In-situ* spectroelectrochemical studies were performed using a Hewlett–Packard 8453A diode array spectrometer. The spectra of transmittance and absorption for **PI** were taken *in-situ* under different potentials. Additionally, the method of square wave potential was employed to look the switch ability of the **PI** film between its neutral and doped condition.

For the investigation of the thermal analysis of PI film, DSC 910/TA and Perkin–Elmer TGA systems were used. FT-IR spectra were recorded with a Bruker Vertex 70 Spectrophotometer.

The four-probe technique was used for the estimations of electrical conductivity. The designation of electrical contacts was made by painting pure silver paste over the surface of film employing a proper contact shape.

Preconcentration of Ag^+ ions was performed using the PI film (100 mC/cm^2) under a constant potential of -0.5 V for 30 s in $0.1 \text{ M TBAClO}_4/\text{acetonitrile}$ containing various concentration of AgBF_4 solution, and then voltammetric recognition of the silver content was carried out in the same electrolytic medium at a scan rate of 50 mV/s .

CHAPTER 3

RESULTS AND DISCUSSION

3.1. Thermosensitive Biodegradable mPEG-PLLA Block Copolymers: Syntheses, Characterizations and Applications in Drug Delivery Systems

Camptothecin and its derivatives, especially FDA approved topotecan and irinotecan, become more popular every day in the clinical studies due to their therapeutic effects on human cancer. Sales of these two anti-cancer drugs reached to US-\$1 billion in annual worldwide reports [142]. Intensive research on these drugs was performed for last 10 years to improve their clinical performance. One of the major shortcomings of camptothecin family is the hydrolyzation of the lactone ring moiety of the drug under physiological conditions *i.e.* at pH 7 or above, revealing low biologic activity and high toxicity [143]. Thus, lactone ring was a crucial structural requirement for both passive diffusion of drug into cancer cells as well as desired drug interaction with the pharmacological target topoisomerase 1.

Here, we describe how we developed an efficient and simple strategy for maintaining lactone moiety of camptothecin and topotecan via biodegradable biocompatible PLLA-mPEG diblock thermo-sensible gels for a model application of local injection in breast cancer as well as potential application in the primary malignant brain tumor. This methodology may constitute an alternative approach over treatments of surgery, radiotherapy or chemotherapy via systemic way,

which produced only modest increases in median survival time from a few months to over a year for primary malignant brain tumors. Also, this system avoids using organic solvents, which may cause toxicity, aggregation problems, and extensive washing steps in the nanoparticle and liposome formulations [144, 145]. The last but not the least; blood brain barrier, which is a very crucial physical and physiologic barrier regulating the entrance of molecules to the brain, can be bypassed by the local injection of these drug loaded polymeric gels to directly the tumor, and this platform provides high drug concentrations at the target site without causing systemic toxicity.

3.1.1. Synthesis of Poly(L-Lactide) Homopolymer

Synthesis of poly(L-lactide) was carried out using L-lactide as monomer, benzyl alcohol as coinitiator, stannous octoate ($\text{Sn}(\text{Oct})_2$) as catalyst. Mechanism of L-lactide polymerization is coordination-insertion, which was discussed in Figure 1.3 at introduction part. Stannous octoate was selected for three main reasons. First, the catalysis is highly efficient. It has almost complete conversion even at catalyst/monomer ratios as high as $1:10^4$ [4]. Second, 99 % optically pure poly(L-lactide) can be synthesized even at $150\text{ }^\circ\text{C}$. Third, its toxicity is considerably low compared to other heavy metal salts.

The molecular weight of the PLLA homopolymer was determined by the ratio of the intensity of phenyl protons of benzyl alcohol and methyl protons of lactide unit in ^1H NMR (Table 3.1).

Table 3.1 The molecular weight of PLLA homopolymers

ID	\bar{M}_n	RU of Lactide	Lactide /Sn (Oct)₂	Lactide / BzOH
19	4200	58	100	21
20	7670	105	225	48

RU: Repeating unit

3.1.2. Syntheses of mPEG-PLLA Diblock Copolymers

The block copolymerization reaction of mPEG with L-lactide is shown in Figure 3.1. PLLA-mPEG diblock copolymer was synthesized in the presence of stannous octoate under argon atmosphere. Polymerization mechanism is the similar way with poly(L-lactide) mechanism.

Two different molecular weights of mPEG (2000 and 5000 g/ mol) were used to synthesize copolymers because higher molecular weight of PEG (above ~10k) is inappropriate for filtration through membrane of human kidney due to being wide hydrodynamic radius of the PEG in aqueous phase [23]. Also, we adjusted hydrophobic PLLA length by changing amount of L-lactide at constant mass of hydrophilic mPEG as seen in Table 3.2.

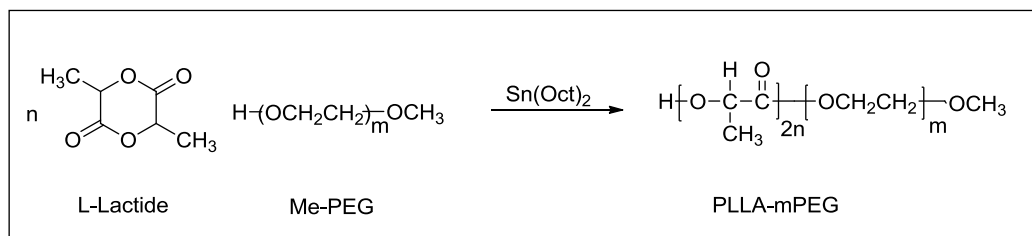


Figure 3.1 PLLA-mPEG polymerization starting from L-lactide and mPEG

Table 3.2 The molecular weight of PLLA-mPEG diblock copolymers

ID	\bar{M}_n (g/mol)	RU of Lactide	Lactide/Sn (Oct)₂	Mw of mPEG	Lactide/ mPEG
21	10120	112	140	2000	58
22	7305	73	84	2000	35
23	3665	23	42	2000	18
24	5645	50	42	2000	18
25	12900	110	140	5000	58
26	8860	54	84	5000	35
27	7500	35	56	5000	23

RU: Repeating unit

PLLA-mPEG copolymers were characterized by ¹H NMR and ¹³C NMR spectroscopy. Main chain units and PEG-connecting part have resonances in the 5.2–5.1 ppm range (CH) and in the 1.5–1.4 ppm range (CH₃). Signal at 3.63 ppm is CH₂ units in PEG block while peak at 3.38 is methoxy protons at the end of PEO segment. On the other hand, carbonyl carbon, methine carbon, and methyl carbon in lactide blocks showed peaks at 169, 69, and 17 ppm, respectively. Methylene carbon in the PEG segment had resonance at 71 ppm. Methylene and methine carbons were identified by using DEPT-90. The α-methylene protons of PLA-connecting PEG units (PLA-COO-CH₂-) and CH protons of the hydroxylated lactyl end units showed peaks in the range of 4.1-4.3 ppm. No peaks at in the 5.0–4.9 ppm range and at 4.0 ppm proved an absence of carboxylated lactyl end units and of free lactic acid [30]. This showed that homopolymerization of L-lactide did not take place as side product. The representative ¹H NMR spectrum of diblock copolymer was shown in Figure 3.2.

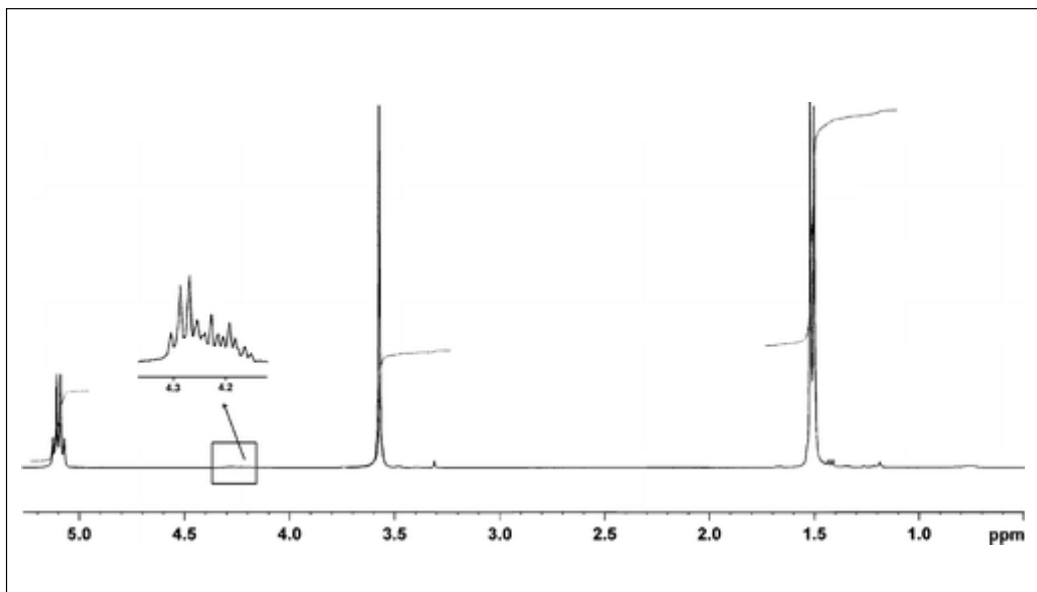


Figure 3.2 Representative $^1\text{H-NMR}$ of copolymer **21**

Copolymers were characterized with FTIR and ATR-FTIR, as well. Representative FTIR spectrum of copolymer **25** was shown in Figure 3.3. The -C=O vibration of the copolymer was observed at 1757 cm^{-1} . The -C-H vibrations of both blocks overlapped around 2950 cm^{-1} . Also, the -C-O-bending of the poly(L-lactide) and mPEG units of the copolymer was observed between 1040 to 1220 cm^{-1} along with -C-H bending of the copolymer.

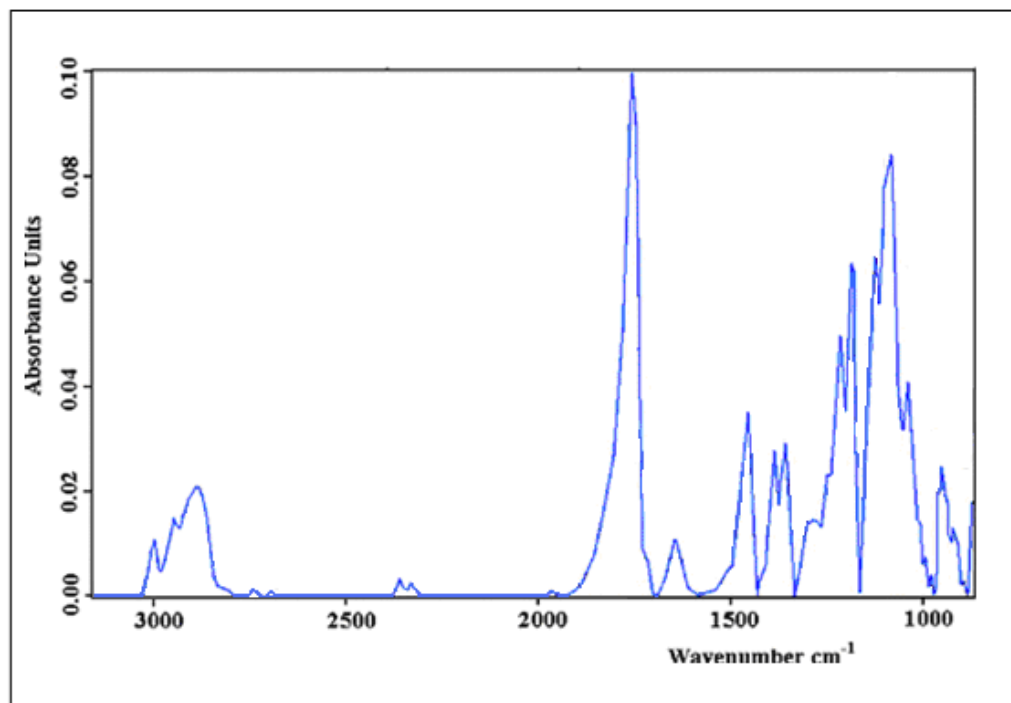


Figure 3.3 FTIR spectrum of copolymer **25**

3.1.3. Properties of mPEG-PLLA Diblock Copolymers

3.1.3.1. Copolymer Film Preparation

For the surface characterization, films of PLLA homopolymer **19**, diblock copolymers **21** and **25** were prepared using the solvents of chloroform and toluene at 20 mg/mL polymer concentration. A mechanical dipper with a removal rate of 67 mm/min was used for coating of glass slides with polymer solution. At each experiment, the slides were kept in 2 min inside of polymer solution. A vacuum oven was employed to dry coated slides [132].

3.1.3.2. Comparison of Surface ATR of Copolymer Films

One alternative to the analysis of the surface composition of blend and copolymer films is to perform ATR-FTIR spectroscopy [146,147]. ATR-FTIR spectra of films of both copolymer **21** and **25** having equal Mn of poly(L-lactide) units (Table 3.2, Mn: 8000 g/mol for lactide parts) were compared. Both -C-H vibrations of poly(L-lactide) and mPEG units of the copolymer overlapped around 2950 cm^{-1} . While -C-H vibrations of the L-lactide part came around 2917 cm^{-1} (left side of the broad peak), the -C-H vibrations of PEG were observed around 2870 cm^{-1} (right shoulder), as shown in Figure 3.4.

In addition, it was observed that the intensity of the -C-H vibrations of PEG increased when the PEG composition of copolymers raised for the constant mass of the poly(L-lactide) part at the surface, as depicted in Figure 3.4.

For quantitative comparisons, we converted transmittance spectrum into absorbance spectrum. For both copolymers the area of all -C-H vibrations seen between 2850 and 2950 cm^{-1} was quantitatively compared with carbonyl vibration of copolymer at 1757 cm^{-1} . It was observed that carbonyl vibrations of copolymer **21** and **25** had the same values as a result of having equal molecular weight of L-lactide units.

The -C-H/-C=O ratio for copolymer **21** was 0.39, while the same ratio for copolymer **25** was 0.86. Similar results were observed when a peak around 1460 cm^{-1} belonging to -C-H vibrations of the PEG and L-lactide units was compared to vibration of the poly(L-lactide) units. As a result, when the PEG component on diblock copolymer increased, the -C-H vibrations of PEG raised at the surface.

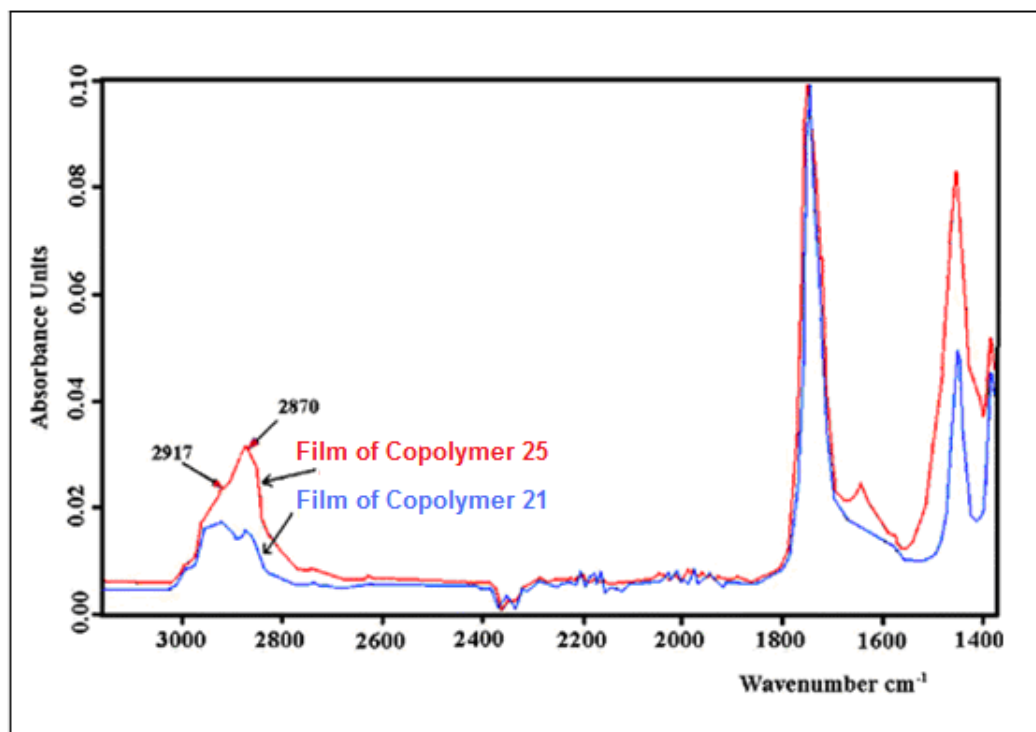


Figure 3.4 Comparison of surface ATR of copolymer Films **21** and **25**

3.1.3.3. Comparison of Bulk FTIR and Surface ATR

-CH₂- of mPEG in the bulk of copolymer **25** was compared with -CH₂- of mPEG of the film of copolymer **25** using with FTIR and ATR-FTIR instruments. While one unit -C=O corresponds to 0.42 -C-H for bulk by the FTIR spectrum, one unit -C=O corresponds to 0.86 -C-H for film by the ATR-FTIR spectrum. Similar results were observed when -CH₂- vibrations of bulk and film of copolymer **21** were examined. One unit carbonyl corresponds to 0.15 -C-H for the bulk of copolymer **21**, while one unit carbonyl corresponds to 0.39 -C-H for the film of copolymer **21**. It was understood that the areas of -CH₂- of mPEG in both of the films were higher than those of the bulk of both copolymers. It seems

that $\text{-CH}_2\text{-}$ of mPEG in the copolymer **21** and copolymer **25** films mostly takes their position at the surface rather than inside. (Figure 3.5)

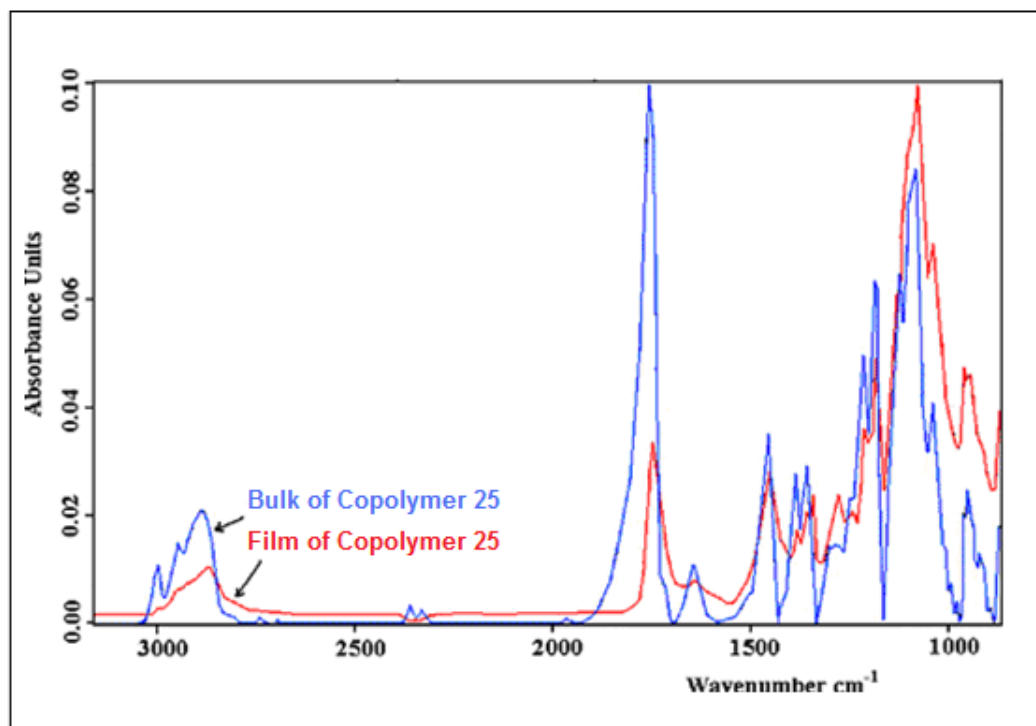


Figure 3.5 Comparisons of bulk FTIR and surface ATR of copolymer **25**

3.1.3.4. Surface Free Energy Properties and Contact Angle Measurements

Surface free energy properties of two types of amphiphilic and semicrystalline diblock copolymers containing poly(l-lactic acid) coupled to (methoxy poly(ethylene glycol) (PLLA-mPEG) having differing block lengths of PEG were investigated by using static and dynamic contact angle measurements, and compared with results obtained from PLLA and MePEG homopolymers. The contact angle results were evaluated by using the van Oss–Good method (acid–base method), and it was determined that the Lewis base surface tension

coefficient (γ^-) of the copolymers increased with an increase of the PEG molar content at the copolymer surface. This result is in good agreement with the transmission FTIR and ATR-FTIR results but not proportional to them, indicating that the surfaces of the copolymers are highly susceptible and that the molecular rearrangement takes place upon contact with a polar liquid drop.

The dynamic contact angle measurements showed that the strong acid–base interaction between the oxygen atoms in the copolymer backbone of the relatively more hydrophilic PEG segments with the Lewis acidic groups of the polar and hydrogen-bonding water molecules enabled the surface molecules to restructure (conformational change) at the contact area, so that the PEG segments moved upward, whereas the apolar methyl pendant groups of PLLA segments buried downward.

Basically the equilibrium water contact angles (θ_e) for homopolymer **19**, copolymer **21**, copolymer **25**, MePEG 2000 and MePEG 5000 were found as 70°, 66°, 49°, 41° and 24°. When the θ_e results are considered, they decrease with the increase of PEG molar content as expected from the hydrophilicity of the PEG blocks due to the presence of polar and hydrogen-bonding oxygen containing ethylene oxide segments within the macromolecule. When the surface free energy components (acid-base) approach is applied, it is clearly seen that the values of the Lewis base surface free energy component (γ_s^-) and total surface free energy of the polymeric substrate (γ_s^{tot}) were mainly variable with a change in the PEG content of the copolymers. The increase of (γ_s^-) with the increase of the PEG content was continuous. [i.e. (γ_s^-): 9.33, 12.37, 20.61, 33.76, 48.93 for homopolymer **19**, copolymer **21**, copolymer **25**, MePEG 2000 and MePEG 5000, respectively]. Finally, surface free energy properties and contact angle measurements of those polymers were studied in depth by the group of Prof. Erbil, and detailed data can be found in literature [132].

3.1.4. Determination and Regulation of Thermosensitivity of the Polymers

To determine of sol-gel temperature, various amounts of copolymer **23** and distilled water were firstly mixed to prepare suspensions of 3, 5, 10, and 30 % (mg/ μ l). All suspensions formed a sol property at room temperature. It was concluded that it was a requirement to increase the polymer concentrations to obtain suspension having gel property at room temperature. Then 45 % polymer suspension was tested to find gel to sol temperature. While the suspension was gel at RT, it started to flow immediately at 35-37 °C.

We selected the copolymer **23** as the reference sample for the future gel formations. On the other hand, we tested possible gel-to sol properties of other copolymers (Table 3.3). Among them, suspension of copolymer **26** at 30 % formed a gel at RT while it was sol at 30 °C. Lastly, copolymers **22**, **24** and **25** at low concentration (3 %) were not homogeneously suspended because of higher lactide content relatively to m-PEG moiety in diblock chain.

Table 3.3 Determination of sol-gel temperature

ID	Sol Gel Temp. °C	Conc. % (mg/ μ l)
19	N.O.	3
20	N.O.	3
21	N.O.	3
22	N.O.	3
23	37	45
24	N.O.	3
25	N.O.	3
26	30	30
27	V.S.	30

N.O.: Not Observed, VS: very soluble

3.1.5. Camptothecin Class Topoisomerase I Anticancer Drugs: Structures, Clinic Limitations and Properties

3.1.5.1. Camptothecin

Camptothecin (CPT), pentacyclic quinoline alkaloid, was firstly isolated from the Chinese tree *camptotheca acuminata* in 1966 (Figure 3.6) [148].

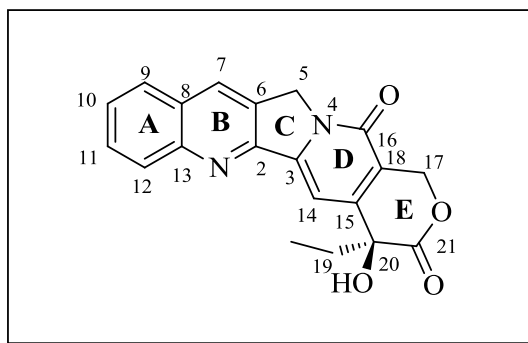


Figure 3.6 Structure of camptothecin

It has been pointed out that camptothecin remarkably shows anticancer property by inhibiting DNA topoisomerase I [149]. Extraction of CPT from the intact plants, *Camptotheca acuminata* and *Nothapodytes foetida*, is the main source of CPT for pharmaceutical market (Figure 3.7). Its semi-synthetic derivatives synthesized from CPT plants are topotecan and irinotecan anticancer agents. These two anti-cancer drugs have been approved by FDA and have nearly US \$1 billion in annual reported worldwide sales [142].



Figure 3.7 CPT producing plants

3.1.5.2. Clinic Limitation for CPT Derivatives

Hydrolyzation of the lactone ring moiety of camptothecin under physiological conditions *i.e.* at pH=7 or above leads to an inactive and more water soluble carboxylate form (Figure 3.8) [150-153]. The clinical results showed that biological activity of carboxylate form was weak with regard to xenograph models and unexpected side effects consisting of hemorrhagic cystitis and myelotoxicity, which led to suspension of the trials [154,155]. CPT took more attentions just after its cellular target was discovered as DNA topoisomerase I. Thus, more water soluble CPT derivatives such as topotecan and irinotecan were synthesized for clinical applications [149,156,157].

In conclusion, closed α -hydroxy lactone ring moiety must be intact for antitumor activity because lactone ring was a crucial structural requirement for both passive diffusion of drug into cancer cells as well as desired drug interaction with the pharmacological target topoisomerase 1 [143].

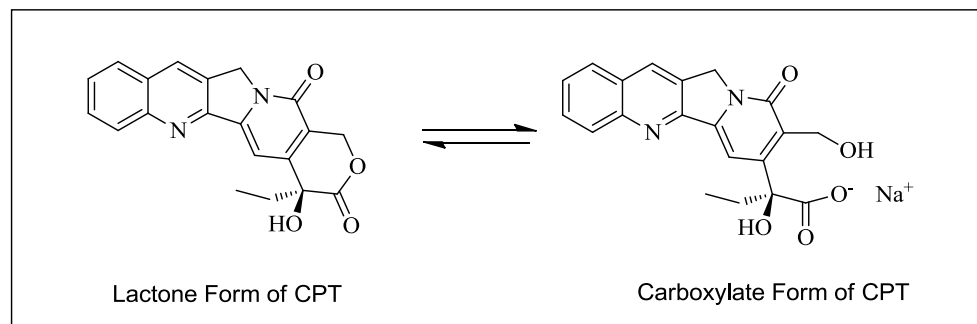


Figure 3.8 Camptothecin hydrolysis to water soluble sodium salt.

3.1.5.3. Topotecan (TPT)

Topotecan, an analogue of CPT, (9-[[dimethylamino) methyl]-10-hydroxycamptothecin) (Figure 3.9) carries superior properties like higher water solubility and biological activity than CPT. It was approved by FDA for use as antitumor agent in the treatment of recurrent ovarian cancer in 1996 as well as for patients small-cell lung cancer (SCLC) in 1998. TPT activity against a variety of tumor types such as head and neck, prostate, breast, melanoma, cervical, gastric, pancreatic, myelodysplastic syndrome, myeloma, renal cell, glioma, uterine hepatocellular cancer has been observed [158-160].

As with CPT, lactone form of TPT readily goes through a nonenzymatic reversible hydrolysis at physiological pH, leading to carboxylate form. Therefore, formulation method of topotecan plays important role for efficient therapy. Liposomal encapsulation can be regarded as one of the ways for the delivery of TPT. Liposomal encapsulation provided the protection of lactone species inside liposome, which increased survival rates in animal xenograft models when compared with free topotecan [144,161,162].

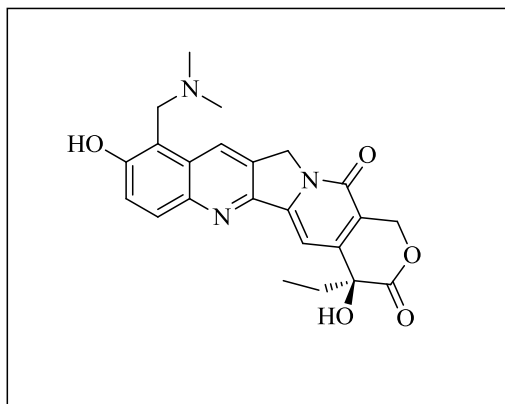


Figure 3.9 Structure of topotecan

Synthesis of semi-synthetic of topotecan was accomplished in two steps starting from 20(S)-CPT. First, 20(S)-CPT was converted into 10-hydroxy CPT through a reduction-oxidation sequence followed by introducing dimethyl amine in aqueous formaldehyde and acetic acid (Figure 3.10) [163].

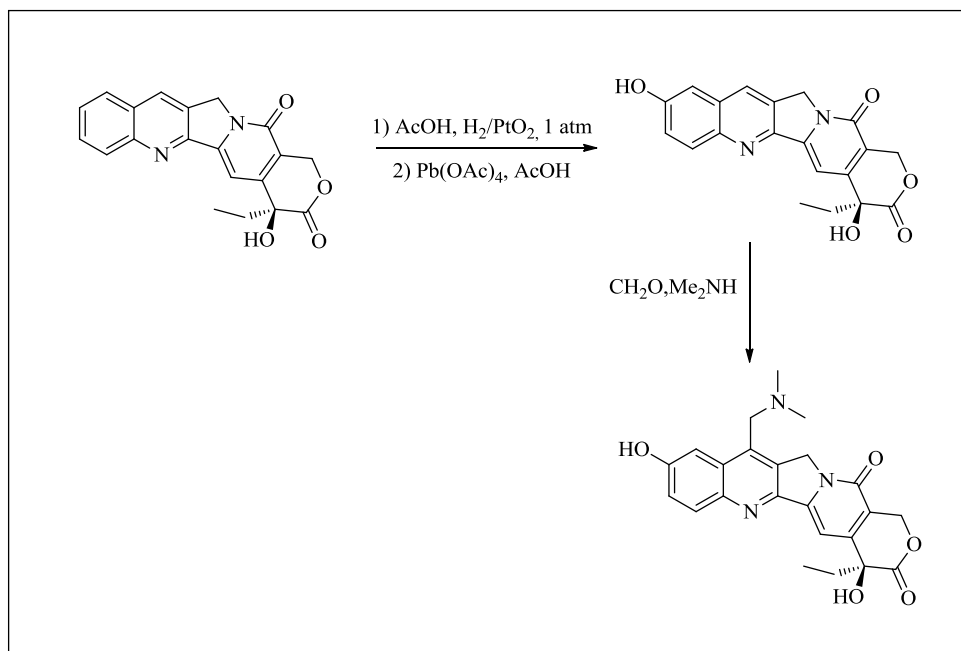


Figure 3.10 Synthesis of topotecan

3.1.5.4. Mechanism of Action of Camptothecin with Topoisomerase 1

Human DNA topoisomerase I is composed of a 765-amino-acid nuclear enzymes [164]. It alters topological states of DNA structure [157]. It has key role for DNA replication, transcription, and recombination. CPT and its derivatives bind noncovalently topo 1 in cleavable complexes, stabilizes them and interfering with DNA religation [165]. Single and double-strand DNA breaks are produced. Premature termination of replication and inhibition of transcription are observed [166]. It eventually leads to cell death [167,168]. Mechanistic action of CPT to topo I catalytic process is seen in Figure 3.11.

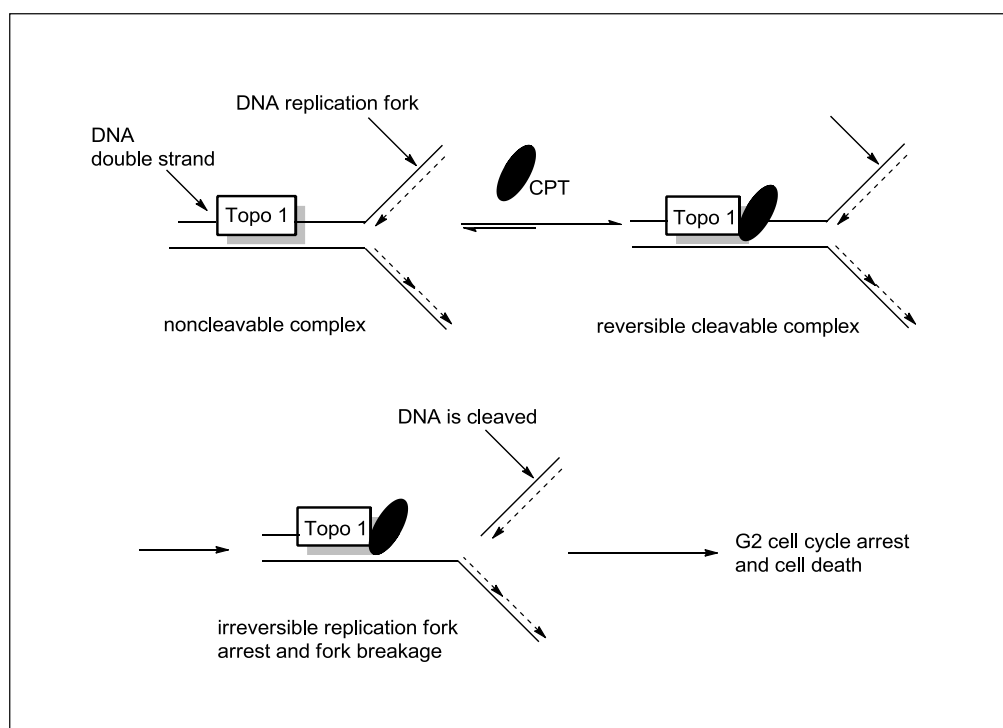


Figure 3.11 Mechanism of action of camptothecin

3.1.6. Thermosensitive mPEG-PLLA Drug Delivery Systems

3.1.6.1. Formulation of the Polymer-Drug Conjugate

Topotecan or camptothecin anti-cancer drugs were efficiently loaded into gels, respectively. Loading ratios of them were selected as 0.015, 1.0, and 10 %. Homogenous dispersion of drugs within gels was obtained for all ratios.

3.1.6.2. Stability of the Drugs

3.1.6.2.1. Fluorescence Spectroscopy Analysis

Hydrolyses of free camptothecin, free topotecan, camptothecin in gel and topotecan in gel at pH: 7.4 were evaluated by the ratio of fluorescence intensities of two different emission wavelengths vs. time. The ratios of intensities at two different emissions of wavelength of pure lactone (R_L) and pure carboxylate (R_C) were also measured for each species and thereafter employed as constants.

Concentrations of ring closed (state of lactone) and opened form (carboxylate) of drugs were referred to as [L] and [C], respectively. Scatchard plots [169] were used to evaluate the [L]/[C] ratio.

An intensity of fluorescence emission intensity $I(\lambda_1)$ of a compound consisting of both lactone and carboxylate states for a specific time could be described as

$$I(\lambda_1) = I_C(\lambda_1) * [C] + I_L(\lambda_1) * [L] \quad (\text{Equation 1})$$

Intensities for fluorescence emission of L and C can be expressed as I_L and I_C .

Similarly for $I(\lambda_2)$,

$$I(\lambda_2) = I_c(\lambda_2) * [C] + I_L(\lambda_2) * [L] \quad (\text{Equation 2})$$

The ratio at fluorescence intensities of the compound at λ_1 and λ_2 wavelengths gives R factor.

$$R = I(\lambda_1) / I(\lambda_2) \quad (\text{Equation 3})$$

Then $[C]/[L]$ ratio can be simply written as

$$[C] / [L] = [I_L(\lambda_2) / I_c(\lambda_2)] * (R_L - R) / (R - R_C) \quad (\text{Equation 4})$$

Lactone fraction $[L, \%]$ in the compound can be determined as

$$[L, \%] = 100 \% / \{ 1 + [I_L(\lambda_2) / I_c(\lambda_2)] * (R_L - R) / (R - R_C) \} \quad (\text{Equation 5})$$

Scatchard plots of hydrolyses are plotted as the percentage of lactone $[L, \%]$ or carboxylate percentage $[C, \%]$ with respect to time (t). Each point is at least three independent data.

3.1.6.2.2. Analysis of R_L and R_C Values of Free CPT and TPT via Fluorescence Spectroscopy

R_L and R_C values are critical factors for the estimation of the lactone percentage $[L, \%]$. Fluorescence spectroscopy was employed to measure intensities of free camptothecin and topotecan in DMSO, further diluted with tris buffer at either acidic or basic pH conditions. Intensities were recorded at two different emission wavelengths as shown in Table 3.4. Then R_L and R_C were found taking the ratio of those intensities measured. Those values were indicated in Table 3.4.

Table 3.4 R_L and R_C values for free CPT and TPT

ID	λ excitation (nm)	λ_1 emission (nm)	λ_2 emission (nm)	R_L	R_C
Free CPT	370	432	480	3.43	2.18
Free TPT	381	516	580	4.86	5.41
CPT in gel	370	432	480	2.39	2.07
TPT in gel	381	516	580	2.89	3.70

3.1.6.2.3. Analysis of R_L and R_C Values for CPT and TPT in Gel via Fluorescence Spectroscopy

Similar methodology above was used for the analysis of R_L and R_C , as well. Intensities of pure carboxylate and lactone forms of CPT and TPT at different emission wavelengths in copolymer gel were measured at both acidic and basic pH conditions. Then R_L and R_C values for CPT and TPT in gel were calculated as shown in Table 3.4.

3.1.6.2.4. Analysis of Lactone Conversion of Free CPT and TPT via Fluorescence Spectroscopy

Kinetics of lactone hydrolysis in free CPT and TPT at pH=7.4 were monitored with dual wavelength fluorescence spectroscopy. Intensities at 432 and 480 nm for CPT and 516 and 580 nm for TPT were measured at different time points. Then, Equation 5 was used to calculate lactone percentage of CPT and TPT at specified time points. Degradation of lactone form in about five hours was around 70 % for CPT and TPT. Detailed data of all measurements and calculations was seen in Table 3.5 and Table 3.6. On the other hand, L % of free CPT and TPT were plotted to time as seen Figure 3.12.

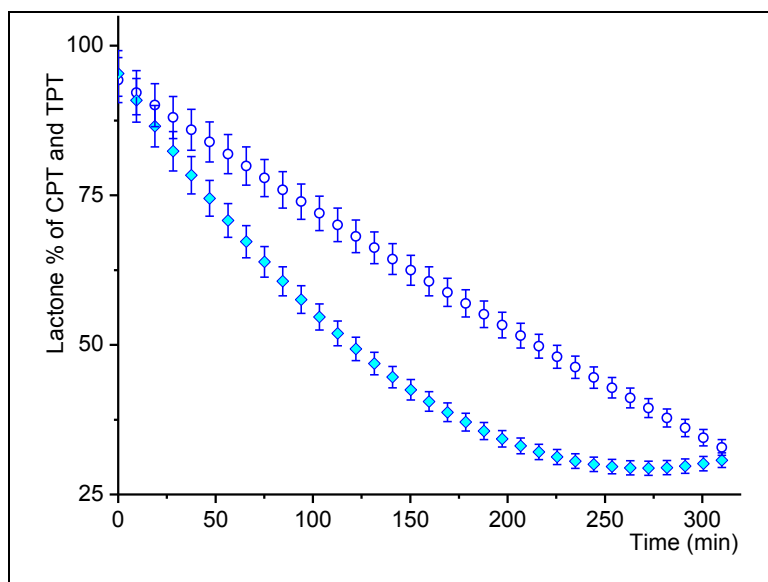


Figure 3.12 L % and C % of free CPT and TPT with FL analysis (a. circle: L % of free TPT in buffer; b. diamond: L % of free CPT in buffer). Polynomial fitting of data was performed.

Table 3.5 Lactone conversion of free CPT

Time(min)	$I(\lambda_1)$	$I(\lambda_2)$	R	R_L	R_C	$I_L(\lambda_2)$	$I_C(\lambda_2)$	L %	C %
0	206	60	3.43	3.43	2.18	60	264	99.91	0.09
20	269	92	2.92	3.43	2.18	60	264	86.40	13.60
40	324	121	2.69	3.43	2.18	60	264	75.13	24.87
60	373	145	2.57	3.43	2.18	60	264	66.53	33.47
80	418	168	2.50	3.43	2.18	60	264	59.77	40.23
100	454	186	2.45	3.43	2.18	60	264	54.50	45.50
120	486	202	2.41	3.43	2.18	60	264	49.26	50.74
140	511	216	2.37	3.43	2.18	60	264	44.28	55.72
160	533	226	2.36	3.43	2.18	60	264	42.28	57.72
180	552	237	2.33	3.43	2.18	60	264	38.21	61.79
200	567	246	2.31	3.43	2.18	60	264	33.72	66.28
220	578	251	2.31	3.43	2.18	60	264	32.91	67.09
240	586	255	2.30	3.43	2.18	60	264	32.35	67.65
260	594	259	2.30	3.43	2.18	60	264	31.42	68.58
280	599	261	2.29	3.43	2.18	60	264	30.45	69.55
300	601	263	2.29	3.43	2.18	60	264	29.70	70.30
310	601	264	2.28	3.43	2.18	60	264	26.91	73.09

Table 3.6 Lactone conversion of free TPT

Time(min)	I(λ_1)	I(λ_2)	R	R _L	R _C	I _L (λ_2)	I _C (λ_2)	L %	C %
0	560	115	4.87	4.86	5.41	115	79	97.77	2.23
20	549	112	4.91	4.86	5.41	115	79	87.14	12.86
40	535	109	4.91	4.86	5.41	115	79	86.71	13.29
60	526	106	4.95	4.86	5.41	115	79	78.59	21.41
80	517	104	4.95	4.86	5.41	115	79	77.21	22.79
100	506	101	4.98	4.86	5.41	115	79	70.24	29.76
120	498	100	4.99	4.86	5.41	115	79	69.63	30.37
140	491	98	5.02	4.86	5.41	115	79	62.17	37.83
160	484	96	5.02	4.86	5.41	115	79	61.90	38.10
180	478	95	5.04	4.86	5.41	115	79	57.91	42.09
200	471	93	5.07	4.86	5.41	115	79	52.47	47.53
220	464	91	5.09	4.86	5.41	115	79	49.72	50.28
240	455	89	5.10	4.86	5.41	115	79	47.39	52.61
260	445	87	5.13	4.86	5.41	115	79	41.24	58.76
280	432	84	5.14	4.86	5.41	115	79	40.38	59.62
300	419	81	5.17	4.86	5.41	115	79	33.95	66.05
310	413	79	5.20	4.86	5.41	115	79	30.29	69.71

3.1.6.2.5. Analysis of Lactone Conversion of CPT and TPT in Gel via Fluorescence Spectroscopy

Kinetics of lactone hydrolysis of 0.015 % CPT and TPT loaded gels were performed at pH= 7.4. It was obtained that 99 % of CPT maintained its lactone form in gel at 310 min. Also, it was found that lactone fraction of TPT in gel was 95 % at 310 min. Detailed data of all measurements and calculations was seen in Table 3.7 and Table 3.8. Also, L % of CPT in gel and TPT in gel vs. time was plotted as seen in Figure 3.13.

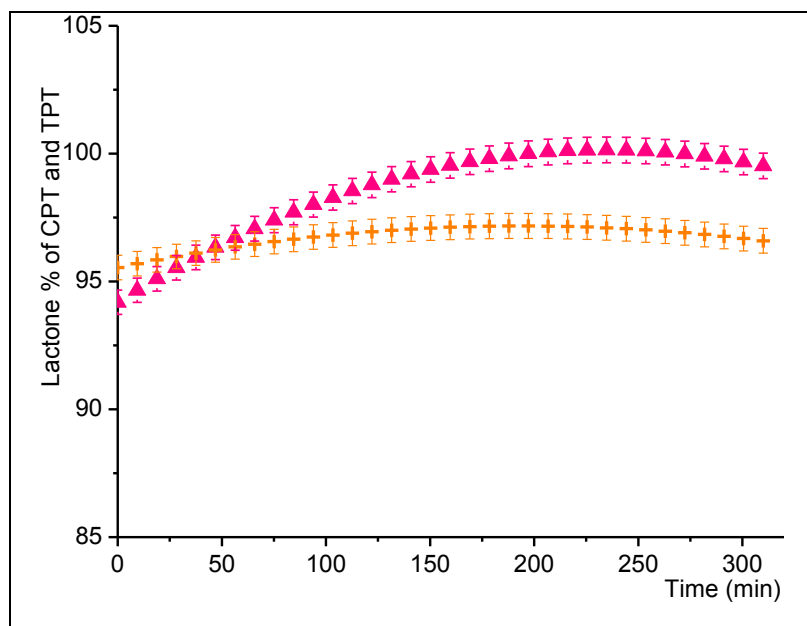


Figure 3.13 Lactone conversion for CPT and TPT in gel, 0.015 % loading via FL (a. up-triangle: L % of CPT in gel; b. plus: L % of TPT in gel). Polynomial fitting of data was performed.

Table 3.7 CPT in gel, 0.015 % loading

Time(min)	$I(\lambda_1)$	$I(\lambda_2)$	R	R_L	R_C	$I_L(\lambda_2)$	$I_C(\lambda_2)$	L %	C %
0	138.60	58.80	2.36	2.39	2.07	58.80	121.00	94.73	5.27
85	75.60	31.96	2.37	2.39	2.07	31.96	71.00	96.40	3.60
175	226.40	94.60	2.39	2.39	2.07	94.60	194.00	100.49	-0.49
260	185.60	77.50	2.39	2.39	2.07	77.50	165.00	100.70	-0.70
310	307.39	129.00	2.38	2.39	2.07	129.00	277.00	98.95	1.05

Table 3.8 TPT in gel, 0.015 % loading

Time(min)	$I(\lambda_1)$	$I(\lambda_2)$	R	R_L	R_C	$I_L(\lambda_2)$	$I_C(\lambda_2)$	L %	C %
0	246.0	84.4	2.91	2.89	3.7	84.4	68	96.24	3.76
85	232.2	79.5	2.92	2.89	3.7	79.5	65	95.40	4.60
175	268.5	92.2	2.91	2.89	3.7	92.2	73	96.57	3.43
260	253.8	87.8	2.89	2.89	3.7	87.8	71	99.90	0.10
310	529.2	181	2.92	2.89	3.7	181	144	94.82	5.18

3.1.6.2.6. HPLC Analysis

Simple and versatile high-performance liquid chromatographic method was used to separate the lactone and carboxylate forms of free CPT and TPT drugs [170]. This two component mobile phase system contains triethylamine acetate (TEAA) and acetonitrile (ACN). In this method, triethyl amine has multiple advantages. It is used for as an ion pairing reagent, a masking agent for underivatized silanols and major buffer constituent for the pH adjustment. Thus, it provides sufficient retention and good separation for carboxylate species on column. On the other hand, ACN was employed to control lactone species of drugs.

3.1.6.2.7. Analysis of Lactone Conversion of Free CPT and TPT via HPLC

Retention time of pure carboxylate and pure lactone of free CPT and TPT was determined at basic pH (9.9) and acidic pH (5.0), respectively. HPLC analysis was performed with C-18 column using ACN- TEAA buffer mobile phase. Carboxylate peak of CPT appeared at 1.51 min while lactone peak gave a signal at 4.21 min. Also, carboxylate peak of TPT was observed at 1.53 min while lactone peak of TPT gave a signal at 3.72 min (data not shown).

When behaviors of CPT and TPT in tris buffer at pH=7.4 were examined with time elapsed, decrease in lactone form and increase in carboxylate form were observed. Lactone to carboxylate conversion of free CPT and TPT was shown in HPLC chromatograms in Figure 3.14. The graph of decomposition of lactone of both free drugs was plotted to time points (Figure 3.15).

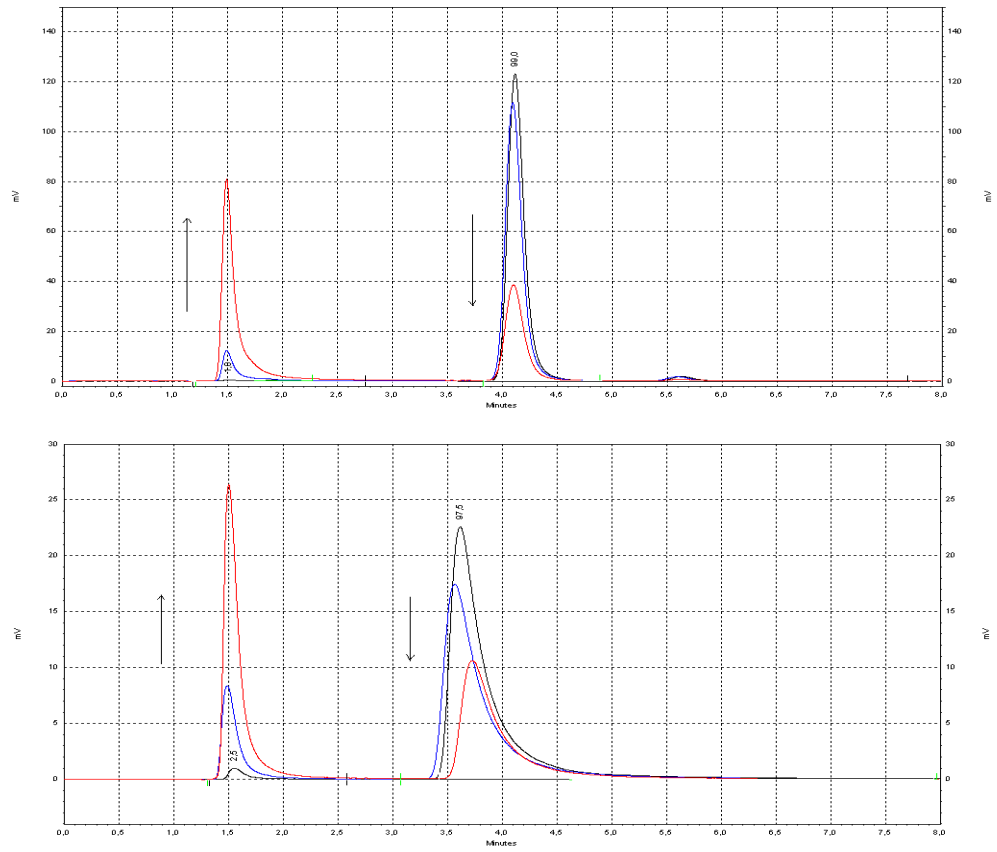


Figure 3.14 HPLC Chromatograms of the conversion of lactone to carboxylate of free CPT and TPT with time elapsed, respectively.

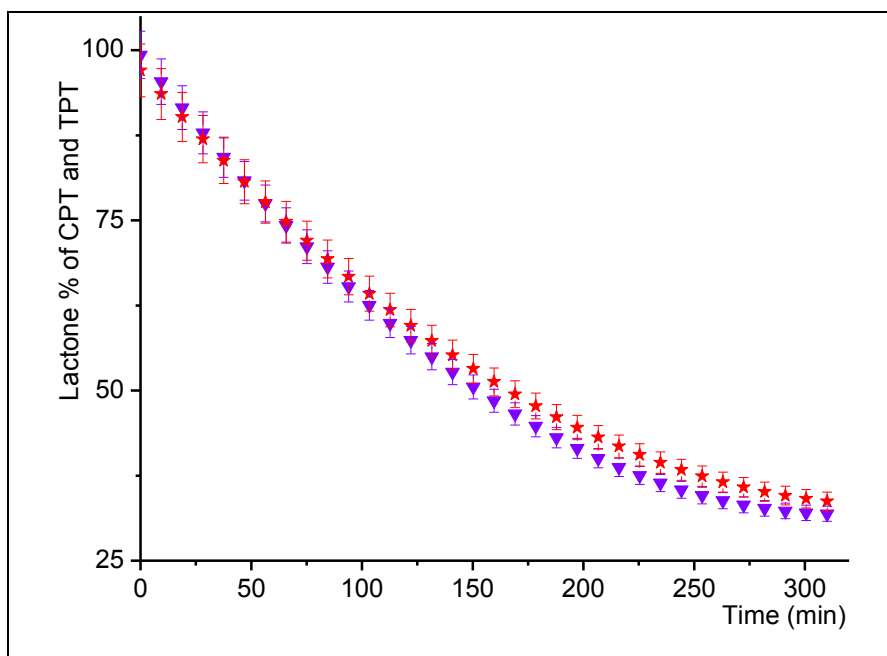


Figure 3.15 Conversions of lactone to carboxylate of free CPT and TPT with HPLC (a. down-triangle: L % of free CPT in buffer; b. star: L % of free TPT in buffer). Polynomial fitting of data was performed.

3.1.6.2.8. Analysis of Lactone Conversion of CPT and TPT in Gel via HPLC

Similar methodology above was used to test which form of drugs exists in gel at pH=7.4 over time. Firstly 0.015 % loading of CPT and TPT into gel was examined with HPLC. It was observed that each drug maintained its lactone form in PLLA-mPEG gel over time (Figure 3.16). We also analyzed higher drug loadings such as 1.0 % and 10 %. They showed similar behaviors as seen in Table 3.9.

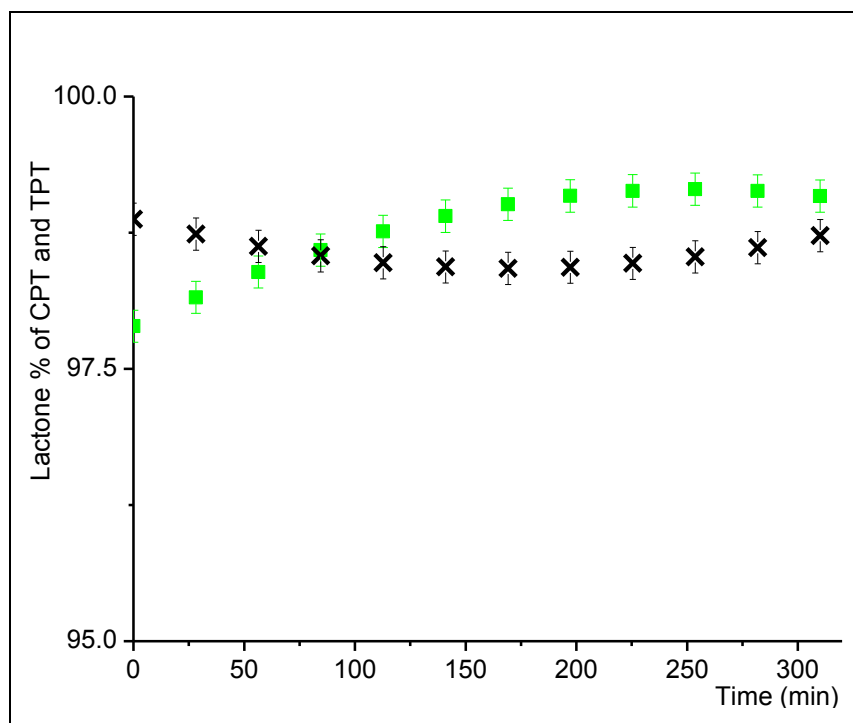


Figure 3.16 CPT and TPT in Gel with HPLC Analysis, 0.015 % loading (a. cross: L % of TPT in gel; b. square: L % of CPT in gel). Polynomial fitting of data was performed.

Table 3.9 L % of CPT and TPT in gel, HPLC analysis

time(min)	CPT in gel, L%		TPT in gel, L %	
	1 % loading	10 % loading	1 % loading	10 % loading
0	99.9	100	99.1	98.6
30	99.9	99.8	99.1	98.1
60	99.9	99.8	99.2	98.4
90	99.9	99.9	98.8	98.4
120	99.9	99.8	98.9	98.7
150	99.9	99.9	98.8	98.6
180	99.9	99.8	97.8	98.8

3.1.6.2.9. Concentration Effect on Drug Stability

As we mentioned previous sections, CPT and TPT maintain its lactone form more than >95 % in PLLA-mPEG gel. We also examined how CPT and TPT behaved concentrated PLLA-mPEG solutions (~200-250 mg/mL) at room temperature. Surprisingly, HPLC measurements revealed that CPT and TPT still keep their intact lactone. Lastly, we tested CPT and TPT in very aqueous polymer solutions (500x dilutions from gel). This formulation slowed down the hydrolysis of CPT at pH 7.4 buffer (Almost 20 % increase in the stability when compared to free drugs at pH 7.4 buffer). Thus, bulk or surface erosion of biodegradable polymer in the tumor environment may trigger slow drug degradation after drug is released. This may enhance the efficiency of therapy.

3.1.6.2.10. Mechanistic Outlook to the Stabilization of CPT via PLLA-mPEG Gels

20-OH group of the lactone ring at camptothecin plays an important role about ring opening of lactone moiety of the drug (Figure 3.17) [150, 171-173]. Proton transfer or stabilization of the transition state via a strong intramolecular hydrogen bonding may facilitate ring opening of the ring after nucleophilic attack at the acyl carbon occurred [150]. Another study was also reported that esterification of the 20-OH of CPT stabilized the lactone ring, supporting this phenomenology [173].

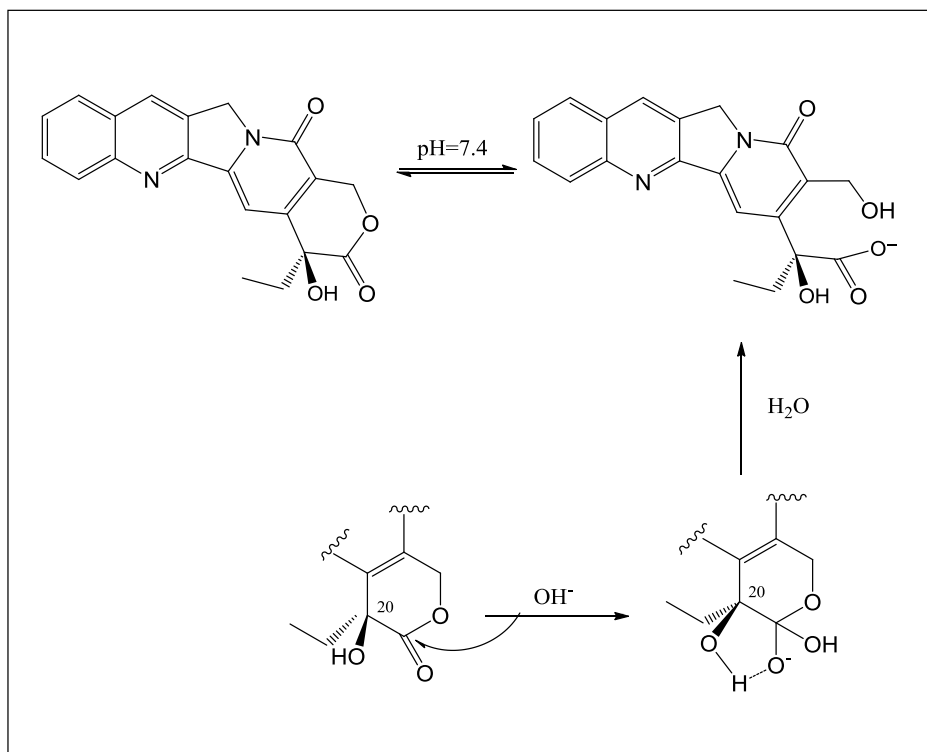


Figure 3.17 Proposed mechanism of conversion of lactone ring to carboxylate form of CPT.

Intermolecular interactions between 20-OH group of lactone moiety and carbonyl groups of lactide units in PLLA-mPEG diblock copolymer most probably reduce the intramolecular hydrogen bonding within lactone moiety of drug molecule. In order to prove our proposal we benefited from ATR-FTIR. Thus, ATR-FTIR spectra of powder CPT (A) was compared to CPT loaded copolymer gel (B) (Figure 3.18).

Highly concentrated copolymer solution (almost like gel) was prepared with PLLA-mPEG and distilled water. It was recorded as background. Then, a 1-2 mg of powder CPT was added into the same vial before it was stirred with high speed vortex for the complete homogenization. ATR-FTIR spectrum of drug loaded gel was recorded, and background was subtracted.

We observed that three bands in the spectra located at 3100-3500, 1360-1390 and 650-720 cm^{-1} had undergone significant changes and should be closely analyzed. In the first range as shown in Figure 3.18(A), band around 3427 cm^{-1} was assigned to O-H stretching vibration of CPT. This band highly shifted to 3658 cm^{-1} due to potential intermolecular hydrogen bonding between carbonyl group of copolymer and hydroxyl group of CPT. (Figure 3.18(B))

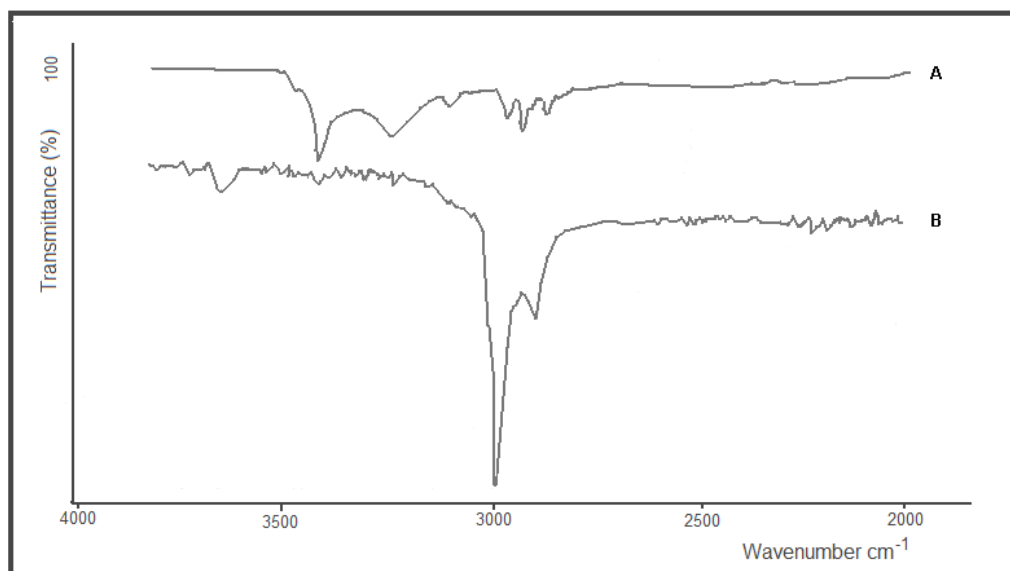


Figure 3.18 ATR-FTIR spectra of powder CPT (A) and CPT loaded copolymer gel (B) in the range of 2000-4000 cm^{-1} .

While the O-H in-plane bending vibration of powder CPT was observed 1387 cm^{-1} with weak small signal in Figure 3.19-A1, that of drug loaded copolymer gel was observed 1389 cm^{-1} with strong broad signal in Figure 3.19-B2. Also, spectral changes between 650-720 cm^{-1} in region A3 and B4 might be resulted from out-of-plane bending of O-H group.

In addition, as expected, there was no shift in carbonyl stretching of lactone ring (1737 cm^{-1}), lactame (1650 cm^{-1}) ring, and aromatic C=C bonds (1578 cm^{-1} and 1600 cm^{-1}) of powder CPT and CPT loaded copolymer gel.

It is known that carboxylate ion gives rise to two bands: asymmetrical stretching band near $1650\text{-}1550$ and a weaker, symmetrical stretching band near 1400 cm^{-1} . These bands didn't appear in the spectrum of drug loaded copolymer gel as shown in Figure-21B, which was one more proof keeping of active lactone ring of CPT in gel.

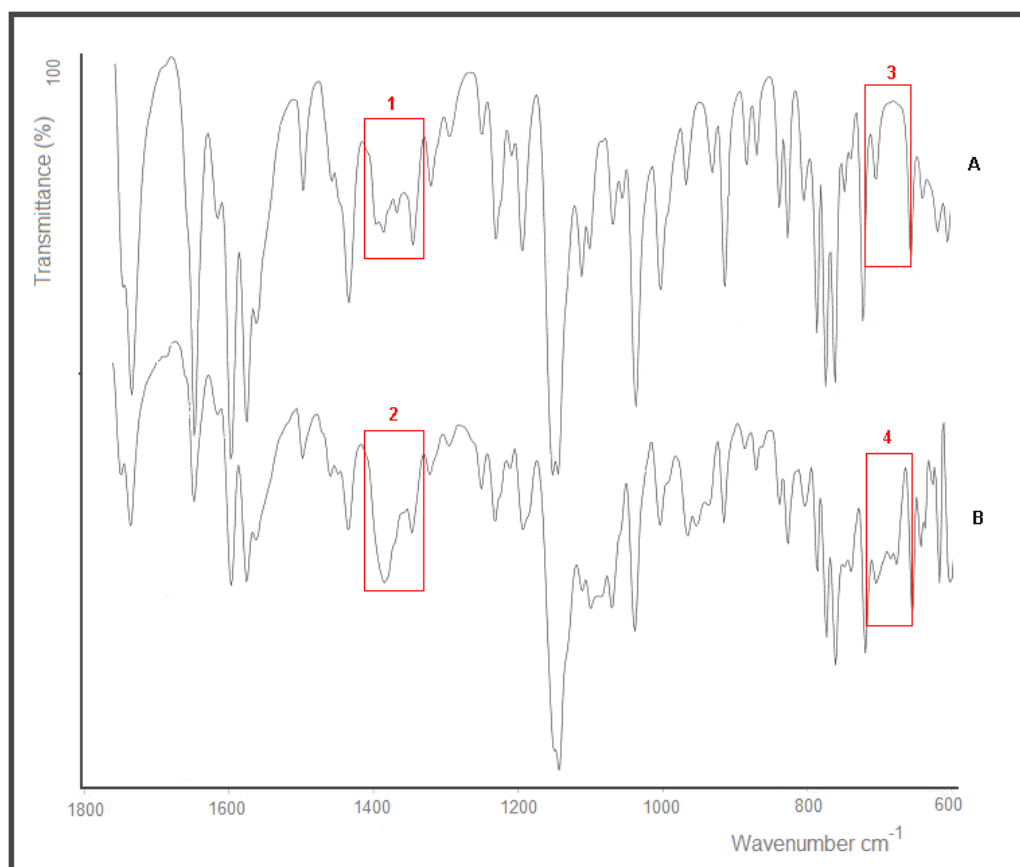


Figure 3.19 ATR-FTIR spectra of powder CPT (A) and CPT loaded copolymer gel (B) in the range of $600\text{-}1800\text{ cm}^{-1}$.

We did not ignore solubility effect of drug crystals in gel, especially for low soluble camptothecin drug. Confocal and optic microscopes were used to examine characteristics of undissolved CPT crystals which might give us a complimentary idea about mechanism for CPT stabilization.

Free CPT suspended water was reported by SEM before [174] and had the image of undissolved lamellar square type of crystals due to low solubility of CPT crystals in water. When the CPT molecules in copolymer gel was examined by confocal and optic microscope, the similar behavior of CPT molecules was observed as shown in Figure 3.20-A and B. Undissolved CPT crystals formed the domains in gel due to low solubility of CPT in water. Undissolved lactone crystals are likely to be very stable and the conversion of lactone ring to water soluble carboxylate form in gel state is quite slow due to potential intermolecular interactions via hydrogen bonding between 2OH group and carbonyl group of lactide units as explained in detail above. Those strong interactions inhibit the formation of the water soluble carboxylate moiety.

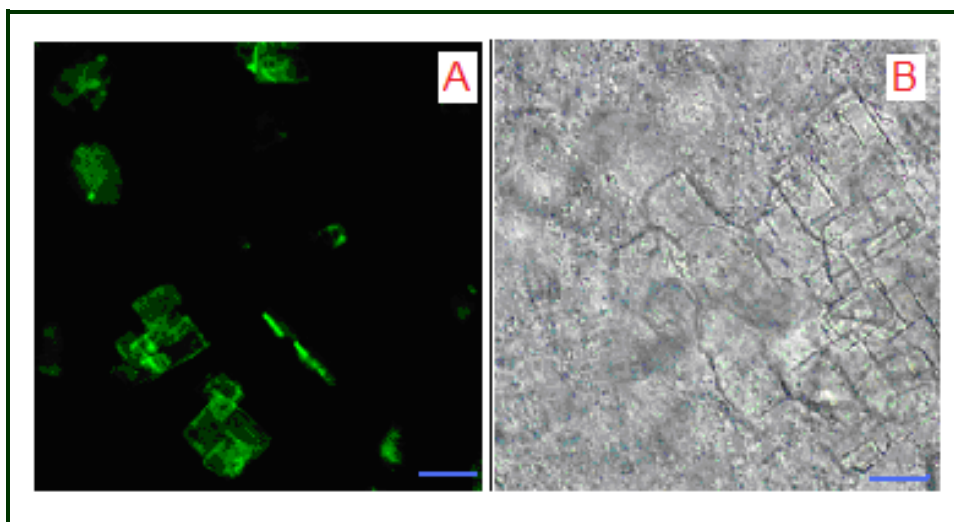


Figure 3.20 Confocal microscope image of drug loaded gel (A); optical microscope image of drug loaded gel (B)

3.1.6.3. Controlled Release of the Drugs

3.1.6.3.1. Standard Curves of Free CPT and TPT

Intensity measurements of various dilute concentrations of free CPT and TPT were carried out for the assignments of standard curves of drugs (no gel at all). They employed to calculate drug mass delivered into supernatant phase from drug loaded gels. Curves obtained were indicated in Figures 3.21 and 3.22.

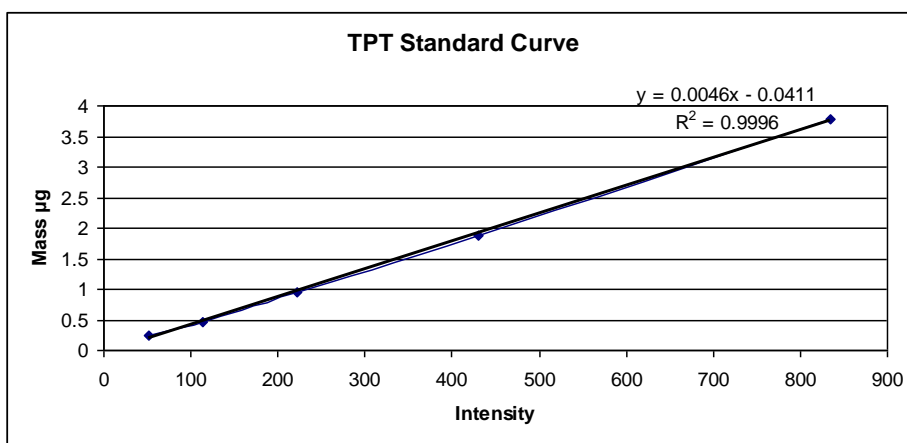


Figure 3.21 TPT standard curve

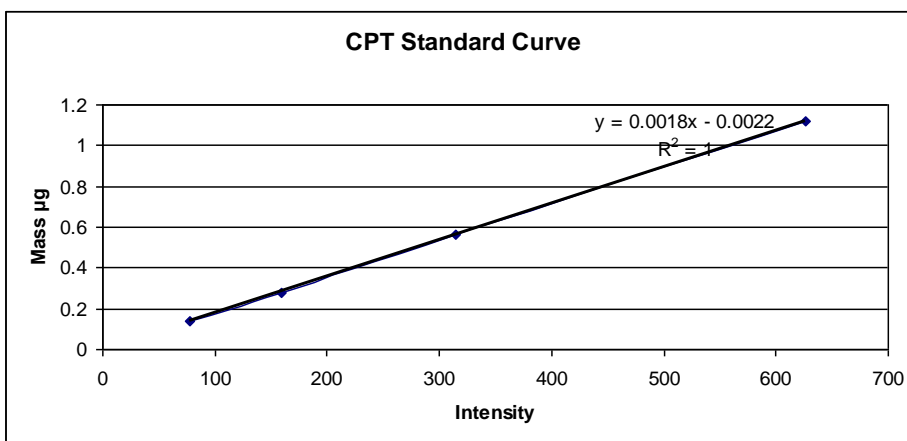


Figure 3.22 CPT standard curve

3.1.6.3.2. Release Studies of CPT and TPT Anticancer Drugs from Gels

Topotecan and camptothecin were loaded into copolymer gel with 0.015 % (0.15 mg drug /g polymer) and 1.0 % (10 mg drug /g polymer) loading ratios **28-31**. A blank formulation **32** (no drug at all) was also prepared for the eliminating of polymer effect on intensity measurements of drugs (Table 3.10). Loading ratios were randomly selected. Formulations were kept in a constant speed at 160 rpm and 35 °C in a shaker. In different time points, supernatants were replaced with the fresh buffer. Measurements were carried out using fluorescence spectroscopy with single read measurements at appropriate wavelengths of drugs shown in Table 2.6.

Table 3.10 Formulations of CPT and TPT loaded gels

ID	Loading %	Drug
28	0.015 (0.15 mg/g)	TPT
29	1.0 (10 mg/g)	TPT
30	0.015 (0.15 mg/g)	CPT
31	1.0 (10 mg/g)	CPT
32	NA	blank

Figure 3.23 shows the release profile of CPT and TPT from PLLA-mPEG gels. Each point represents the amount of drugs left from gels. There was a constant daily release of both 0.015 % and 1.0 % loadings of drugs without any significant burst effect (only 5 to 10 % burst release in a couple of hours). At the end of 23 days, 75 % and 89 % of the total CPT and TPT mass were released from the gels for formulations **30** and **28**, respectively. TPT has hydrophilic character and relatively higher solubility in water while hydrophobic CPT has low water solubility. TPT release is faster than CPT. Thus, TPT moves fast to upper buffer layer. Also, complete release of drugs from gels was observed for the formulations of **29** and **31** at the end of 23rd days (Figure 3.23). Detailed data of

intensity values, calculated mass values at each time points were shown in Tables of 3.11, 3.12, 3.13 and 3.14.

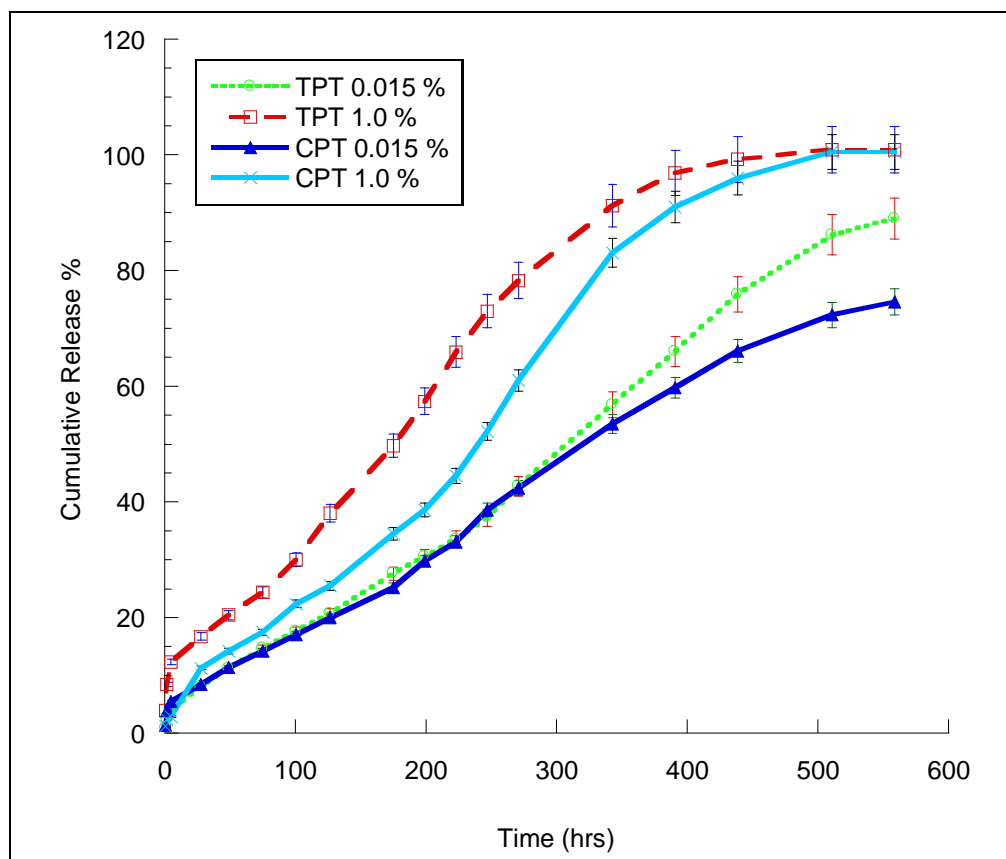


Figure 3.23 CPT and TPT release curves

Table 3.11 Release data of formulation 28

Intensity	Mass (µg)	Cumulative mass (µg)	Cumulative mass %
86	0.35	0.35	0.9
128	0.55	0.90	2.4
123	0.52	1.43	3.8
352	1.58	3.01	8.0
266	1.18	4.19	11.2
299	1.33	5.52	14.7
243	1.08	6.60	17.6
258	1.15	7.74	20.7
573	2.59	10.34	27.6
252	1.12	11.46	30.6
261	1.16	12.62	33.6
310	1.38	14.00	37.3
449	2.02	16.03	42.7
1155	5.27	21.30	56.8
761	3.46	24.76	66.0
814	3.70	28.46	75.9
849	3.86	32.32	86.2
237	1.05	33.37	89.0

Table 3.12 Release data of formulation 29

Intensity	Mass (µg)	Cumulative mass (µg)	Cumulative mass %
13680	62.89	62.89	3.9
15500	71.26	134.15	8.4
13660	62.79	196.94	12.3
15440	70.98	267.92	16.7
12840	59.02	326.95	20.4
13440	61.78	388.73	24.3
19700	90.58	479.31	30.0
27840	128.02	607.33	38.0
40860	187.91	795.25	49.7
26640	122.50	917.75	57.4
29760	136.85	1054.60	65.9
24690	113.53	1168.14	73.0
18480	84.97	1253.10	78.3
44640	205.30	1458.41	91.2
20025	92.07	1550.48	96.9
8100	37.22	1587.70	99.2
5940	27.28	1614.98	100.9
40	0.14	1615.13	100.9

Table 3.13 Release data of formulation 30

Intensity	Mass (µg)	Cumulative mass (µg)	Cumulative mass %
283	0.51	0.5	1.4
523	0.94	1.4	3.9
352	0.63	2.1	5.5
590	1.06	3.1	8.4
625	1.12	4.3	11.4
599	1.08	5.3	14.2
580	1.04	6.4	17.0
615	1.10	7.5	20.0
1102	1.98	9.5	25.2
948	1.70	11.2	29.8
695	1.25	12.4	33.1
1138	2.05	14.5	38.6
795	1.43	15.9	42.4
2317	4.17	20.1	53.5
1293	2.33	22.4	59.7
1337	2.40	24.8	66.1
1292	2.32	27.1	72.3
482	0.87	28.0	74.6

Table 3.14 Release data of formulation 31

Intensity	Mass (μg)	Cumulative mass (μg)	Cumulative mass %
17120	30.81	30.8	1.2
15880	28.58	59.4	2.4
7220	12.99	72.4	2.9
116105	208.99	281.4	11.3
41320	74.37	355.8	14.2
44820	80.67	436.4	17.5
68360	123.05	559.5	22.4
43110	77.60	637.1	25.5
124830	224.69	861.8	34.5
57960	104.33	966.1	38.6
81900	147.42	1113.5	44.5
106380	191.48	1305.0	52.2
121770	219.18	1524.2	61.0
307200	552.96	2077.1	83.1
110360	198.65	2275.8	91.0
68940	124.09	2399.9	96.0
62820	113.07	2512.9	100.5
264	0.47	2513.4	100.5

3.1.6.4. In Vivo and In Vitro Experiments with Polymer-Drug Conjugate

3.1.6.4.1. In Vitro Studies

The cytotoxic efficacy of TPT in the PLLA-mPEG platform (PLLA-mPEG-TPT) was evaluated on cancer cell lines (LLC-1 and 4T1) via MTT assay. The amount of TPT released into the media was determined to range between 363-402 μM in independent experiments. TPT released from the gel exerted cytotoxic effects on LLC-1 tumor cells (Figure 3.24). 4T1 cells were sensitive neither to released TPT nor to fresh TPT solution (Figure 3.25-A). Notably, a very high dose of TPT (200 μM) decreased 4T1 viability (Figure 3.25-B). The effect of TPT on cell survival can be related to the malignant character and the origin of tumors [175]. In a

widely used human breast cancer cell line, MDA-MB-231, sensitivity to TPT was also observed at high drug concentrations [175]. 4T1 mouse mammary carcinoma cells are also aggressive and chemoresistant [176]. Therefore, the insensitivity of 4T1 cells to TPT may be attributed to drug resistance beside the short-time drug exposure, *in vitro* [175-176]. However, this cell line is regarded as a compatible model for studying human breast cancer because of the highly malignant nature of 4T1 [176].

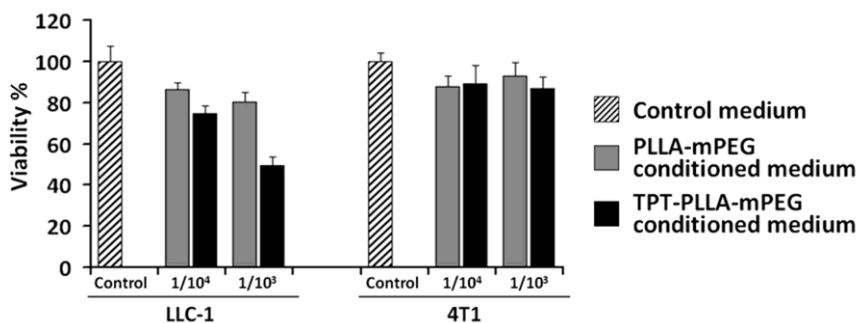


Figure 3.24 Effect of TPT released from PLLA-mPEG gels on the viability of LLC-1 and 4T1 cancer cells. 1×10^4 cells were seeded and $1:10^4$ and $1:10^3$ dilutions of the conditioned media were tested.

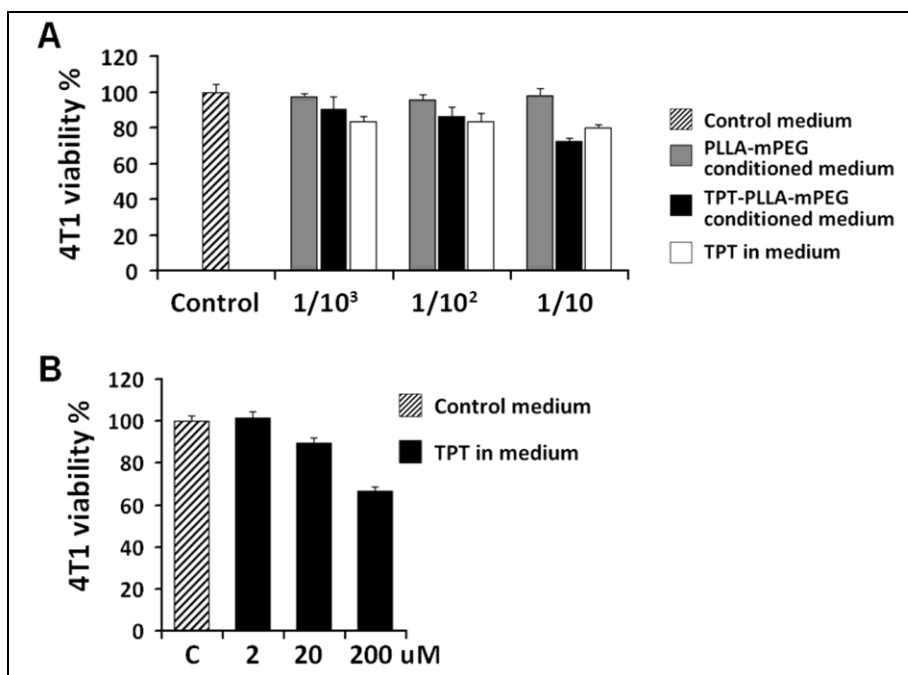


Figure 3.25 Effect of high doses of TPT on the viability of 4T1 cancer cells. Effect of TPT released from PLLA-mPEG gel, TPT solution and PLLA-mPEG conditioned cell culture media on the 4T1 cell viability (A). 3×10^4 cells were seeded and $1:10^3$, $1:10^2$ and $1:10$ dilutions ($0.4 \mu\text{M}$, $4 \mu\text{M}$ and $40 \mu\text{M}$, respectively) of TPT solution or released drug were tested. Dose response for TPT solution was also determined (B).

3.1.6.4.2. In Vivo Studies

Tumors established with 4T1 cells are widely accepted as a superior model compatible to human breast tumors [176] and we challenged the efficacy of TPT-loaded PLLA-mPEG preparation on this model. When compared to positive and negative control groups, the administration of PLLA-mPEG-TPT to the tumor-bearing mice resulted in a significant reduction in tumor size (Figure 3.26-A and B, Figure 3.27). The initial reduction (day 3) seen with the PLLA-mPEG-TPT was compatible with the TPT solution. However, on the seventh day, the tumor size in the group treated with TPT solution reached that of the control group,

whereas PLLA-mPEG-TPT considerably hampered the tumor growth during 14-days of follow-up (Figure 3.26-A and B, Figure 3.27). This result, simply demonstrates the increased *in vivo* stability of TPT when administered in PLLA-mPEG gel. Correspondingly, between the days 14-17, PLLA-mPEG-TPT gel improved the survival rate of mice bearing tumors established with 4T1 cells which were insensitive to TPT, *in vitro* (Figure 3.26-C). In the study of Berrada et al [177] demonstrating treatment of potentially drug-sensitive tumors, the biodegradable polymer gel-CPT preparation was administered directly into the tumor mass however its efficacy was compared with the CPT solution given intraperitoneally. On the other hand, the usage of TPT-insensitive 4T1 cells was the major challenge in our study to test the efficacy of TPT-PLLA-mPEG. In addition, all the agents (control physiological saline, TPT solution, PLLA-mPEG gel and TPT-PLLA-mPEG) were administered to via same route.

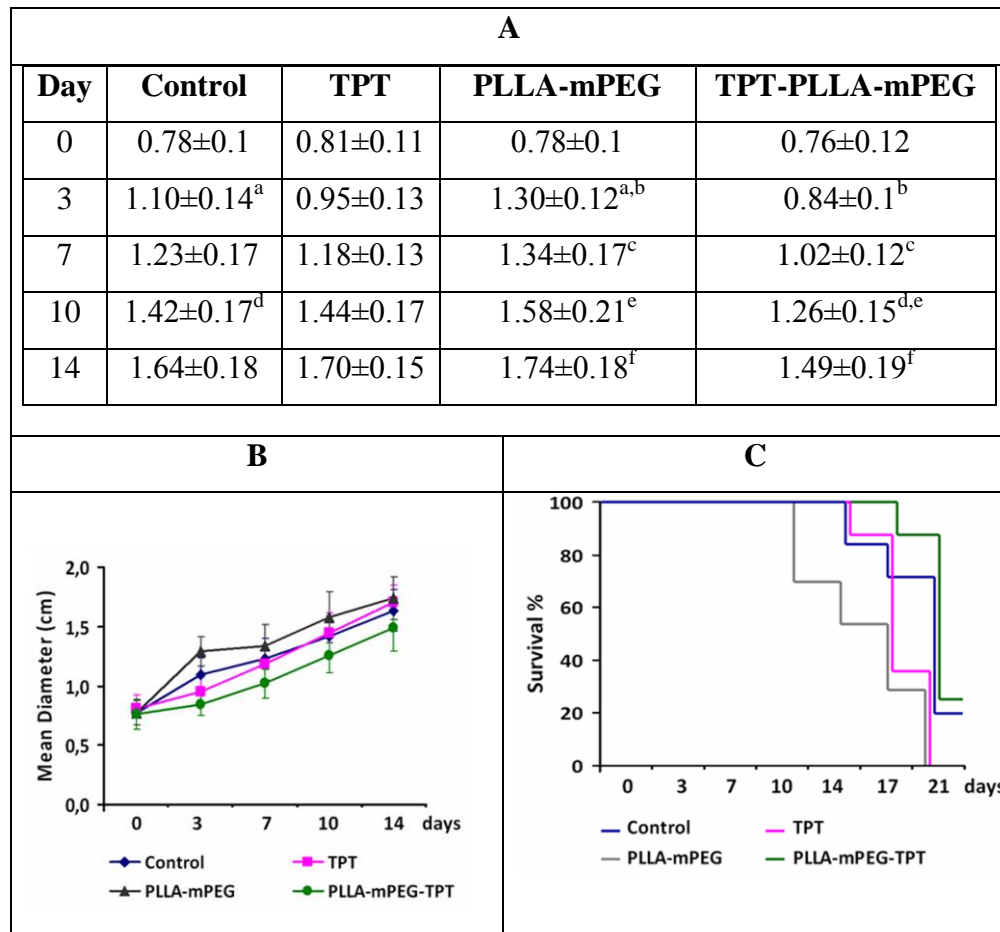


Figure 3.26 Size of 4T1 breast tumours during 14-day follow-up (A and B) and survival percentages of the mice during the treatment period (C).

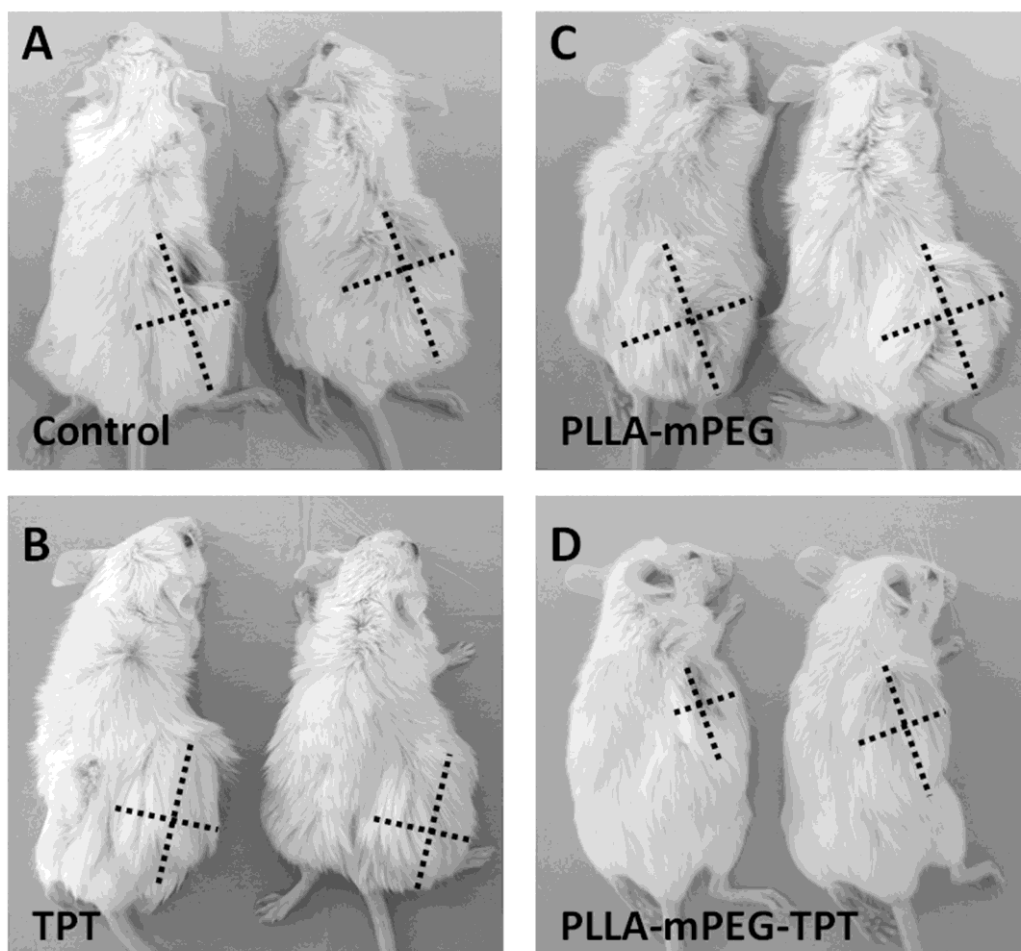


Figure 3.27 Representative photographs of two mice bearing 4T1 tumors from each experimental group. The dashed lines indicate the perpendicular diameters of the tumors.

3.1.7. Performance of the Current Platform vs. Literature

Yu et al [85] recently published a study centered on the use of PEG-CPT drug, which was released from hydrogels formed by a thermally gelling and hydrolytically degradable polymer PLGA-PEG-PLGA. The first major difficulty is whether chemically bonded PEG-CPT is converted into camptothecin itself after its hydrolyzation with the release of the drug. PEG-CPT does not hydrolyze after it is released in Yu's study. Thus, this modification can not be used as a

drug. It is rather prodrug. The second major disadvantage is poor performance of commercial pegylated CPT in clinic Phase 2b trials in patients with gastric or gastroesophageal cancers whose disease progressed following prior chemotherapy. Last, at *in vivo* application of Yu's work, the performance of the PEG-CPT was evaluated towards 5-fluorouracil (5-Fu) as the positive control group. Thus, it is unclear whether chemically modified pegylated-CPT gives better response than CPT itself or not. In our study we strongly point out that the formulation of TPT-gel improves reduction in tumour size and the survival rate of mice when it is compared with TPT solution without gel.

In Gao et al [178] work, 9-nitro-20(S)-camptothecin (9-NC) was loaded into micelles forming from copolymer methoxy poly(ethylene glycol)-b-poly(D,L-lactide) (mPEG-PDLLA, PELA). The lactone form of 9-NC in the micellar solution decreased up to 80% at 160 min, and curve will probably goes down beyond 160 min. In our research, hydrophobic CPT and hydrophilic TPT in gels showed a very high stability of lactone species (> 98%) for 300 mins (time is almost double). Also, we observed that no regular decrease in lactone species with time elapsed. For representative samples, we checked the stability of the drugs even 24 hrs later (data not shown), there was no change in the stability of the drugs. On the other hand, FDA approval of 9-nitro-20(S)-camptothecin (rubitecan or Orathecin) (the drug in Gao study) has been withdrawn its New Drug Application (NDA) due to the treatment of pancreatic cancer patients who have failed at least one prior chemotherapy regimen. Finally, there was no evidence how the stabilized drugs in micelles worked in a cell culture or a model *in vivo* application in that study.

Berrada et al [177] prepared a chitosan based autogelling solution with camptothecin, which remains liquid at low temperature and turn into gel when heated. However, our system bases on PLLA-PEG block copolymer which is

solution at high temperature (around 45°C) and injectable in that form. When it is injected it forms gel with cooling to body temperature (37°C). Second, it is claimed that approximately 80% of intact drug is loaded in chitosan gels although lactone- carboxylate conversion is not experimentally reported in initial solution and latter gel state. In our research, hydrophobic CPT and hydrophilic TPT in gels showed a very high stability of lactone species (> 98%), and mechanistic outlook to the stabilization of the drug via PLLA-mPEG gels was examined in detail. Last, gel-CPT preparation at Berrada et al was tested by giving directly into the tumor mass and compared its efficacy with the CPT solution given intraperitoneally. In our study, we injected all of the agents (physiological saline, TPT solution, PLLA-mPEG gel and TPT-PLLA-mPEG) using the same route.

Shenderova and Burke reported that 10-Hydroxycamptothecin (10-HCPT) was encapsulated into poly(lactide-co-glycolide) (PLGA) microspheres via oil in water emulsion solvent method with the aim of maintaining lactone form of drug. Unreleased 10-HCPT was in the form of lactone (>95 %) in microspheres over two months. However, it was not tested for in vitro cell lines and tumor models in vivo [145].

Hatefi et al prepared semi-crystalline ϵ -caprolactone oligomers prepared with different initiators for loading of camptothecin. CPT-Oligomers having melt characteristics at 45 °C for injection formed a semi solid depot at 37 °C. Camptothecin prior to being released remained the lactone form within polymeric depot [179]. However, in vitro cell lines and tumor models in vivo were not reported.

Barreiro-Iglesias et al reported that micellar solutions of poly(ethylene oxide)-*b*-poly(propylene oxide)-*b*-(polyethylene oxide)-*g*-poly(acrylic acid) (Pluronic-PAA) in combination with CPT was prepared to investigate solubility behavior

and stability of the lactone form of camptothecin (Figure 3.28). Pluronic-PAA micelles slowed down hydrolysis of CPT at pH 8, and solubility of CPT in micellar solution increased 3-4 times when compared to CPT in water [180]. However, in vitro cell lines and tumor models in vivo were not reported. Also, other bottleneck is non-biodegradability of the polymer.

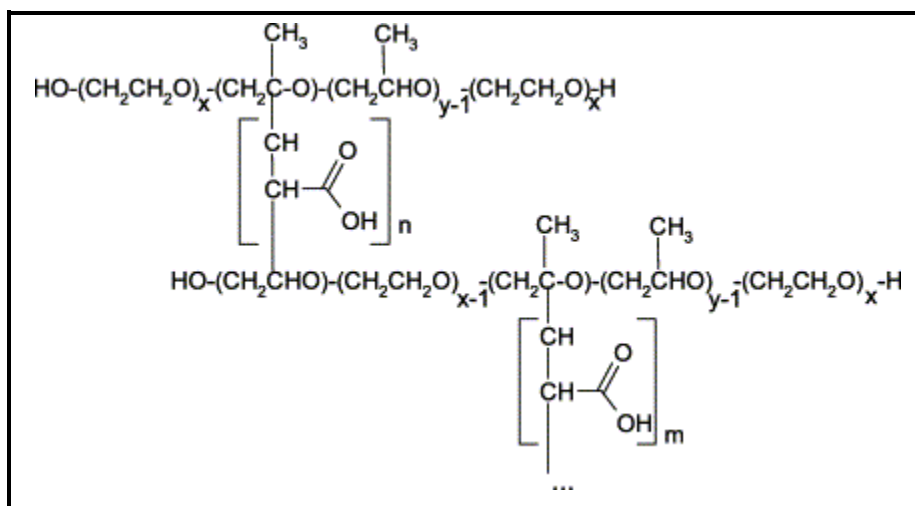


Figure 3.28 Structure of the poly(ethylene oxide)-*b*-poly(propylene oxide)-*b*-poly(ethylene oxide)-*g*-poly(acrylic acid), Pluronic-PAA, copolymers

To conclude, our research not only covers in vitro/ vivo aspects of the produced platform, but also detailed mechanism of drug-polymer interactions, significant chromatographic and spectroscopic analyses and prolonged release of both drugs over weeks. Our platform bases on simple strategy, and it does not require any chemical modifications so no need hydrolysis after it is released, which makes our study unique and valuable.

3.2. Preparation of Polymeric PEG:PSA Particles for the Camptothecin Anticancer Drug Delivery System

3.2.1. Synthesis of Sebacic Acid Prepolymer

As a precursor for melt polymerization of PEG:PSA, prepolymer of sebacic acid is performed in acetic anhydride at reflux temperature under nitrogen atmosphere (Figure 3.29) [71,72]. Characterization is performed with $^1\text{H-NMR}$. Main chain - CH_2 units have resonances in 1.33 ppm, 1.66 ppm and 2.45 ppm. Also, acetyl methyl groups at the ends give a peak at 2.33 ppm.

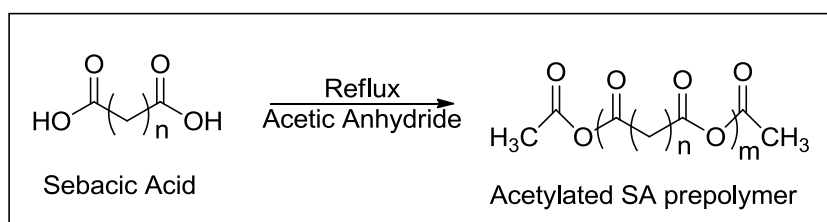


Figure 3.29 The preparation of monomeric SA prepolymer

3.2.2. Synthesis of PEG Prepolymer

As a second precursor for melt polymerization of PEG:PSA, prepolymer of acetylated PEG is prepared from PEG diacid in acetic anhydride at reflux temperature under nitrogen atmosphere (Figure 3.30) [71,72]. Characterization is performed with $^1\text{H NMR}$. While CH_2 units having resonances in 3.65 ppm, and 4.27 ppm, acetyl methyl groups at the ends give a peak at 2.25 ppm.

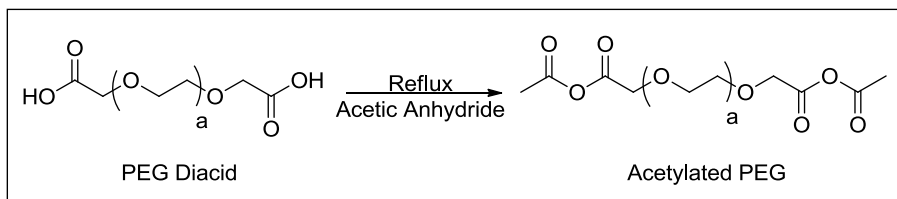


Figure 3.30 The preparation of acetylated PEG prepolymer

3.2.3. Synthesis of PEG:PSA Copolymer

Poly(ether-anhydride) is synthesized by melt polycondensation of acetylated PEG and monomeric SA prepolymer under high vacuum (Figure 3.31). Characterization is performed with ^1H NMR. PEG components give signals at 3.65 ppm and 4.27 ppm while SA components have resonance at 2.45 ppm, 1.66 ppm and 1.33 ppm [71,72].

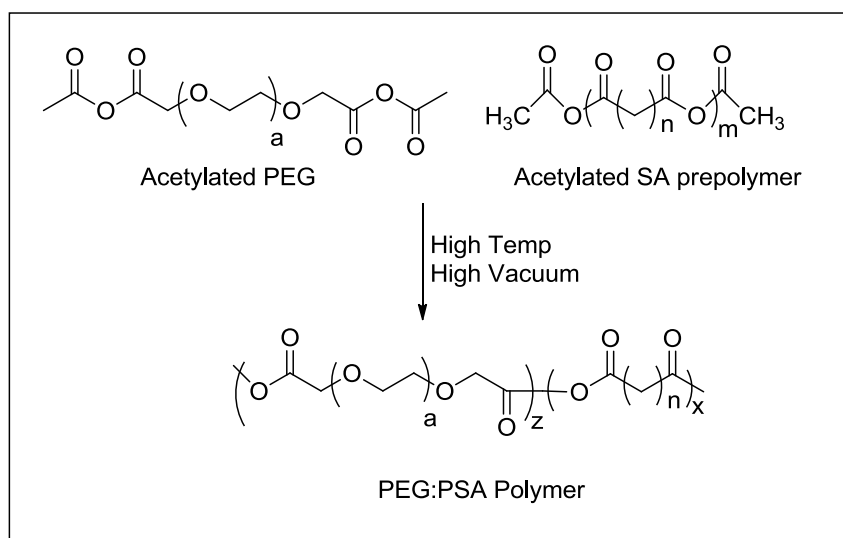


Figure 3.31 The preparation of PEG: PSA copolymer

3.2.4. Nanoparticle and Microparticle formulations of PEG:PSA Copolymer

Nanoprecipitation (Solvent Diffusion) and Single Emulsion methods were performed to formulate camptothecin loaded PEG-SA nanoparticles and microparticles in 1 % PVA aqueous phase. Camptothecin loaded nanoparticles were made with diffusion method. They showed ~360 nm by number as shown in Figure 3.32. On the other hand, drug loaded microparticles were formulated with single emulsion method and characterized with particle size analyzer. They showed average of 14 μm by volume. Also, Particle images are recorded by Confocal, SEM and Light Microscopes, as indicated in Figure 3.33.

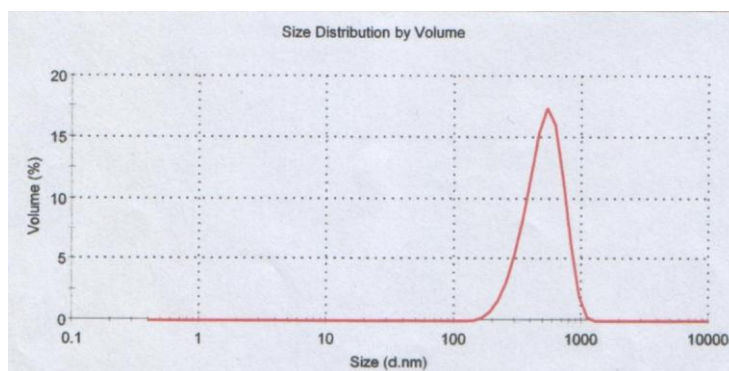


Figure 3.32 Size distribution report by volume for CPT loaded nanoparticles

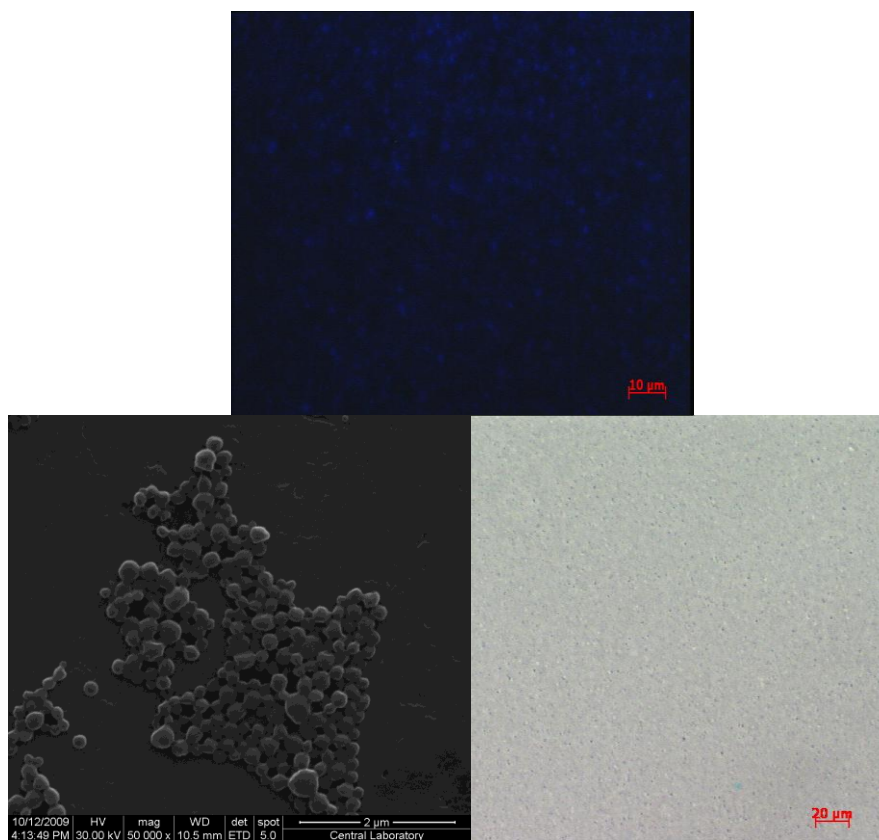


Figure 3.33 Particle images of Confocal, SEM and Light Microscopes

3.2.5. Analysis of CPT loaded particles by HPLC

After the positions of lactone and carboxylate forms of free camptothecin are identified with high performance liquid chromatographic method, lactone and carboxylate forms of CPT in micro and nano particles were examined, and it was found that CPT is very stable in particles. For example, in representative example of CPT loaded microparticules, CPT is in 99.2 % lactone form, as shown in Figure 3.34.

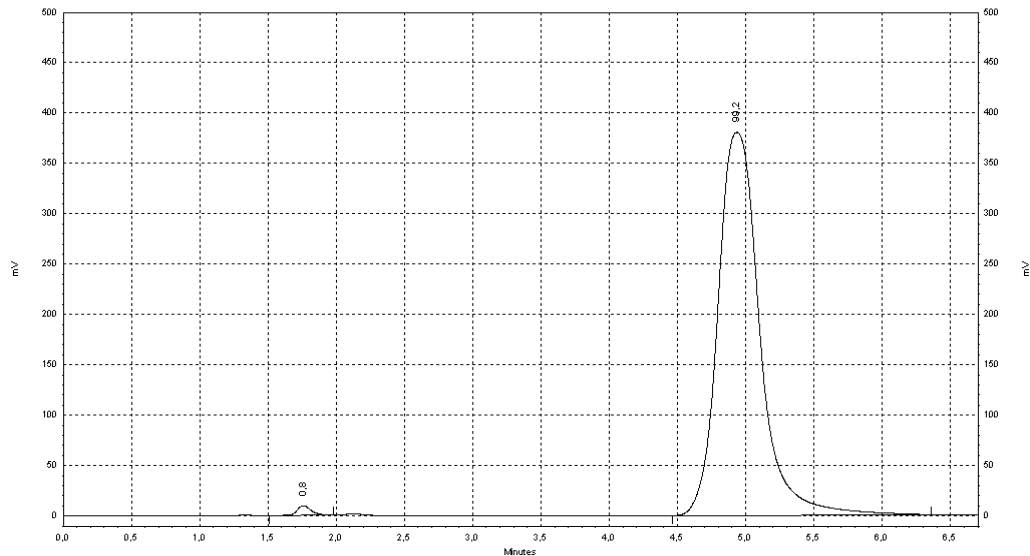


Figure 3.34 Representative HPLC Chromatogram of CPT loaded polymeric microparticles

3.3. Synthesis and Properties of Novel Electrochromic Polythienylpyrrole

3.3.1. Synthesis of 1,1'-Bipyrrole

Synthesis of N-aminophthalimide **10** was performed reacting phthalimide **9** with hydrazine at 5 °C in 75 % yield [133-135]. Then, it was converted into N-phthalimidopyrrole **12** in the presence of 2,5-dimethoxytetrahydrofuran **11** in dioxane in 87 % yield [135-137]. Phthalimidopyrrole **12** reacted with hydrazine monohydrate in methanol at reflux temperature to produce 1-aminopyrrole **13** in 91 % [137, 138]. Treatment of 1-aminopyrrole **13** with 2,5-dimethoxytetrahydrofuran **11** gave 1,1'-bipyrrole **14** in 37 % yield [135] (Figure 3.35).

3.3.2. Synthesis of 1-(1H-pyrrol-1-yl)-2,5-di(thiophen-2-yl)-1H-Pyrrole (SNSN)

1,4-Dithien-2-yl-butane-1,4-dione **17** was firstly synthesized from thiophene **15** and succinyl chloride **16** in dichloromethane at room temperature as reported previously [139]. Then, we synthesized a novel 1-(1H-pyrrol-1-yl)-2,5-di(thiophen-2-yl)-1H-pyrrole (SNSN) **18** from 1-Aminopyrrole **13** and 1,4-Dithien-2-yl-butane-1,4-dione **17** in the presence of p-toluenesulfonic acid (Figure 3.35).

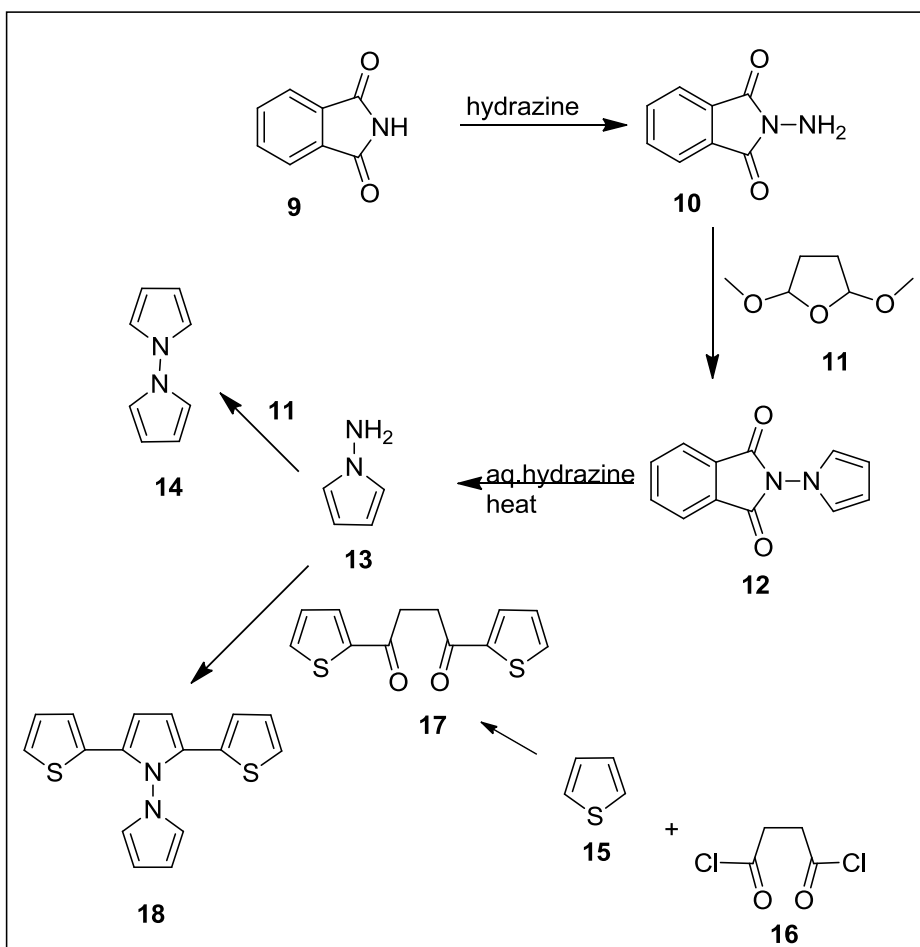


Figure 3.35 Synthesis of dipyrrole and SNSN

3.3.3. Electropolymerization of SNSN

Cyclic voltammetry was used to investigate the redox behavior of 1,1'-bipyrrole in a 0.1 M TBAP/DCM electrolyte solution. An irreversible oxidation (E_{ox}) at 1.14 V during the first anodic scan corresponded to a radical formation on bipyrrole as shown in Figure 3.36(a). Following scans displayed the disappearance of that peak, revealing no film formation on the electrode surface with repetitive cycling or constant potential electrolysis. The reason of this might be twisted structure of bipyrrole rings with an $\sim 80^\circ$ interplanar angle [135].

To overcome this problem, we attached thiophene rings to the 2- and 5- positions of one pyrrole ring to increase the planarity of the molecule electropolymerization. Due to external thiophene rings in monomer, single irreversible oxidation peak shifted to 0.98 V vs Ag/AgCl as seen in the first cycle in Figure 3.36 (b). This value is compatible with the redox behavior of SNS ($E_{ox} = 0.94$ V) [95]. Slight difference in oxidation peak between SNS and SNSN indicates that pyrrole substitution to SNS makes little contribution to the electronic structure of the trimeric system when compared to aromatic subunits like fluorene, naphthyl and benzene in Table 3.15 [103,110,111]. For instance, the electronic density of the system increased in the presence of aromatic subunits in SNSF ($E_{ox} = 0.77$ V vs Ag/AgCl) [92] and SNSNP ($E_{ox} = 0.77$ V vs Ag/AgCl) [111]. This lowered the oxidation potential of SNS unit. Then, we observed a new reversible redox couple at following cycles. The formation of an electroactive polymer was understood with a continuous increase in the current value after consecutive cycles.

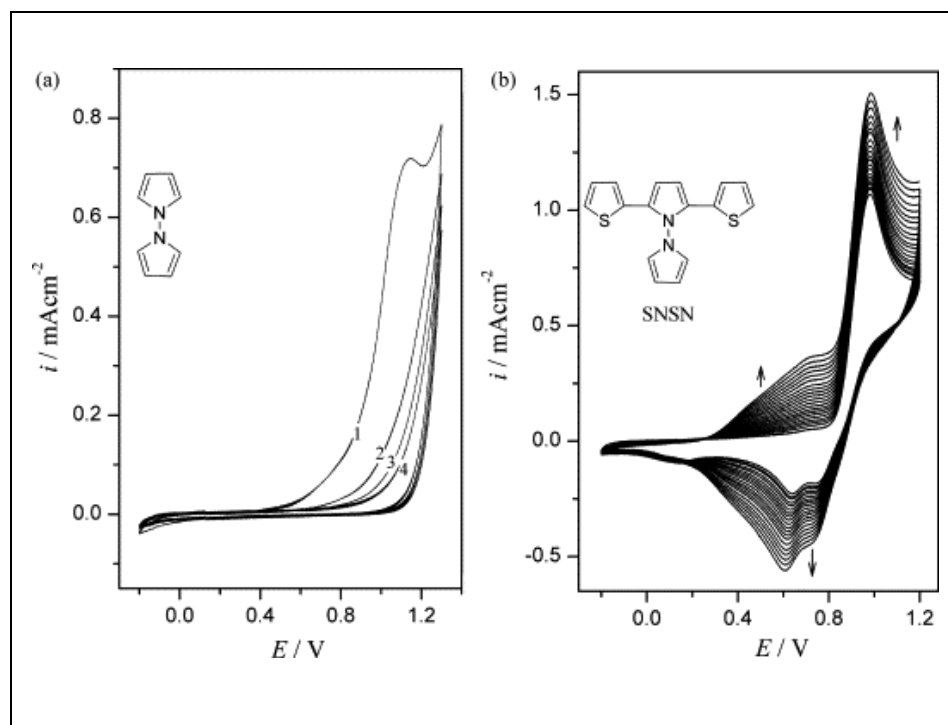


Figure 3.36 Cyclic voltammetry of 1,1'-bipyrrole and SNSN

Table 3.15 Electrochemical and/or optical data for SNS, SNSN, SNSF and SNSNP as well as their polymers.

Monomer	$E_{\text{ox}}(\text{V})$	Polymer	$E_{\text{p},1/2}(\text{V})$	$\lambda_{\text{abs,max}}$ (nm)	$\lambda_{\text{em,max}}$ (nm)	E_{g} (eV)	(%) ΔT
SNSN	0.98	PSNSN	0.64	444	527	2.21	18
SNS ^a	0.94	PSNS ^a	0.60	430	–	2.88	–
SNSF ^b	0.77	PSNSF ^b	0.54	445	543	2.18	21.7
SNSNP ^c	0.77	PSNSNP ^c	0.61	423	537	2.33	18.2

^{a,b,c} estimated from refs. [95], [110] and [111], respectively.

Redox and optical properties of polymer film was also investigated. In order to investigate the redox properties of the PSNSN film it was scanned between 0.0 V and 1.0 V. A single and well-defined reversible redox couple ($E_{p,1/2}$) around 0.64 V was obtained as seen in Figure 3.37a. This value is higher than PSNS ($E_{p,1/2} = 0.60$ V), PSNSF ($E_{p,1/2} = 0.54$ V) and PSNSNP ($E_{p,1/2} = 0.61$ V). Beside this, PSNSN film maintained well-defined and promising reversible characteristics even at higher scan rates. Also, a non-diffusional redox process was observed when peak currents were plotted to the corresponding scan rates (Figure 3.37b). Also, according to equation 1 the current peak depends linearly on scan rate.

$$i_p = n^2 F^2 \Gamma v / 4RT \quad (\text{equation 1})$$

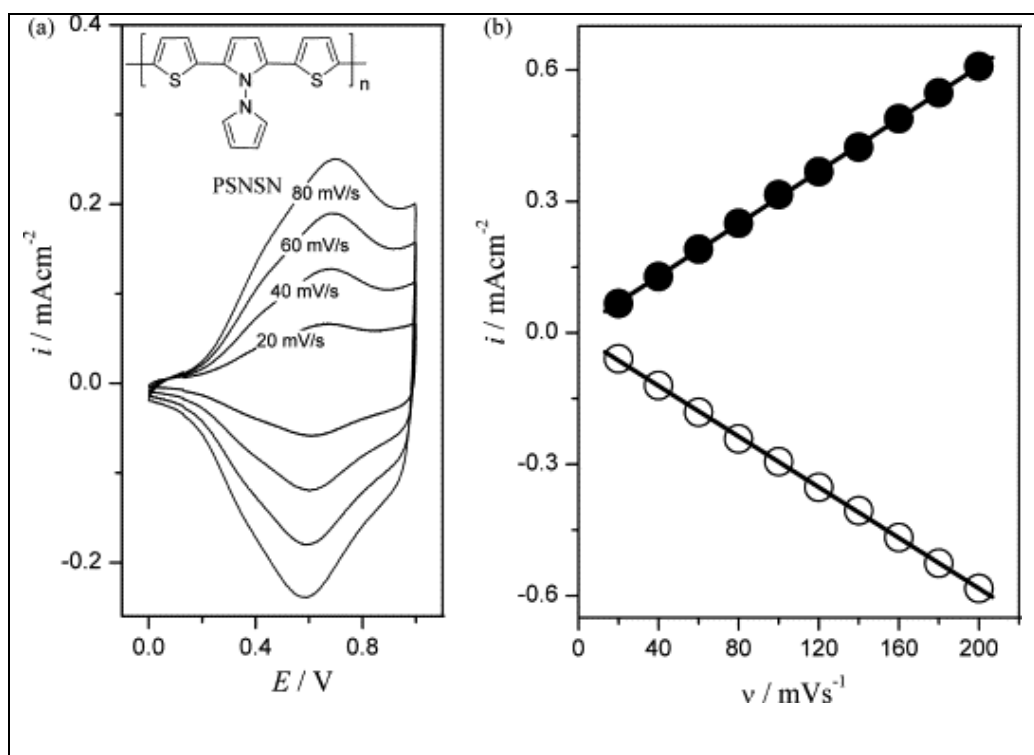


Figure 3.37 (a) Redox behavior of PSNSN film at different scan rates and (b) relationship of anodic and cathodic current peaks as a function of scan rate in 0.1 M TBAP/DCM.

3.3.4. Characterization of PSNSN with FTIR

Three main peaks of dithienylpyrrole at 697 cm^{-1} (for α -H of thiophene rings), 763 cm^{-1} (for β -H of pyrrole ring), and 844 cm^{-1} (for β/β' -H of thiophene rings) play important role to predict the proceeding of polymerization via the coupling of thiophene rings or pyrrole rings [95,103,110,111,181]. Electropolymerization mechanism of SNS was elucidated when the vibrations of α -coupling of the external thiophene rings were examined with FTIR.

The vanishing of 697 cm^{-1} and the appearance of a broad band at 792 cm^{-1} due to the β -H of the thiophene rings were ascribed to the α -coupling between the external thiophene rings as seen in Figure 3.38.

Vibrations at 716 cm^{-1} , 1009 cm^{-1} and 3104 cm^{-1} belong to α -H of pyrrole ring to the central ring of the SNS system [181] and the rest gets unchanged during polymerization. This shows that electropolymerization did not perform over the coupling of pyrrole rings. Peaks of ClO_4^- dopant ion at 1052 cm^{-1} and 621 cm^{-1} were indication of occurrence of polymerization (Figure 3.39).

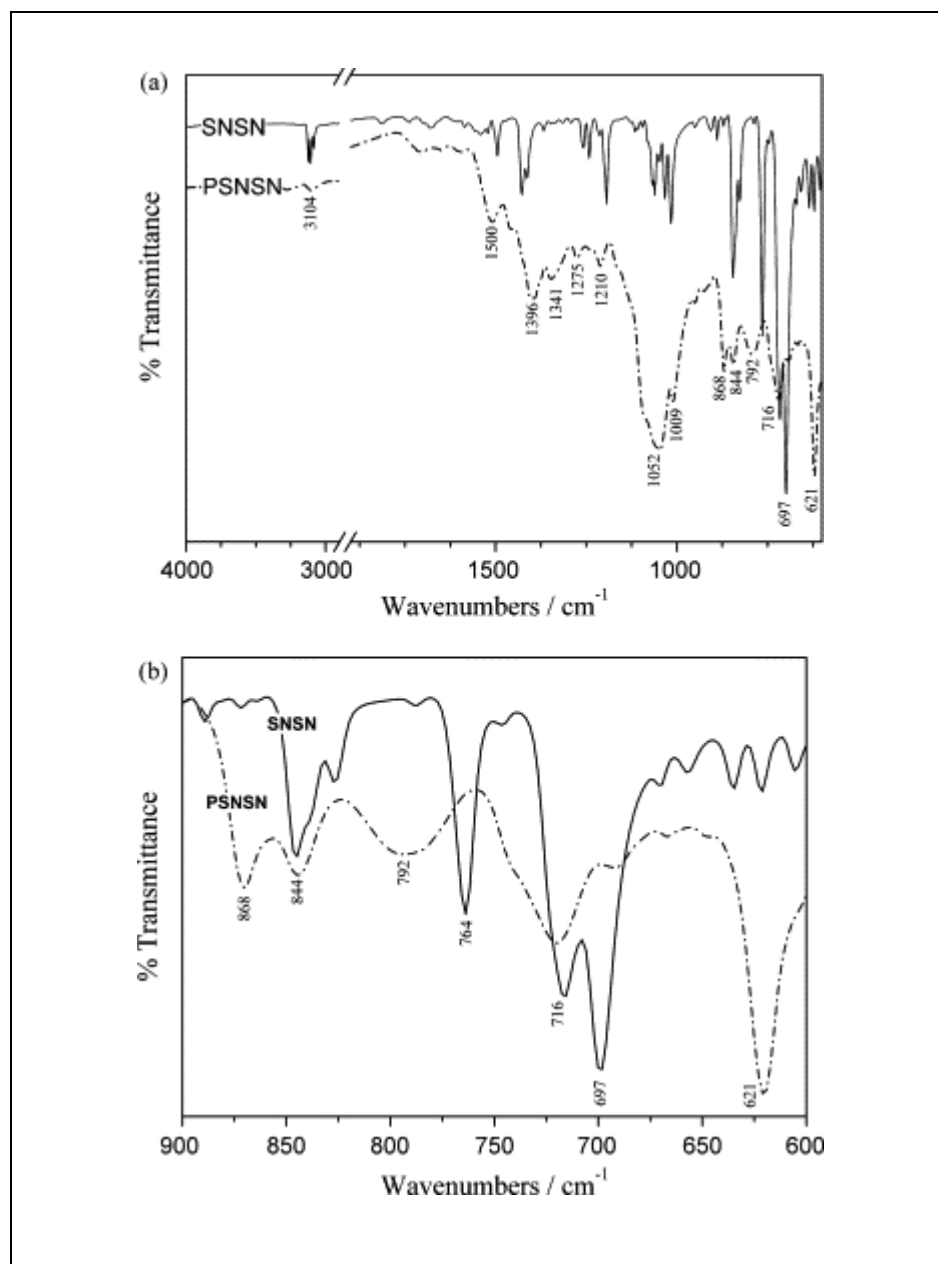


Figure 3.38 FT-IR spectra of SNSN and PSNSN (a) between 4000 cm^{-1} and 600 cm^{-1} and (b) between 900 cm^{-1} and 600 cm^{-1} .

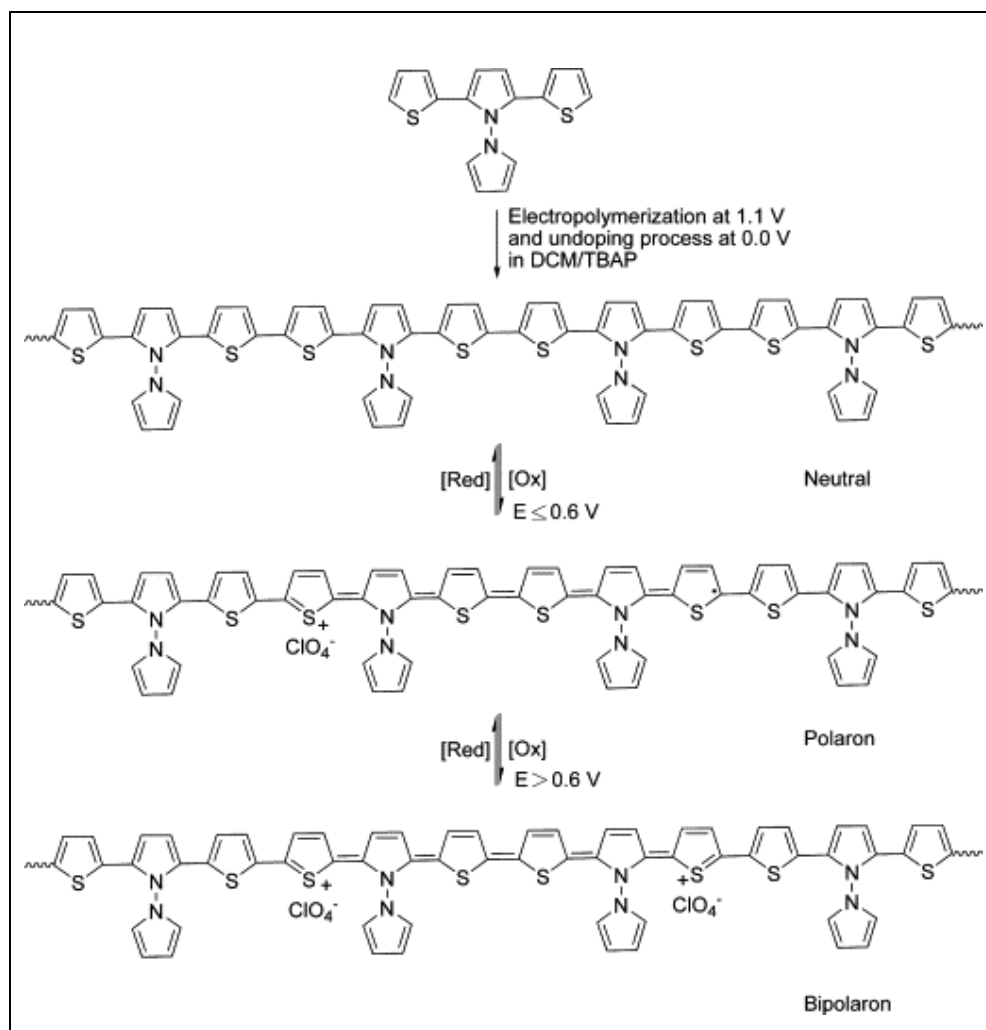


Figure 3.39 Polymerization of SNSN

3.3.5. Electro-Optical Properties of SNSN and of Its Derived Polymer PSNSN

The electronic absorption changes were recorded during SNSN electrolysis in 1.1 V vs. Ag wire. Two novel broad bands appeared in beginning of the electrolysis followed by formation of violet colored polymer film at the ITO surface. The absorption bands at 460 nm, 775 nm, 810 nm and 900 nm can be

closely related with the presence of SNSN charge species and of the p-doped polymer film. (Figure 3.40)

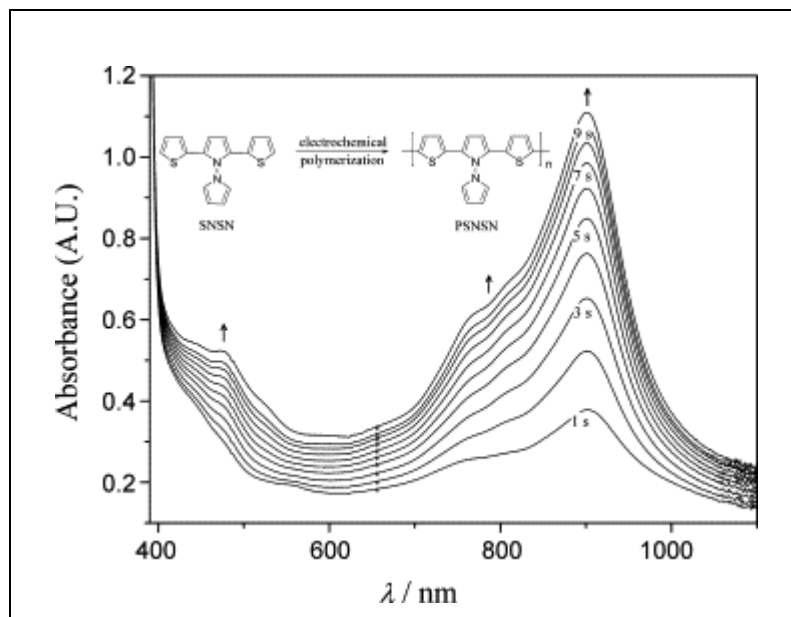


Figure 3.40 The changes in the electronic absorption spectra of 3.0×10^{-2} M of SNSN in 0.1 M TBAP/DCM during in situ electrolysis at 1.1 V.

Then, alterations on electronic absorption spectra applying sequential potential were monitored in situ in order to have an idea about electro-optical properties of the polymer films. The fully neutral state was initially observed at a potential of 0.0 V and then the band gap (E_g) of PSNSN film was calculated as 1.77 eV by the initiation on the low energy end of the $\pi - \pi^*$ transition at 444 nm. This value is in good agreement with PSNS (430 nm, 2.88 eV), PSNSF (445 nm, 2.18 eV) and PSNSNP (423 nm, 2.33 eV) in Table 3.15.

SNSN film displayed a color alteration from orange to violet via oxidation as seen in Figure 3.41. While the intensity of the $\pi - \pi^*$ transition band decreased polaron band at 661 nm and bipolaron at 1000 nm were observed with the

stepwise increase in applied potential as shown in Figure 3.41. This is another expression of highly conductive state of the polymer films (Figure 3.39).

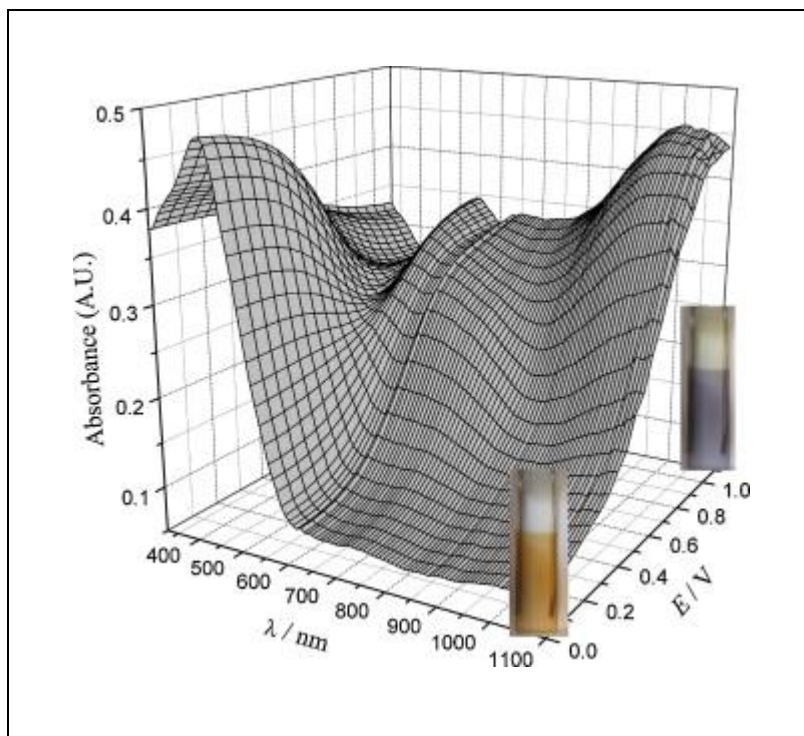


Figure 3.41 Electronic absorption spectra of PSNSN in 0.1 M TBAP/DCM at various applied potentials between 0.0 V and 1.1 V.

3.3.6. Studies of Switching and Stability of PSNSN

Switching and stability play important role for the practical use of electrochromic materials. The square wave potential method was performed for evaluation of switching ability of PSNSN film. Neutral and oxidized states were 0.0 V and 1.1 V with a residence time of 10 s in the electrolyte solution. The percentage transmittance changes (ΔT %) between the neutral and oxidized states were measured, and it was found 18% for 444 nm and 33 % for 661 nm in the visible region as well as 45 % for 1000 nm in the near-infrared region. The time elapsed

between highest and lowest transmittance values is called as the switching time. It was found as ca. 1.0 s. This value is fairly enough for usage of the polymer film in optical displays and electrochromic devices. A reversible and reproducible redox response of film even after multiple scans were observed, e.g., retained electro-optical activity of the polymer film is 64 % at 444 nm, 51 % at 661 nm and 68 % at 1000 nm after the first 500 cycles, as seen in Figure 3.42.

Despite the fact that the stability of PSNSN film was not superior to PSNSF, maintaining 53% of its electroactivity after the first 1500 cycles recorded between neutral and oxidized forms at 445 nm, it was more stable than PSNS without any substituents. Different from PSNS, the PSNSN film did not display any electro-dissolution during switching between its redox states [95].

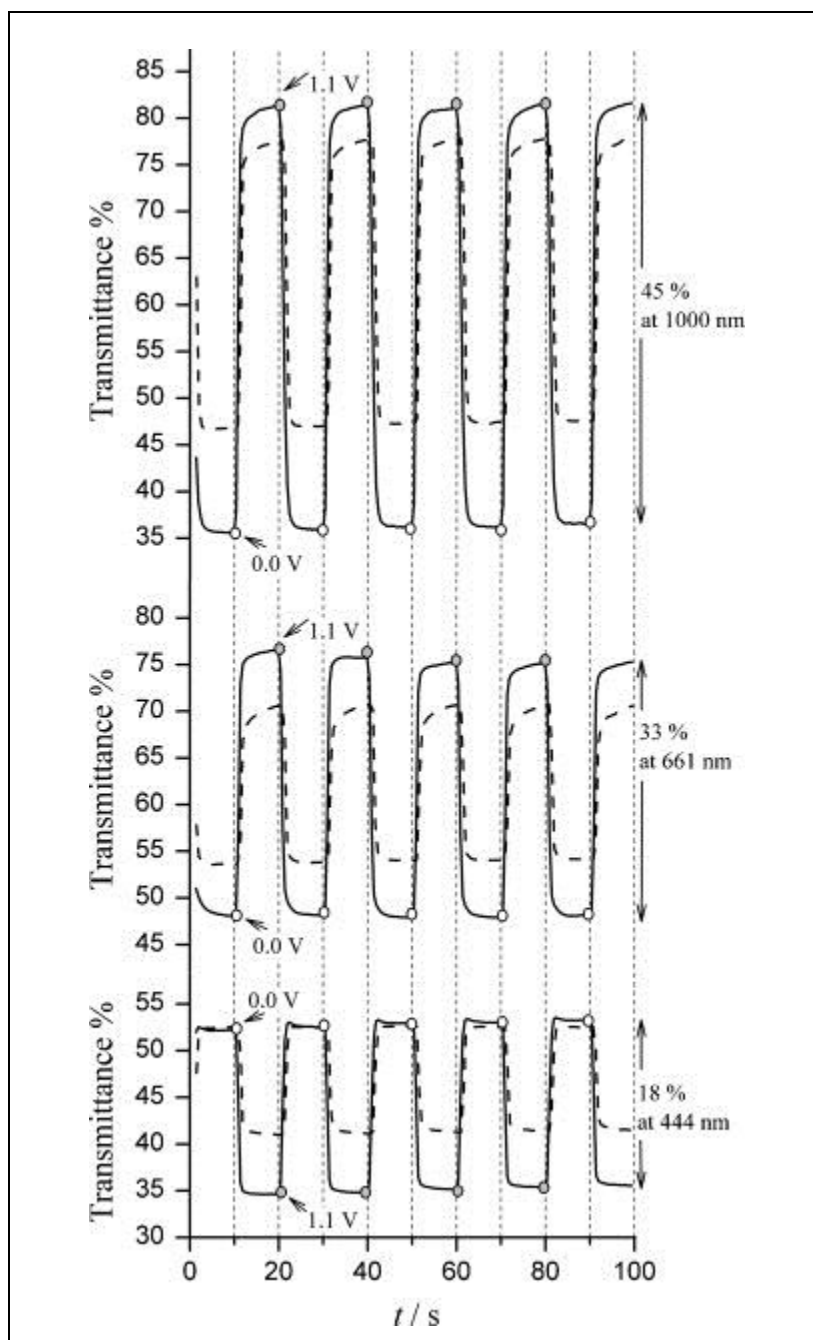


Figure 3.42 Optical transmittance changes for PSNSN at 444 nm, 661 nm and 1000 nm in 0.1 M TBAP/DCM after 1st (—) and 500th (- - -) cycles while the polymer was switched between 0.0 V and 1.1 V with a switch time of 10 s.

3.3.7. Spectroscopic Studies

Solubility of the polymer film in *N,N*-dimethylformamide (DMF) may find potential application for the construction of light emitting diodes and optical displays. Fluorescence spectra of both the monomer and its polymer in DMF were recorded as seen in Figure 3.43. While SNSN showed emission peaks at 395 and 413 nm with blue color, corresponding polymer displayed two emission bands at longer wavelengths at 527 and 547 nm with a yellow color.

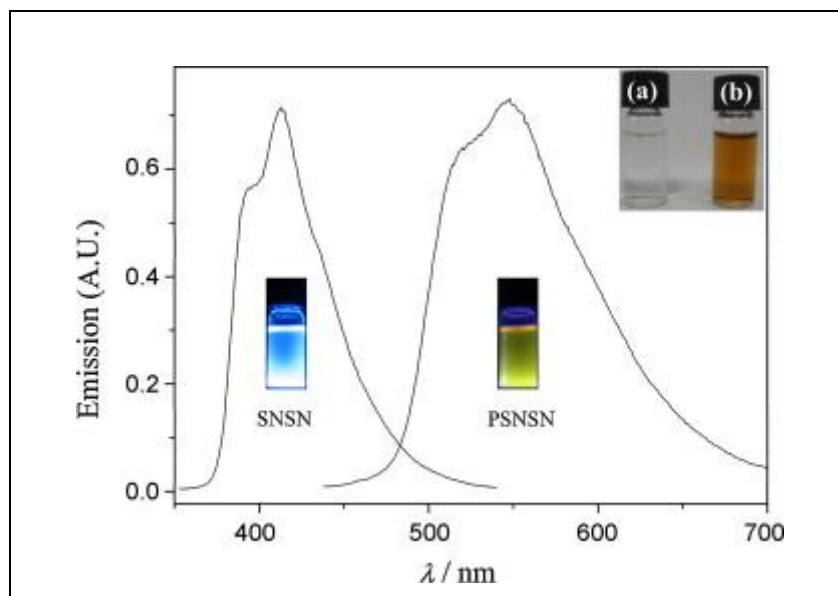


Figure 3.43 Emission spectra of SNSN (excited at 350 nm) and PSNSN (excited at 440 nm) in DMF. Inset: the colors of (a) SNSN and (b) PSNSN in DMF under ambient light.

3.3.8. Building Block System for Development of Electrochemical Reactors

Enantiopure fine chemicals can be produced by electrochemical reactor consisting of specific enzymes like dehydrogenases, mediators and NAD^+ (Figure 3.44 a, b, ERUDES FP7 project). Here, the redox mediator helps to lower the potential for the NAD^+ reduction.

2,5-Di(2-thienyl)pyrroles consist of thiophene and pyrrole rings interconnected by their α -positions, and are undoubtedly of interest in the preparation of electroconductive materials ("organic metals"). The aim of the present work is starting from 1,4-bis(2-thienyl)butane-1,4-dione and a functionalized amine to synthesize 2,5-Di(2-thienyl)pyrroles (SNS) with several spacers that can be bound to mediators, cofactors, and enzymes. These molecules can be polymerized on an electrode surface in order to obtain all of the components for the electrochemical reactor, which are summarized in Figure 3.44c.

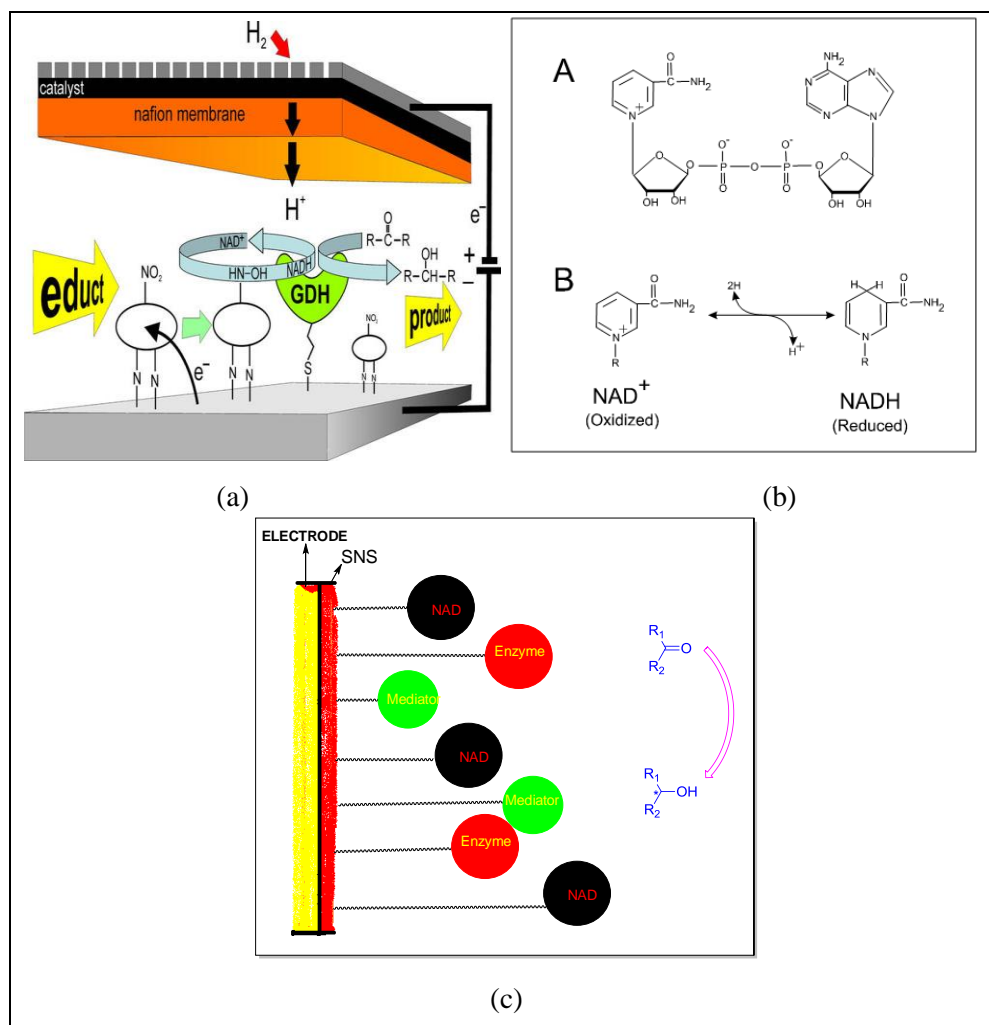


Figure 3.44 Design of electrochemical reactor

3.3.8.1. Synthesis of a SNS-Mediator

Starting from thiophene (**15**) and succinyl chloride (**16**) in the presence of AlCl_3 via a Friedel-Crafts acylation reaction 1,4 diketone **17** was synthesized in good yield. Condensation of **17** with ethylenediamine **34** furnished 2-(2,5-di(thiophen-2-yl)-1H-pyrrol-1-yl)ethanamine (**35**), which then reacted with the monobromomethyl derivative of 4,4-bipyridine to obtain SNS-bipyridine derivative **38**. The reaction of **38** with Rh complex derived the mediator **39**, as shown in Figure 3.45.

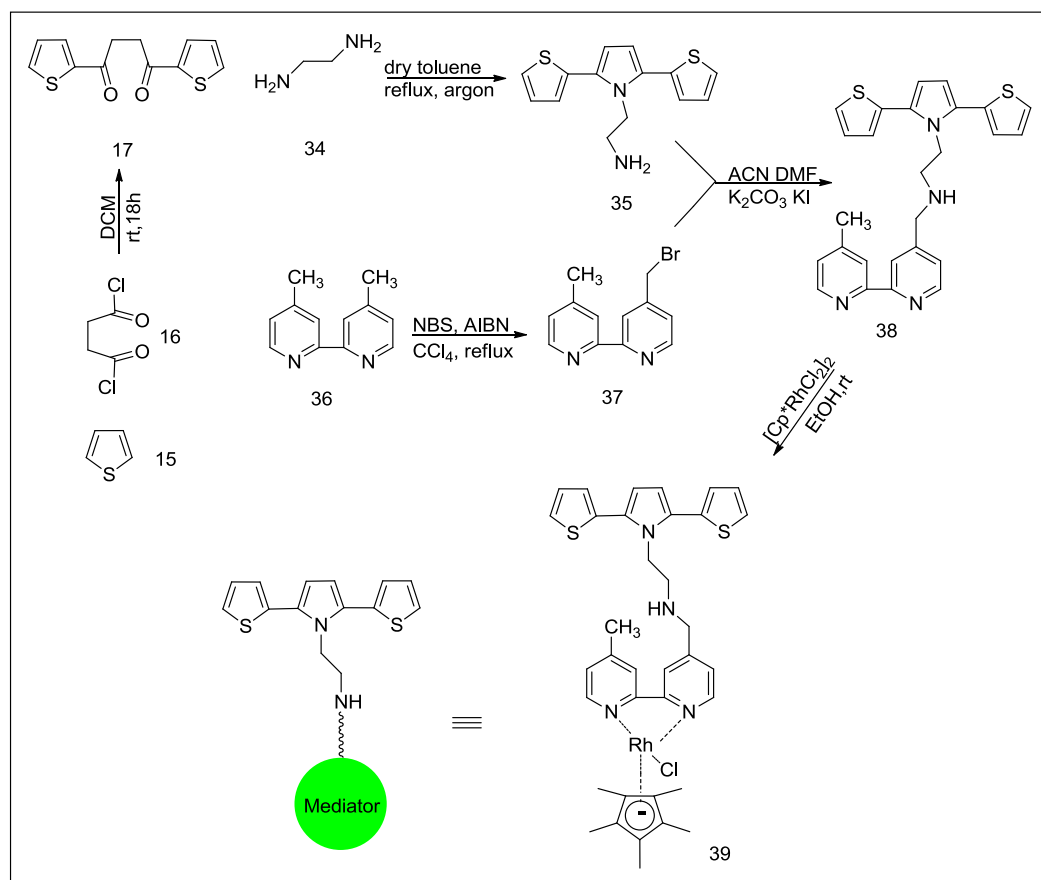


Figure 3.45 Synthesis of Mediator

3.3.8.2. Synthesis of SNS-NAD⁺

For the synthesis of SNS-NAD, the amine derivative **35** is reacted with *p*-formylboronic acid **40** and, after reductive amination, the phenylboronic acid derivative **41** was obtained in good yield. The reaction of boronic acid derivative **41** with NAD⁺ (**44**) gives SNS-NAD complex **45** via the formation of boronic acid ester with a five membered ring diol **45** (Figure 3.46).

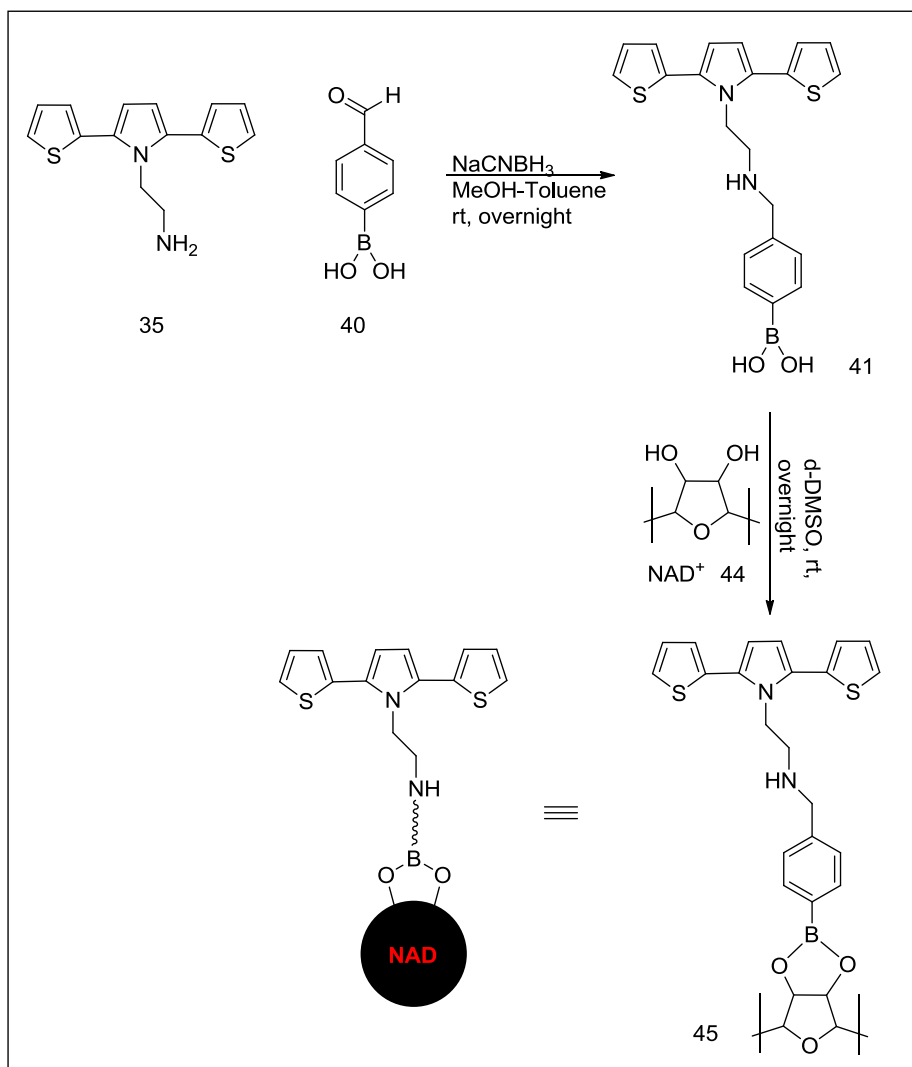


Figure 3.46 Synthesis of NAD- SNS Complex

Using the same reaction of formylthiopheneboronic acid **42**, the boronic acid-SNS derivative **43** is synthesized (Figure 3.47).

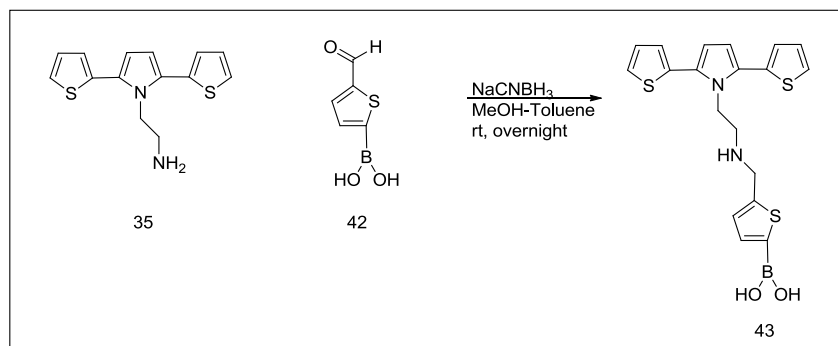


Figure 3.47 Synthesis of the compound **43**

3.3.8.3. Electropolymerization of SNS-Ethylene Amine (SNS-EA) **35**

The monomer **35** (SNS-EA) was successfully polymerized via cyclic voltammetry in 0.1 M tetrabutylammonium perchlorate (TBAP) in dry DCM (2 ml) (Figure 3.48) [182]. Also, a black polymer was covered onto working electrode. A platinum disk (0.02 cm^2), wires of platinum and silver were employed as the working, counter and pseudo-reference electrodes, respectively. In the next step, we are in the process of the attachment of the enzyme into functional $-\text{NH}_2$ group of poly (SNS-EA).

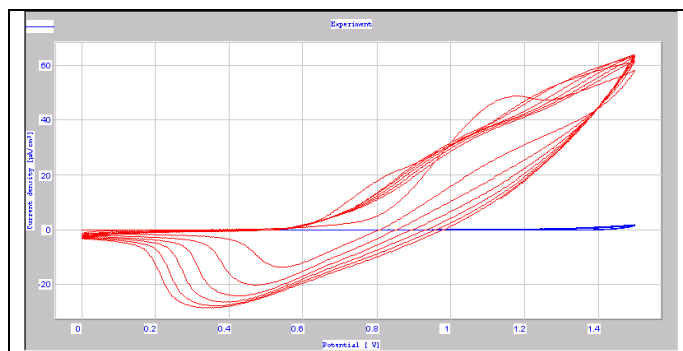


Figure 3.48 Electropolymerization of SNS-ethylene diamine **35** (red) and monomer free medium (blue)

3.3.8.4. Electropolymerization of SNS-EA-Bipyridine **38**

The polymerization of SNS-EA-Bipy **38** was tested in 0.1 M tetrabutylammonium perchlorate (TBAP) in dry DCM at scan rate of 250 mV/s. Upon repetitive cycling in the various potential ranges, the current intensities decreased after each cycling, and the electrode was not coated with the polymer of SNS-EA-Bipy **38** (Figure 3.49). We also observed that no polymerization was obtained with the addition of a drop of boron trifluoride diethyl etherate (yellow color formation after addition of etherate).

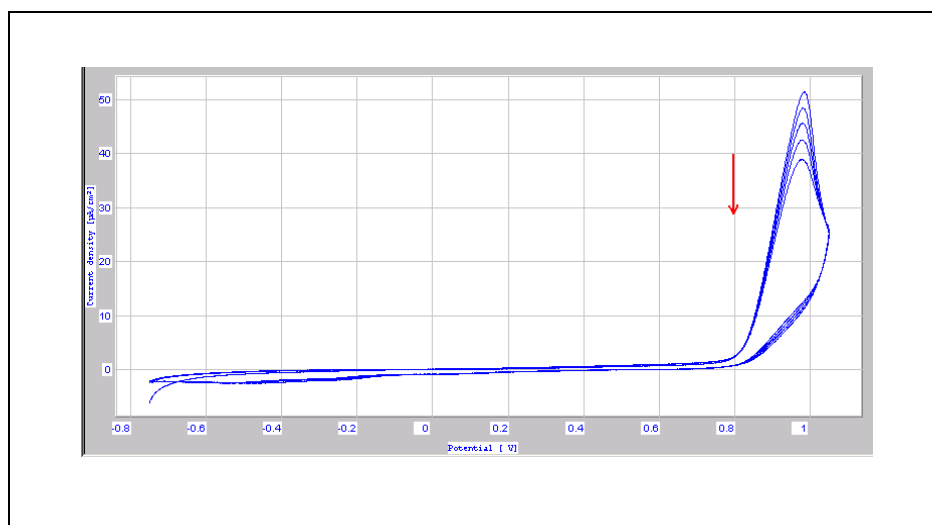


Figure 3.49 Electropolymerization of SNS-EA-Bipy. A platinum disk (0.02 cm²), wires of platinum and silver were employed as working, counter and pseudo-reference electrodes, respectively.

3.3.8.5. Electropolymerization of SNS-EA-Bipy-Rh Complex **39**

SNS-EA-Bipy-Rh Complex **39** was tested in 0.1 M TBAP in dry DCM at scan rate of 250 mV/s. Upon repetitive cycling in the various potential ranges, the current intensities decreased after each cycling, and the electrode was not coated with the polymer of SNS-EA-Bipy-Rh complex **39** (Figure 3.50). Polymerization

did not occur with the addition of a drop boron trifluoride diethyl etherate, as well.

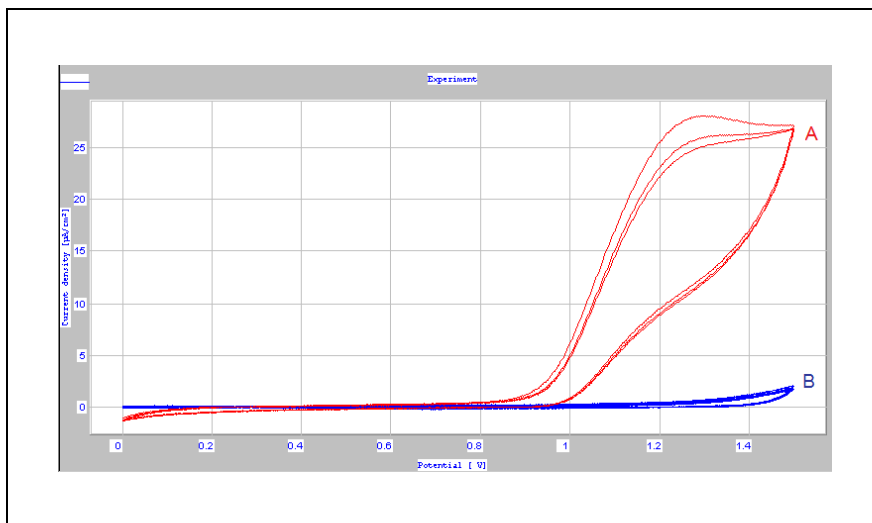


Figure 3.50 Electropolymerization of SNS-EA-Bipy-Rh Complex **39** (A) and monomer free medium (B). A platinum disk (0.02 cm²), wires of platinum and silver were employed as working, counter and pseudo-reference electrodes, respectively.

3.3.8.6. Electro-copolymerization of SNS-EA-Bipyridine Rh Complex **39** with Pyrrole

Pyrrole was first polymerized in 0.1 M TBAP in dry DCM-ACN mixture (4:1) at scan rate of 100 mV/s (Figure 3.51-A). We investigated cyclic voltammetry of the copolymer in the presence of pyrrole and SNS-EA-Bipy Rh complex **39** under the experimentally same conditions. There was a significant alteration in the voltammogram. The current growth between subsequent cycles and the oxidation potential (shifted to left) of the compound were unsimilar than those of pyrrole and SNS-EA-Bipy Rh Complex, which in fact, could be interpreted as the formation of copolymer (Figure 3.51-B).

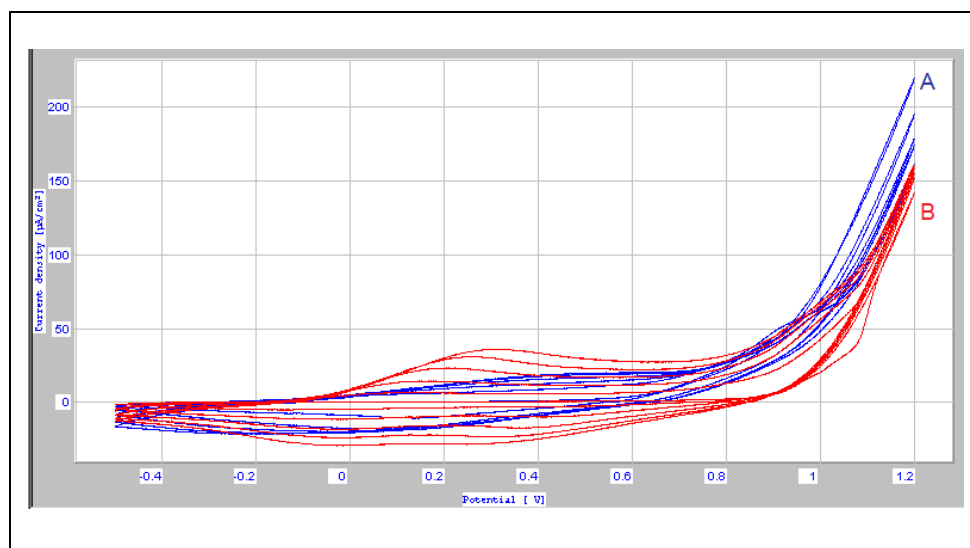


Figure 3.51 Electropolymerization of pyrrole (A) and copolymer of SNS-EA-Bipy Rh Complex **39** (B). A platinum disk (0.02 cm²), wires of platinum and silver were employed as working, counter and pseudo-reference electrodes, respectively.

3.3.8.7. SNS-EA-Bipy Rh Complex-Pyrrole **39** After NAD Addition

Copolymer film of SNS-EA-Bipy Rh complex **39** before and after the addition of NAD was tested in 10 mM of pH= 8.8 phosphate buffer without monomers with cyclic voltammetry. However, a sharp decrease in the current intensities was observed upon repetitive cycling before and after the addition of NAD (Figure 3.52-A: before NAD addition; Figure 3.52-B: after NAD addition). Also, different concentrations of NAD did not make significant difference in the current intensities in cyclic voltammogram.

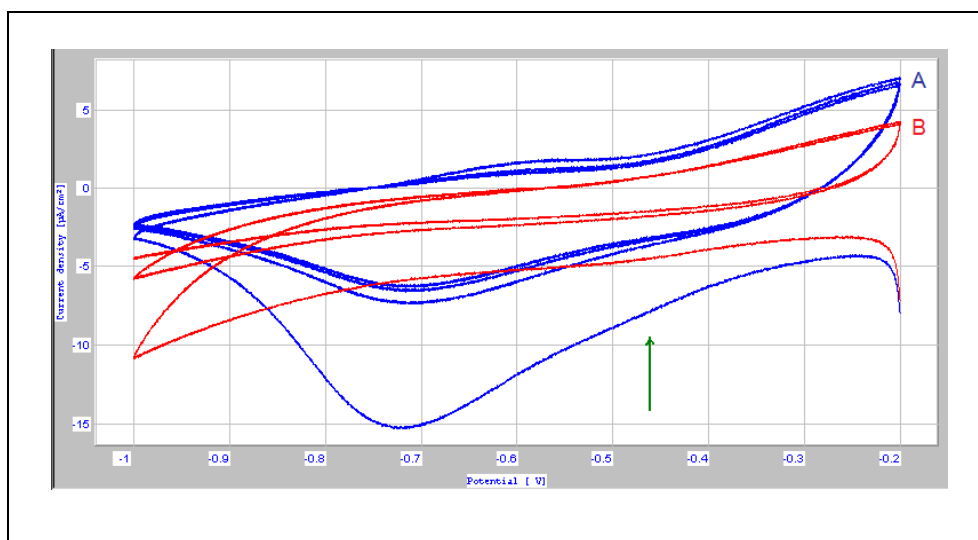


Figure 3.52 Copolymer film of SNS-EA-Bipy Rh complex **39** before (A) and after (B) the addition of NAD.

3.3.8.8. Electropolymerization of SNS-EA-pBA and Copolymerization with 3,4-Ethylene Dioxythiophene (EDOT)

4-((2-(2,5-Di(thiophen-2-yl)-1H-pyrrol-1-yl)ethylamino)methyl) phenylboronic acid monomer **41** (SNS-EA-PBA) was tested for the polymerization in 0.1 M tetrabutylammonium Perchlorate (TBAP) in dry DCM. Upon repetitive cycling in the potential range of 0.0–1.6 V, a new reversible redox couple with a concomitant increase in the current intensities after each cycling was observed. However, the electrode was not coated with the polymer of SNS-EA-PBA (Figure 3.53, A- red cycles). On the other hand, by dissolving the monomer and the comonomer in the same solvent and applying an appropriate potential, conducting copolymer may be obtained onto the electrode surface. Thus, we tried to make a copolymer of SNS-EA-PBA **41** with 3,4-ethylenedioxythiophene (EDOT) in the same medium. Copolymer of SNS-EA-PBA-EDOT was successfully obtained with the formation of a black film on working electrode (B- blue cycles in Figure 3.53).

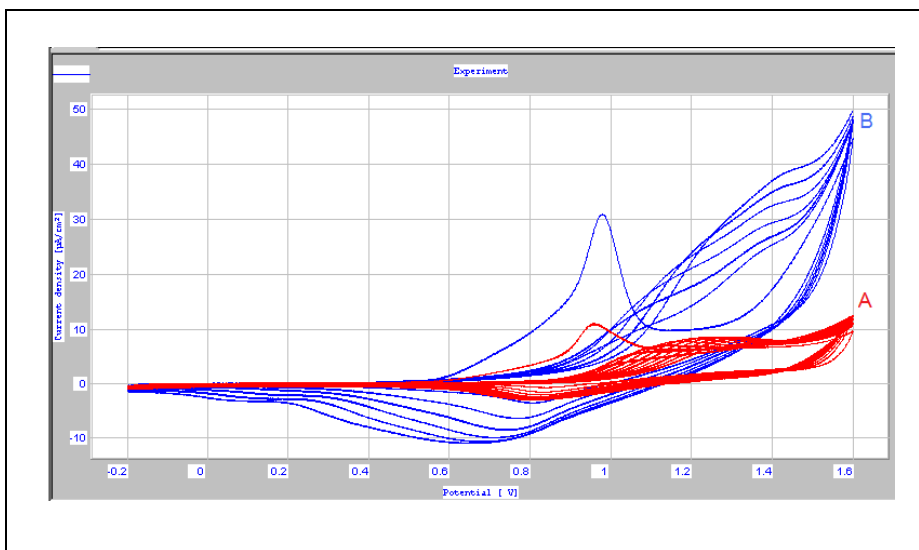


Figure 3.53 Electropolymerization of SNS-EA-PBA (A-red) and its copolymer with EDOT (B-blue). A platinum disk (0.02 cm^2), wires of platinum and silver were employed as working, counter and pseudo-reference electrodes, respectively.

3.3.8.9. Film Stability of SNS-EA-PBA-EDOT in Various Mediums

Copolymer film of SNS-EA-PBA-EDOT was first tested in 0.1 M TBAP in dichloromethane (DCM) without monomer with cyclic voltammetry. After five repetitive cycles, there was no change in the current density which indicates the stability of the copolymer film (Figure 3.54-A). However, the copolymer film was not stable in 0.1 M LiClO_4 in water when it was scanned between 0.0 and 0.9 V. A decrease in the current intensities was observed upon repetitive cycling (Figure 3.54-B). Also, it was observed that the film disintegrated into small pieces in water. Thus, a thinner film was deposited with only 3-4 cycling. It was unluckily dissolved in water during repetitive cycles.

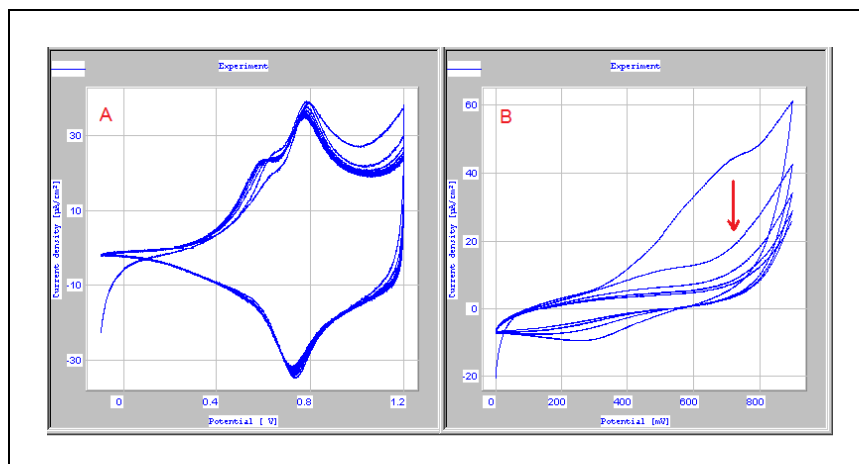


Figure 3.54 Film stability of SNS-EA-PBA-EDOT in 0.1 M TBAP in DCM (A) and 0.1 M LiClO₄ in water (B)

3.3.8.10. Electropolymerization of SNS-EA-PBA with Thiophene

The copolymerization of SNS-EA-PBA **41** with thiophene was tested in 0.1 M tetrabutylammonium perchlorate (TBAP) in dry DCM at scan rate of 100 mV/s. Upon repetitive cycling in the various potential ranges, the current intensities decreased after each cycling, and the electrode was not coated with the copolymer of SNS-EA-PBA-Thiophene (Figure 3.55).

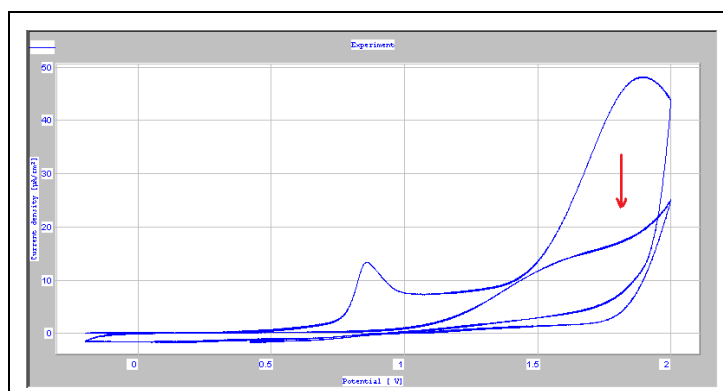


Figure 3.55 Electropolymerization of SNS-EA-PBA-Thiophene. A platinum disk (0.02 cm²), wires of platinum and silver were employed as working, counter and pseudo-reference electrodes, respectively.

3.3.8.11. Electropolymerization of Pyrrole and Its Copolymer with SNS-EA-PBA 41

Pyrrole was first polymerized in 0.1 M TBAP in dry DCM-ACN mixture (4:1) at a scan rate of 100 mV/s (Figure 3.56-A). To explore the copolymer we carried out the studies of cyclic voltammetry in the presence of pyrrole under experimentally the same conditions. There was a significant alteration in the voltammogram. The current growth between subsequent cycles and the oxidation potential (shifted to left) of the compound were unsimilar than those of pyrrole and SNS-EA-PBA **41**, which in fact, could be interpreted as the formation of copolymer (Figure 3.56-B).

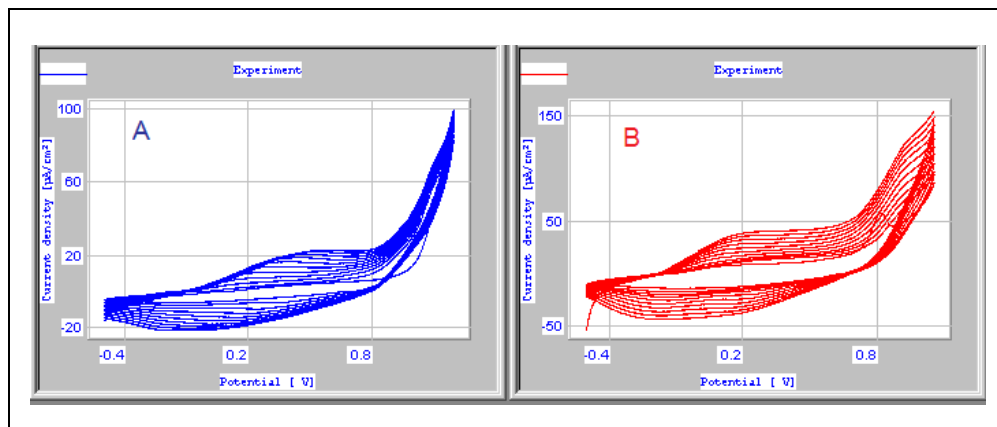


Figure 3.56 Electropolymerization of pyrrole (A) and copolymer of SNS-EA-PBA-Pyrrole (B). A platinum disk (0.02 cm^2), wires of platinum and silver were employed as working, counter and pseudo-reference electrodes, respectively.

3.3.8.12. Film Stability of SNS-EA-PBA-Pyrrole Before and After NAD Immobilizations

Copolymer film of SNS-EA-PBA-pyrrole was tested in 0.1 M LiClO_4 in water in the absence of monomer with cyclic voltammetry. After some repetitive cycles,

there was no change in current intensity which indicated the stability of the copolymer film (Figure 3.57-A). However, a decrease in the current intensities was observed upon repetitive cycling after NAD immobilization was performed (Figure 3.57-B).

NAD immobilization: 18 mM NAD solution was prepared in DI-water. The copolymer coated electrode was immersed into NAD solution. It was stirred over half an hour in a shlenk tube (Figure 3.57-C).

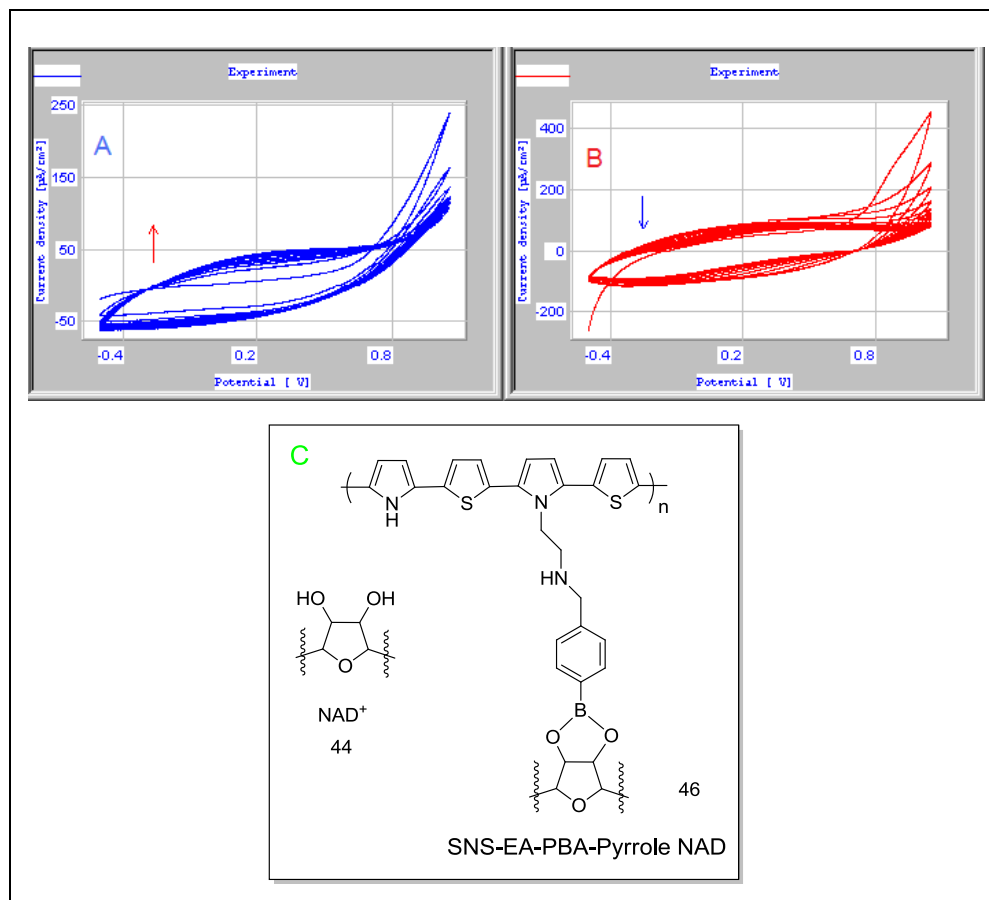


Figure 3.57 Film stability of SNS-EA-PBA- pyrrole in 0.1 M LiClO₄ in water before (A) and after (B) NAD immobilization; (C) structure of immobilization of NAD to SNS-EA-PBA-Pyrrole

the first cycle. Moreover, a growth in the current intensity of the redox couple after each successive scans confirms the formation of an electroactive polymer film on the working electrode surface. Based on the foregoing results, it can be concluded that the first oxidation peak at 1.1 V can be attributed to the oxidation of monomer **I** and the second to the overoxidation of the oligomeric species formed in the vicinity of the working electrode.

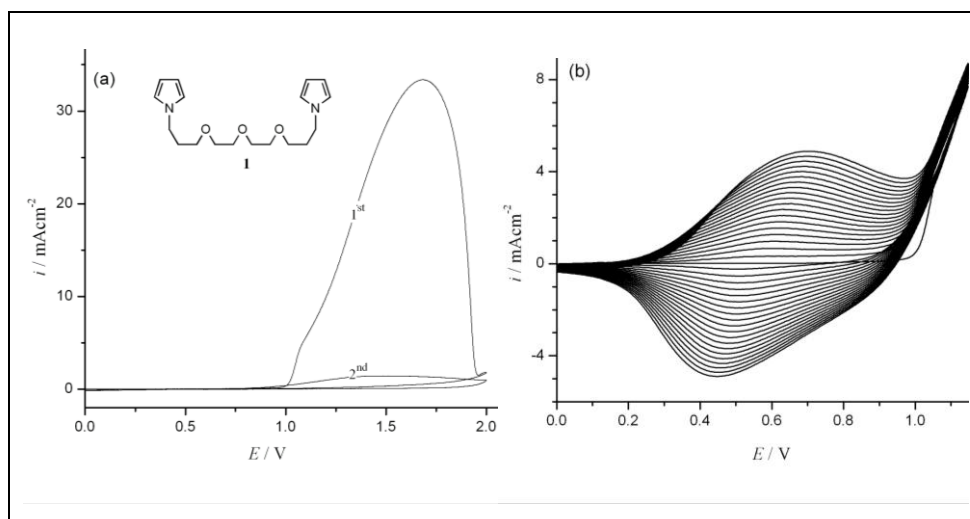


Figure 3.59 Cyclic voltammograms of 3.0×10^{-2} M sample **I** in 0.1 M TBAClO₄/acetonitrile solution (a) between 0.0 V and 2.0 V and (b) repetitive cycling between 0.0 V and 1.1 V at a 100 mV/s scan rate.

The **PI** was polymerized via the constant potential electrolysis at 1.1 V vs. Ag/AgCl on a Pt electrode by passing a total charge of 100 mC/cm^2 . The coated electrode was then placed into an electrolytic solution after it was rinsed with acetonitrile. The **PI** film shows a single and well-defined reversible redox couple ($E_{\text{pa}} = 0.58 \text{ V}$, $E_{\text{pc}} = 0.55 \text{ V}$ vs. Ag/AgCl) while the potential was applied between 0.0 V and 0.9 V (Figure 3.60a).

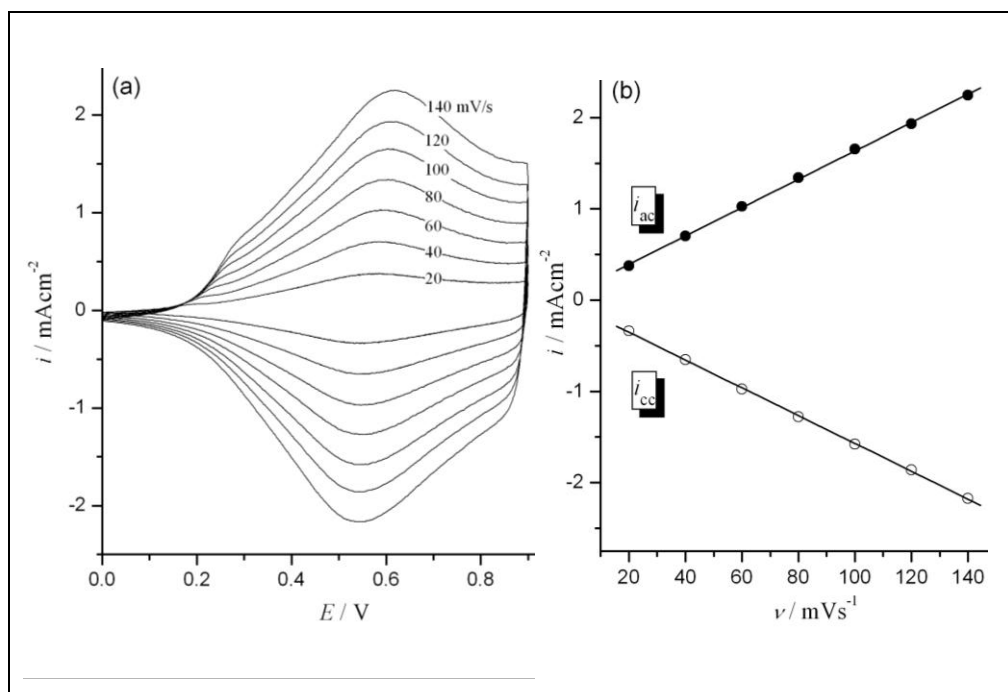


Figure 3.60 (a) Scan rate dependence of PI film (100 mC/cm^2) on a platinum disk electrode in 0.1 M TBAClO_4 in ACN solution at various scan rates between 20 mV/s and 140 mV/s . (b) Dependence of anodic (i_{ac}) and cathodic (i_{cc}) current peaks on the scan rate for neutral and oxidized PI.

The film can be repeatedly cycled between its neutral and oxidized states without any significant decomposition, even after hundreds of cycles, which indicates the stability of the polymer film. It is acquired that peak currents for both anode (i_{ac}) and cathode (i_{cc}) grow linearly with the increments at scan rate. That is indication of non-diffusional redox process and good adhesive between PI film and working electrode (Figure 3.60(b)).

The FT-IR spectrum of the polymer film was consistent with the structure. LiClO_4 electrolyte was employed instead of TBAClO_4 , which prevents the overlapping of the methylene group bands in polymer and TBAClO_4 . The peaks at 2865 and 2931 cm^{-1} and 1122 and 1091 cm^{-1} are assigned to the methylene and etheric groups, respectively, remained unaltered upon polymerization. The

absence of 3100 cm^{-1} indicates a 2,5-coupling. The peaks at 1144 cm^{-1} and 625 cm^{-1} in **PI** spectrum might be resulting from the presence of ClO_4^- dopant. In the light of this information, a plausible structure for **PI** was able to be provided, such as the one shown in Figure 3.61.

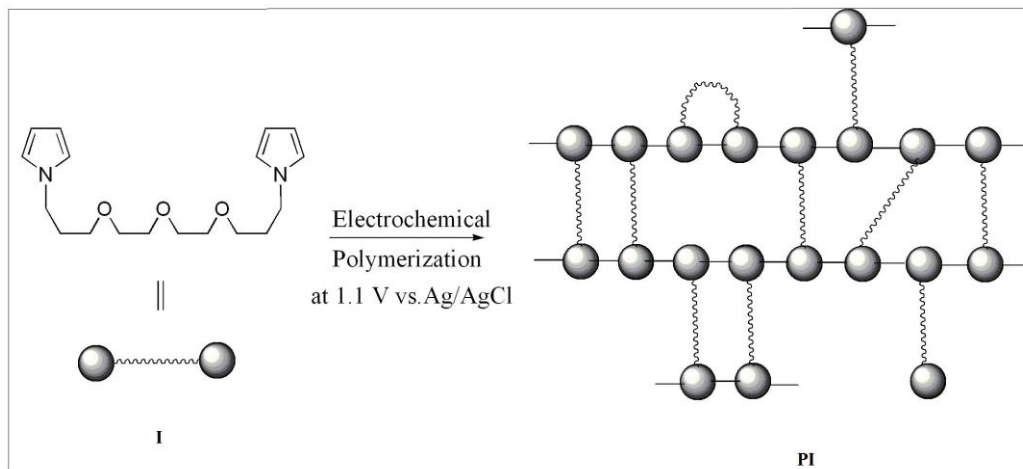


Figure 3.61 Electrochemical polymerization of monomer **I**.

3.4.2. Spectroelectrochemical Behavior of **PI**

The electro-optical properties of **PI** were firstly elucidated via the changes in absorption upon doping in the electrolyte solution without monomer. **PI** film was coated on ITO and then the transition between the neutral and doped states was monitored in the absorption spectrum. The electronic absorption spectrum of the neutral state of the **PI** film displayed an absorption band at 315 nm and from its onset, the band gap (E_g) was calculated as 2.71 eV.

At the time of oxidation, valence-conduction band (π - π^*) transition at 315 nm (3.94 eV) diminished and the absorbance at 484 nm (2.56 eV) increased, pointing out polaron formation (Figure 3.62a). At higher oxidation levels ($E_{p,a} \geq 0.4\text{ V}$) polarons coupled to form bipolarons [183]. Therefore, a new broad band

intensified at 1000 nm (1.24 eV), which was attributed to the highly conducting state of the polymer film [184-186].

Polymer films on ITO display various colors while different potentials are applied. Figure 3.62a shows how the color of the polymer film can be tuned from transparent yellow (at the neutral state) to light pink (at the intermediate state) and finally to blue (at the oxidized state). The hope here is that the polymeric materials at various oxidation states might be suitable for many applications like displays and electrochromic devices.

Determination of response times and optical contrast in **PI** film on indium tin oxide were made from difference at transmittance. Therefore, the method of square wave potential step along with optical spectroscopy was utilized in order to take a look at the switching ability of **PI** between redox states. The **PI** film on ITO was successfully switched between 0.0 mV and 800 mV versus silver-wire for 10 seconds. The difference in the transmittance between the oxidized and neutral states was measured as 16.77 % (at 315 nm), 17.53 % (at 484 nm), and 73.04 % (at 1,000 nm) (Figure 3.62b). The charge passed at 95% of the full optical switch was used to evaluate response time since the color change could not be distinguished with the naked eye after this point. The response time was found to be 0.8 s from the oxidized into neutral cases. This indicates that **PI** might be quickly switched to the neutral case.

The long cycle life is also important parameter in the spectroelectrochemical study. Switching was performed by assigning potential steps of 1.0 s between 0.0 V and 0.8 V. After switching 500 times, the polymer film keeps its high redox stability, in turn retaining approx. 75 % of its optical activity.

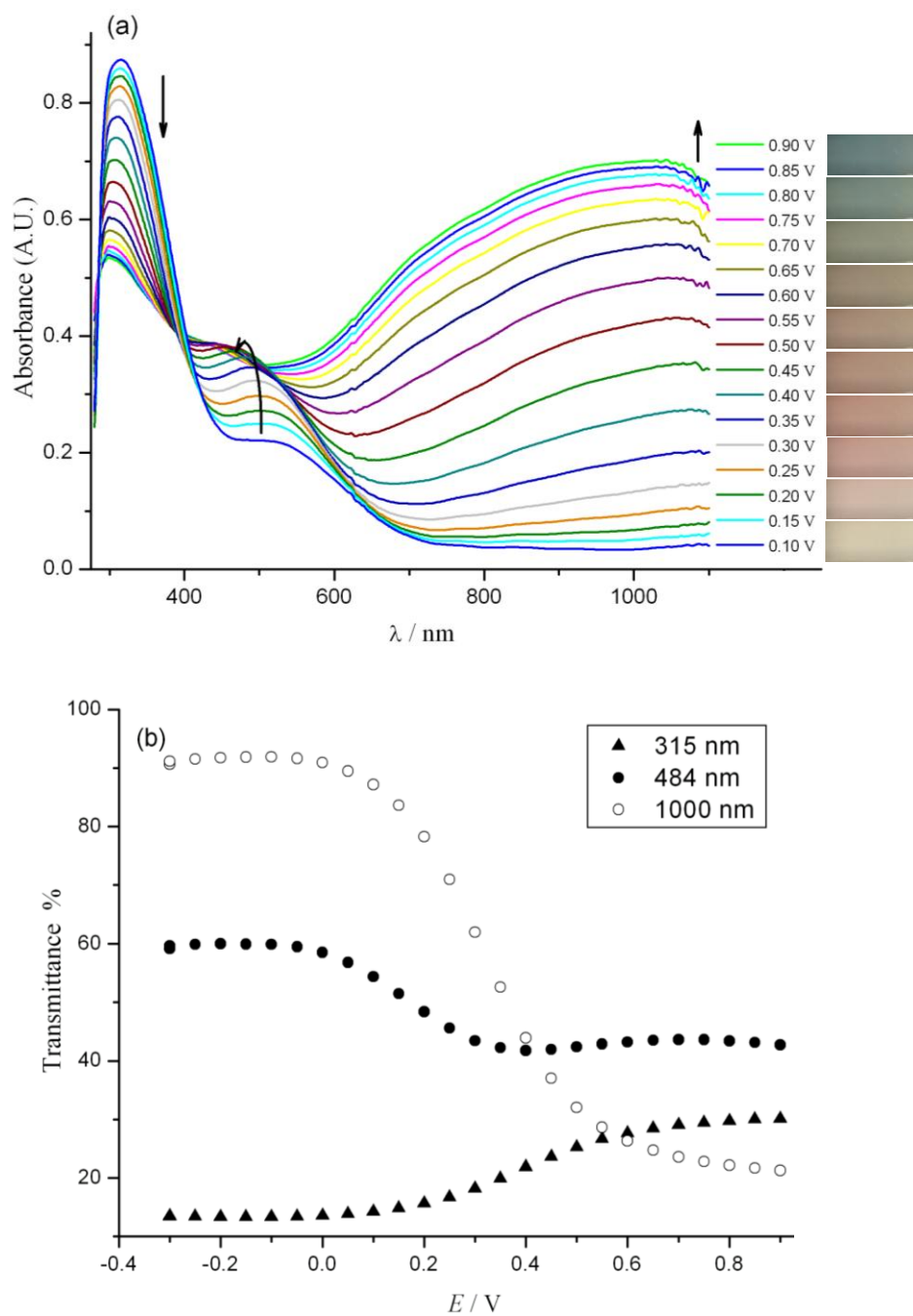


Figure 3.62 (a) *In-situ* absorption spectra for PI (50 mC/cm² on ITO) was enrolled at 0.1 M TBAClO₄ in ACN at several applied potentials (vs. Ag-wire) and (b) Optical responses of PI (50 mC/cm² on ITO) at 315 nm, 484 nm, and 1000 nm as a function of applied potentials in 0.1 M TBAClO₄/acetonitrile (vs. Ag-wire).

3.4.3. Thermal Behavior of PI

DSC thermogram for PI film has two exothermic transitions at 175 °C and 280.5 °C. The first exotherm might be thought as an organizational process and the latter could be attributed to dopant loss. TGA was also used to confirm the DSC measurement. A TGA thermogram for the polymer showed two maximum weight losses at 300 °C and 430 °C under an inert atmosphere. They are connected with dopant loss and the degradation of ethyleneoxide-chains, respectively (Figure 3.63). The PI losses are approx. 32% and 16% of its weight at 300 °C and 430 °C, respectively, and the rest contains basically PPy moiety. After 800 °C, nearly 34 % of the polymer remained. These results indicate that PI possesses high thermal stability.

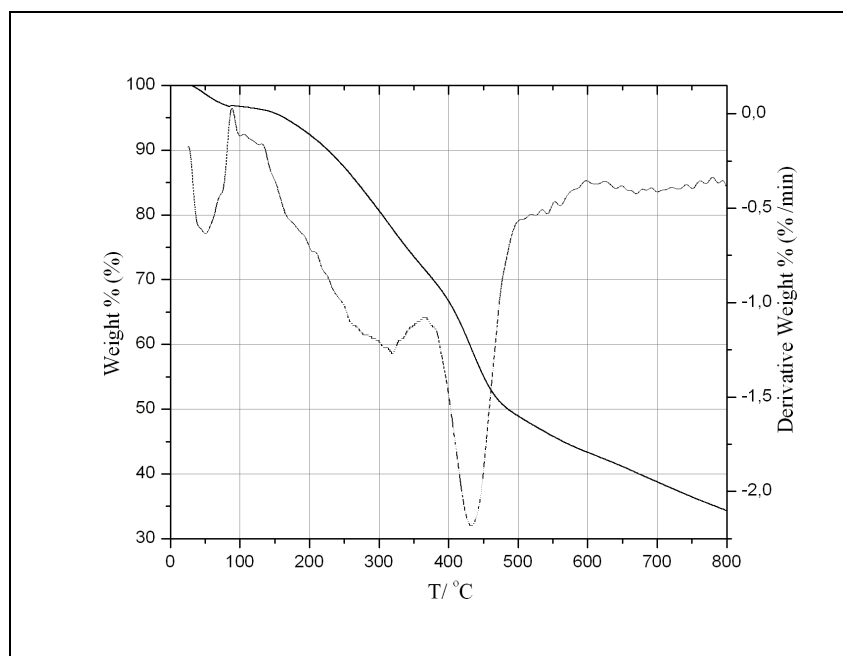


Figure 3.63 TGA thermogram of PI (polymerization charge of 5 C/cm²)

3.4.4 Electrical Properties

The current–voltage (I–V) characteristics of the **PI** (5 C/cm^2) at 300 K were performed in the voltage range of 0.1–2.5 V. The curve of I–V is linear and is not dependent on the reversal current. This behavior indicates the ohmic nature of contacts. The conductivity (σ) of the films was measured as $2.5 \times 10^{-4} \text{ S/cm}$.

PI was compared to polypyrroles (PPy) regarding conductivity. The reason for the lower conductivity of **PI** is steric effect of the flexible spacer that greatly disturbs the ring–ring planarity, and makes the process of hopping between chains much more difficult (Table 3.16).

Table 3.16 Voltammetric and spectroelectrochemical data with the conductivities of PPy and P-I at 300 K.

Polymers	$E_{m,a}$ (V)	$E_{p,a}$ (V)	λ_{max} (nm)	E_g (eV)	σ (Ωcm) ⁻¹
PPy	1.05	0.10	400	2.50	60.5
PI	1.10	0.58	315	2.71	2.5×10^{-4}

3.4.5. Voltammetric Recognition of Na⁺ Ions

Sodium recognition in food, blood and soil is increasingly important. One of the essential mineral substance nutrients in the human body is sodium ion. Some reports use different analytical systems and spectrophotometric techniques in various clinical, pharmaceutical and environmental samples [187-192]. Also, carbon paste electrode modified with layered birnessite-type manganese oxide and anodized indium tin oxide electrode were lastly tested [193,194]. Simple and efficient sensors towards Na⁺ is still needed, thus polymeric P-I type film was constructed for the detection of sodium ions using with cyclic voltammetry. The complexing properties of **PI** towards alkali cations (Li⁺, Na⁺ and K⁺) was

investigated in an acetonitrile medium, in which **PI** was grown by passing a total charge of 100 mC/cm^2 at 1.1 V. Changes in the voltammogram of the polymer film were monitored during the addition of a small amount of cations to a monomer-free electrolytic solution. Among the cations, Na^+ ion leads to a modification of the redox behavior of the polymer film. Figure 3.64 depicts the response of the polymer with respect to increasing ion concentration. The anodic peak for polymer oxidation shifted negative ($\Delta E = -90 \text{ mV}$ for $6.0 \times 10^{-2} \text{ M NaClO}_4$) and stabilized after 2 scans. Positive shifts are usually observed when complexations occur in close vicinity to the electroactive reporters, the observation of a negative displacement is probably due to conformational change in pseudo-cage side of polymeric structure after complexation with Na^+ ion as reported previously [103]. It is also noteworthy that the redox behavior of the polymer film stayed the same by changing ionic strength of the medium since the polymer film did not give any response towards Li^+ and K^+ .

The results may conclude that the ionic radius of Na^+ ion fits the cavity sizes in the polymer structure and the polymer film has a selective voltammetric response towards Na^+ among alkali cations, in turn revealing the electrical transduction of the chemical information.

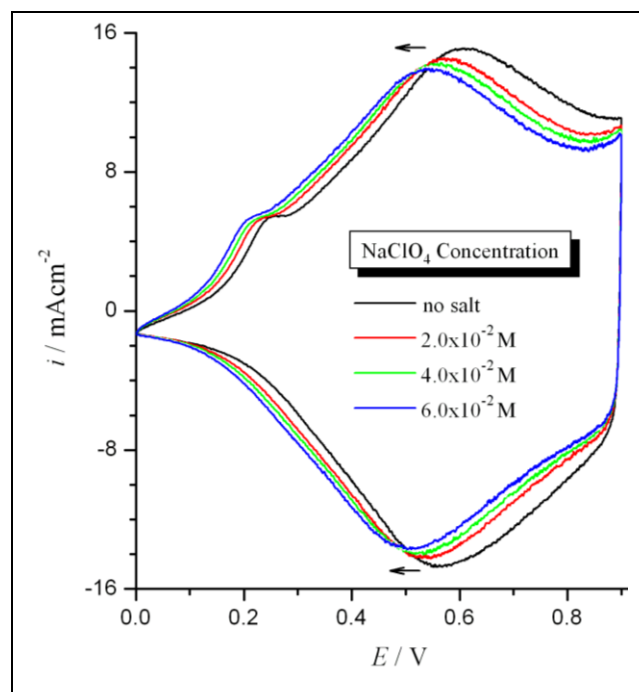


Figure 3.64 Voltammetric responses of the PI (100 mC/cm^2) with respect to an increasing Na^+ ion concentration in a $0.1 \text{ M TBAClO}_4/\text{acetonitrile}$ solution at a scan rate of 50 mV/s .

3.4.6. Preconcentration and Voltammetric Recognition of Ag^+ Ions

An analogue of PI with shorter flexible intra-chains was previously examined using large scale process for the detection of radioactive silver species from nuclear power plants besides the detection of silver species with the impedance spectroscopy [117,118,120]. We tested the PI for the extraction of silver ions to examine upper limit of length of intra-chains between pyrrole moieties. The preconcentration of silver ions on the PI surface was carried out by electrochemical deposition, in which the presence of silver was confirmed by voltammetric experiments. When PI coated electrode was treated at -0.5 V in a monomer-free solution containing Ag^+ , the cyclic voltammogram displayed a distinct oxidation peak that was attributed to metallic silver (Fig. 3.65a). The attributed silver oxidation peak on the first anodic scan nearly disappeared in

subsequent scans. The amount of accumulated silver could be calculated from the integration of the anodic peak, in which these increase along with the Ag^+ concentration (Fig. 3.65b).

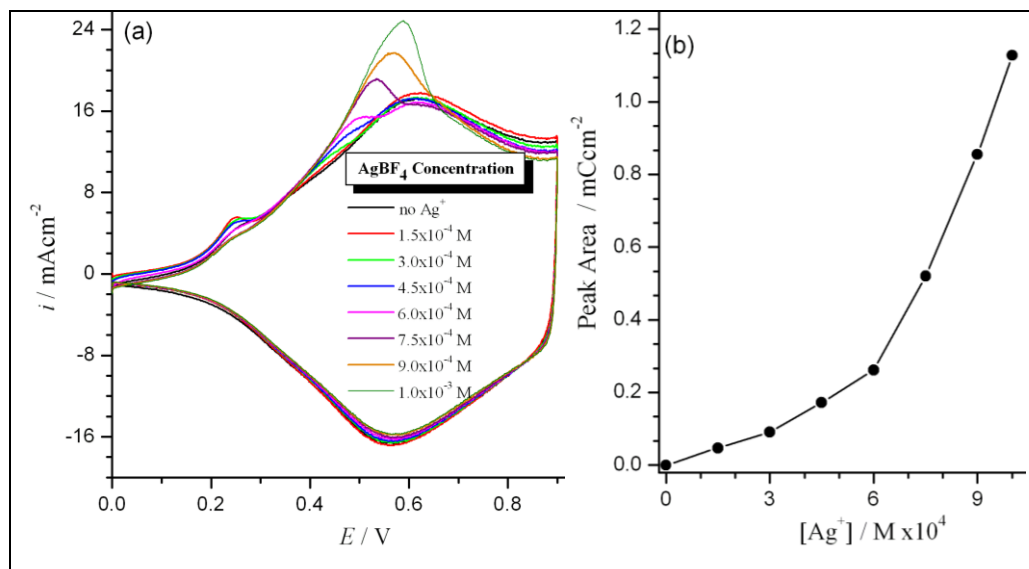


Figure 3.65 (a) Cyclic voltammograms recorded for PI (100 mC/cm^2) after 30 s conditioning at -0.5 V in various concentrations of AgBF_4 in a $0.1 \text{ M TBAClO}_4/\text{acetonitrile}$ solution at a scan rate of 50 mV/s and (b) the amount of the charge of accumulated silver calculated by the integration of the anodic peak.

SEM also verified the presence of a crystalline metallic Ag that was deposited on the polymer surface. The SEMs revealed crystals with an average cross-section from 20 to $30 \mu\text{m}$ on PI (Fig. 3.66b). The same conditions were applied for the PI film without any Ag^+ ions in the solution (Figure 3.66a). When the reduction potential or conditioning time was increased, metallic silver was deposited onto the polymer surfaces (Figure 3.66c). It is also in progress of the homogenous silver coatings of PI films for sensing of biologically active substances via surface enhanced Raman spectroscopy (SERS) method.

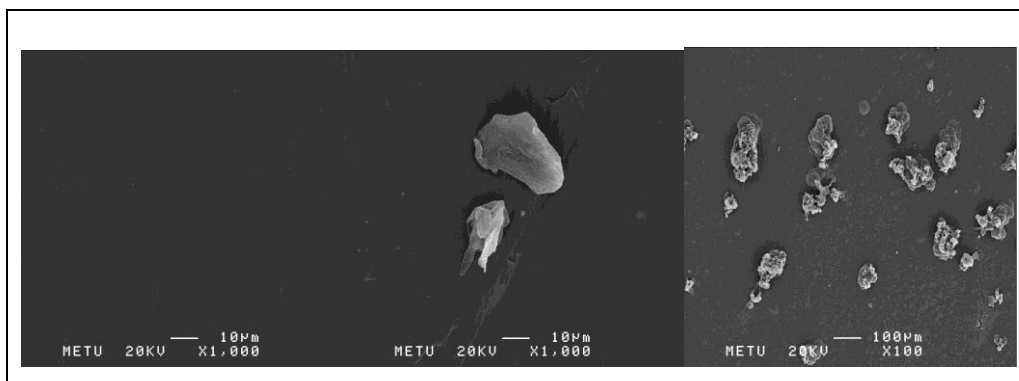


Figure 3.66 SEM pictures obtained (a) PI without Ag^+ ions, (b) PI after the applied -0.5 V for 5 minutes in a 0.1 M TBAClO_4 /acetonitrile solution containing 1.0×10^{-3} M AgBF_4 . (c) PI after the applied -1.0 V for 5 min in a 0.1 M TBAClO_4 /acetonitrile solution containing 1.0×10^{-3} M AgBF_4 .

CHAPTER 4

CONCLUSIONS

4.1. Thermosensitive Biodegradable mPEG-PLLA Block Copolymers: Syntheses, Characterizations and Applications in Drug Delivery Systems

Most challenging problem for the topotecan and camptothecin anti-cancer drugs is the conversion of active lactone ring into inactive toxic carboxylate form at physiological conditions (pH= 7.4) in body. To overcome this difficulty, an efficient and simple platform based on PLLA-PEG diblock polymeric gels was designed to maintain topotecan and camptothecin in the form of lactone, especially for brain tumor therapies such as local injection. The sol-gel transition temperature of the matrix was firstly adjusted by altering chemically the length of each component. Aqueous solutions of appropriate copolymers synthesized showed sols at around 45° C, suitable for the injection, then a gel with subsequent rapid cooling to body temperature. Spectroscopic and chromatographic analyses confirmed that high stabilization of lactone species of CPT and TPT within this polymer matrix (>95 %, Figure 4.1), efficient homogenous drug loadings at 0.015 %, 1.0 % and 10 %, sustained-release matrix of CPT and TPT anticancer drugs over three weeks were succeeded. Stabilization mechanism of anticancer drugs with polymer matrix was elucidated by primarily ATR-FTIR, confocal microscopy and light microscopy. Lastly, the cytotoxic efficacy of PLLA-mPEG-TPT platform was evaluated on cancer cell lines (LLC-1 and 4T1) via MTT assay, and then the administration of PLLA-mPEG-TPT to the mice bearing

breast tumours established with 4T1 cells resulted in a significant reduction in tumor size and better survival percentages.

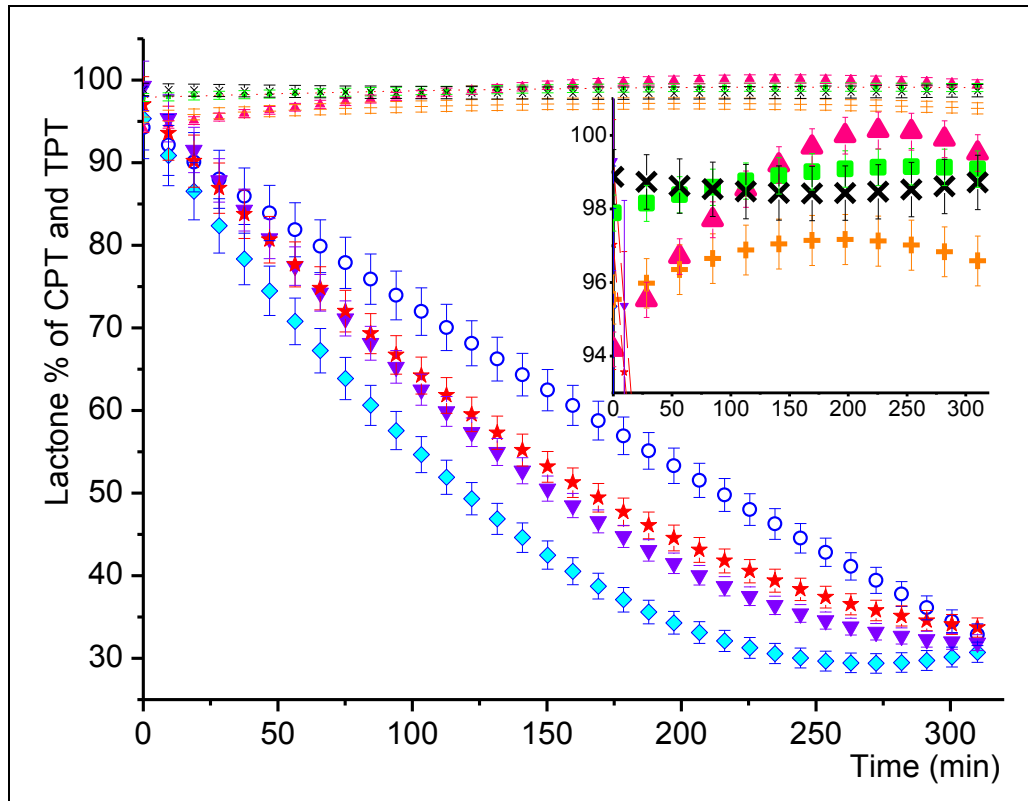


Figure 4.1 Stability of CPT and TPT in gels (0.015 %) versus rapid hydrolysis in physiological environment (circle: L % of free TPT in buffer analyzed with FL; diamond: L % of free CPT in buffer analyzed with FL; up-triangle: L % of CPT in gel analyzed with FL; plus: L % of TPT in gel analyzed with FL; down-triangle: L % of free CPT in buffer analyzed with HPLC; star: L % of free TPT in buffer analyzed with HPLC; cross: L % of TPT in gel analyzed with HPLC; square: L % of CPT in gel analyzed with HPLC).

We basically synthesized two different molecular weight poly (L-lactide) (**19** and **20**) from L-lactide and Sn(Oct)₂ via ring opening polymerization (Table 3.17). As expected, these homopolymers did not show any sol-gel property even at low concentration (3 %) due to hydrophobic character of the polymer. Number average molecular weight of homopolymer increased when higher mass of L-lactide is employed (i.e. **19** vs **20**). Then, we synthesized PLLA-mPEG diblock copolymers, **20-27**, from L-lactide and mPEG2k or mPEG5k in toluene at reflux temperature. The reason for the usage of low molecular is that higher molecular weight of PEG (above ~10k) is inappropriate for filtration through membrane of human kidney due to being wide hydrodynamic radius of the PEG in aqueous phase [23]. As shown in Table 3.17, Number average molecular weight of copolymer is closely variable with L-lactide mass. It was obtained that copolymers **21-22** did not display sol-gel property at low concentration. It is highly possible that those copolymers are still highly hydrophobic. We decided to shorten the poly(L-Lactide) length more. Therefore, we synthesized copolymer **23** via same methodology above. After undesired results for copolymer **23** at the concentrations of 3, 5, 10 and 30 %, suitable sol-gel characteristics for polymer suspension **23** was found at 45 %. While that suspension was gel at room temperature, it started to flow immediately at 35-37 °C.

Table 3.17 Syntheses and sol-gel characteristics of PLLA and PLLA-mPEG polymers

ID	\bar{M}_n	Lactide /Sn(Oct) ₂	Lactide (g)	Sn(Oct) ₂ (mg)	Time (h)	Toluene (mL)	Conc. %
19	4200	100	3.0	84	3.0	45	3
20	7670	225	6.8	84	3.0	45	3
21	10120	140	5.0	100	10.5	120	3
22	7305	84	3.0	100	10.5	120	3
23	3665	42	1.5	100	10.5	120	3, 5, 10, 30, 45
24	5645	42	1.5	100	24	120	3
25	12900	140	5.0	100	10.5	120	3
26	8860	84	3.0	100	10.5	120	30
27	7500	56	4.0	200	10.5	120	30

4.2. Preparation of Polymeric PEG:PSA Particles for the Camptothecin Anticancer Drug Delivery System

In order to keep camptothecin in active and non-toxic lactone form, it was decided to use biodegradable and FDA approved PEG-SA copolymer. CPT was encapsulated in PEG-SA nano- and micro- particles. CPT showed excellent stability within particles. CPT loaded particles are planned to use in vivo studies to treat various malignant tumors via systemic delivery.

4.3. Synthesis and Properties of Novel Electrochromic Polythienylpyrrole

First, 1,1'-bipyrrole was synthesized in four steps from hydrazine, for the objective of examining of its electropolymerization characteristics, especially to see the contribution of N- pyrrole substitution having no further linkage between pyrroles (Figure 4.2). While investigating of the redox behavior of 1,1'-bipyrrole in a 0.1 M TBAP/DCM electrolyte solution via cyclic voltammetry, an irreversible oxidation (E_{ox}) at 1.14 V during the first anodic scan corresponded to a radical formation on

bipyrrole. However, following scans indicated the disappearance of that peak, which caused no film formation on the electrode surface with repetitive cycling or constant potential electrolysis. One possible explanation is that twisted structure of bipyrrole rings with an $\sim 80^\circ$ interplanar angle [135] may inhibit the electropolymerization of 1,1'-bipyrrole.

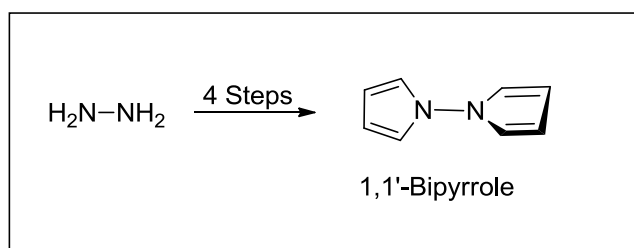


Figure 4.2 1,1'-bipyrrole

Then, a novel 1-(1H-pyrrol-1-yl)-2,5 di(thiophen-2-yl)-1H-pyrrole (SNSN) was synthesized from thiophene and hydrazine in 5 steps (Figure 4.3). Attaching thiophene rings to the 2- and 5- positions of pyrrole ring might decrease the effect of planarity hassle on the electropolymerization. Thus, a single irreversible oxidation peak shifted to 0.98 V vs Ag/AgCl followed by observation of a new reversible redox couple at following cycles, causing the formation of an electroactive polymer.

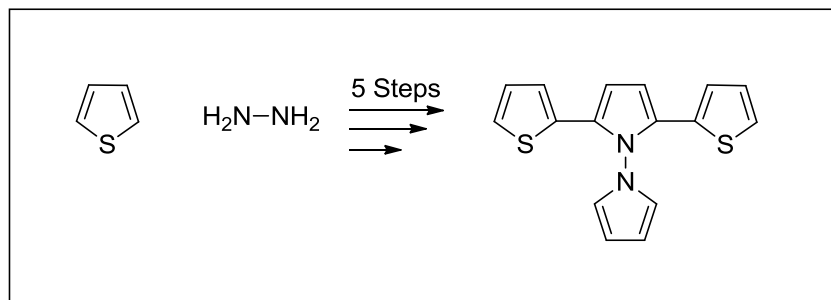


Figure 4.3 1-(1H-pyrrol-1-yl)-2,5 di(thiophen-2-yl)-1H-pyrrole (SNSN)

When redox and optical properties of polymer film were also examined by scanning the film between 0.0 V and 1.0 V, a single and well-defined reversible redox couple ($E_{p,1/2}$) around 0.64 V was obtained, and the redox couple continued its well-defined and promising reversible characteristics even at higher scan rates. Then, the proceeding of polymerization via the coupling of thiophene rings or pyrrole rings was investigated with FTIR. It was observed that α -H of pyrrole ring connected to the central ring of the SNS system remained unchanged during polymerization while α -coupling between the external thiophene rings was observed. This indicates that electropolymerization occurred through SNS backbone.

The fully neutral state was initially observed at a potential of 0.0 V and then the band gap (E_g) of PSNSN film was calculated as 2.21 eV by the initiation on the low energy end of the $\pi - \pi^*$ transition at 444 nm. This value is in good agreement with PSNS (430 nm, 2.88 eV), PSNSF (445 nm, 2.18 eV) and PSNSNP (423 nm, 2.33 eV) in Table 3.15.

Finally, optical contrasts were 18 % for 444 nm and 33 % for 661 nm in the visible region as well as 45 % for 1000 nm in the near-infrared region, and switching time was measured as 1.0 s. Lastly, fluorescence characteristics of SNSN and pSNSN were investigated. In light of the findings, the PSNSN may be a very promising candidate for optical displays.

4.4. Pyrrole Coupling Chemistry: Investigation of Electroanalytic Spectroscopic and Thermal Properties of N-Substituted Poly(Bis-Pyrrole) Films

N-substituted polyetheral polypyrrole PI film was synthesized via electrochemical polymerization in acetonitrile containing 0.1 M TBAClO₄ in order

to investigate ion sensing properties. P-I film has been fully characterized by electroanalytic, spectroscopic, thermal, and four probe techniques. It was found that P-1 possesses good stability and a reversible redox process. The polymer film also demonstrates multi-electrochromic behavior, which shows transparent yellow in the neutral state, light pink in the intermediate state, and blue in the oxidized state. These noticeable characteristics also make P-I a good candidate for any practical use, such as electrochromic devices and displays. In addition, the polymer film exhibits a selective voltammetric response towards Na^+ ion among the alkali series in an organic medium. Moreover, PI film was used to detect Ag^+ ions without precipitants or complexing ligands. SEM images also verified metallic silver on the film surface. These prominent features make PI a good candidate for any practical use, such as for the recovery of metals and ion sensors. Critical point for the use of this kind of pseudo cage polymers for ion sensing purposes is that the length of intra-chains between pyrrole moities. For example, it was reported that short intrachains of polybisPy did not respond towards rare earth ions like La(III), Eu(III) and Yb(III) while longer one has a response towards them [121] because longer flexible chains provide cavity for the insertion of metals for the complexation. Thus, pseudo cage polymers having suitable length of flexible intrachains like P1 films form suitable platform for ion sensing purposes.

REFERENCES

1. Bajpai, A; Shukla, S.; Saini, R.; Tiwari, A. *Stimuli Responsive Drug Delivery Systems - From Introduction to Application*. **2010** Smithers Rapra Technology.
2. Middleton, J. C.; Tipton, A. J. *Biomaterials* **2000**, *21*, 2335.
3. Sinclair, R. G. *J. Macromol Sci-Pure Appl. Chem.* **1996**, *A 33* (5), 585.
4. Nijenhuis, A. J.; Grijpma D.W.; Pennings, A. J. *Macromolecules* **1992**, *25*, 6419.
5. Kricheldorf, H. R.; Saunders, K.; Boettcher, C. *Polymer*, **1995**, *36*, 1253.
6. Kricheldorf, H. R.; Berl, M; Scharnagl, N. *Macromolecules* **1988**, *21*, 286.
7. Kricheldorf, H. R.; Sumbel, M.; Kreiser-Saunders, I. *Macromolecules* **1991**, *24*, 1944.
8. Herold, D. A.; Keil, K.; Bruns, D. E. *Biochem. Pharmacol.* **1989**, *38*, 73.
9. Cohn, D.; Younes, H. J. *Biomed. Mater. Res.* **1988**, *22*, 993.
10. Zhu, K. J.; Xiangzhou, L.; Shilin, Y. *J. Appl. Polym. Sci.* **1990**, *39*, 1.
11. Kricheldorf, H. R.; Meier-Haack, J. *Makromol. Chem.* **1993**, *194*, 715.
12. Hu, D. S.-G.; Liu, H.-J. *Polym. Bull.* **1993**, *30*, 669.
13. Cerrai, P.; Tricoli, M.; Lelli, L.; Guerra, G. D.; Sbarbati Del Guerra, R.; Cascone, M. G.; Giusti, P. *J. Mater. Sci.: Mater. Med.* **1994**, *5*, 308.
14. Jedlinski, Z.; Kurcok, P.; Walach, W.; Janeczek, H.; Radecka, I. *Makromol. Chem.* **1993**, *194*, 1681.

15. Sawhney, A.; Pathak, C. P.; Hubbell, J. A. *Macromolecules* **1993**, *26*, 581.
16. Hagan, S. A.; Davis, S. S.; Illum, L.; Davies, M. C.; Garnett, M. C.; Taylor, D. C.; Irving, M. P. and Tadros, Th. F. *Langmuir* **1995**, *11*, 1482.
17. Lewis, D. H. *Drugs Pharm. Sci.* **1990**, *45*, 1.
18. Manolova, N.; Baranovski, V.; Rashkov, I; Maximova, V. *Eur. Polym. J.* **1993**, *29*, 721.
19. Yokoyama, M.; Fukushima, S.; Uehara, R.; Okamoto, K.; Kataoka, K.; Sakurai, Y. and Okano, T., *J. Control. Release* **1998**, *50*, 79.
20. Sutton, D.; Wang, S.; Nasongkla, N.; Gao, J.; Dormidontova, E.E., *Exp. Biol. Med.*, **2007**, *232*(8), 1090-9.
21. Lee, J.; Cho, E. C. and Cho, K., *J. Control. Release* **2004**, *94*, 323.
22. Hagan, S. A.; Coombes, A.G.A.; Garnett, M.C.; Dunn, S.E.; Davies, M.C.; Illum, L. and Davis, S.S. *Langmuir* **1996**, *12*, 2153.
23. Jeong, B.; Bae, Y. H.; Lee, S. D.; Kim, S. W. *Nature* **1997**, *388*, 860.
24. Kim, S. Y.; Shin, I. G. and Lee, Y. M. *J. Control. Release* **1998**, *56*, 197.
25. Jeong, B.; Lee, D.S.; Shon, J.I.; Bae Y.H.; Kim, S.W. *J. Polym. Sci.: Part A* 1999, *37*, 751.
26. Kim, S. K.; Seo, K. S.; Khang, G.; Cho, S. H.; Lee, H. B. *J. Polym. Sci.: Part A* **2004**, *42*, 5784.
27. Lee, H. J.; Go, A. K.; Oh, S. H.; Lee, K. E.; Yuk, S. H. *Biomaterials* **2005**, *26*, 671.
28. Dai, Z.; Piao, L.; Zhan, X.; Deng, M.; Chen, X.; Jing, X. *Colloid Polym Sci.* **2004**, *282*, 343.
29. Li, S.; Vert, M. *Macromolecules* **2003**, *36*, 8008.

30. Espartero, J. L.; Li, S. M.; Rashkov, I.; Manolova, N.; Vert, M. *Macromolecules* **1996**, *29*, 57.
31. Li, S.; Anjard, S.; Rashkov, I. and Vert, M. *Polymer* **1998**, *39*, 5421.
32. Agrawal, S. K.; Sanabria-DeLong, N.; Coburn, J. M.; Tew, G. N. and Bhatia, S. R. *J. Control. Release* **2006**, *112*, 64-71.
33. Kim, K. W.; Chung, S.; Chin, I. J.; Kim, M. N.; Yoon, J. S. *J. Appl. Polym. Sci.* **1999**, *72*, 341.
34. Sun, J.; Hong, Z.; Yang, L.; Tang, Z.; Chen, X.; Jing, X. *Polymer* **2004**, *45*, 5969.
35. Fujiwara, T.; Miyamoto, M.; Kimura, Y. *Macromolecules* **2000**, *33*, 2782.
36. Fujiwara, T.; Kimura, Y. *Makromol. Biosci.* **2002**, *2*, 11-23.
37. Scholz, C.; Iijima, M.; Nagasaki, Y.; Kataoka, K. *Macromolecules* **1995**, *28*, 7295.
38. Nagasaki, Y.; Okada, T.; Scholz, C.; Iijima, M.; Kato, M.; Kataoka, K. *Macromolecules* **1998**, *31*, 1473.
39. Otsuka, H.; Nagasaki, Y. and Kataoka, K. *Biomacromolecules* **2000**, *1*, 39-48.
40. Kubies, D.; Machova, L.; Brynda, E.; Lukas, J.; Rypacek, F. *J. Mat. Sci. Mater. In Med.*, **2003**, *14*, 143-149.
41. Kim, H. D.; Bae, E. H.; Kwon, I.C.; Pal, R. R.; Nam, J. D.; Lee, D. S. *Biomaterials* **2004**, *25*, 2319.
42. Kumari, A.; Yadav, S.K.; Yadav, C.S. *Colloids and Surfaces B: Biointerfaces*, **2010**, *75*, 1-18.
43. Ikada, Y.; Tsuji, H. *Macromol Rapid Commun.* **2000**, *21*, 117-132.

44. Middleton, J.C.; Tipton, A.J. *Medical Plastics & Biomaterials*. **1998**; 5(2), 30-39.
45. Huh, K.M.; Cho, Y.W.; Park, K., *Drug. Del. Tech.* **2003**, 3, 42–49.
46. Yu, L.; Ding, J. *Chem. Soc. Rev.*, **2008**, 37, 1473–1481.
47. Allcock, H.R. 2003. *Chemistry and Applications of Polyphosphazenes*. Wiley, Hoboken, NJ.
48. Allcock, H.R.; Kwon, S. *Macromolecules*, **1988**, 21, 1980–1985.
49. Allcock, H.R.; Pucher, S.R.; Scopelianos, A.G. *Macromolecules*, **1994**, 27, 1071–1075.
50. Allcock, H.R.; Pucher, S.R.; Scopelianos, A.G. *Macromolecules*, **1994**, 27, 1–4.
51. Allcock, H.R., Fuller, T.J., Mack, D.P., Matsumura, K., Smeltz, K.M. *Macromolecules*, **1977**, 10, 824–830.
52. Allcock, H.R.; Singh, A., Ambrosio, A.M.; Laredo, W.R. *Biomacromolecules*, **2003**, 4, 1646–1653.
53. Allcock, H.R.; Fuller, T.J.; Matsumura, K. *Inorg. Chem.*, **1982**, 21, 515–521.
54. Andrianov, A.K., Marin, A. *Biomacromolecules*, **2006**, 7, 1581–1586.
55. Allcock, H.R.; Kugel, R.L. *J. Am. Chem. Soc.*, **1965**, 87, 4216–4217.
56. Allcock, H.R.; Kugel, R.L.; Valan, K.J., *Inorg. Chem.*, **1966**, 5, 1709–1715.
57. Allcock, H.R., Kugel, R.L., *Inorg. Chem.*, **1966**, 5, 1716–1718.
58. Allcock, H.R.; Cook, W.J.; Mack, D.P. *Inorg. Chem.*, **1972**, 11, 2584–2590.

59. Allcock, H.R.; Coley, S.M.; Manners, I.; Visscher, K.B.; Parvez, M. *Inorg. Chem.* **1993**, *32*, 5088-5094.
60. Allcock, H.R. *J. Inorg. Organomet. Polym. Mater.*, **2006**, *16*(4), 277–294 and Appendix, 437–459.
61. Allcock, H.R.; Kim, Y.B. *Macromolecules*, **1994**, *6*, 516–524.
62. Allcock, H.R.; Ngo, D.C. *Macromolecules*, **1992**, *25*, 2802–2810.
63. Singler, R.E.; Hagnauer, G.; Schneider, N.S.; LaLiberte, B.R.; Sacher, R.E.; Matton, R.W. *J. Polym. Sci.*, **1974**, *12*, 433–444.
64. Allcock, H.R.; Austin, P.E.; Neenan, T.X.; Sisko, J.T.; Blonsky, P.M.; Shriver, D.F. *Macromolecules*, **1986**, *19*, 1508–1512.
65. Maher, A.E.; Allcock, H.R. *Macromolecules*, **2005**, *38*, 641–642.
66. Song, S.C.; Lee, S.B.; Jin, J.I.; Sohn, Y.S. *Macromolecules*, **1999**, *32*, 2188–2193.
67. Hou, S.; McCauley, L.K.; Ma, P.X. *Macromol. Biosci.*, **2007**, *7*, 620–628.
68. Shuai, X.; Tan, H. *Journal of Applied Polymer Science*, **1997**, *66*, 1891–1898.
69. Domb, A.J.; Langer, R. *Journal of Polymer Science: Part A: Polymer Chemistry*, **1987**, *25*, 3373-3386.
70. Kumara, N.; Langer, R.S.; Domb, A. *Advanced Drug Delivery Reviews*, **2002**, *54*, 889–910.
71. Fu, J.; Fiegel, J.; Hanes, J. *Macromolecules*, **2004**, *37*, 7174-7180.
72. Fu, J.; Fiegel, J.; Krauland, E.; Hanes, J. *Biomaterials*, **2002**, *23*, 4425–4433.
73. Lee, J.; Joo, M.K.; Oh, H.; Sohn, Y.S.; Jeong, B. *Polymer*, **2006**, *47*, 3760–3766.

74. Tang, B.C.; Dawson, M.; Lai, S.K.; Wang, Y.Y.; Zeitlin, P.; Boyle, M.P.; Fu, J.; Hanes, J. *Proc Natl Acad Sci U S A.*, **2009**, *106*(46), 19268-73.
75. Tang, B. C.; Fu, J.; Watkins, D. N.; Hanes, J. *Biomaterials*, **2010**, *31*, 339–44.
76. Petka, W.A.; Harden J.L.; McGrath K.P.; Wirtz, D.; Tirrell, D.A. *Science*, **1998**, *281*, 389 -392.
77. Jeong, B.; Lee, K.M.; Gutowska, A.; An, Y. H. *Biomacromolecules*, **2002**, *3*, 865.
78. Lee, P. Y.; Cobain, E.; Huard, J.; Huang, L. *Molecular Therapy*, **2007**, *15*, 1189.
79. Lee, J.; Bae, Y.H.; Sohn, Y. S.; Jeong, B. *Biomacromolecules*, **2006**, *7*, 1729-1734.
80. Shim, W. S.; Kim, J. H.; Kim, K.; Kim, Y. S.; Park, R. W.; Kim, I. S.; Kwon, I. C.; Lee, D. S. *Int. J. Pharm.*, **2007**, *331*, 11
81. Zentner, G.M.; Rathi, R.; Shih, C.; Mcrea, J.C.; Seo, M.H.; Oh, H.; Rhee, B.G.; Mestecky, J.; Moldoveanu, Z.; Morgan, M.; Weitman, S. *J. Controlled Release*, **2001**, *72*, 203-215.
82. Vukelja, S. J.; Anthony, S. P.; Arseneau, J. C.; Berman, B. S.; Cunningham, C. C.; Nemunaitis, J. J.; Samlowski, W. E.; Fowers, K. D. *Anti-Cancer Drugs*, **2007**, *18*, 283.
83. DuVall, G.A.; Tarabar, D.; Seidel, R.H.; Elstad, N.L.; Fowers, K.D., *Anticancer Drugs*, 2009, *20*, 89–95.
84. Tyagi, P.; Li, Z.; Chancellor, M.; De Groat, W.C.; Yoshimura, N.; Huang, L., *Pharm. Res.* **2004**, *21*, 832–837.
85. Yu, L.; Chang, G.T.; Zhang, H.; Ding, J.D. *Int. J. Pharm.*, **2008**, *348*(1-2), 95-106.

86. Guerin, C.; Olivi, A.; Weingart, J. D.; Lawson, H.C.; Brem, H. *Investigational New Drugs*, **2004**, *22*, 27-37.
87. Brem, H.; Piantadosi, S.; Burger, P.C.; Walker, M.; Selker, R.; Vick, N.A.; Black, K.; Sisti, M.; Brem, S.; Mohr, G.; et al *Lancet*, **1995**, *345(8956)*, 1008-1012.
88. Ghandehari, H.; Kopeckova, P.; Kopecek, J. *Biomaterials* **1997**, *18*, 861–872.
89. Aikawa, K.; Matsumoto, K.; Uda, H.; Tanaka, S.; Tsuchiya, S. *Int. J. Pharm.* **1998**, *167*, 97–104.
90. Aikawa, K.; Mitsutake, N.; Uda, H.; Tanaka, S.; Tsuchiya, S. *Int. J. Pharm.* **1998**, *168*, 181–188.
91. Lu, J.; Choi, E.; Tamanoi, F.; Zink, J.I. *Small* **2008**, *4*, 421–426.
92. Rapoport, N.Y.; Christensen, D.A.; Fain, H.D.; Barrows, L.; Gao, Z. *Ultrasonics*, **2004**, *42*, 943–950.
93. Schweiger, L.F.; Ryder, K.S.; Morris, D.G.; Glidle, A.; Cooper, J.M.; *J. Mater. Chem.* **2000**, *10*, 107
94. McLeod, G. G.; Galin, J. C.; Truong, N. D.; Watson, S. D.; Pethrick, R. A.; Mahboubian-Jones, M. G. B.; Francois, J. *Polymer*, **1986**, *27*, 455-8.
95. Ferraris, J. P.; Hanlon, T. R. *Polymer*, **1989**, *30*, 1319.
96. Carrasco, J.; Figueras, A.; Otero, T.F.; Brillas, E. *Synthetic Metals*, **1993**, *61*, 253-258.
97. Brillas, E.; Carrasco, J.; Oliver, R.; Estrany, F.; Vilar, J.; Morlans, J.M. *Electrochimica Acta*, **2000**, *45*, 4049-4057.
98. Niziurski-Mann, R. E.; Scordilis-Kelley, C.; Liu, T. L.; Cava, M. P.; Carlin, R. T. *J. Am. Chem. Soc.*, **1993**, *115* (3), 887–891.

99. Brillas, E.; Garrido, J.A.; Fernandez, V.; Cabot, P.L.; Perez, E.; Centellas, F.; Carrasco, J.; Rodriguez, R.M. *Synthetic Metals*, **1999**, *101*, 24.
100. Yanai, H.; Yoshizawa, D., Tanaka, S.; Fukuda, T.; Akazome, M.; Ogura, K. *Chemistry Letters*, **2000**, 238.
101. Tuncagil, S.; Odaci D.; Yildiz E.; Timur, S.; Toppare L. *Sensors and Actuators B*, **2009**, *137*, 42–47.
102. Tuncagil, S.; Varis, S.; Toppare L. *Journal of Molecular Catalysis B: Enzymatic*, **2010**, *64*, 195-9.
103. Algi, F.; Cihaner, A. *Tetrahedron Letters*, **2008**, *49*, 3530–3533.
104. Liu, Y.X.; Summers, M.A.; Edder, C. Frechet, J.M.J.; McGehee M.D. *Advanced Materials*, **2005**, *17*, 2960.
105. Tarkuc, S.; Sahmetlioglu, E.; Tanyeli, C.; Akhmedov, I.M.; Toppare, L. *Electrochimica Acta*, **2006**, *51*, 5412.
106. Arslan, A.; Turkarslan, O.; Tanyeli, C.; Akhmedov, M. I.; Toppare, L. *Materials Chemistry and Physics*, **2007**, *104*, 410.
107. Yigitsoy, B.; Varis, S.; Tanyeli, C.; Akhmedov, I. M.; Toppare, L. *Thin Solid Films*, **2007**, *515*, 3898-3904.
108. Varis, S.; Ak, M.; Akhmedov, I.M.; Tanyeli, C.; Toppare, L. *J. Electroanal. Chem.*, **2007**, *603*, 8–14.
109. Yildiz, E.; Camurlu, P.; Tanyeli, C.; Akhmedov, I.M.; Toppare, L. *J. Electroanal. Chem.*, **2008**, *612*, 247–256.
110. Cihaner, A.; Algi, F. *Journal of Electroanalytical Chemistry*, **2008**, *614*, 101–106.
111. Cihaner, A.; Algi, F. *Electrochimica Acta*, **2008**, *53*, 2574.
112. Freeman, R.; Willner, I. *Nano Lett.* **2009**, *9*, 322– 326
113. Cheikhou, K.; Tzedakis, T. *AIChE Journal* **2008**, *54*; 1365-1376.

114. Kornberger, P.; Gajdzik, J.; Natter, H.; Wenz, G.; Giffhorn, F.; Kohring, G.W.; Hempelmann, R. *Langmuir* **2009**, *25*, 12380–12386
115. Chane-Ching, K.I.; Lacroix, J.C.; Baudry, R.; Jouini, M.; Aeiyaich, S.; Lion, C.; Lacaze, P.C. *J. Electroanal. Chem.* **1998**, *453*, 139.
116. Horwitz, C.P. *Chem. Mater*, **1989**, *1*, 463.
117. Leclerc, O. *Eur. Pat. Appl.* **1995**, AN 1995:721071.
118. Simonet, J.; Gache, Y.; Simonet-Gueguen, N.; Leclerc, O. *Denki Kagaku* **1994**, *62*, 1211.
119. Cihaner, A. *J. Electroanal. Chem.* **2007**, *605*, 8.
120. Cihaner, A.; Onal, A.M. *J. App. Polymer Sci.* **2008**, *108*, 2373.
121. Koksel, B.; Cihaner, A.; Kaya, M.; Volkan, M.; Onal, A.M. *J. Appl. Polymer Sci.*, **2008**, *108*, 2707.
122. Cihaner, A. *J. Macromol. Sci. Part A Pure Appl Chem*, **2006**, *43*, 1379.
123. Mousty, C.; Galland, B.; Cosnier, S. *Electroanal.* **2001**, *13*, 186.
124. Cristea, C.; Mousty, C.; Cosnier, S.; Popescu, I.C. *Electrochim. Acta* **2005**, *50*, 3713.
125. Tabbá, H.D.; Cavaleiro, J.A.S.; Jeyakumar, D.; Neves, M.G.P.M.S.; Smith, K.M. *J. Org. Chem.* **1989**, *54*, 1945.
126. Pozo-Gonzalo, C.; Pomposo, J.A.; Rodriguez, J.; Schmidt, E.Y.; Vasil'tsov, A.M.; Zorina, N.V.; Ivanov, A.V.; Trofimov, B.A.; Mikhaleva, A.I.; Zaitsev, A.B. *Synth. Met.* **2007**, *157*, 60.
127. Ghosh, T.; Maiya, B.G.; Wong, M.W. *J. Phys. Chem. A* ,**2004**, *108*, 11249.
128. Chen, C.L.; Chen, Y.H.; Chen, C.Y.; Sun, S.S. *Org. Lett.* **2006**, *8*, 5053.
129. Cabaj, J.; Sołoducho, J.; Nowakowska, A.; Chyla, A. *Electroanal.* **2006**, *18*, 801.
130. Sołoducho, J. *Synth. Met.* **1999**, *99*, 181.
131. Yadav, J.S.; Subba Reddy, B.V.; Satheesh, G. *Tetrahedron Lett.* **2004**, *45*, 3673.

132. Mert, O.; Doganci, E.; Erbil, H. Y.; Demir, A. S., *Langmuir*, **2008**, 24(3), 749-757.
133. Kirkpatrick, J. L.; Patel, N. R.; Rulter, J. L. *U.S. Patent*, **1982**, 4,-292,071; Chem. Abstr. **1982**, 96, 64200.
134. Patel, N. R.; Rulter, J. L. *U.S. Patent*, **1981**, 4,264,502.; Chem. Abstr. **1981**, 95, 80725.
135. Dey S. K.; Lightner, D. A. *J. Org. Chem.* **2007**, 72, 9395-9397.
136. Flitsch, W.; Kramer, U.; Zimmerman, H. *Chem. Ber.* **1969**, 102, 3268-3276.
137. Flitsch, H.; Lult, F.-J. *Liebig's Ann. Chem.* **1987**, 893-894.
138. Drew, H. D.; Halt, H. H. *J. Chem. Soc.* **1937**, 16-26.
139. Schweiger, L. F.; Ryder, K. S.; Morris, D. G.; Glidlec, A; Cooper, J. M.; *J. Mater. Chem.*, **2000**, 10, 107-114.
140. Cooke, G.; Garety, J. F.; Jordan, B.; Kryvokhyzha, N.; Parkin, A.; Rabani, G.; Rotello, V. M., *Org. Lett.* **2006**, 8, 2297-2300.
141. Strouse, G. F.; Schoonover, J. R.; Duesing, R.; Boyde, S.; Jones, Jr., W. E.; Meyer, T. J., *Inorg. Chem.* **1995**, 34, 413-481.
142. Oberlies, N.H.; Kroll, D.J. *J. Nat. Prod.*, **2004**, 67(2), 129-135.
143. Wani, M. C.; Ronman, P. E.; Lindley, J. T.; Wall, M. E. *J. Med. Chem.* **1980**, 23, 554.
144. Tardi, P.; Choice, E; Masin, D; Redelmeier, T; Bally, M; Madden, T.D., *Cancer Res.*, **2000**, 60, 3389-3393.
145. Shenderova, A.; Burke T.G.; Schwendeman, S.P. *Pharmaceutical Research*, **1997**, 14, 1406.
146. Paragkumar, T. N.; Edith, D.; Jean-Luc, S. *Appl. Surf. Sci.* **2006**, 253, 2758
147. Tretinnikov, O. N.; Ohta, K. *Langmuir*, **1998**, 14, 915.
148. Wall, M. E.; Wani, M. C.; Cook, C. E.; Palmer, K. H.; McPhail, A. T.; Sim, G. A. *J. Am. Chem. Soc.* **1966**, 88, 3888.

149. Hsiang, Y.H.; Hertzberg, R.; Hecht, S.; Liu, L.F. *J. Biol. Chem.*, **1985**, 260(27), 14873-14878.
150. Fassberg, J.; Stella, V. J., *J. Pharm. Sci.* **1992**, 81, 676-684.
151. Wani, M. C.; Nicholas, A. W.; Manikumar, G.; Wall, M. E. *J. Med. Chem.* **1987**, 30, 1774-1779.
152. Wani, M. C.; Nicholas, A. W.; Wall, M. E. *J. Med. Chem.* **1987**, 30, 2317-2319.
153. Jaxel, C.; Kohn, K. W.; Wani, M. C.; Wall, M. E.; Pommier, Y. *Cancer Res.* **1989**, 49, 5077-5082.
154. Moertel, C. G.; Schutt, A. J.; Reitemeier, R. J.; Hahn, R. G. *Cancer Chemother. Rep.*, **1972**, 56, 95.
155. Gottlieb, J. A.; Luce, J. K. *Cancer Chemother. Rep.*, **1972**, 56, 103.
156. Dancy, J.; Eisenhauer, E. A. *Br. J. Cancer*, **1996**, 74, 327.
157. Pommier, Y.; Pourquier, P.; Fan, Y.; Strumberg, D. *Biochim. Biophys. Acta* **1998**, 1400, 83.
158. Burris, III HA; Hanauske, A.R.; Johnson R.K.; Marshall M.H.; Kuhn, J.G.; Hilsenbeck, S.G.; Von Hoff, D.D. *J. Natl. Cancer Inst.*, **1992**, 23, 1816-20.
159. Creemers, G.J.; Lund, B.; Verweij, J. *Cancer Treat Rev.*, **1994**; 20, 73-96.
160. Burris, III H.A.; Fields S.M. *Hematol. Oncol. Clin. North Am.*, **1994**, 8, 333-55.
161. Burke, T.G.; Gao, X. *J. Pharm. Sci.* **1994**, 83, 967-969.
162. Subramanian, D.; Muller, M.T. *Oncol. Res.*, **1995**, 7, 461-469.
163. Kingsbury, W. D.; Boehm, J. C.; Jakas, D. R.; Holden, K. G.; Hecht, S. M.; Gallagher, G.; Caranfa, M. J.; McCabe, F. L.; Faucette, L. F.; Johnson, R. K.; Hertzberg, R. P. *J. Med. Chem.* **1991**, 34, 98.
164. Stewart, L.; Ireton G.C.; Parker, L.H.; Madden, K.R.; Champoux, J.J. *J. Biol. Chem.*, **1996**, 271, 7593-7601.

165. Fan, Y.; Weinstein, J.N.; Kohn, K.W.; Shi, L.M.; Pommier, Y. *J. Med. Chem.*, **1998**, *41*, 2216-2226.
166. Bendixen, C.; Thomsen, B.; Alsner, J.; Westergaard, O. *Biochemistry*, **1990**, *29*, 5613-5619.
167. Legarza, K.; Yang, L.-X. *Anticancer Res.*, **2006**, *26*, 3301.
168. Hsiang, Y.-H.; Lihou, M. G.; Liu, L. F. *Cancer Res.* **1989**, *49*, 5077.
169. Chourpa, I.; Millot, J.-M.; Sockalingum, G.D.; Riou, J.-F.; Manfait, M. *Biochimica et Biophysica Acta (BBA)/General Subjects*, **1998**, *1379*, 353-366.
170. Warner, D.L.; Burke, T.G. *Journal of Chromatography B: Biomedical Sciences and Applications*, **1997**, *691*, 161-171.
171. Wall, M. E. In *Biochemistry and Physiology of the Alkaloids*; Mothes, K., Schrieber, K., Schulte, H. R., Eds.; Akademie-Verlag: Berlin, **1969**; p 77.
172. Nicholas, A. W.; Wani, M. C.; Manikumar, G.; Wall, M. E.; Kohn, K. W.; Pommier, Y. *J. Med. Chem.*, **1990**, *33*, 972.
173. Zhao, H.; Lee, C.; Sai, P.; Choe, Y. H.; Boro, M.; Pendri, A.; Guan, S.; Greenwald, R. B. *J. Org. Chem.*, **2000**, *65* (15), 4601-4606.
174. Kumar, V.; Kang, J.; Hohl, R. J. *Pharm-Dev-Technol.*, **2001**, *6*(3), 459-67.
175. Lin, S. S.; Sun, L.; Zhang, Y. K.; Zhao, R. P.; Liang, W. L.; Yuan, S. T.; Zhang, L. Y. *Acta Pharmacol. Sin.*, **2009**, *30*(5), 628.
176. Pulaski, B. A.; Ostrand-Rosenberg, S. *Curr. Protoc. Immunol.*, **2001**, Chapter 20, Unit 20.2.
177. Berrada, M.; Serreqi, A.; Dabbarh, F.; Owusu, A.; Gupta, A.; Lehnert, S. *Biomaterials*, **2005**, *26*(14), 2115.
178. Gao, J.M.; Ming, J.; He, B.; Gu, Z.W.; Zhang, X.D. *Biomed. Mater.*, **2008**, *3*, 15013.
179. Hatefi, A.; Knight, D.; Amsden, B. *Journal of Pharmaceutical Sciences*, **2004**, *93*, 1195.

180. Barreiro-Iglesias, R.; Bromberg, L.; Temchenko, M.; Hatton, T. A.; Concheiro, A.; Alvarez-Lorenzo, C. *Journal of Controlled Release*, **2004**, *97*, 537-549
181. Just, P.E.; Chane-Ching, K.I.; Lacroix, J.C.; Lacaze, P.C. *Electrochim. Acta*, **2001**, *46*, 3279.
182. Rockel, H.; Huber, J.; Gleiter, R.; Schuhmann, W. *Adv Mater*, **1994**, *6*, 568-571
183. Harbeke, G.; Meier, E.; Kobel, W.; Egli, M.; Kiess, H.; Tosatti, E. *Solid State Commun.* **1985**, *55*, 419.
184. Yakushi, K.; Lauchlan, L.J.; Clarke, T.C.; Street, G.B. *J. Chem. Phys.*, **1983**, *79*, 4774.
185. Sato, M.; Tanaka, S.; Kaeriyama, K. *Synth. Met.* **1986**, *14*, 279.
186. Chung, T.C.; Kaufman, J.H.; Heeger, A.J.; Wudl, F. *Phys. Rev. B*, **1984**, *30*, 702.
187. Akhtar, P.; Too, C.O.; Wallace, G.G. *Anal. Chim. Acta*, **1997**, *339*, 211.
188. Hu, W.; Hasebe, K.; Iles, A.; Tanaka, K. *Analyst* **2001** *126*, 555.
189. Doku, G.N.; Gadzekpo, V.P.Y. *Talanta* **1996**, *43*, 735.
190. Krejcova, A.; Cernohorsky, T.; Curdova, E. *J. Anal. At. Spectrom.* **2001**, *16*, 1002.
191. I. Nemcova, S. Cihelník, P. Rychlovský, L. Antalova, *Anal. Lett.* **2004**, *37*, 2721.
192. Budic, B. *J. Anal. At. Spectrom.* **1998**, *13*, 869.
193. Martinez, M.T.; Lima, A.S.; Bocchi, N.; Teixeira, M.F.S. *Talanta* **2009**, *80*, 519.
194. Lin, J-L.; Hsu, H.-Y. *Sensors* **2010**, *10*, 1798.

APPENDIX A

HPLC

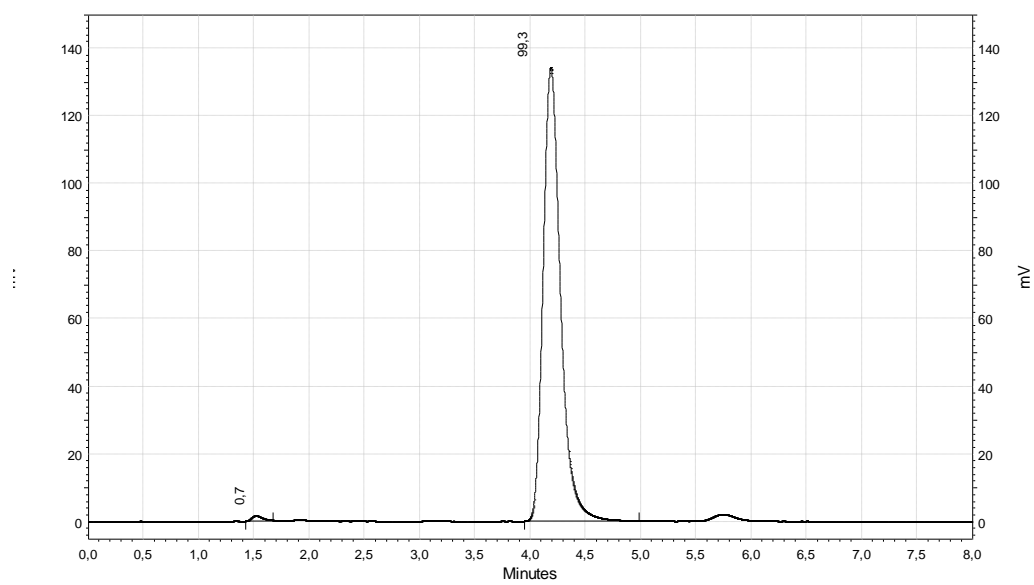


Figure A.1. First measurement of three independent data for free CPT in tris buffer at pH=7.4 at t=0 min

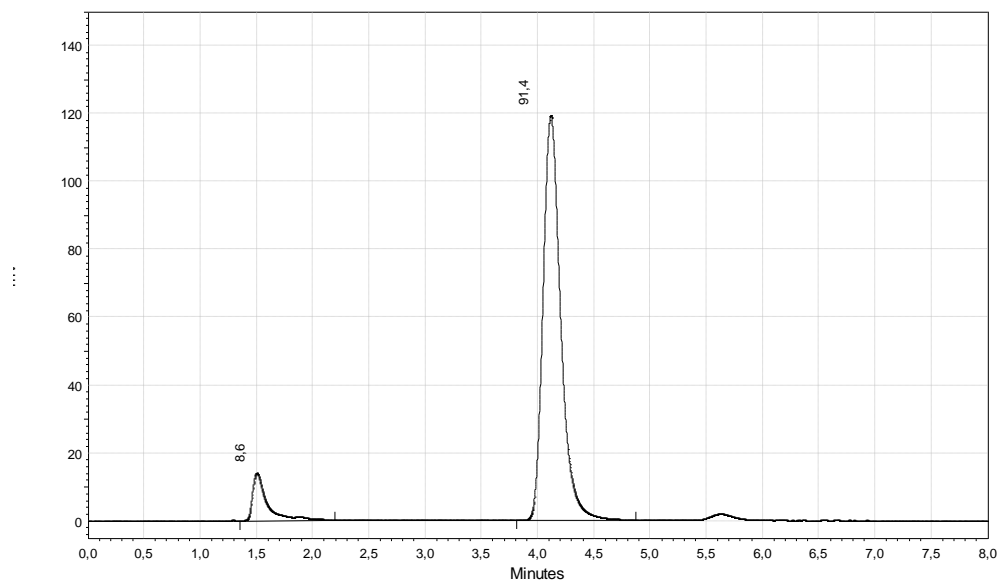


Figure A.2. First measurement of three independent data for free CPT in tris buffer at pH=7.4 at t=20 min

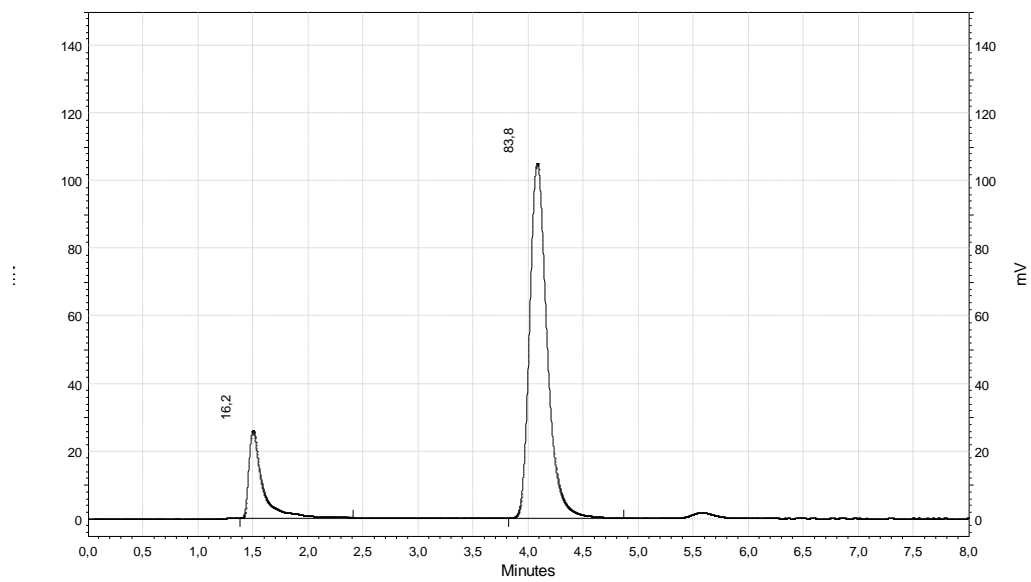


Figure A.3. First measurement of three independent data for free CPT in tris buffer at pH=7.4 at t=39 min

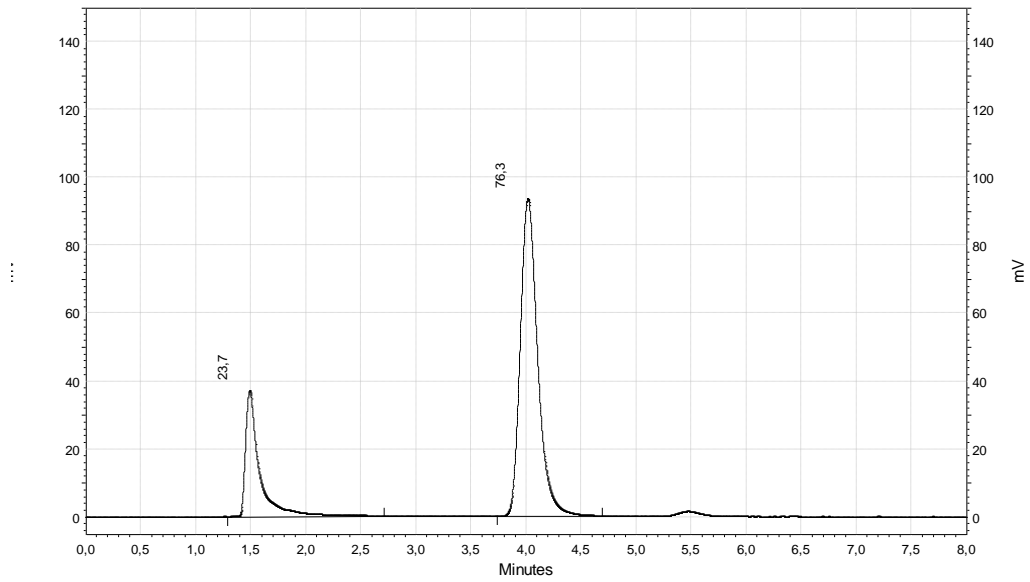


Figure A.4. First measurement of three independent data for free CPT in tris buffer at pH=7.4 at t=58 min

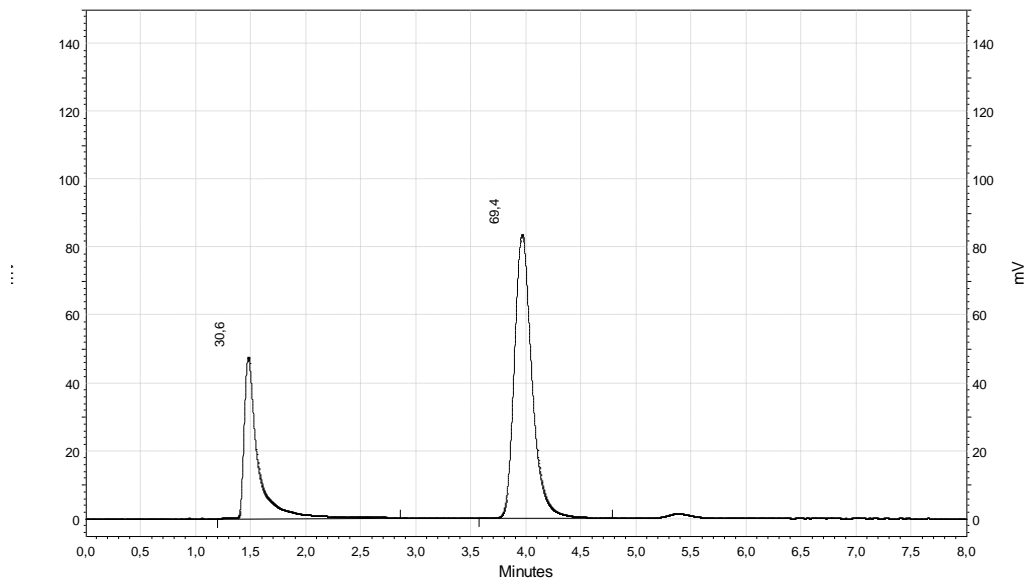


Figure A.5. First measurement of three independent data for free CPT in tris buffer at pH=7.4 at t=78 min

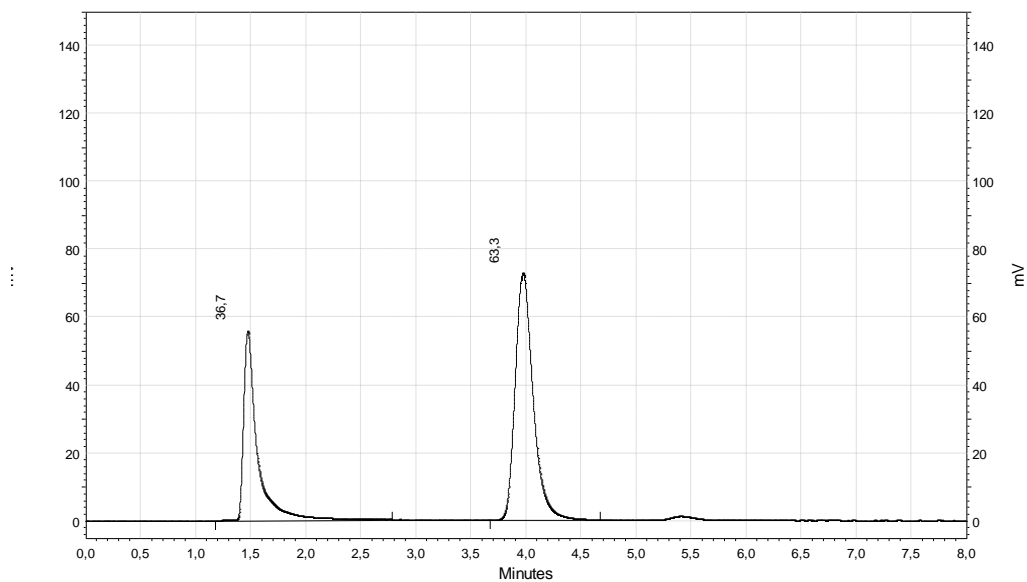


Figure A.6. First measurement of three independent data for free CPT in tris buffer at pH=7.4 at t=97 min

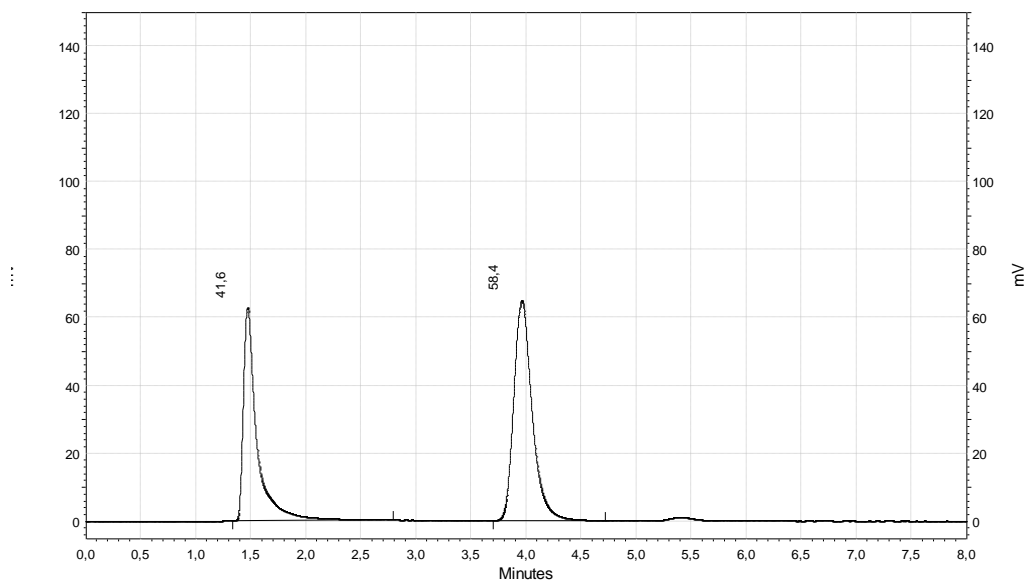


Figure A.7. First measurement of three independent data for free CPT in tris buffer at pH=7.4 at t=117 min

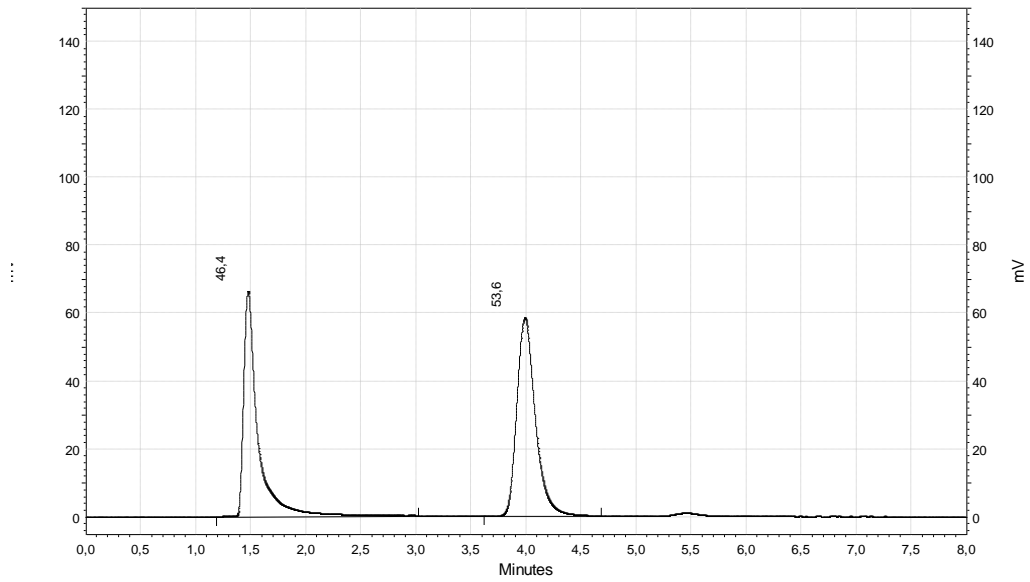


Figure A.8. First measurement of three independent data for free CPT in tris buffer at pH=7.4 at t=136 min

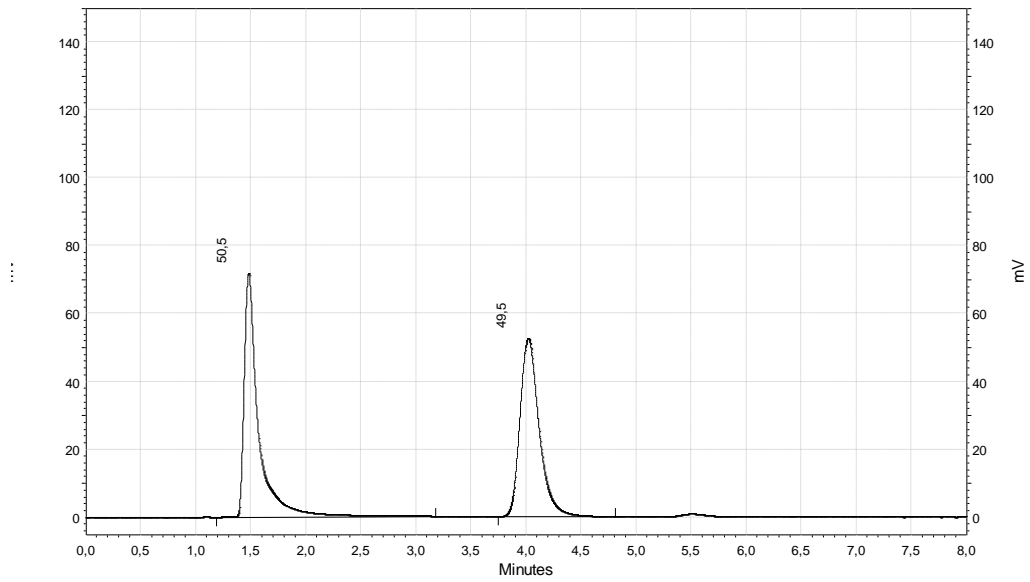


Figure A.9. First measurement of three independent data for free CPT in tris buffer at pH=7.4 at t=155 min

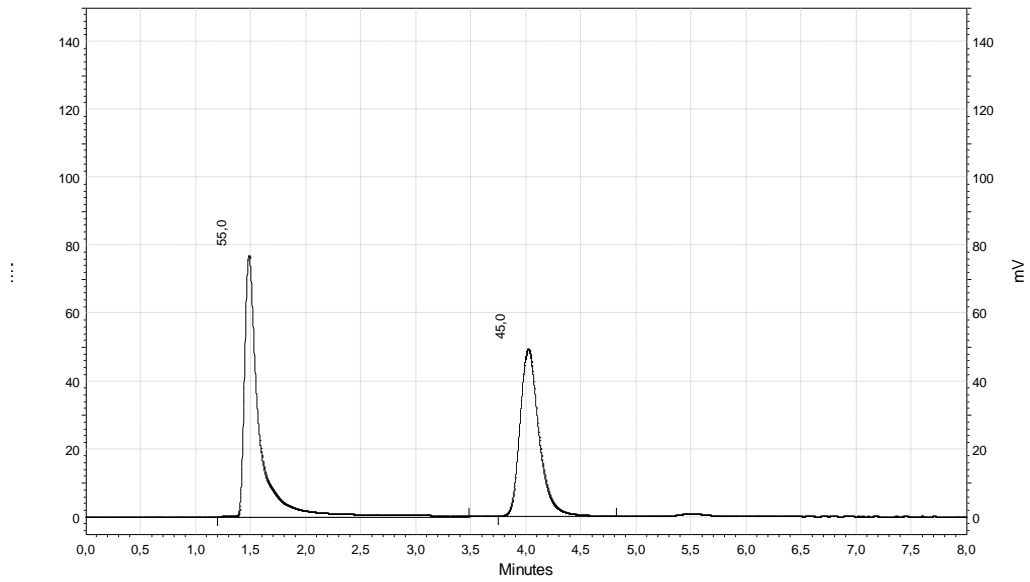


Figure A.10. First measurement of three independent data for free CPT in tris buffer at pH=7.4 at t=175 min

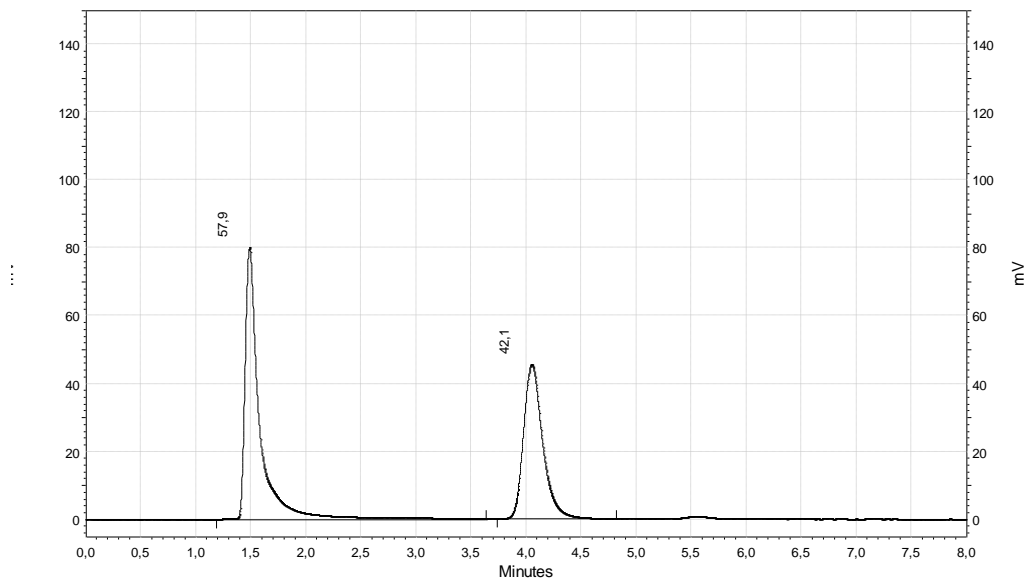


Figure A.11. First measurement of three independent data for free CPT in tris buffer at pH=7.4 at t= 194 min

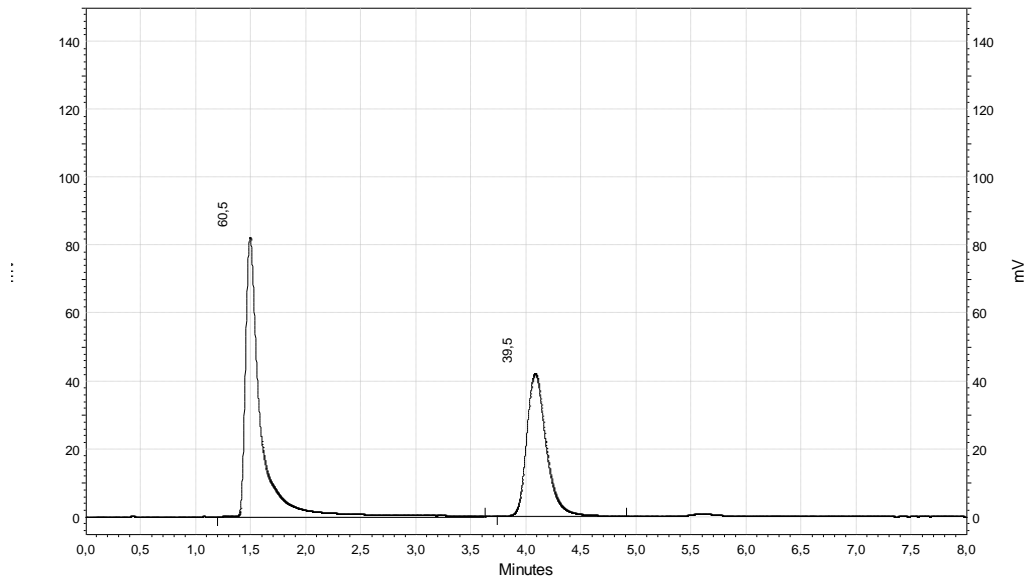


Figure A.12. First measurement of three independent data for free CPT in tris buffer at pH=7.4 at t=213 min

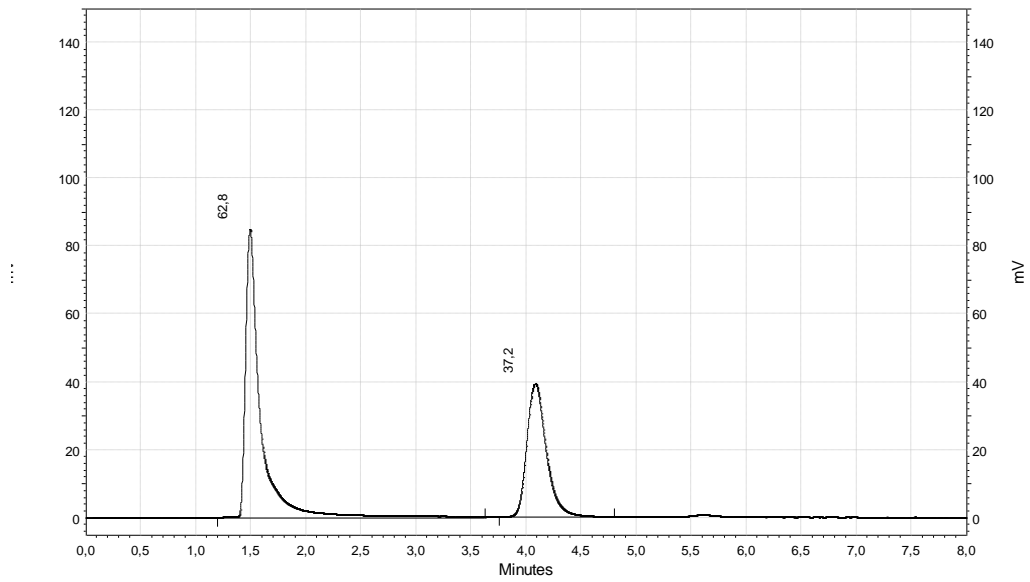


Figure A.13. First measurement of three independent data for free CPT in tris buffer at pH=7.4 at t=232 min

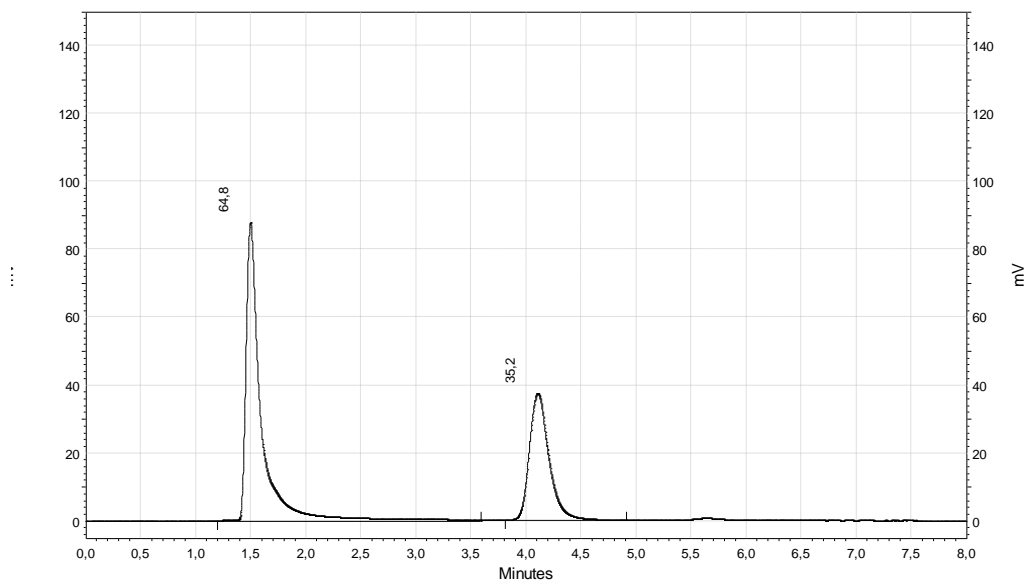


Figure A.14. First measurement of three independent data for free CPT in tris buffer at pH=7.4 at t=252 min

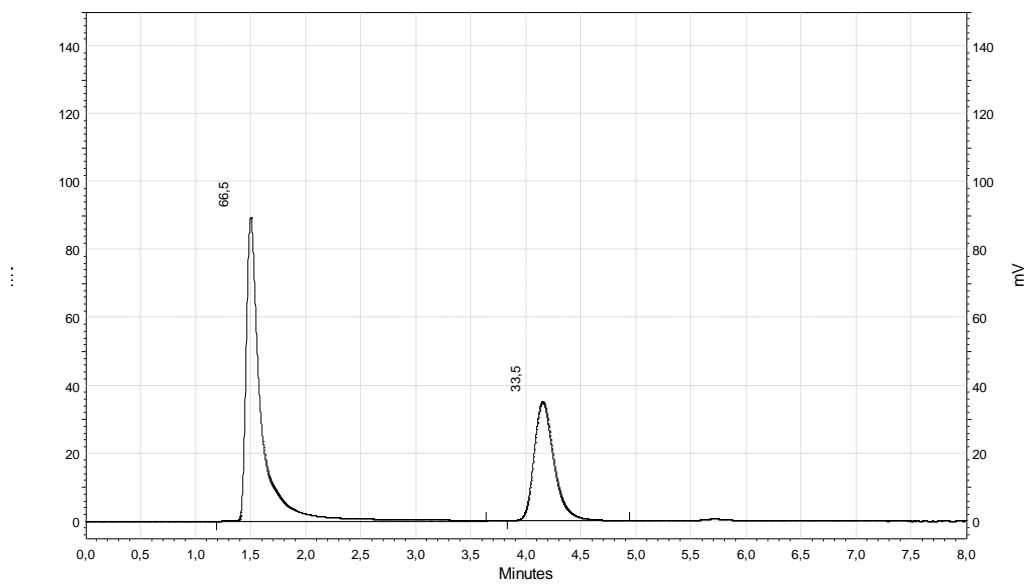


Figure A.15. First measurement of three independent data for free CPT in tris buffer at pH=7.4 at t=271 min

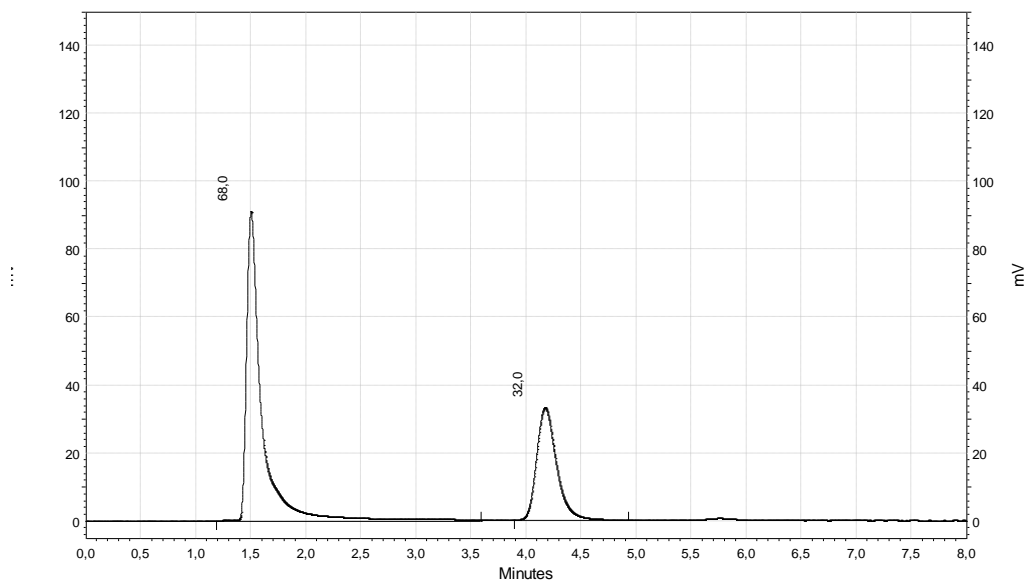


Figure A.16. First measurement of three independent data for free CPT in tris buffer at pH=7.4 at t=290 min

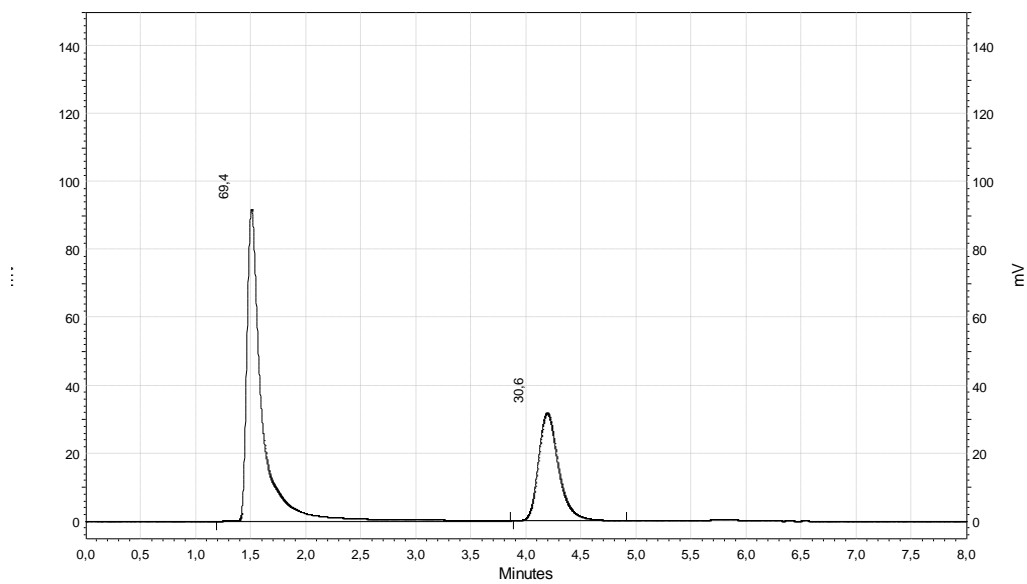


Figure A.17. First measurement of three independent data for free CPT in tris buffer at pH=7.4 at t=310 min

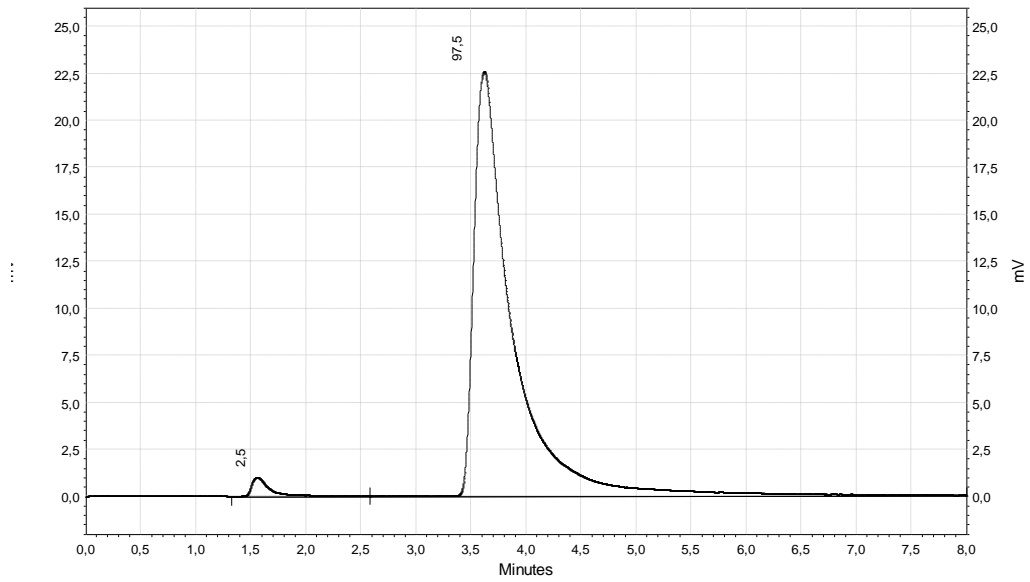


Figure A.18. First measurement of three independent data for free TPT in tris buffer at pH=7.4 at t=0 min

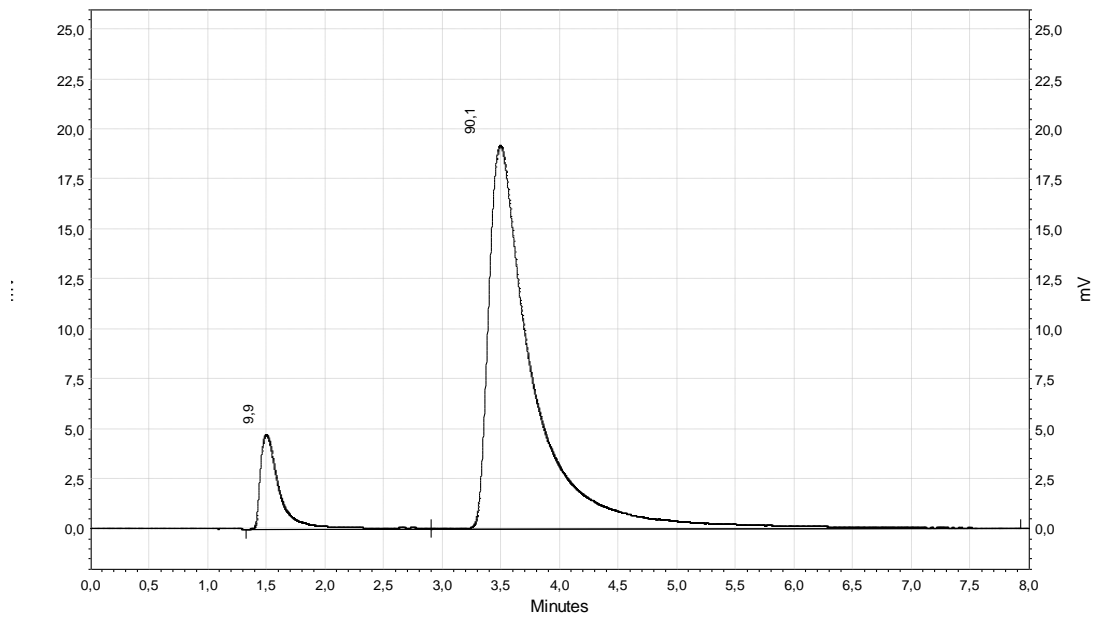


Figure A.19. First measurement of three independent data for free TPT in tris buffer at pH=7.4 at t=20 min

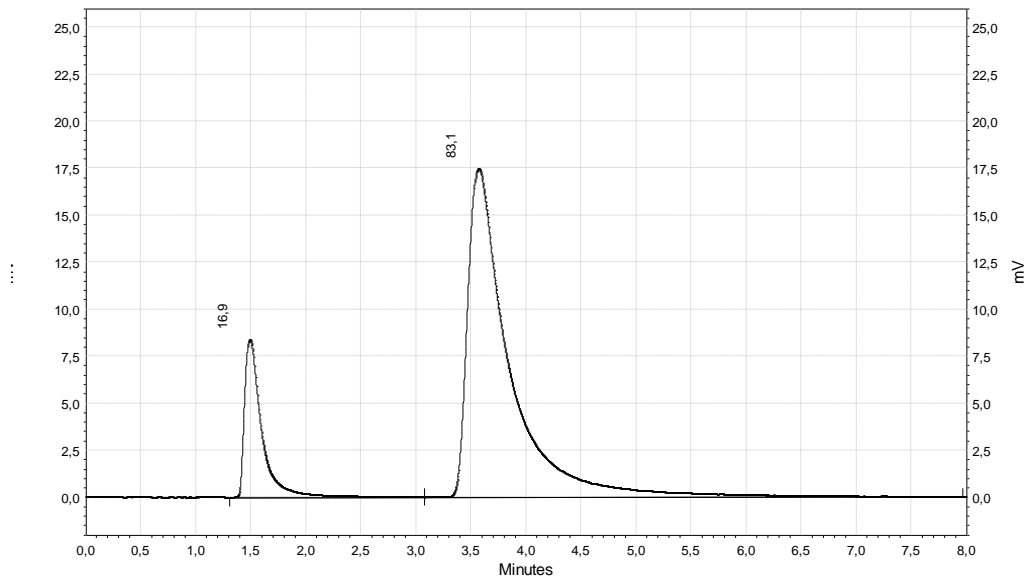


Figure A.20. First measurement of three independent data for free TPT in tris buffer at pH=7.4 at t=39 min

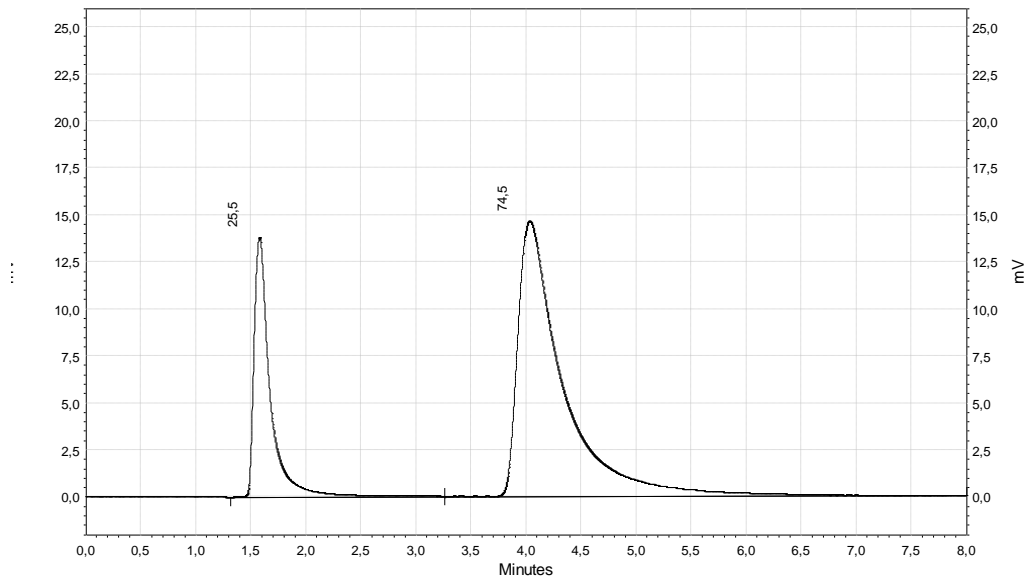


Figure A.21. First measurement of three independent data for free TPT in tris buffer at pH=7.4 at t=58 min

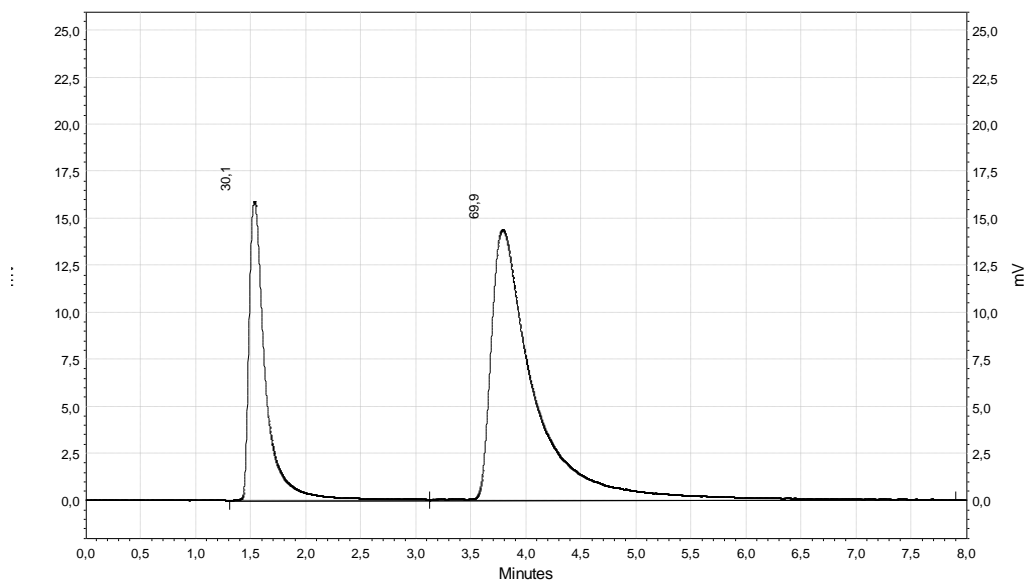


Figure A.22. First measurement of three independent data for free TPT in tris buffer at pH=7.4 at t=78 min

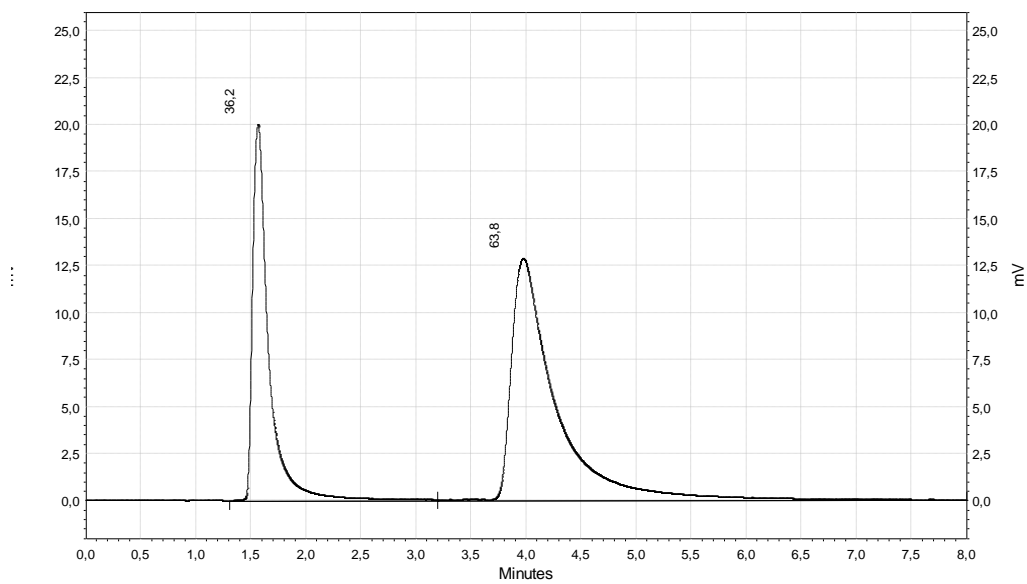


Figure A.23. First measurement of three independent data for free TPT in tris buffer at pH=7.4 at t=97 min

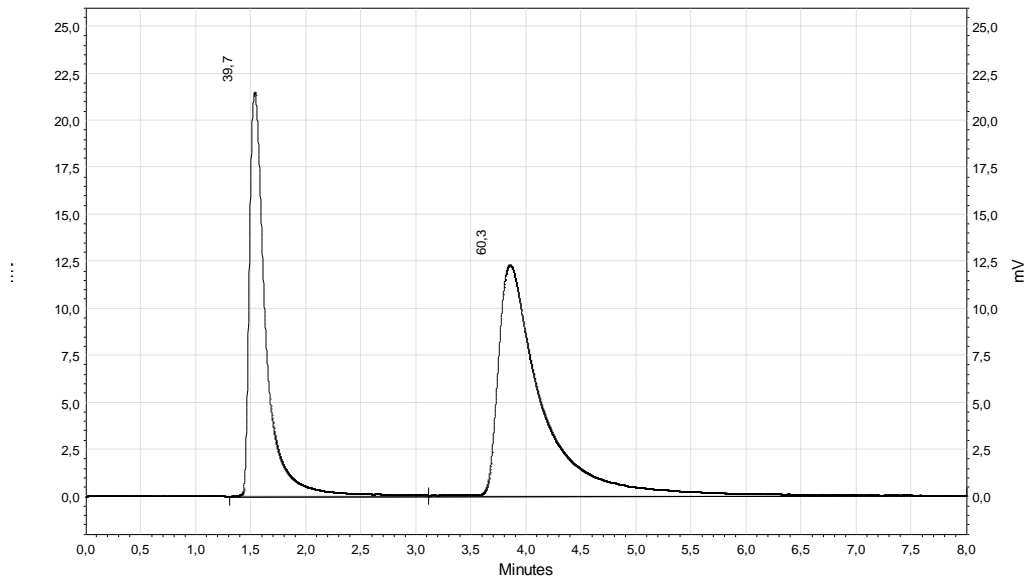


Figure A.24. First measurement of three independent data for free TPT in tris buffer at pH=7.4 at t=117 min

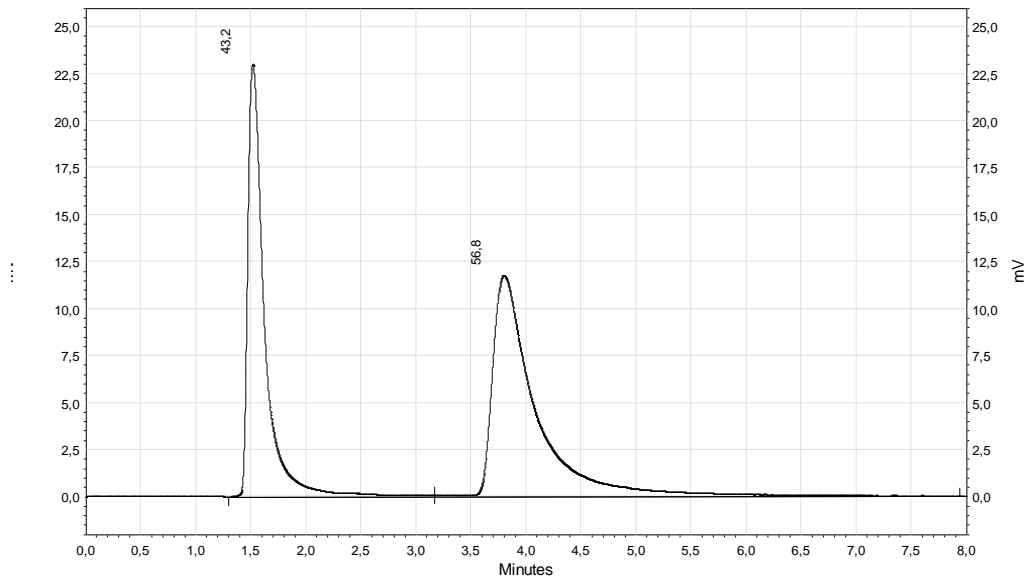


Figure A.25. First measurement of three independent data for free TPT in tris buffer at pH=7.4 at t=136 min

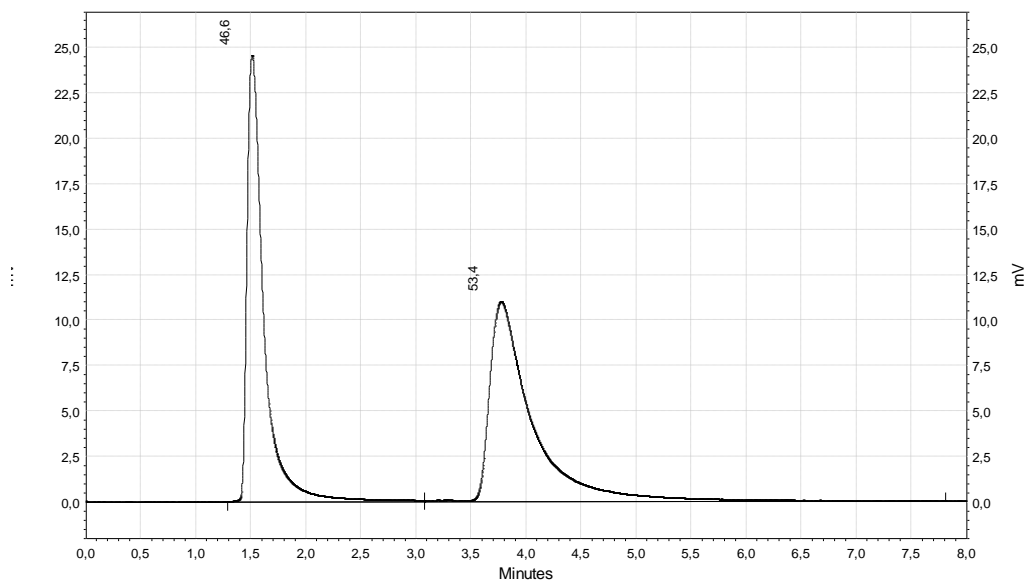


Figure A.26. First measurement of three independent data for free TPT in tris buffer at pH=7.4 at t=155 min

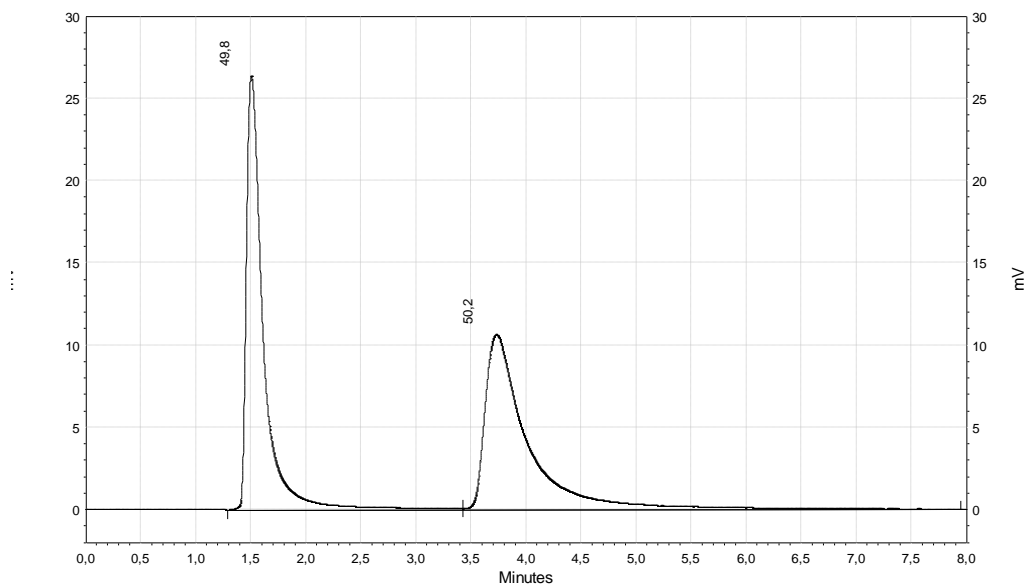


Figure A.27. First measurement of three independent data for free TPT in tris buffer at pH=7.4 at t=175 min

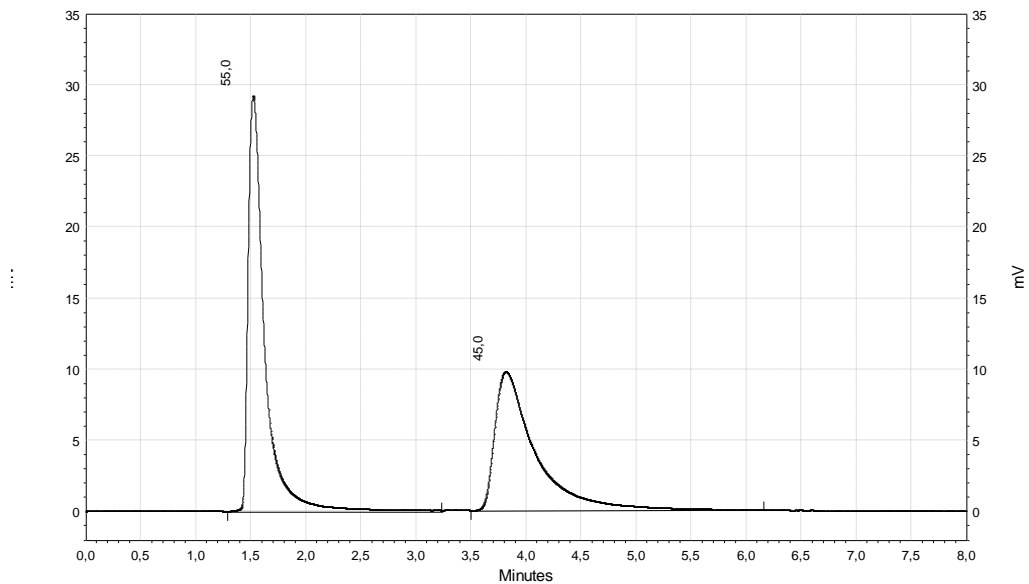


Figure A.28. First measurement of three independent data for free TPT in tris buffer at pH=7.4 at t=194 min

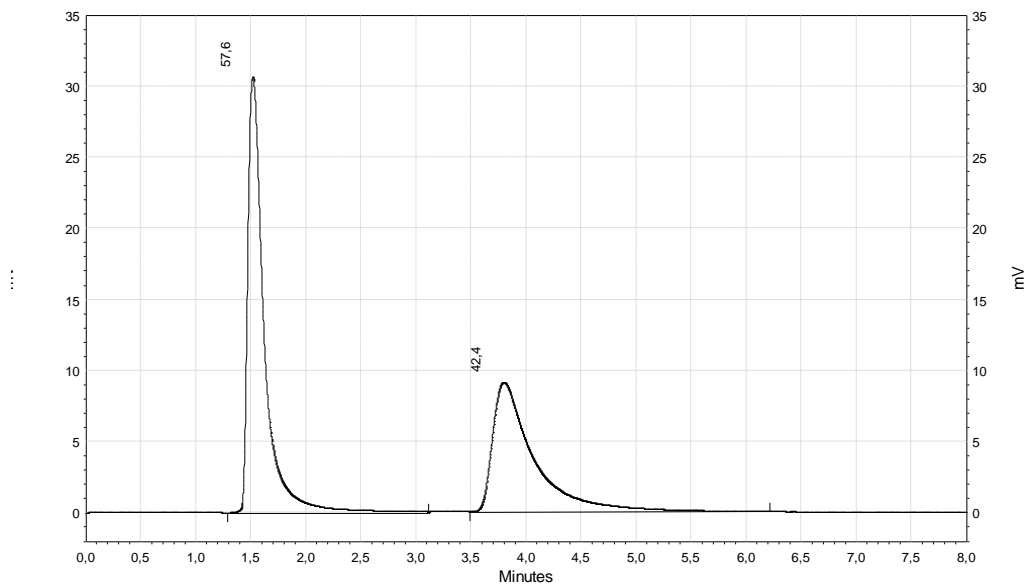


Figure A.29. First measurement of three independent data for free TPT in tris buffer at pH=7.4 at t=213 min

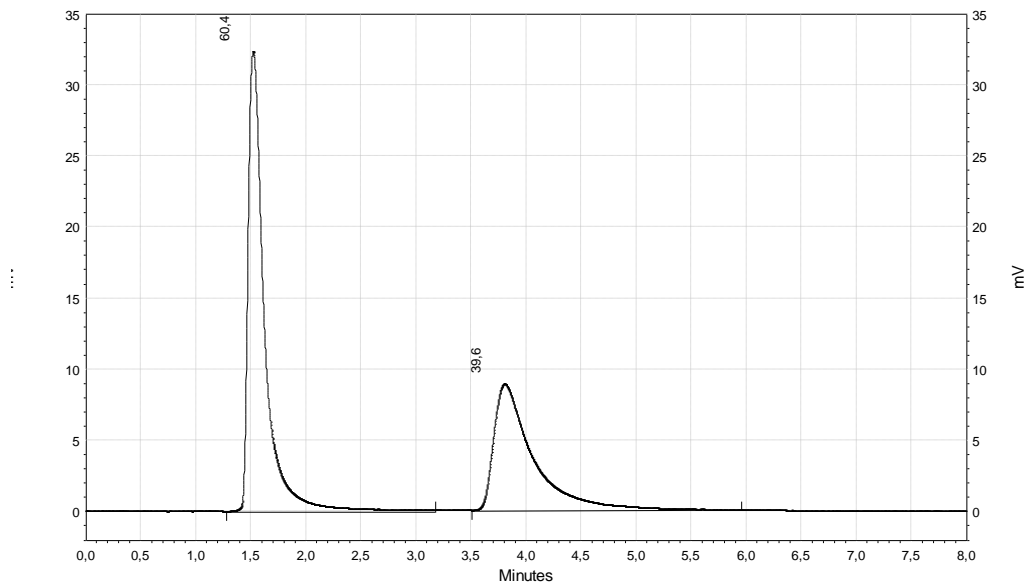


Figure A.30. First measurement of three independent data for free TPT in tris buffer at pH=7.4 at t=232 min

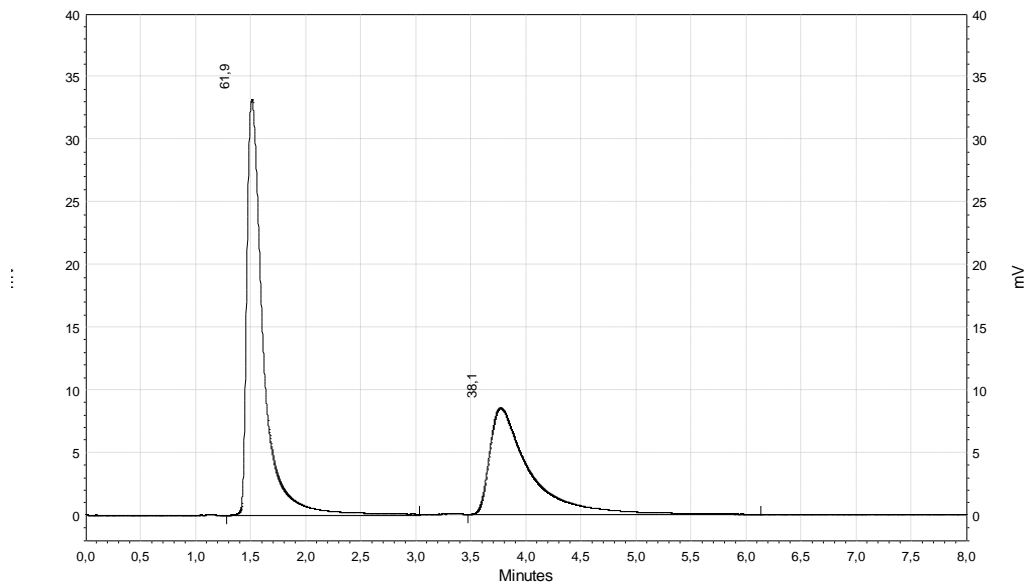


Figure A.31. First measurement of three independent data for free TPT in tris buffer at pH=7.4 at t=252 min

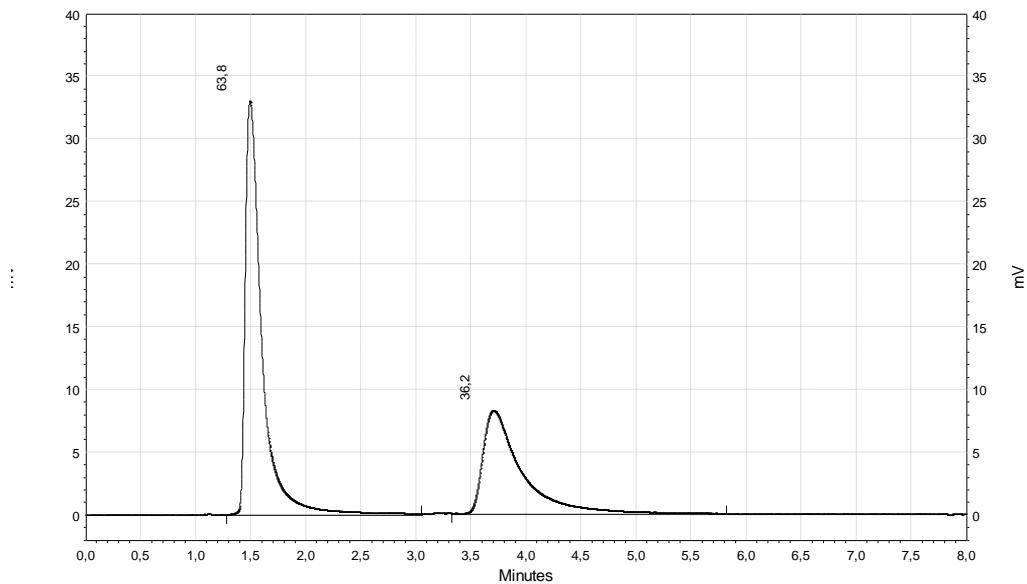


Figure A.32. First measurement of three independent data for free TPT in tris buffer at pH=7.4 at t=271 min

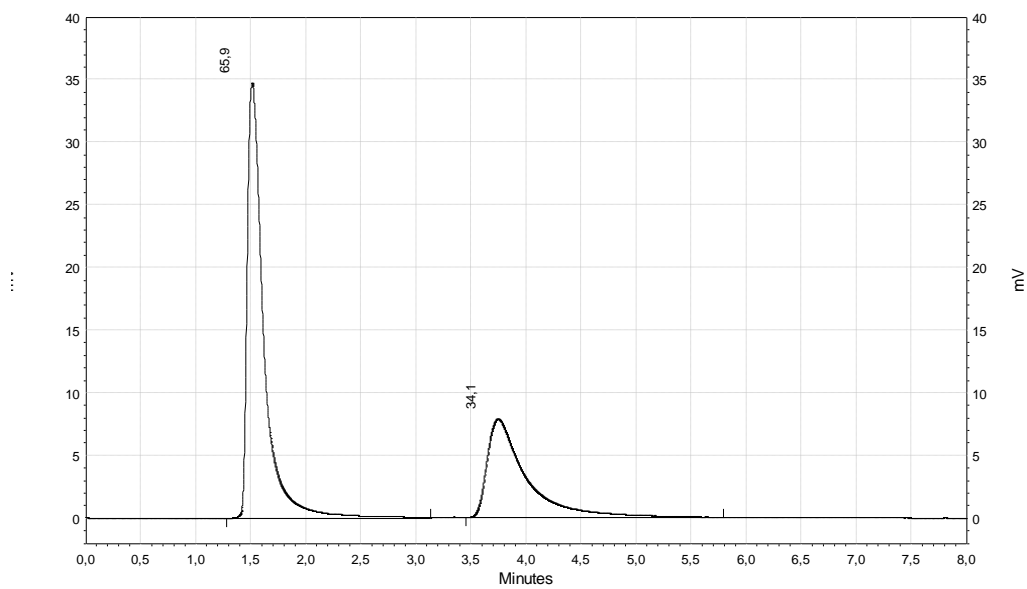


Figure A.33. First measurement of three independent data for free TPT in tris buffer at pH=7.4 at t=290 min

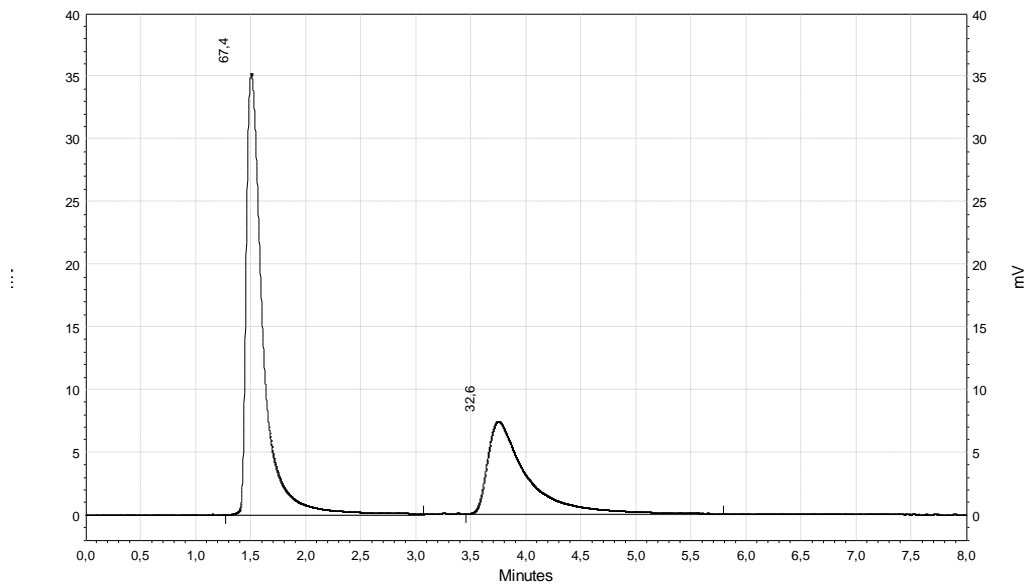


Figure A.34. First measurement of three independent data for free TPT in tris buffer at pH=7.4 at t=310 min

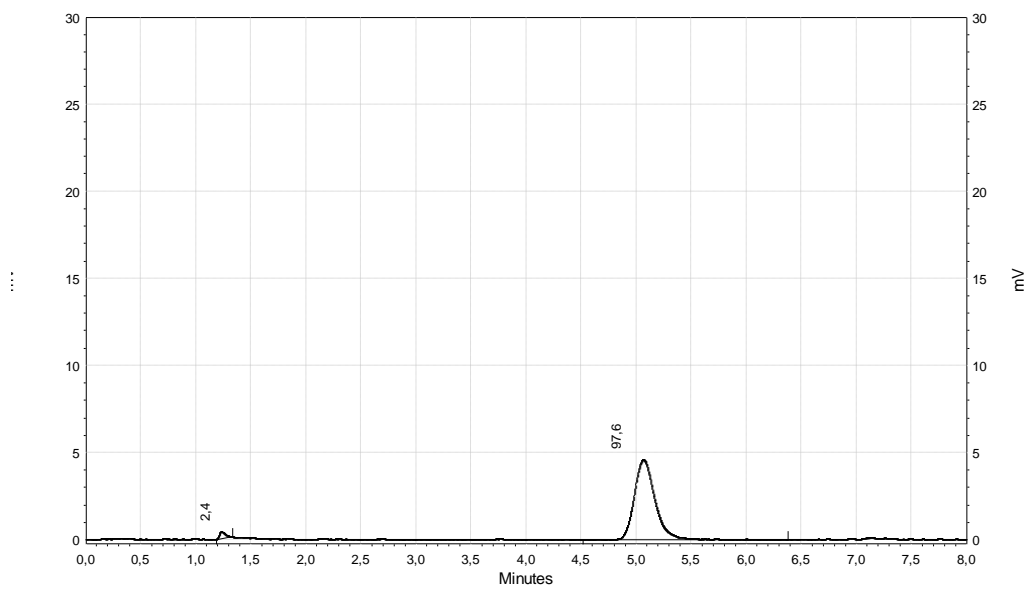


Figure A.35. First measurement of three independent data for CPT in gel at 0.015% loading at t= 0 min

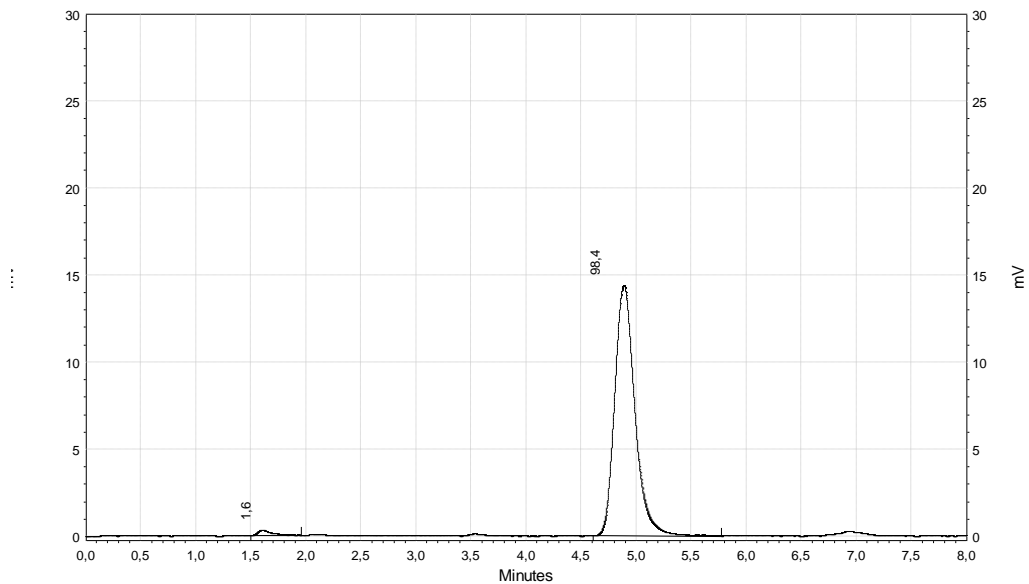


Figure A.36. First measurement of three independent data for CPT in gel at 0.015% loading at $t = 45$ min

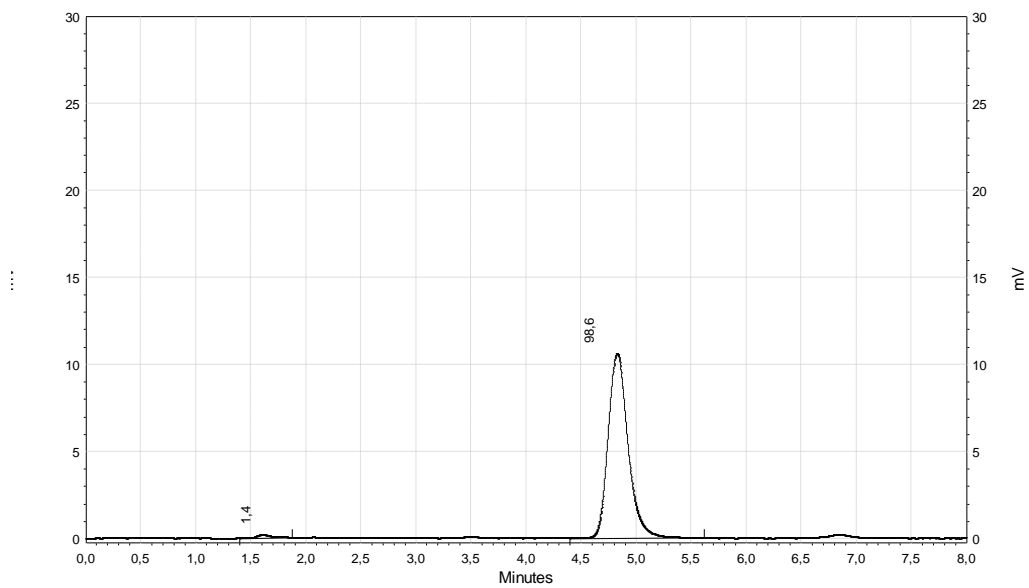


Figure A.37. First measurement of three independent data for CPT in gel at 0.015% loading at $t = 90$ min

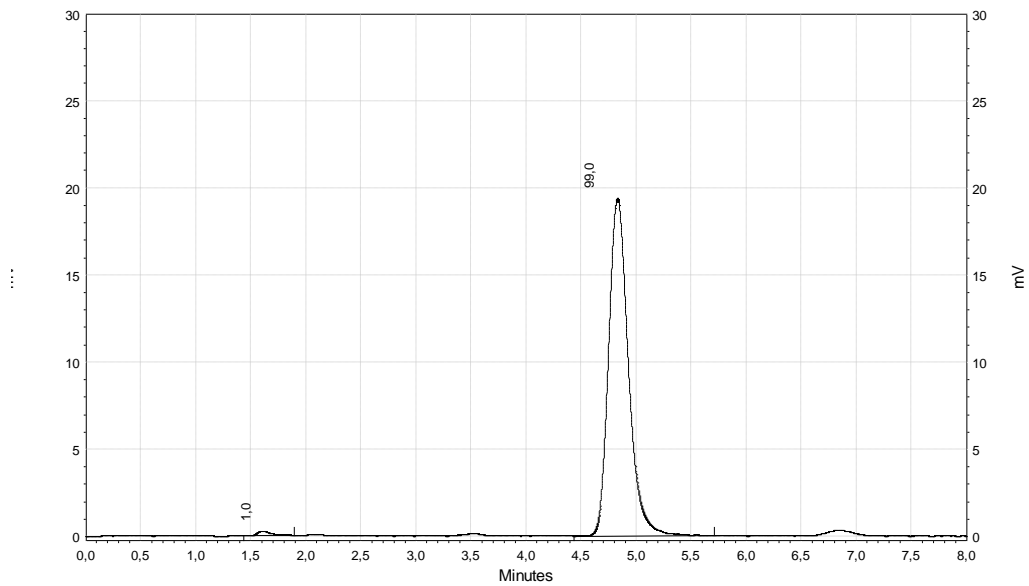


Figure A.38. First measurement of three independent data for CPT in gel at 0.015% loading at $t= 135$ min

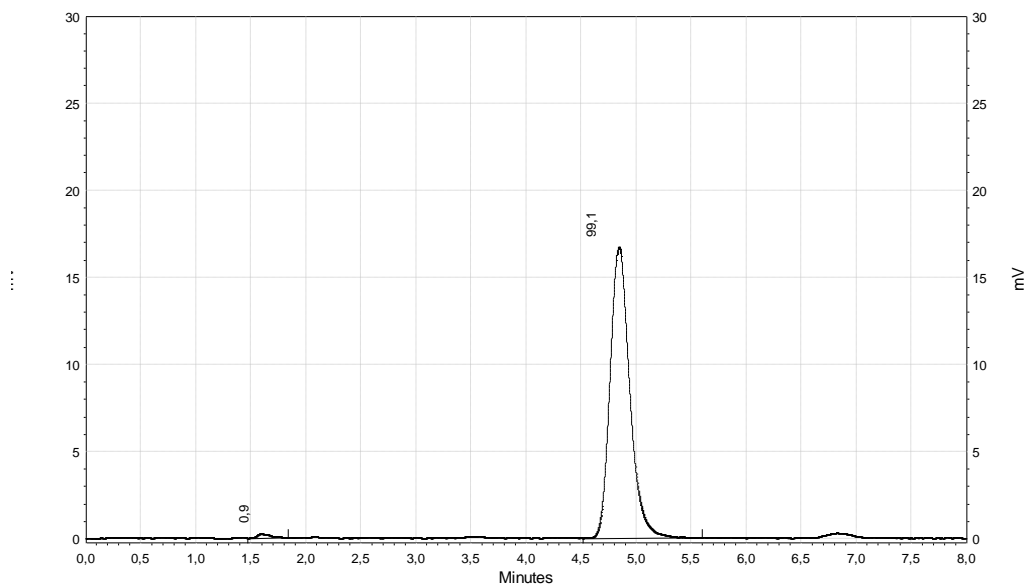


Figure A.39. First measurement of three independent data for CPT in gel at 0.015% loading at $t= 180$ min

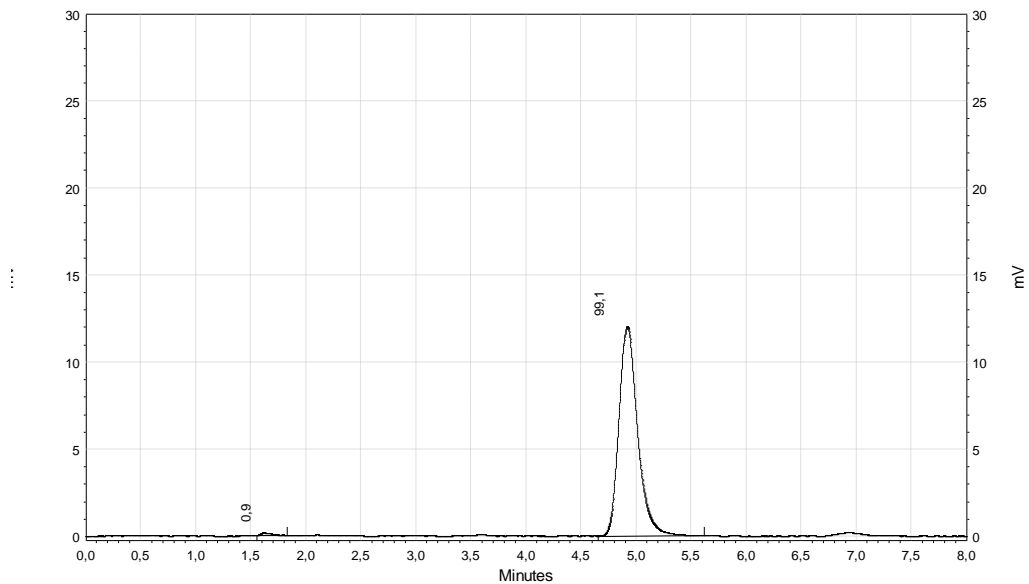


Figure A.40. First measurement of three independent data for CPT in gel at 0.015% loading at $t=225$ min

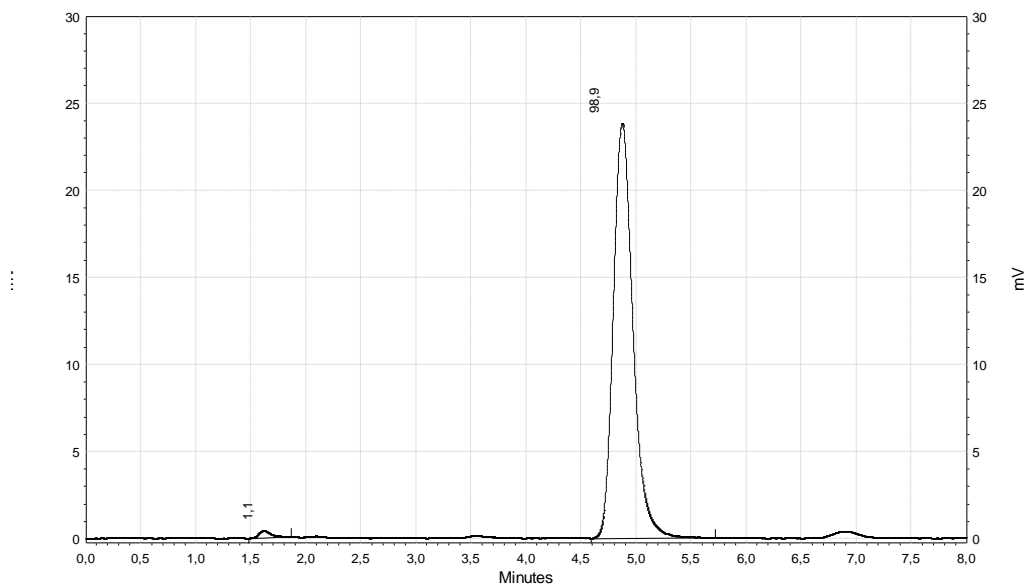


Figure A.41. First measurement of three independent data for CPT in gel at 0.015% loading at $t=270$ min

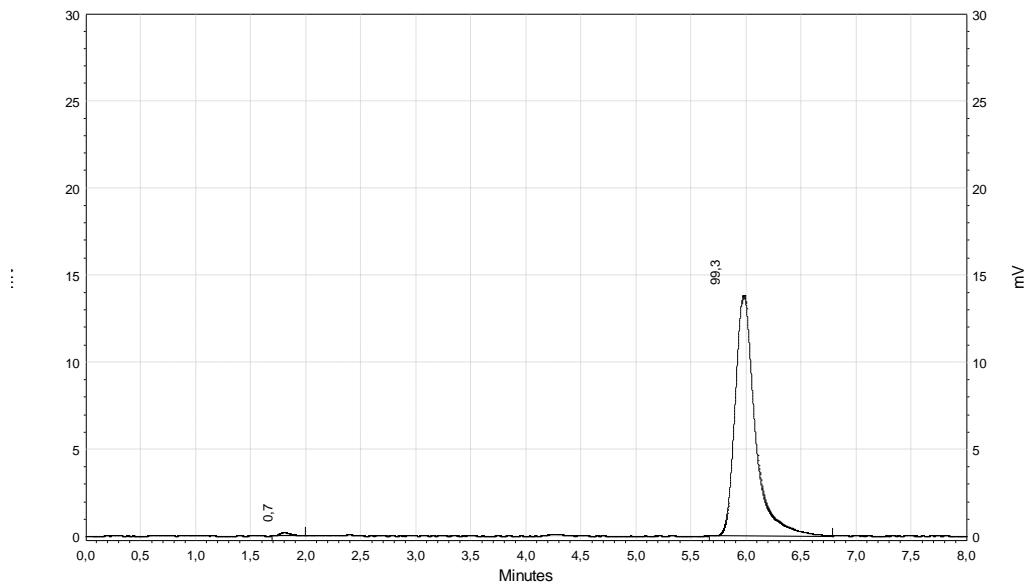


Figure A.42. First measurement of three independent data for CPT in gel at 0.015% loading at t= 315 min

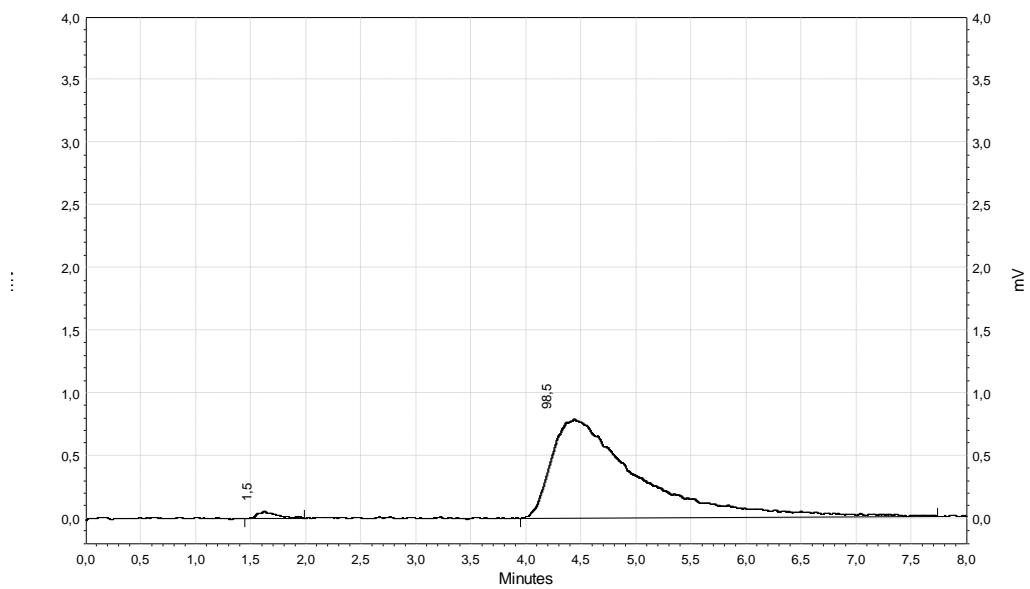


Figure A.43. First measurement of three independent data for TPT in gel at 0.015% loading at t= 0 min

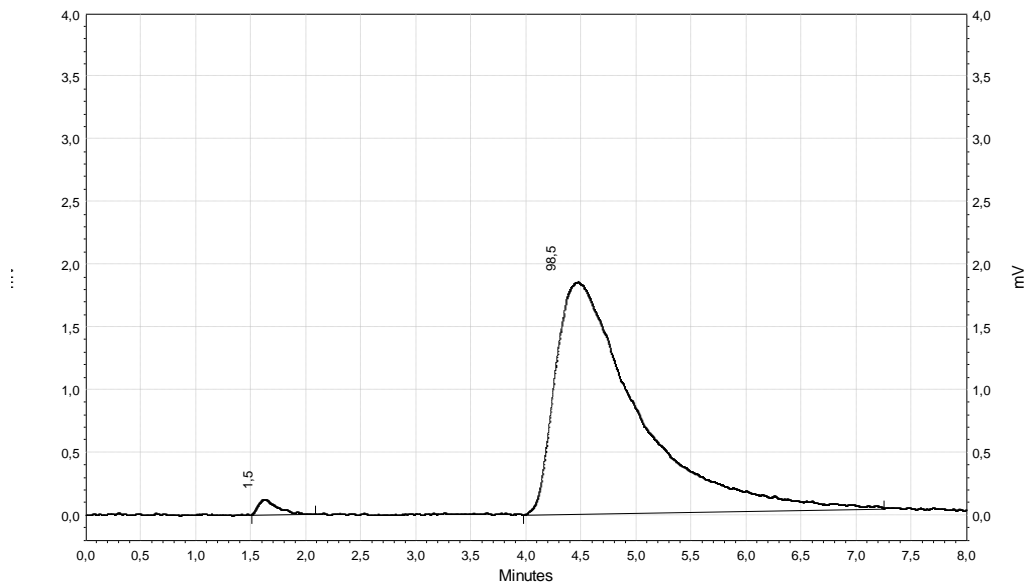


Figure A.44. First measurement of three independent data for TPT in gel at 0.015% loading at $t=45$ min

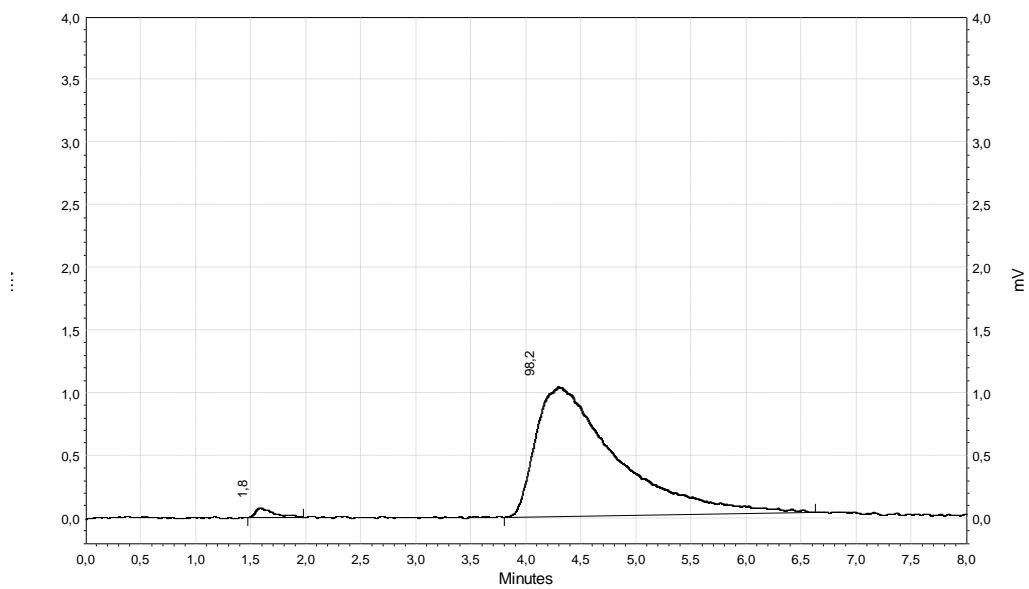


Figure A.45. First measurement of three independent data for TPT in gel at 0.015% loading at $t=90$ min

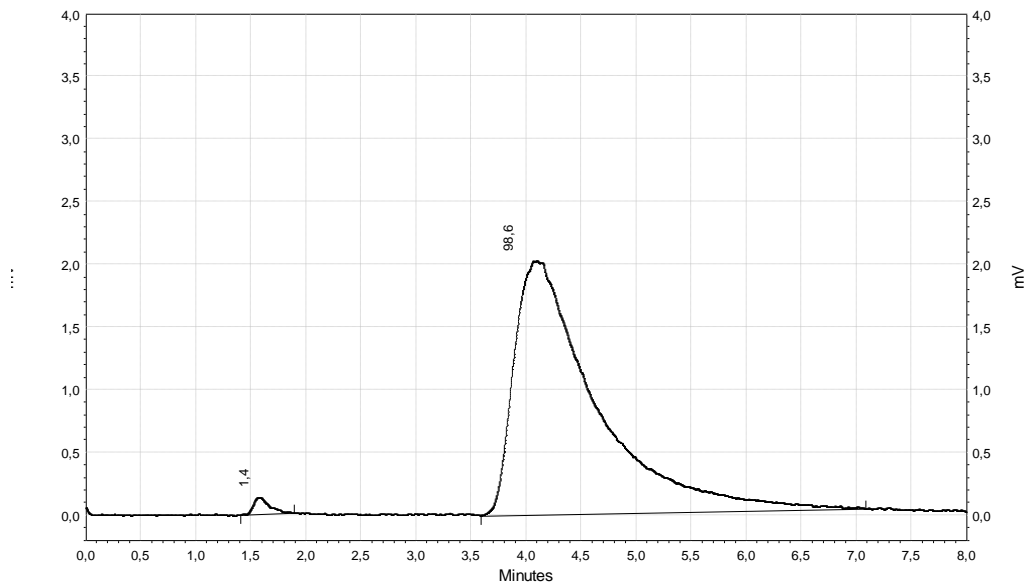


Figure A.46. First measurement of three independent data for TPT in gel at 0.015% loading at $t=135$ min

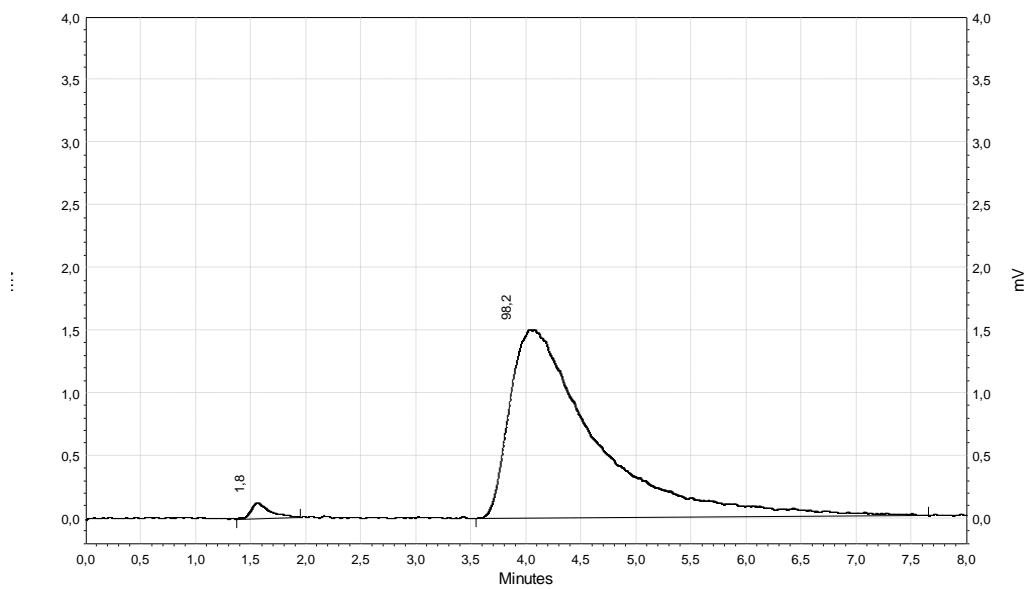


Figure A.47. First measurement of three independent data for TPT in gel at 0.015% loading at $t=180$ min

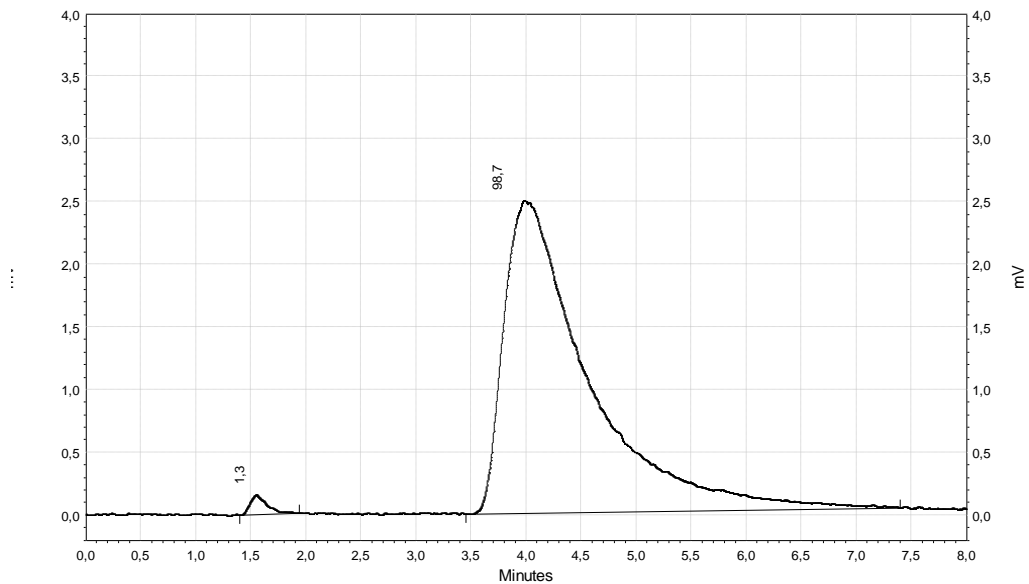


Figure A.48. First measurement of three independent data for TPT in gel at 0.015% loading at $t= 225$ min

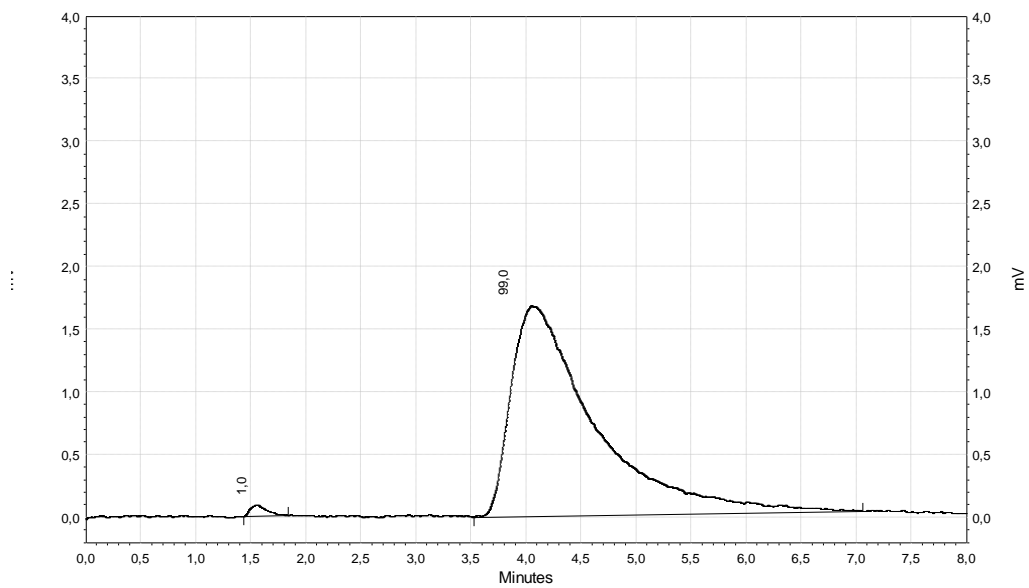


Figure A.49. First measurement of three independent data for TPT in gel at 0.015% loading at $t= 270$ min

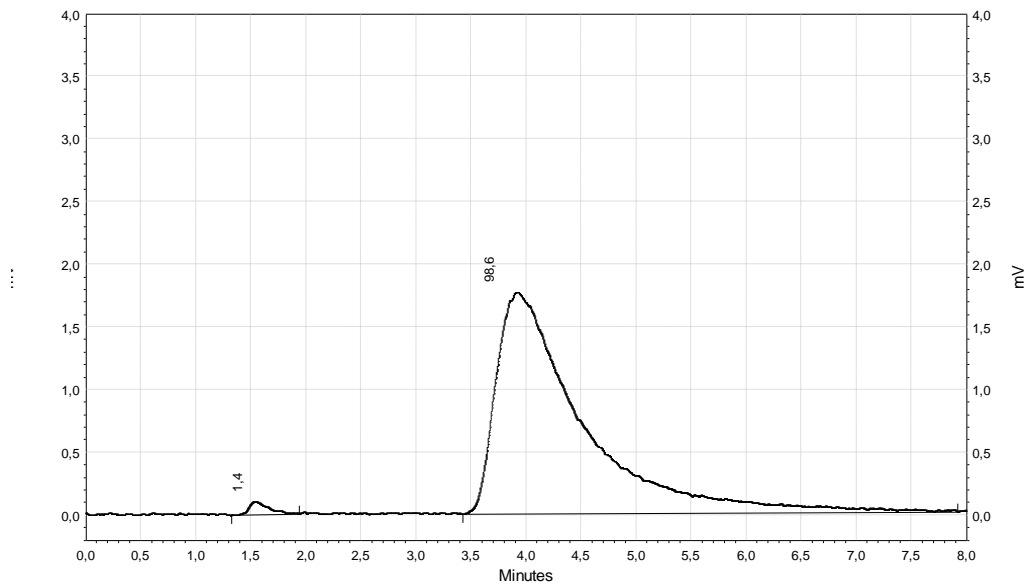


Figure A.50. First measurement of three independent data for TPT in gel at 0.015% loading at $t = 315$ min

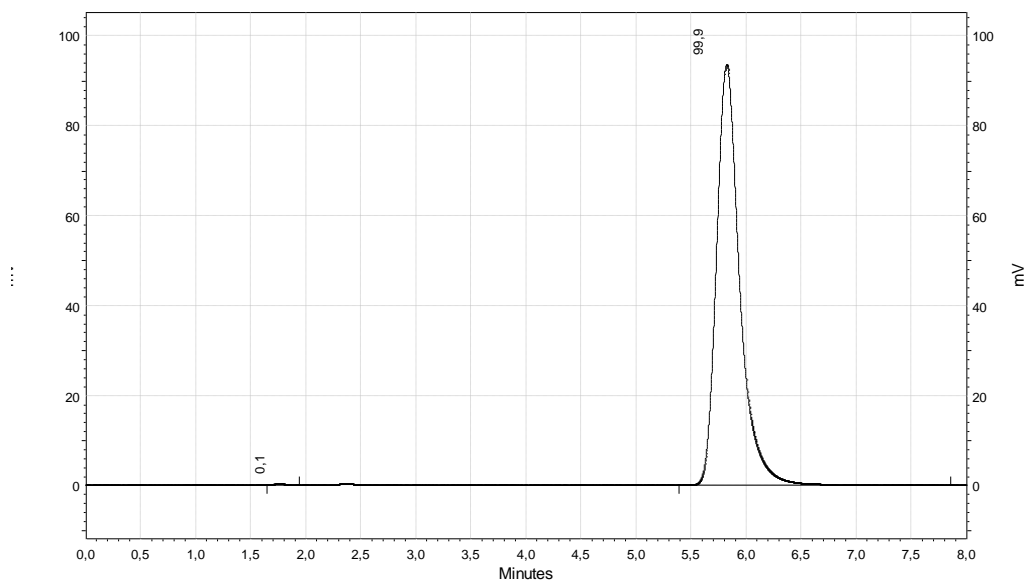


Figure A.51. First measurement of three independent data for CPT in gel at 1.0% loading (representative example), $t = 120$ min

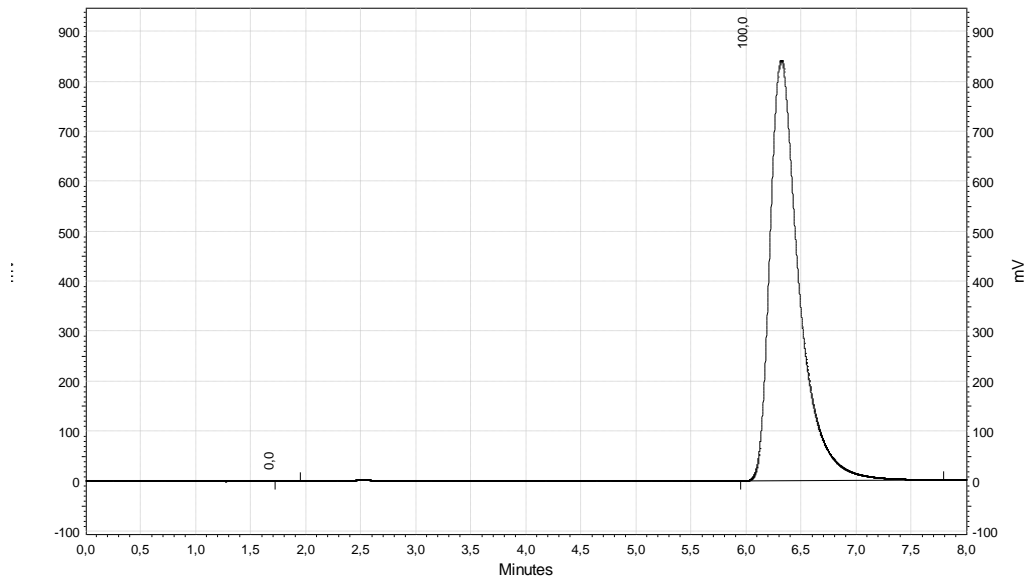


Figure A.52. First measurement of three independent data for CPT in gel at 10.0% loading (representative example), $t= 120$ min

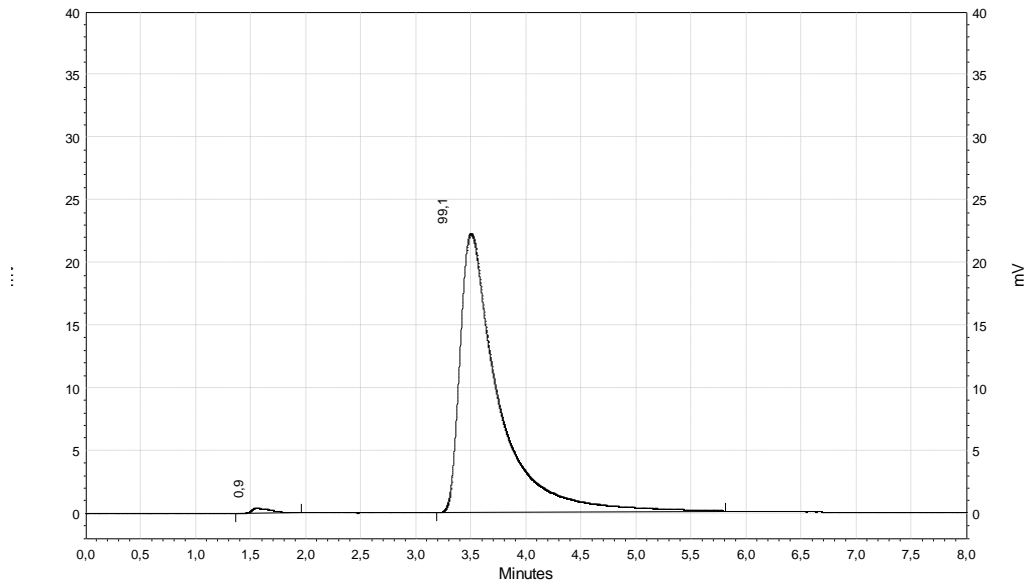


Figure A.53. First measurement of three independent data for TPT in gel at 1.0% loading (representative example), $t= 120$ min

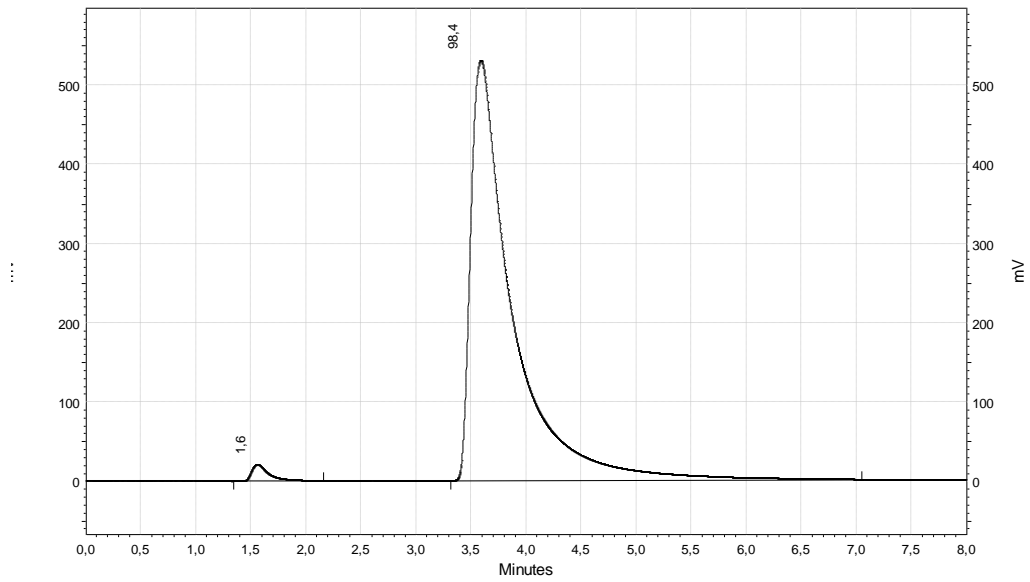


Figure A.54. First measurement of three independent data for TPT in gel at 10.0% loading (representative example), $t=120$ min

APPENDIX B

NMR

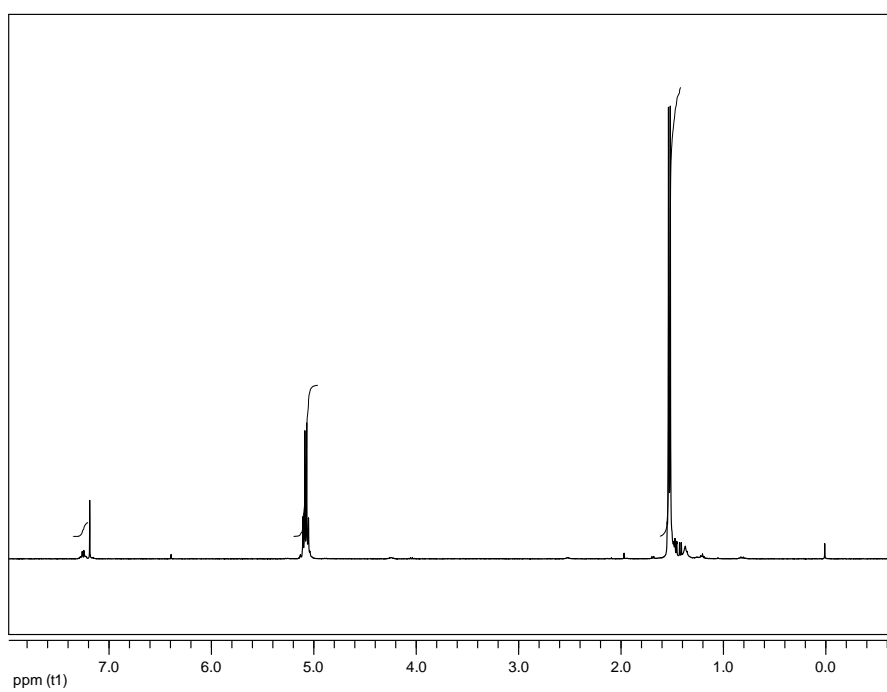


Figure B.1. ^1H spectrum of polymer 19

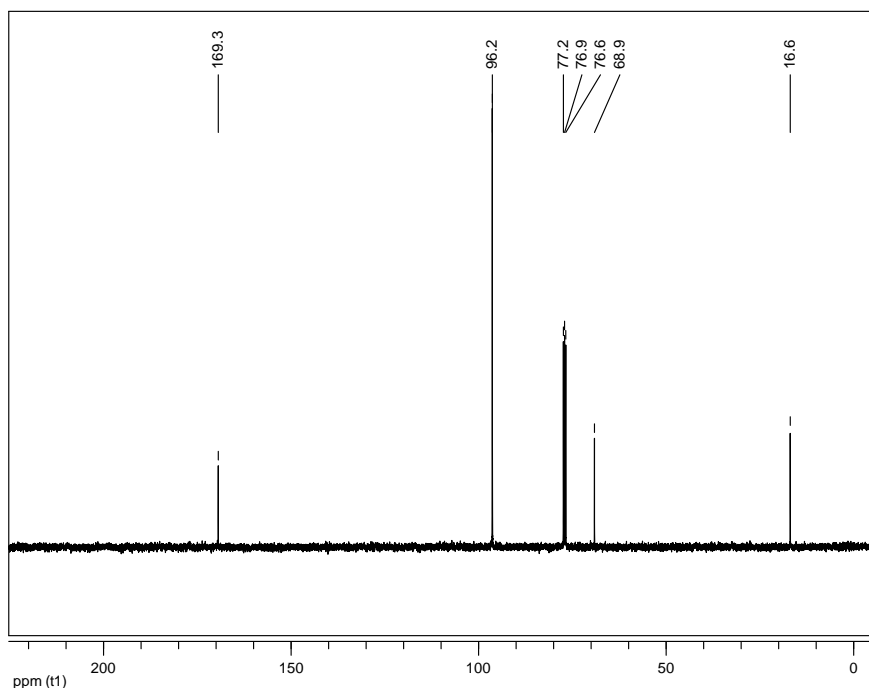


Figure B.2. ^{13}C spectrum of polymer 19

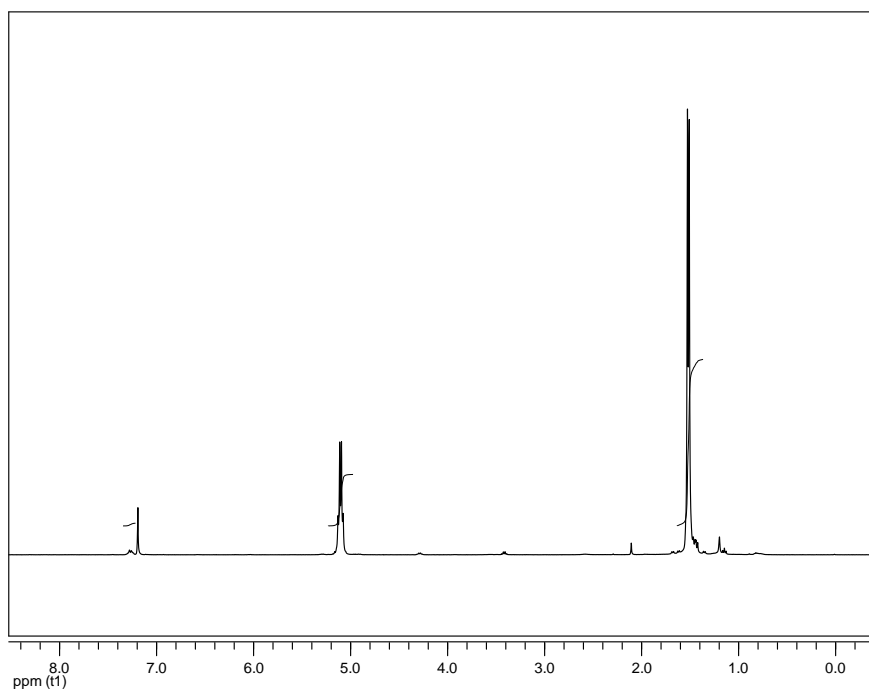


Figure B.3. ^1H spectrum of polymer 20

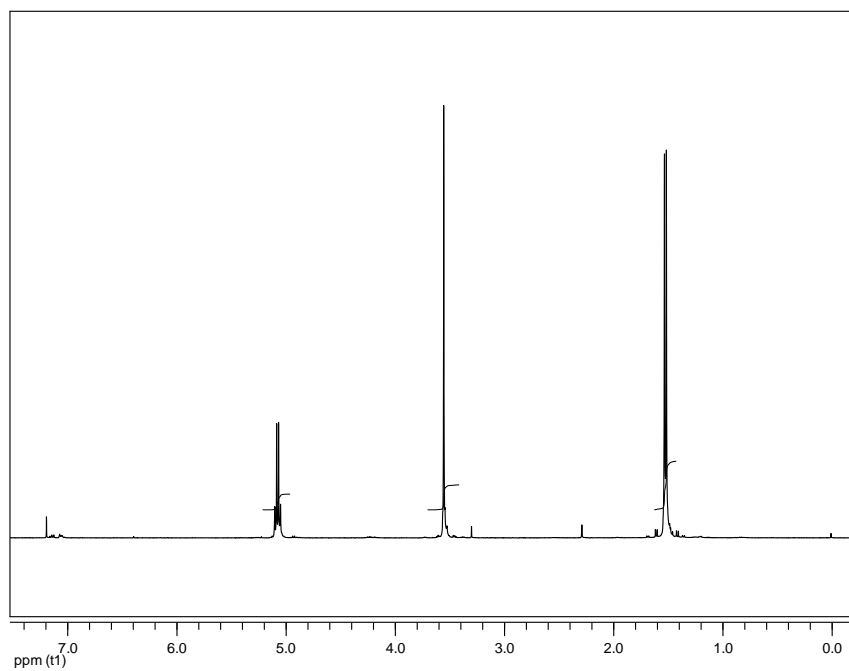


Figure B.4. ^1H spectrum of polymer 21

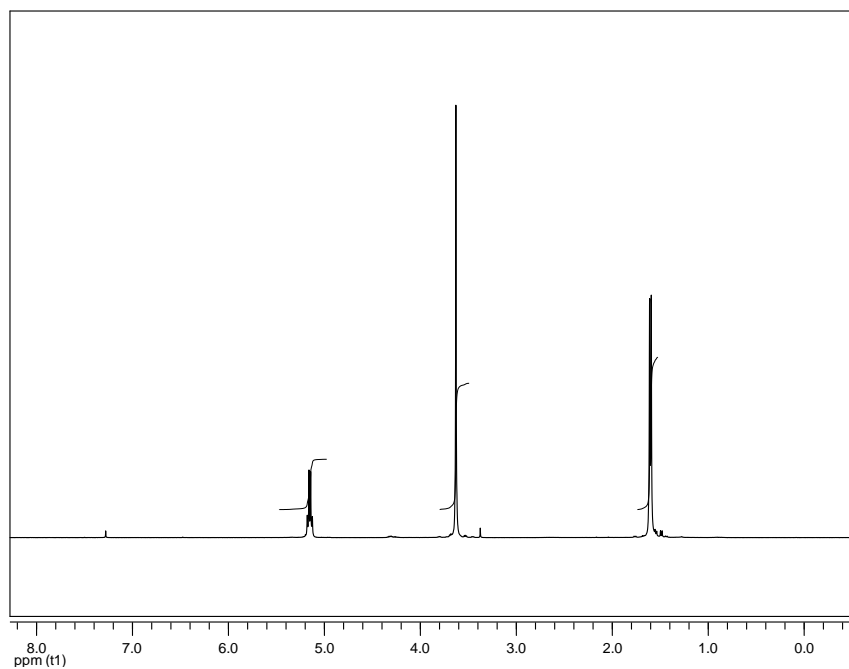


Figure B.5. ^1H spectrum of polymer 22

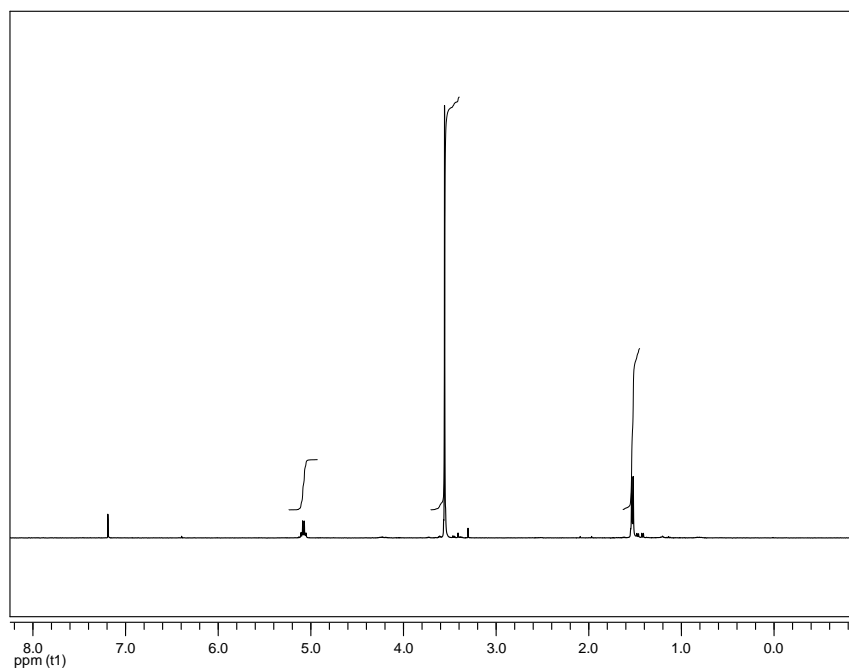


Figure B.6. ¹H spectrum of polymer 23

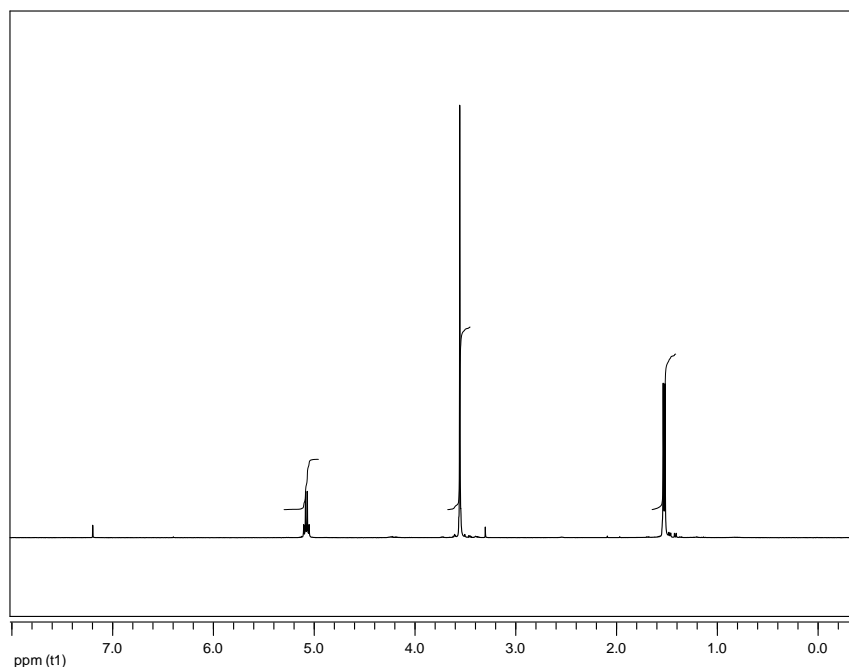


Figure B.7. ¹H spectrum of polymer 24

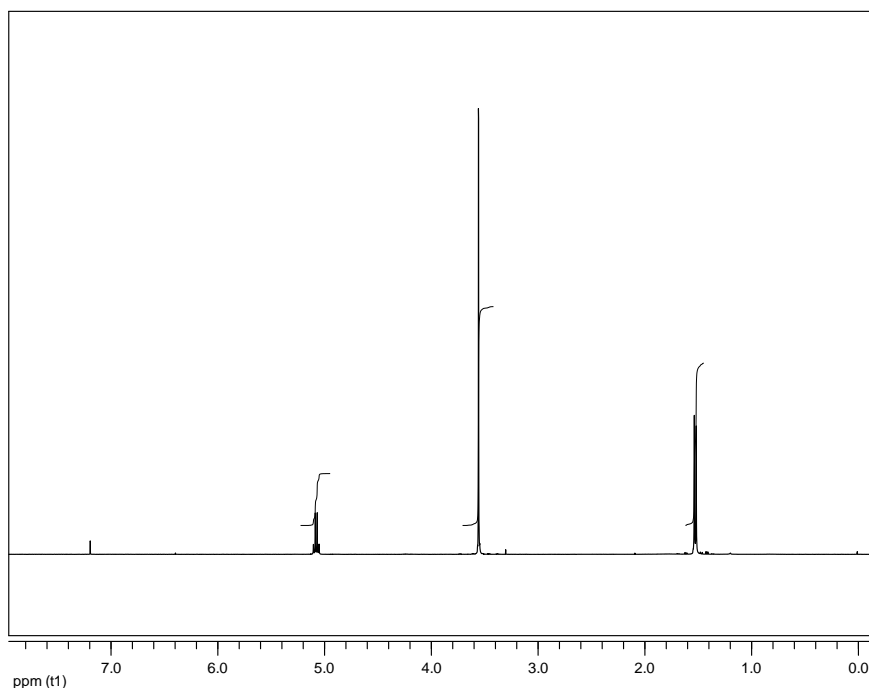


Figure B.8. ^1H spectrum of polymer 25

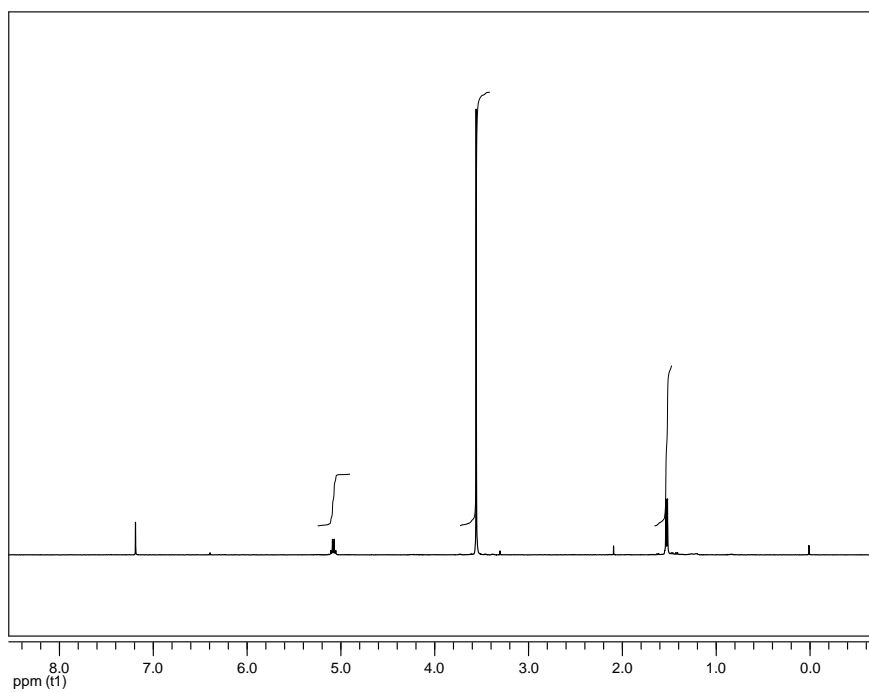


Figure B.9. ^1H spectrum of polymer 26

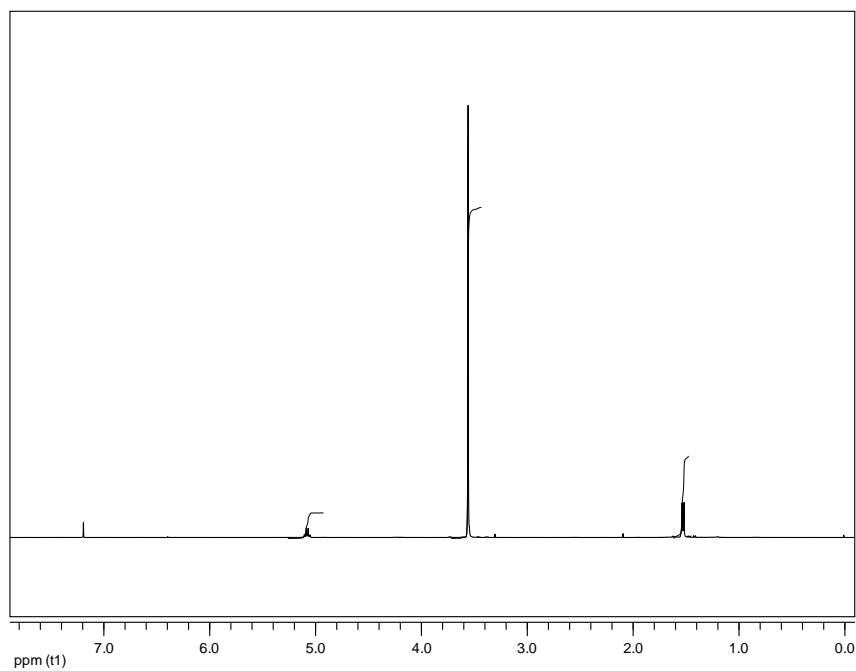


Figure B.10. ^1H spectrum of polymer 27

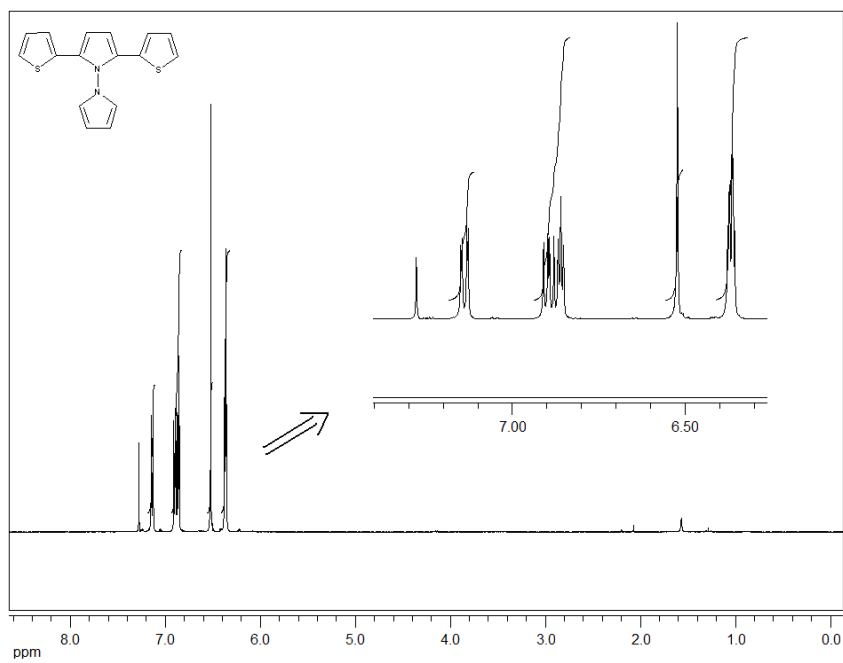


Figure B.11. ^1H spectrum of SNSN 18

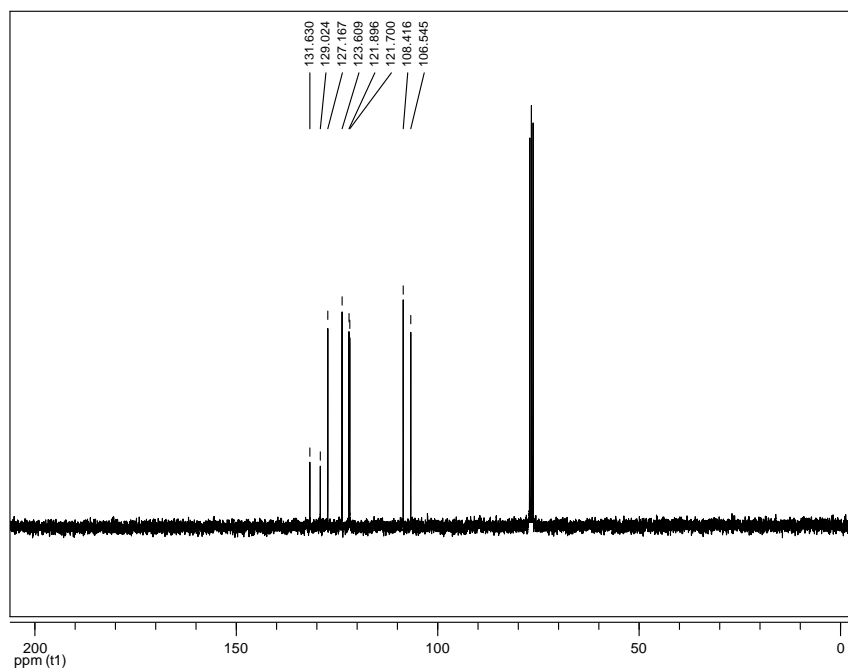


Figure B.12. ^{13}C spectrum of SNSN 18

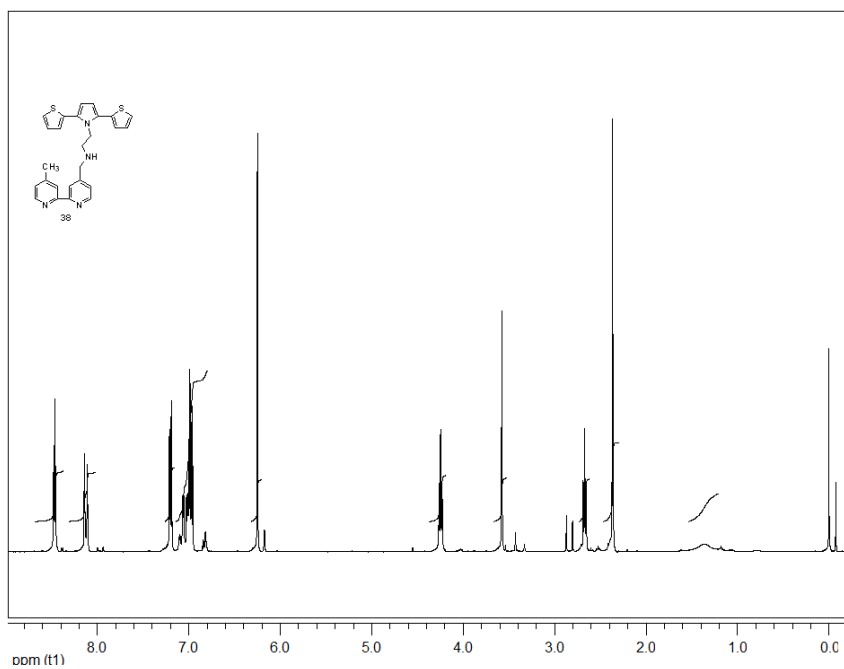


Figure B.13. ^1H spectrum of the compound 38

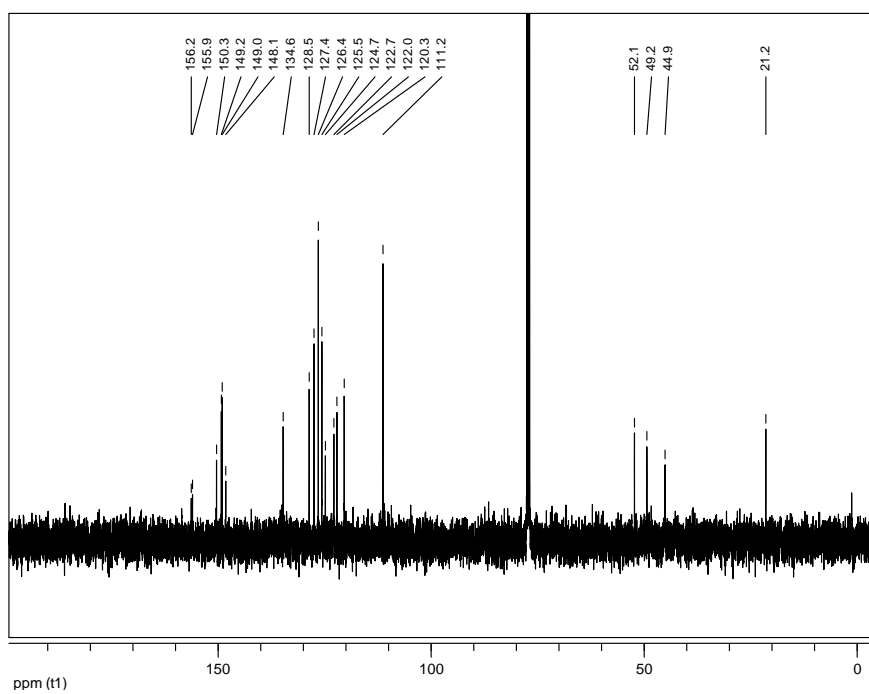


Figure B.14. ^{13}C spectrum of the compound 38

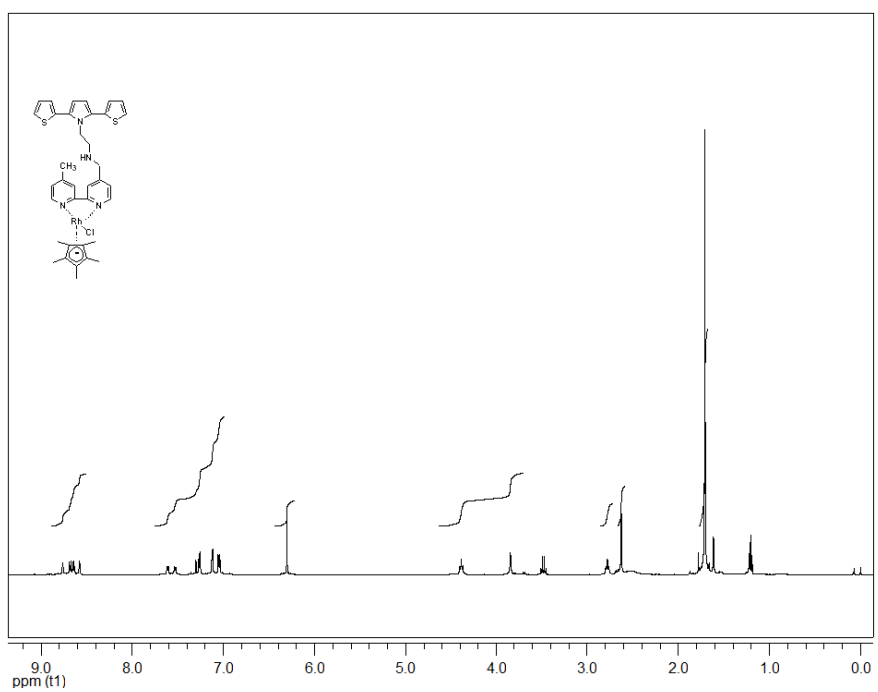


Figure B.15. ^1H spectrum of the compound 39

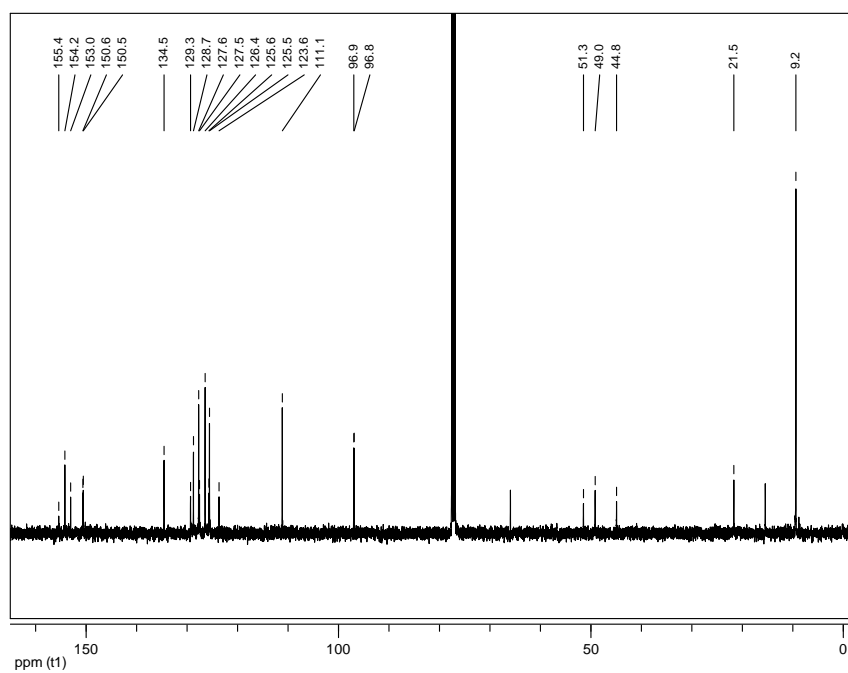


Figure B.16. ^{13}C spectrum of the compound 39

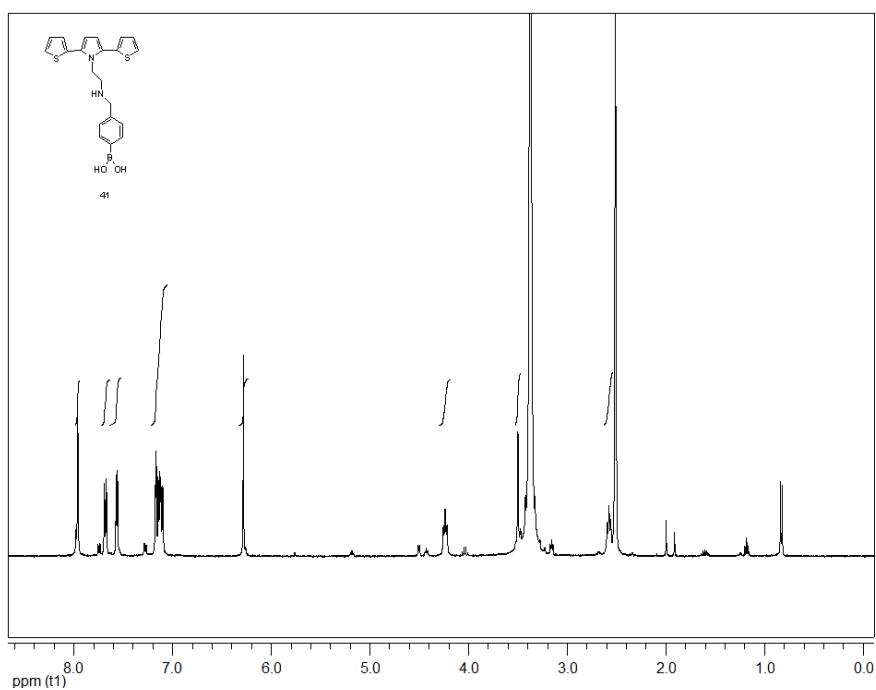


Figure B.17. ^1H spectrum of the compound 41

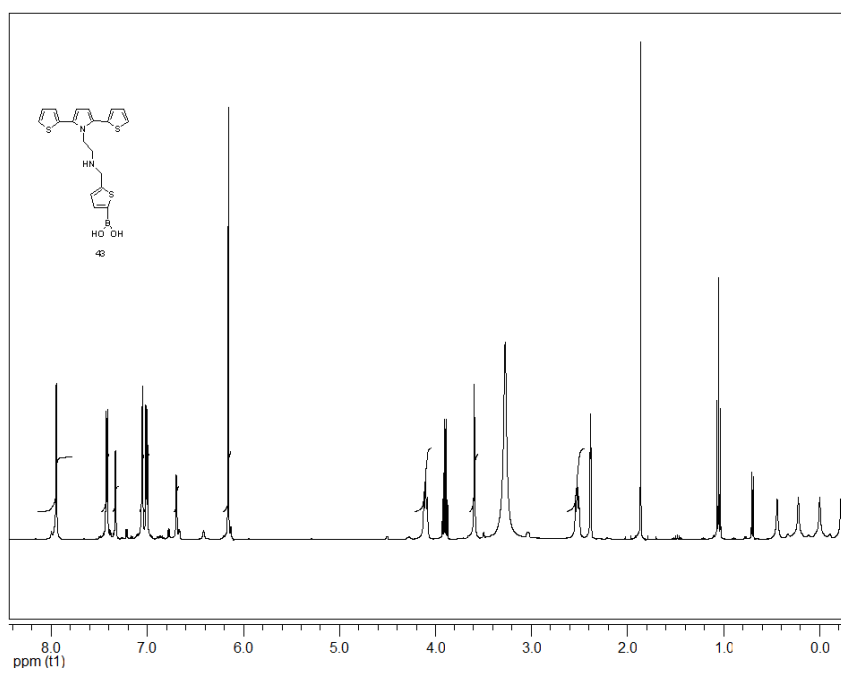


Figure B.18. ¹H spectrum of the compound 43

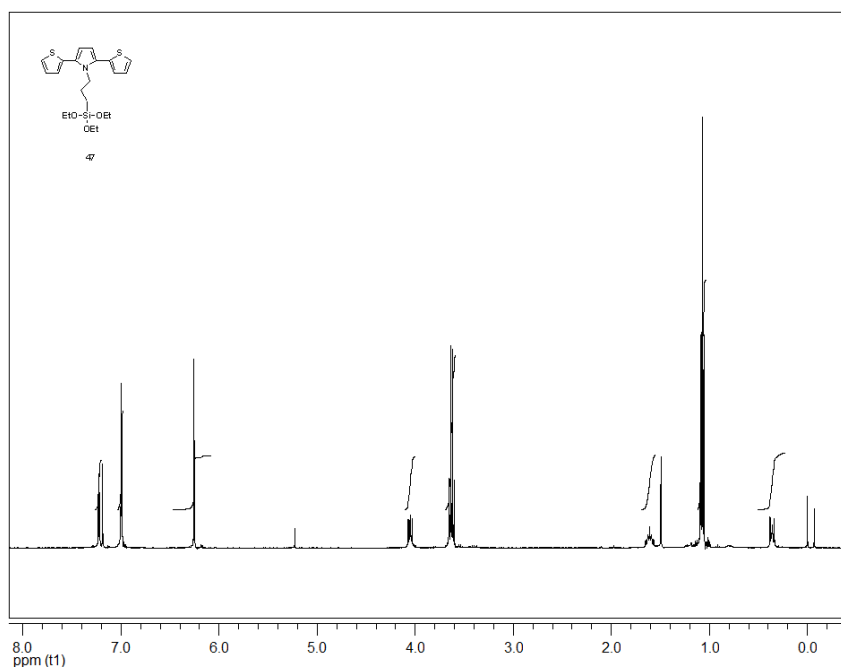


Figure B.19. ¹H spectrum of the compound 47

CURRICULUM VITAE

PERSONAL INFORMATION

Surname, Name: Mert, Olcay

Nationality: Turkish (T.C.)

Date and Place of Birth: 24 March 1981, Saray- Tekirdağ

Marital Status: Single

Phone: +90 312 210 5340

Fax: +90 312 210 3200

E-mail: omert6@gmail.com

EDUCATION

Degree	Institution	Year of Graduation
BS	Kocaeli Univ. Dept. of Chem.	2002
High School	Ali Naki Erenyol Lisesi, T.dağ	1997

WORK EXPERIENCE

Year	Place	Enrollment
2000, Two Months	SETAS Chemistry, Turkey	Training Student
2001, Two Months	TUBITAK, MAM, Turkey	Training Student
2003-	METU Dept. of Chem., Turkey	Research Assistant
2008, One Year	Johns Hopkins Univ., USA	Visiting Scientist

FOREIGN LANGUAGES: English

ALL PUBLICATIONS OF THE WRITER

1- Erbil H. Y., Demirel A. L., Avcı Y., Mert O., Transformation of a Simple Plastic into a Superhydrophobic Surface, **Science**, 2003, Vol.299, 1377-1380.

2- Ozturk T., Ertas E., Mert O., Dithienothiophenes, Review Article, **Tetrahedron**, 2005, 61,11055-11077.

3- Mert O., Sahin E., Ertas E., Ozturk T., Aydin E.A., Toppare L. Electrochromic Properties of Poly(diphenyldithieno[3,2-b;2',3'-d]thiophene), **Journal of Electroanalytical Chemistry**, 2006, 591,53-58.

4- Ozturk T., Ertas E., Mert O., Use of Lawesson's Reagent in Organic Syntheses, **Chemical Reviews**, 2007, 107(11), 5210-5278.

5- Mert O.; Doganci E.; Erbil H. Y.; Demir A. S. Surface Characterization of Poly(L-lactic acid)-Methoxy Poly(ethylene glycol) Diblock Copolymers by Static and Dynamic Contact Angle Measurements, FTIR, and ATR-FTIR, **Langmuir**, 2008, 24(3), 749-757.

6- Cihaner A., Mert O., Demir A. S., A novel electrochromic and fluorescent polythienylpyrrole bearing 1,1'-bipyrrole, **Electrochimica Acta**, 54(4), 2009, 1333-1338.

7- Ozturk T., Ertas E., Mert O., Use of Phosphorus Pentasulfide in Organic Syntheses (P_2S_5), Review Article, **Chemical Reviews**, 110(6), 3419-3478, 2010.

8- Lai S.K., Suk J.S., Pace A., Wang Y.Y., Yang M., Mert O., Chen J., Kim J., Hanes J. Drug carrier nanoparticles that penetrate human chronic rhinosinusitis mucus. **Biomaterials**, In Press.

9- Mert O., Esendađlı G., Dođan A.L., Demir A.S. Injectable Biodegradable Polymeric System for Preserving the Active form and Delayed-Release Of Camptothecin Anticancer Drugs, Submitted.

10- Mert O., Lai S.K., Ensign L., Yang M., Wang Y.Y., Wood J., Hanes J. A poly(ethylene glycol)-based surfactant for formulation of drug-loaded mucus penetrating particles, 2011, submitted.

ALL PATENTS OF THE WRITER

1. “Superhydrophobic Polypropylene Film and Coating Method”, Turkish Patent, Application Number: 21652, 28 February 2004, H. Y. Erbil, A. L. Demirel, Y. Avcı and O. Mert.

2. “Surfactants that improve stability and performance of drug-loaded particles”, S.K. Lai, O. Mert, L. Ensign, M. Yang, J. Hanes. *Patent Pending*.

“The mucus penetrating particle technology described in this patent is being developed by Kala Pharmaceuticals, Boston, USA”

POSTER PRESENTATIONS

National:

- Olcay Mert, Turan Ozturk, Ayhan S. Demir, The Synthesis of Dinitrophenyl and Diaminophenyl Based Dithieno [3,2-b:2',3'-d] Thiophene Compounds, Poster Presentation, 2004, Kars, TURKEY
- Erdinç Doğanç, Olcay Mert, H.Yildirim Erbil, Ayhan S. Demir, Synthesis and Characterization of PLLA-PEG Copolymers Surfaces, Poster Presentation, 2006, Kayseri, TURKEY
- Olcay Mert, Ayhan S. Demir, Injectable Biodegradable Polymers for Drug Delivery Systems, Poster Presentation, 2007, Malatya, TURKEY
- Olcay Mert, Atilla Cihaner and Ayhan S. Demir, A novel electrochromic and fluorescent polythienylpyrrole bearing 1,1'-bipyrrole, Poster Presentation, 2010, Zonguldak, TURKEY
- Olcay Mert and Ayhan S. Demir Injectable Biodegradable Polymers For The Delivery Of Camptothecin Anti-Cancer Drugs, Oral Presentation, 2010, Kocaeli, TURKEY

International:

- Olcay Mert, Ayhan S. Demir, Turan Öztürk and Serap Eröksüz, Synthesis of dithieno [3,2-b:2',3'-d] thiophene derivatives from 1,8 diketones, Poster Presentation, 2006, American Chemical Society, San Francisco, USA.

- Olcay Mert and Ayhan S. Demir, Injectable Biodegradable Polymers For The Delivery Of Camptothecin Anti-Cancer Drugs, Poster Presentation, Macro2010, 2010, Glasgow, UK.
- Olcay Mert, Ayhan S Demir, Building block system for the development of electrochemical reactors, Poster Presentation, 2010, EU FP7 ERUDES Consortium Progress & Management Meeting, Kuşadası, Turkey.

